



Ludwig-Maximilians-Universität München

Fakultät Biologie

Bereich Genetik

**Protein kinase A mediated adaptation of
trypanosomes to the insect host environment**

Kristina Malenica

München 2022

Dissertation der Fakultät für Biologie der
Ludwig-Maximilians-Universität München

Erster Gutachter: **Prof. Dr. Michael Boshart**
Biozentrum der Ludwig-Maximilians-Universität München
Bereich Genetik

Zweiter Gutachter: **PD Dr. Bettina Bölter**
Biozentrum der Ludwig-Maximilians-Universität München
Bereich Botanik

Datum der Abgabe: 19.05.2022

Datum der mündlichen Prüfung: 04.08.2022

Eidesstattliche Versicherung

Ich versichere hiermit an Eides statt, dass die vorgelegte Dissertation von mir selbständig und ohne unerlaubte Hilfe angefertigt ist.

München, 25.08.2022

(Ort, Datum)

Kristina Malenica

(Unterschrift)

Erklärung

Hiermit erkläre ich,

- dass die Dissertation nicht ganz oder in wesentlichen Teilen einer anderen Prüfungskommission vorgelegt worden ist.
- dass ich mich zu keinem früheren Zeitpunkt anderweitig einer Doktorprüfung unterzogen oder eine Dissertation eingereicht habe.

München, 25.08.2022

(Ort, Datum)

Kristina Malenica

(Unterschrift)

I.	List of Abbreviations	IV
II.	ABSTRACT	V
III.	ZUSAMMENFASSUNG	VI
1	INTRODUCTION.....	1
1.1	<i>Metabolic adaptation</i>	<i>1</i>
1.1.1	Metabolic adaptation during <i>Trypanosoma brucei</i> differentiation	1
1.1.2	Glycosomes: specialized compartments.....	5
1.2	<i>Nutrient sensing by protein kinases</i>	<i>8</i>
1.3	<i>Protein kinase A (PKA).....</i>	<i>10</i>
1.3.1	The PKA signaling pathway	10
1.3.1.1	PKA activation mechanism.....	10
1.3.1.2	How is subunit specificity conferred?	12
1.3.1.3	PKA subunits in <i>T. brucei</i>	13
1.3.1.4	Known and potential functions of PKA in single cellular parasites	19
1.4	<i>Aims of the thesis.....</i>	<i>20</i>
2	MATERIALS AND METHODS	21
2.1	<i>Materials.....</i>	<i>21</i>
2.1.1	Oligonucleotides	21
2.1.2	Plasmids.....	23
2.1.3	<i>E. coli</i> strains	27
2.1.4	<i>Trypanosoma brucei</i> cell lines.....	28
2.1.5	Antibodies.....	33
2.1.6	Antibiotic stock solutions	34
2.2	<i>Methods.....</i>	<i>35</i>
2.2.1	<i>Trypanosoma brucei</i>	<i>35</i>
2.2.1.1	Cultivation of BSF trypanosomes	35
2.2.1.2	Cultivation of PCF trypanosomes.....	36
2.2.1.3	Freezing and thawing of stabilates	36
2.2.1.4	Generation of transgenic <i>Trypanosoma</i> lines	36
2.2.1.5	Differentiation of trypanosomes	39
2.2.2	<i>E. coli</i>	40
2.2.2.1	Cultivation.....	40
2.2.2.2	Preparation of competent cells	40
2.2.2.3	Transformation	41
2.2.3	Nucleic acids	41
2.2.3.1	Standard cloning procedures	41
2.2.3.2	Isolation of gDNA from <i>T. brucei</i>	43
2.2.4	Proteins.....	43

2.2.4.1	Recombinant protein expression in <i>E. coli</i>	43
2.2.4.2	Purification of recombinant proteins.....	43
2.2.4.3	Affinity purification of antibodies.....	44
2.2.4.4	Generation of anti-PKAC3 antibody.....	45
2.2.4.5	Protein quantification.....	45
2.2.4.6	Absolute quantification of PKA subunits in <i>T. brucei</i> lysates.....	46
2.2.4.7	Preparation of <i>T. brucei</i> lysates for SDS-PAGE.....	47
2.2.4.8	SDS-PAGE.....	47
2.2.4.9	Coomassie staining of SDS gels.....	47
2.2.4.10	Western blot analysis.....	47
2.2.4.11	Immunoprecipitation by GFP-trap.....	48
2.2.5	Cell fractionations.....	49
2.2.5.1	Glycosome enrichment by differential centrifugation.....	49
2.2.5.2	Glycosome purification by Optiprep density gradient.....	49
2.2.5.3	Glycosome purification by sucrose density gradient.....	50
2.2.5.4	Protease protection assay of glycosome enriched fractions.....	50
2.2.5.5	Preparation of glycosome enriched fractions for proteomics.....	51
2.2.6	Microscopy.....	52
2.2.6.1	Methanol fixation.....	52
2.2.6.2	PFA-fixation.....	52
2.2.6.3	Trypanosoma staging (RBP6).....	52
2.2.6.4	Imaging of GFP-tagged lines.....	53
2.2.7	<i>In vivo</i> cellular assays.....	53
2.2.7.1	Glycerol-depletion assay.....	53
2.2.7.2	Glycerol-depletion phosphoproteome.....	54
2.2.7.3	Alamar Blue assay.....	57
2.2.7.4	Purine response assays in pleomorphic cells.....	57
2.2.7.5	NMR.....	58
2.2.7.6	BioID.....	58
3	RESULTS.....	60
3.1	<i>Tools for TbPKA analysis.....</i>	<i>60</i>
3.1.1	Purification of recombinant PKA subunits from <i>E. coli</i>	60
3.1.2	Generation of an anti-PKAC3 antibody.....	62
3.1.3	Quantification of absolute PKA amounts in <i>T. brucei</i> lysates.....	63
3.2	<i>Generation of a PKAC knockout series.....</i>	<i>65</i>
3.2.1	Generation of Δ PKAC2.....	66
3.2.2	Generation of Δ PKAC1/2.....	69
3.2.3	Generation of Δ PKAC1/2/3.....	71
3.2.4	Comparison of RXXS*/T* phosphorylation in PKA knockouts.....	72

3.3	<i>Identification of possible PKA targets in PCF using a multi-omics approach</i>	73
3.3.1	Δ PKAC2 proteome	74
3.3.2	Δ PKAC2 phosphoproteome	76
3.3.3	Interactome by BioID	78
3.3.3.1	Bloodstream forms	79
3.3.3.2	Procyclics	81
3.3.3.3	Data exploration	82
3.3.4	Structural modeling of PKAC1 and PKAC2	86
3.4	<i>Possible role of PKAC2 in the regulation of metabolism</i>	89
3.4.1	Glycosomal localization of PKAC2	89
3.4.1.1	Fluorescence microscopy of GFP-PKAC2	90
3.4.1.2	Glycosome purification	90
3.4.2	Regulation of carbohydrate metabolism	93
3.4.2.1	Growth analysis under different carbon sources	94
3.4.2.2	Role of PKA in carbon source metabolism	95
3.4.2.3	Carbon source preferences of early PCF by NMR	111
3.4.3	Regulation of purine metabolism	113
4	DISCUSSION	115
4.1	<i>Functions of PKA in PCF</i>	115
4.1.1	Role of PKA in metabolism	115
4.1.1.1	Effects of PKAC2 on central carbon metabolism	115
4.1.1.2	Environmental sensing through glycolytic metabolites	124
4.1.1.3	PKA and nucleoside metabolism	125
4.1.2	PKA is not essential for basic cellular viability in PCF	126
4.2	<i>Redundancy of PKAC1 and PKAC2</i>	127
5	REFERENCES	131
6	CURRICULUM VITAE	143
7	ACKNOWLEDGEMENTS	145
8	SUPPLEMENTARY DATA	146

I. List of Abbreviations

α-KG	alpha-ketoglutarate	PDK1	Phosphoinositide-dependent kinase-1
AC	Adenylate cyclase	PDT	Population doubling time
ADR	Arginine deprivation response	PEPCK	Phosphoenolpyruvate-carboxykinase
AKAP	A-kinase anchoring protein	PEX14	Peroxisomal membrane protein PEX14
AMPK	AMP-activated protein kinase	PFR	Paraflagellar rod
AMP	Adenosine monophosphate	PIP39	PTP1-interacting protein, 39 kDa
ATP	Adenosine triphosphate	PK	Proteinase K
BARP	Brucei alanine-rich protein	PKA	Protein kinase A
BioID	Proximity-dependent biotin identification	PKAR	Protein kinase A regulatory subunit
BiP	Luminal binding protein 1	PKAC	Protein kinase A catalytic subunit
BSA	Bovine serum albumin	PKI	PKA inhibitor peptide
BSF	Bloodstream form	PM	Phosphomimetic
C-KAP	Catalytic kinase anchoring protein	PPDK	Pyruvate phosphate dikinase
cAMP	Cyclic adenosine monophosphate	PPP	Pentose phosphate pathway
CNB	Cyclic nucleotide binding domain	PTM	Post-translational modification
CREB	cAMP response element	PTS	Peroxisomal targeting signal
DAPI	4',6-diamidino-2-phenylindole	RBP6	RNA binding protein 6
DTT	Dithiothreitol	RNAi	RNA interference
EMF	Epimastigote form	ROS	Reactive oxygen species
ER	Endoplasmatic reticulum	RT	Room temperature
FAZ	Flagellar attachment zone	SDS-PAGE	Sodium dodecylsulfate polyacrylamide gel electrophoresis
FDR	False discovery rate	SIF	Stumpy induction factor
GFP	Green fluorescent protein	Stdev	Standard deviation
GlcNAc	N-acetylglucosamine	TCA	Trichloroacetic acid
GO	Gene Ontology	UGP	UTP-glucose-1-phosphate uri- dyltransferase
GPCR	G-protein coupled receptor	UTR	Untranslated region
IDH	Isocitrate dehydrogenase	VSG	Variant surface glycoprotein
IPTG	Isopropyl β -D-1-thiogalactopyranoside		
LFQ	Label-free quantification		
MCF	Metacyclic form		
MS	Mass spectrometry		
NADPH	Nicotinamide adenine dinucleotide phosphate		
NMR	Nuclear magnetic resonance		
OE	Overexpression		
ORF	Open reading frame		
PA	Phosphoablative		
PBS	Phosphate buffered saline		
PCF	Procyclic form		
PDE	Phosphodiesterase		

II. ABSTRACT

The protozoan parasite *Trypanosoma brucei* encounters changing environments during its complex life-cycle involving a mammalian host and the tsetse fly vector. The mammalian life cycle stage (bloodstream form = BSF) inhabits the bloodstream and tissue spaces, which represents a highly stable and tightly regulated environment in terms of pH, temperature and nutrients. Due to the stable supply of glucose in mammalian blood the BSF parasite relies on glycolysis for energy generation. In contrast to that, the environment in the tsetse fly (procyclic form = PCF) varies along the alimentary tract. Insects are poikilotherm and the pH varies between the three main fly tissues, including the midgut, the proventriculus and the salivary glands. Furthermore, transmission to the tsetse fly is accompanied by a severe change in nutrient availability. Glucose is rapidly consumed in the tsetse fly midgut, glycerol might be transiently released during breakdown of erythrocyte membranes after the blood meal while amino acids are highly abundant. These environmental changes during transmission from the mammalian host to the fly vector and its different tissues requires metabolic reprogramming and is accompanied by morphological changes. Proline metabolism takes place in the mitochondrion, while glucose and glycerol are metabolized in specialized peroxisomes, the so-called glycosomes. The changes need to be initiated via signaling events. Protein kinases in general are involved in the signaling cascades that transduce environmental signals into a cellular response. We could confirm that one of the protein kinase A (PKA) catalytic subunits (PKAC2) localizes to glycosomes of fly stage trypanosomes and identified metabolic enzymes regulated in abundance upon PKAC2 knockout. Therefore, we focused on unraveling a potential regulatory role in carbon metabolism. We found that depletion of the glycolytic carbon sources leads to increased phosphorylation of a protein band by PKA or a related kinase *in vivo*. Using a series of PKA knockouts we could show that the phosphorylation event observed by glucose and glycerol-depletion is a PKA mediated event that depends on PKAC2, but not on the regulatory subunit (PKAR). Using a phosphoproteomic approach, we could map the phosphorylation event to the two residues T122 and S123 on PEX14, a key component of the glycosomal import machinery. To address the question of physiological relevance, we generated homozygous phosphoablative and phosphomimetic mutants and compared for glycosomal protein content upon glycerol-depletion. We discuss the potentially important-regulated candidates, including the phosphatase PIP39, a known regulator of trypanosome development.

III. ZUSAMMENFASSUNG

Der einzellige Parasit *Trypanosoma brucei* durchläuft in seinem komplexen Lebenszyklus einen Säugerwirt und die Tsetse Fliege (= Vektor), was zu schwankenden Umweltbedingungen führt. Im Säugerstadium (Blutstromform = BSF) befinden sich die Parasiten in der Blutbahn und in Gewebe Zwischenräumen, die eine sehr stabile und streng regulierte Umgebung in Bezug auf pH-Wert, Temperatur und Nährstoffe darstellt. Aufgrund der stabilen Versorgung mit Glukose im Blut ist der BSF-Parasit auf die Glykolyse zur Energiegewinnung angewiesen. Im Gegensatz dazu schwankt die Umgebung im Verdauungstrakt der Tsetse Fliege. Insekten sind poikilotherm und der pH-Wert variiert zwischen den besiedelten Organen der Fliegen, dazu gehören der Mitteldarm, der Proventriculus und die Speicheldrüsen. Darüber hinaus geht die Übertragung auf die Tsetse-Fliege mit einer starken Veränderung der Nährstoffverfügbarkeit einher. Glukose wird im Mitteldarm der Tsetse-Fliege schnell konsumiert, Glycerol kann während des Abbaus der Erythrozytenmembranen nach der Blutmahlzeit vorübergehend freigesetzt werden, während Aminosäuren extrem abundant sind. Diese Umweltveränderungen während der Übertragung vom Säugerwirt auf den Fliegenvektor und seine verschiedenen Organe erfordern eine metabolische Anpassung und werden von morphologischen Veränderungen begleitet. Der Prolinstoffwechsel findet im Mitochondrium statt, während Glukose und Glycerol in spezialisierten Peroxisomen, sogenannten Glykosomen, verstoffwechselt werden. Diese Änderungen müssen über Signalwege initiiert werden. Proteinkinasen sind an diversen Signalkaskaden beteiligt, die Umweltsignale in eine zelluläre Antwort umwandeln. Wir konnten zeigen, dass eine der katalytischen Untereinheiten der Proteinkinase A (PKA, hier: PKAC2) im prozyklischen Stadium eine zusätzliche glykosomale Lokalisation zeigt und konnten metabolische Enzyme identifiziert, die als Reaktion auf PKAC2-Knockout in ihrer Expression reguliert werden. Daher fokussierten wir uns darauf, eine potenzielle regulatorische Rolle der PKA im Kohlenstoffstoffwechsel zu identifizieren. Der Entzug von glykolytischen Kohlenstoffquellen führt zu einer erhöhten Phosphorylierung einer Proteinbande durch PKAC2 oder einer verwandten Kinase. Mit Hilfe einer Reihe von PKA-Knockouts konnten wir zeigen, dass das durch Glukose- und Glycerol-Depletion beobachtete Phosphorylierungsereignis von der PKAC2, aber nicht von der regulatorischen Untereinheit (PKAR), abhängig ist. Durch Phosphoproteomics konnten wir das Phosphorylierungsereignis den beiden Positionen T122 und S123 auf PEX14 zuordnen, einer Schlüsselkomponente der glykosomalen Importmaschinerie. Um die Frage der physiologischen Relevanz zu beantworten, haben wir homozygote phosphoablative und

phosphomimetische Mutanten generiert und die Abundanz glykosomaler Proteine nach Glycerol-Entzug verglichen. Abschließend diskutieren wir die potenziell Import-regulierten Kandidaten, einschließlich PIP39, einer Phosphatase, die eine Schlüsselrolle in der Entwicklung der Trypanosomen spielt.

1 INTRODUCTION

1.1 Metabolic adaptation

All living organisms are exposed to their respective environments. These environments often change either due to natural rhythms or unexpected perturbations. The organisms therefore need to sense and adapt to these changes, often by modifying their metabolic pathways. Plants for example are exposed to fluctuating weather conditions and must cope with a variety of stresses, like heat, draught, or light availability. Additionally, they need to switch their metabolism from photosynthesis during daytime to respiration at night on a daily basis.

Cell populations, for example bacterial biofilms are exposed to a changing environment. While the biofilm is growing, metabolites and nutrients form gradients throughout this structure leading to different cell layers and metabolic activity of the residing cells (Crabbe et al., 2019). Many pathogenic organisms are exposed to dramatic environmental changes during transmission or when entering an intracellular state.

Not only pathogenic or parasitic, but also free-living organisms are exposed to their surroundings and need to respond accordingly, for example by exponential growth during permissive times and formation of spores and cysts during restrictive times (reviewed in (Stewart, 2015)).

1.1.1 Metabolic adaptation during *Trypanosoma brucei* differentiation

Overview of the life cycle

Trypanosoma brucei is a protozoan parasite and causative agent of sleeping sickness in humans and Nagana in cattle. It is characterized by a complex life cycle involving two hosts providing very different environments. In the mammalian host, two types of so-called bloodstream forms (BSF) are known: the long slender BSF divide in the mammalian bloodstream until a high level of parasitemia is reached. At that point, the cells undergo differentiation to cell-cycle arrested short stumpy forms, which is induced by a quorum sensing mechanism of the stumpy induction factor (SIF). This differentiation process limits the parasitemia and allows host survival (reviewed in (Rojas and Matthews, 2019)). Furthermore, these cells are metabolically primed for the uptake by the insect vector, the tsetse fly (*Glossina spec.*) (reviewed in (Kabani et al., 2009; MacGregor et al., 2012)). During the bloodmeal, the tsetse fly ingests both forms of parasites. The long slenders mostly die off, while the short stumpys differentiate further into procyclic forms (PCF) in the tsetse midgut (Rico et al., 2013). Procyclic forms

resume proliferation and progress towards the salivary glands, a process that includes migration through different tissues and undergoing additional differentiation steps (de-

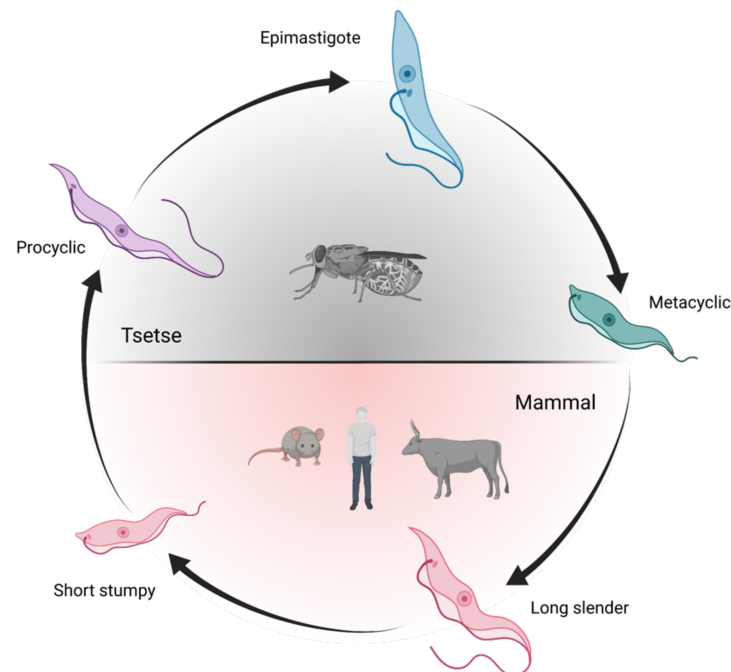


Figure 1: *Trypanosoma brucei* life cycle. Long slender cells proliferate in the mammalian bloodstream until they differentiate into short stumpy forms. They are taken up by tsetse flies during their bloodmeal and differentiate further into procyclic forms, then epimastigote forms and finally metacyclics. These metacyclics are transmitted to a new mammalian host. Figure was created with BioRender.com

scribed in more detail in paragraph Metabolism of Procyclic forms). In the salivary glands they differentiate into metacyclic cells, which are again primed for the transfer to a new mammalian host (Figure 1). After transmission they differentiate into slender BSF and the cycle resumes (Walsh and Hill, 2021).

Metabolism of BSF

The proliferating long slender BSF cells mainly reside in the mammalian bloodstream which provides a highly regulated

and stable environment in terms of temperature, pH, oxygen and nutrient levels. Glucose levels in particular are very tightly regulated in mammalian blood and kept stable at around 5 mM (<https://hmdb.ca>)(Wishart et al., 2018). Therefore, it is not surprising that the BSF stage specialized on glycolysis for energy generation (reviewed in (Smith et al., 2017)). Other energy generating pathways are extremely downregulated and the mitochondrion is highly reduced, both in size and active pathways (Figure 2). Therefore, glucose-depletion in this stage is lethal. The stumpy cells however, are primed for uptake by the insect vector (reviewed in (Kabani *et al.*, 2009; MacGregor *et al.*, 2012)). This priming includes the reactivation of the mitochondrial metabolic pathways (Dejung et al., 2016; Gunasekera et al., 2012; Tyler et al., 1997), which circumvents the glucose-dependency.

Metabolic and gene expression data are limited to the forms that can be cultured *in vitro*. The mammalian form of *T. brucei* colonizes the blood and interstitial spaces of tissues, including the brain, adipose tissue or skin. These extra vascular forms were described to have a different morphology, indicating the need for some metabolic re-programming (Dwinger et al., 1988). However, there are no experimental data available for these special forms. One recent study described differences in mRNA transcript levels of genes involved in fatty acid metabolism in adipose tissue forms (Trindade et al., 2016).

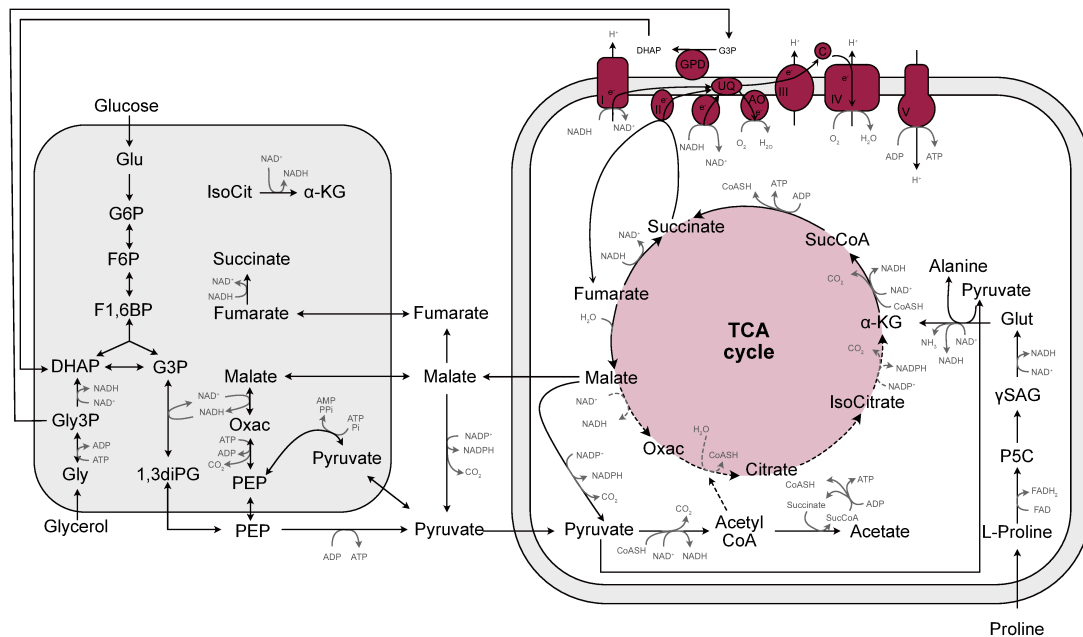


Figure 2: Energy generation in long-slender BSF *T. brucei*. Energy generation is dependent on glucose breakdown to pyruvate, which is a major excretion product. Some pyruvate however can be further metabolized to acetate, which is finally excreted. Based on (Michels et al., 2021). Enzymes: 1: hexokinase, 2: glucose-6-phosphate-isomerase, 3: phosphofructokinase, 4: aldolase, 5: triosephosphate-isomerase, 6: glycerol-3-phosphate-dehydrogenase, 7: glyceraldehyde-3-phosphate-dehydrogenase, 8: phosphoglycerate kinase, 9: phosphoglycerate mutase, 10: enolase, 11: pyruvate kinase, 12: phosphoenolpyruvate carboxykinase, 13: malate dehydrogenase, 14: fumarate reductase, 15: fumarase, 16: pyruvate dehydrogenase, 17: acetate:succinate CoA transferase, 18: succinyl-CoA synthase, 19: acetyl-CoA thioesterase, 20: L-threonine dehydrogenase, 21: 2-amino-3-ketobutyrate CoA-transferase, 22: NADH dehydrogenase, 23: NADH dehydrogenase, 24: Ubiquinone, 25: trypanosome alternative oxidase, 26: ATP synthase, 27: FAD-dependent glycerol-3-phosphate dehydrogenase

Metabolism and differentiation of procyclic forms

Once the short stumpy forms are taken up by the tsetse fly during the blood meal, the parasites differentiate into procyclic cells (PCF stage). Procyclics have a fully active mitochondrion and can utilize different carbon sources. Glucose and glycerol both feed the glycolytic pathway, which is localized within a specialized compartment, the glycosome. In contrast to BSF, they can additionally utilize amino acids for energy generation by the TCA cycle and oxidative phosphorylation (Allmann et al., 2021; Smith et al., 2017; Wargnies et al., 2018) (Figure 3). Proline is a highly available amino acid and

used by the tsetse fly for fueling the flight muscles (Balogun, 1974; Bursell, 1963). For procyclic *T. brucei* proline is essential *in vitro* in the absence of glucose (Mantilla et al., 2017). However, glucose is preferentially metabolized if available (Lamour et al.,

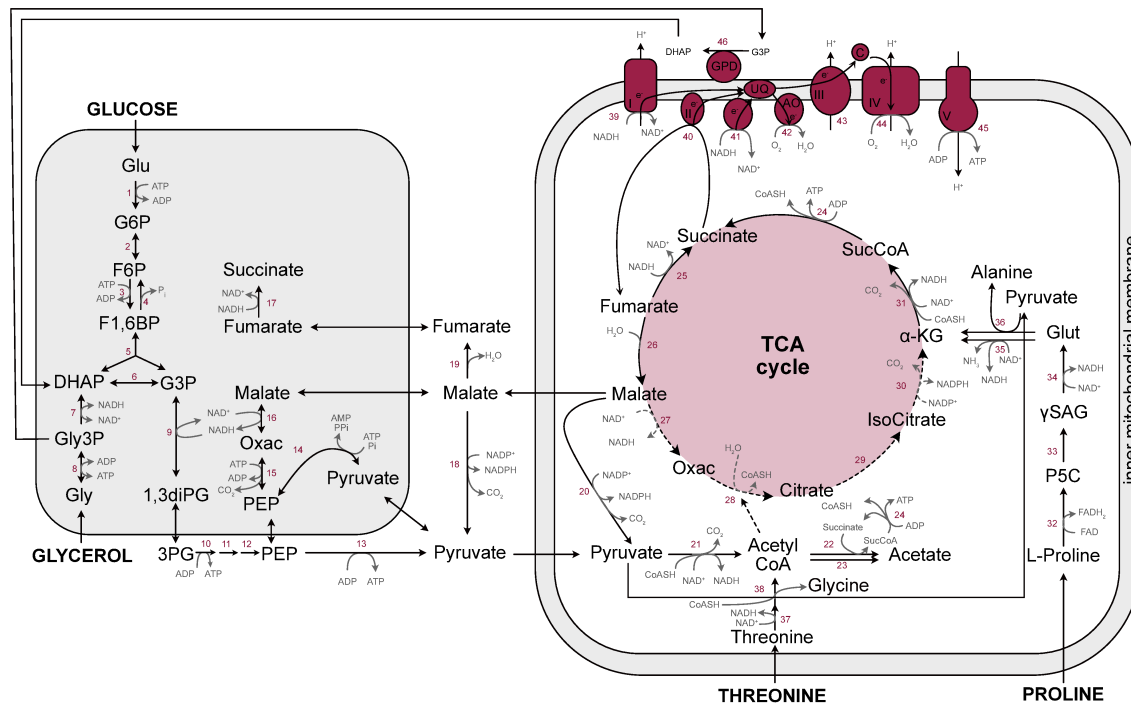


Figure 3: Energy generation in PCF *T. brucei*. Glucose and glycerol feed the glycolytic pathways in the glycosome to generate pyruvate. This is further broken down into acetate or can enter the TCA cycle. Proline is broken down to glutamate and α -ketoglutarate, which enters the TCA cycle. The respiratory chain is fully active. Based on (Michels *et al.*, 2021; Wargnies *et al.*, 2018). Enzymes: 1: hexokinase, 2: glucose-6-phosphate-isomerase, 3: phosphofructokinase, 4: pfructose-1,6-bisphosphatase, 5: aldolase, 6: triose-phosphate-isomerase, 7: glycerol-3-phosphate-isomerase, 8: glycerol kinase, 9: glyceraldehyde-3-phosphate dehydrogenase, 10: phosphoglycerate kinase, 11: phosphoglycerate mutase, 12: enolase, 13: pyruvate kinase, 14: pyruvate phosphate dikinase, 15: phosphoenolpyruvate carboxykinase, 16: malate dehydrogenase, 17: fumarate reductase, 18: malic enzyme, 19: fumarase, 20: malic enzyme, 21: pyruvate dehydrogenase complex, 22: acetate:succinate CoAtransferase, 23: acetyl CoA thioesterase, 24: succinyl-CoA synthetase, 25: fumarate reductase, 26: fumarase, 27: malate dehydrogenase, 28: citrate synthase, 29: aconitase, 30: isocitrate dehydrogenase, 31: α -ketoglutarate dehydrogenase, 32: proline dehydrogenase, 33: spontaneous reaction, 34: pyrroline-5-carboxylate dehydrogenase, 35: glutamate dehydrogenase, 36: alanine aminotransferase, 37: threonine dehydrogenase, 38: 2-amino-3-ketobutyrate CoA-transferase, 39: NADH dehydrogenase (complex I), 40: succinate dehydrogenase (complex II), 41: NADH dehydrogenase, 42: Trypanosome alternative oxidase, 43: complex III, 44: complex IV, 45: ATP synthase, 46: FAD-dependent glycerol-3-phosphate dehydrogenase, UQ: ubiquinone pool, C: cytochrome C

2005). Within the tsetse fly, trypanosomes pass a variety of different tissues and undergo multiple stages of differentiation (Figure 4). After the blood meal, the parasites are transported to the crop, where they are exposed to dehydration stress (Bastin, 2019). Later, the contents of the crop are transported to the midgut. Here, the trypanosomes are facing an environment that is characterized by an alkaline pH (Weiss *et al.*, 2019) and the presence of digestive enzymes. The nutrients from the blood meal are used up not only by the parasites, but also by the tsetse fly itself. Therefore, glucose, the main carbon source in BSF forms, is eliminated within a short period of time (reviewed in (Smith *et al.*, 2017)) and the trypanosomes need to make use of their

extended metabolic network. Additionally, the tsetse fly midgut harbors several microbial endosymbionts, which can have an influence on the environment and vary between individual flies (Griffith et al., 2018). After arrival in the midgut, the parasites differentiate into procyclic forms. The differentiation takes place in the posterior midgut and eventually the procyclics migrate to the proventriculus. In the proventriculus, they can pass the newly synthesized peritrophic matrix to enter the ectoperitrophic space or differentiate into epimastigote forms (Rose et al., 2020; Rotureau and Van Den Abbeele, 2013). The peritrophic matrix is composed of chitin, which is a polymer of N-acetyl-glucosamine (GlcNAc). This sugar blocks glucose transporters of *T. brucei* (Ebikeme et al., 2008), meaning that even if glucose was available here, the parasites might not be able to import it. From the proventriculus, the parasites migrate towards the salivary glands, where they attach to the epithelial cells via the flagellum (Rotureau et al., 2012; Tetley and Vickerman, 1985). After attachment, they finally give rise to metacyclics that are primed for transmission.

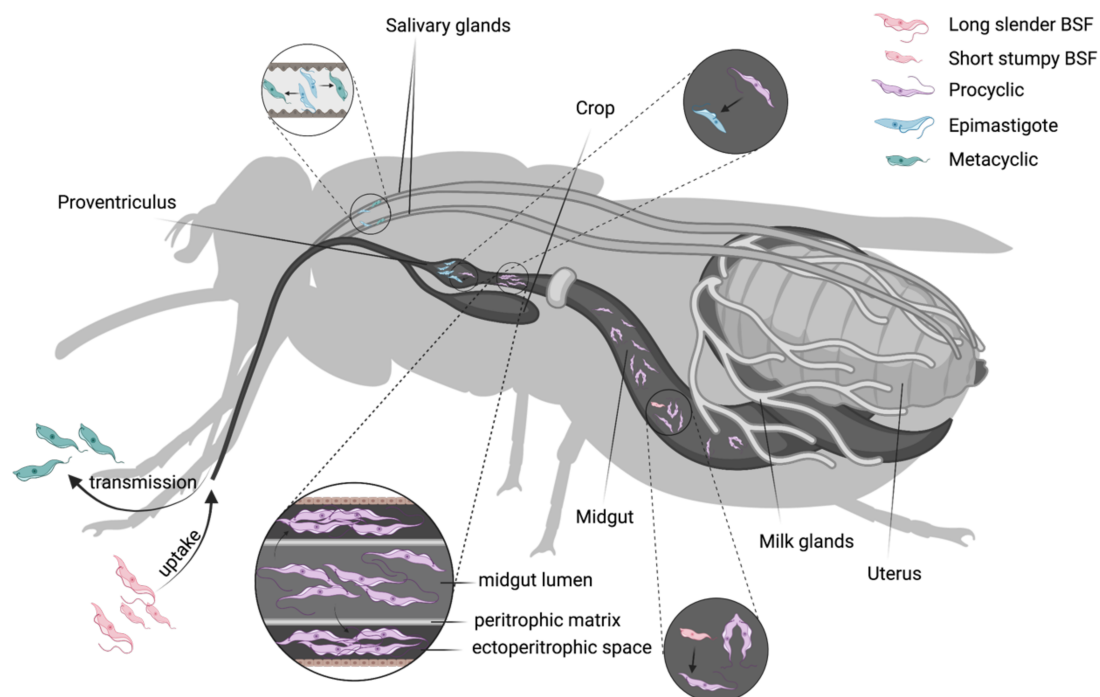


Figure 4: Trypanosome migration through the tsetse fly. Short stumpy cells are taken up during the bloodmeal and transported to the midgut. Here they differentiate into procyclics and migrate towards the proventriculus where they differentiate into epimastigotes. Here, they cross the peritrophic matrix and proceed to the salivary glands. After attachment to the salivary gland epithelium, they differentiate into metacyclics and are finally transmitted to the next mammalian host. Figure generated with BioRender.com.

1.1.2 Glycosomes: specialized compartments

Glycosomes are specialized peroxisomes found in kinetoplastids. These compartments are extremely important in metabolic adaptation and heavily remodeled during differentiation from BSF to PCF (Herman et al., 2008; Vertommen et al., 2008). The

first six (PCF)/seven (BSF) enzymes of glycolysis are located within this organelle (Gualdron-Lopez et al., 2013a) and constitute up to 95% of all protein content (Misset et al., 1986) in BSF, hence the name glycosome. In PCF cells, the first six enzymes compose up to 50% of all protein content (Hart et al., 1984). In higher eukaryotes, the glycolytic pathway is localized within the cytosol. Proper localization of these enzymes is extremely important in *Trypanosoma brucei*, especially in BSF which heavily rely on glucose as an energy source due to complete downregulation of mitochondrial energy generation pathways. Proper import of proteins is ensured by the glycosomal import machinery comprised of the so-called PEX proteins. The import machinery is conserved compared to that of peroxisomes. Glycosomal proteins are marked by a peroxisomal targeting signal (PTS). There are two types of PTS, the PTS1 and PTS2. The PTS1 is a C-terminal tripeptide sequence (SLK or a variation thereof (Opperdoes and Szikora, 2006)) that is recognized by the receptor protein PEX5. In contrast, PTS2 is a 9 amino-acid motif located close to the N-terminus: [RK]-[LVI]-X5-[HQ]-[LA] (Opperdoes and Szikora, 2006) which is recognized by the receptor PEX7. After binding of the cargo, the receptor proteins interact with a docking/translocation complex in the glycosomal membrane. The docking/translocation complex is comprised of at least two components: PEX13 and PEX14. Depending on the organism studied, further PEX proteins can be involved. The docking occurs via PEX14/PEX5 interaction and is conserved in most eukaryotic organisms (Smith and Aitchison, 2009) and results in the release of the cargo proteins into the glycosomes. PTS2 carrying cargo is hypothesized to interact with the docking/translocation complex via interaction of PEX7 with PEX5 (Gualdron-Lopez et al., 2013a). The PEX5 receptor is finally recycled from the membrane by an ubiquitylation-dependent mechanism (Gualdron-Lopez et al., 2013b) (Figure 5). RNAi-mediated knock-down of PEX14 is lethal in BSF and PCF when glucose is present in the medium (Furuya et al., 2002; Haanstra et al., 2008; Kessler and Parsons, 2005). This effect can be explained by the lack of feedback regulation in kinetoplastid glycolysis. The first two steps of glycolysis (hexokinase and phosphofructokinase) consume ATP, which is later recovered and can be utilized to fuel the initial enzymatic reactions (See Figure 2, Figure 3). Similarly, glycerol degradation requires ATP in the first reaction by glycerol-kinase. Most eukaryotic systems have feedback regulation mechanisms to avoid extremely high activities of these ATP-consuming enzymes and the resulting ATP-depletion (Aleshin et al., 1998; Locasale, 2018). Trypanosomes lack these regulations but use compartmentalization instead. Glycosomal ATP-consuming and ATP-producing reactions are in equilibrium. This equilibrium is disturbed when glycolytic enzymes are mislocalized to the cytoplasm and cause a severe ATP-depletion. In PCF, the effects are less pronounced when the

parasites are cultured in a medium devoid of glycolytic carbon sources (Haanstra *et al.*, 2008).

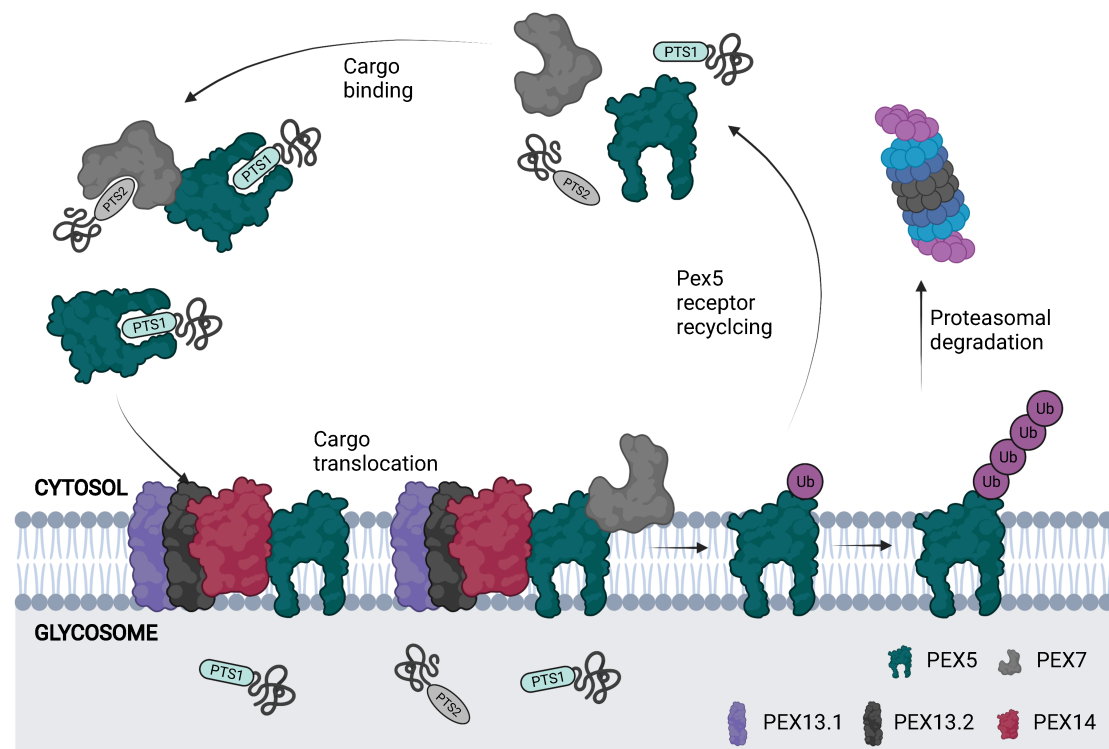


Figure 5: Simplified model of glycosomal protein import in *T. brucei*. Glycosomal proteins are recognized by their PTS1 and PTS2 signals by PEX5 and PEX7, respectively. The receptors bind to the docking complex composed of PEX13.1, PEX13.2 and PEX14, after which the cargo is released into the glycosome. PEX5 is subsequently ubiquitinated and either recycled or degraded in the proteasome. Figure was created with BioRender.com.

Even though enzymes of carbon source metabolism compose most of the protein content in glycosomes, there are more pathways which localize to this compartment. The oxidative branch of the pentose-phosphate pathway takes place in glycosomes and is necessary to provide precursors for nucleotide biosynthesis (Duffieux *et al.*, 2000; Heise and Opperdoes, 1999). Additionally, enzymes of nucleoside metabolism are localized to the glycosomes as well, like some enzymes of the pyrimidine biosynthetic pathway or purine salvage. Purine salvage is essential to the parasites since they cannot synthesize the purine ring *de novo* (el Kouni, 2003).

Glycosomes also appear to be involved in lipid metabolism. Some genes of the ether lipid biosynthetic pathway were found in this organelle (Opperdoes, 1984; Zomer *et al.*, 1999; Zomer *et al.*, 1995). Two enzymes (enoyl-CoA hydratase and 3-hydroxyacyl-CoA dehydrogenase) of β -oxidation are reported (Hart *et al.*, 1984; Wiemer *et al.*, 1996), but no metabolic activity could be attributed to the two annotated genes that encode these enzymes (Allmann *et al.*, 2014).

In other eukaryotes, the main function of peroxisomes is the detoxification of hydrogen peroxide by catalase. In kinetoplastids, this enzyme is missing. However, they do have

mechanisms to fight reactive oxygen species by a modified glutathione, called trypanothione and parts of the trypanothione detoxification system are localized in glycosomes (Müller et al., 2003).

1.2 Nutrient sensing by protein kinases

Nutrients are essential for growth and development of all living organisms. However, they are not always available in unlimited amounts. Therefore, changing levels need to be sensed in order to cope with fluctuations. A number of kinases have been demonstrated to be involved in nutrient sensing and regulation of downstream metabolic processes. Prokaryotes for example use the two-component systems for transformation of extracellular information into an intracellular response. The first step (component) of this system is a membrane-bound histidine kinase that phosphorylates a response-regulator in response to a specific stimulus. This usually results in a change of gene expression to cope with the newly sensed environmental conditions (Mascher et al., 2006).

In eukaryotes, nutrient sensing pathways involve multimeric kinase complexes. AMP-activated protein kinase (AMPK) is a heterotrimeric Ser/Thr kinase that acts as a cellular energy sensor (Davies et al., 1994; Ross et al., 2016). Kinase activity is regulated by the AMP to ATP ratio (Corton et al., 1994). When AMP concentrations are elevated, the molecule allosterically activates AMPK by causing a conformational change, rendering the Thr172 in the activation loop accessible for phosphorylation by other kinases (Carling et al., 1987). Phosphorylation of this threonine residue is crucial for AMPK activity (Hawley et al., 1996; Stein et al., 2000). Upon activation, AMPK can phosphorylate substrates involved in catabolic processes and thereby activate them, which results in increased ATP synthesis. Additionally, the kinase inactivates proteins involved in anabolic processes by phosphorylation (reviewed in (Garcia and Shaw, 2017)). Physiologically, AMPK was shown to be activated in response to glucose starvation in pancreatic beta cells, which results in an ATP-deficit (Salt et al., 1998). Alternatively, AMPK activity can be regulated by nucleotide-independent mechanisms. The phosphorylation of Thr172 can be catalyzed by CAAMK in response to elevated Ca^{2+} levels (Hawley et al., 2005; Hurley et al., 2005; Woods et al., 2005). Moreover, phosphorylation of the C-terminus of AMPK α subunit by Protein kinase A (PKA) was shown to inhibit its activity (Heathcote et al., 2016; Horman et al., 2006; Hurley et al., 2006).

Another kinase involved in metabolic sensing, is the Ser/Thr kinase mTOR, which was shown to participate in the regulation of cell growth in response to nutrient availability (reviewed in (Saxton and Sabatini, 2017)). This kinase is part of the mTOR complex 1 (mTORC1) and mTOR complex 2 (mTORC2). In the context of metabolic sensing and

adaptation, mTORC1 is more relevant, while mTORC2 mainly focuses on regulation of cell proliferation. In the mammalian system mTORC1 predominantly promotes anabolic processes, like protein synthesis (Holz et al., 2005), de novo lipid synthesis (Porstmann et al., 2008) and nucleotide synthesis (Ben-Sahra et al., 2013; Robitaille et al., 2013), mainly by phosphorylation of transcription factors, which subsequently alter gene expression (reviewed in (Ma and Blenis, 2009)). Activity of mTORC1 also increases translation of the transcription factor HF1 α , which upregulates enzymes of the glycolytic pathway (Duvet et al., 2010). These anabolic processes are only promoted during growth permissive phases, which lead to mTORC1 activation by growth factors (reviewed in (Kim et al., 2013)). In contrast to that, the kinase is inhibited by intracellular and environmental stresses, like low energy or nutrient levels and oxidative stress. One of the upstream acting components in this case, is AMPK. It can sense low energy levels and is activated by AMP/ADP (Corton *et al.*, 1994). AMPK can then directly inhibit mTORC1 (Gwinn et al., 2008; Inoki et al., 2003; Shaw et al., 2004).

This example shows that these pathways are often interconnected. The signaling network is very well described in the baker yeast *Saccharomyces cerevisiae*. This organism prefers glucose as the primary carbon source but can also survive on non-fermentable carbon sources. A complex of AMPK (Snf1 in yeast) and the protein phosphatase PP1 (in yeast termed Reg1/Glc7 \rightarrow regulatory and catalytic subunits) regulates nuclear and cytoplasmic localization of the zinc-finger protein Mig1. At high glucose levels, Mig1 localizes to the nucleus and represses expression of genes involved in aerobic respiration, gluconeogenesis as well as transporters of non-fermentable carbon sources (De Vit et al., 1997; Treitel and Carlson, 1995). When glucose levels drop, Snf1 is activated by phosphorylation of Thr210 in the activation loop (McCartney and Schmidt, 2001) and can subsequently phosphorylate Mig1 on multiple sites (DeVit and Johnston, 1999; Ostling and Ronne, 1998; Treitel et al., 1998). This phosphorylation results in cytoplasmic localization and induction of the repressed genes (De Vit *et al.*, 1997). Glc7 acts antagonistically to Snf1 and presumably promotes Mig1 nuclear localization by dephosphorylation and hence inhibition of Snf1 (Sanz et al., 2000). In addition to that, AMPK represses TORC1, leading to downregulation of protein synthesis at nutrient-restrictive times (reviewed in (Saxton and Sabatini, 2017)). TORC1 acts in parallel with Protein kinase A (PKA) to regulate expression of ribosomes and genes involved in protein synthesis to determine the growth rate in response to nutrient availability (Kunkel et al., 2019). While TORC1 appears to set expression levels for steady-state growth conditions, PKA is responsible for boosts during times of transition (Kunkel *et al.*, 2019). When glucose becomes available after periods of starvation, cAMP levels transiently increase (Kraakman et al., 1999; van der Plaats, 1974) and lead

to PKA activation. This triggers a downstream response that favors protein synthesis (Lippman and Broach, 2009; Zurita-Martinez and Cardenas, 2005).

1.3 Protein kinase A (PKA)

1.3.1 The PKA signaling pathway

1.3.1.1 PKA activation mechanism

Protein kinase A is one of the best studied kinases since its discovery by (Walsh et al., 1968) and conserved from single cellular organisms to primates. PKA has been extensively studied in the past three decades (reviewed in (Taylor et al., 2021)) and by now serves as a prototype for AGC protein kinases. It is composed of a regulatory (R) and a catalytic (C) subunit and most organisms encode multiple isoforms of each. In higher eukaryotes, the regulatory subunit dimerizes via the dimerization/docking (D/D) domain and each of these regulatory subunits binds one catalytic subunit to yield a heterotetrametric holoenzyme (R_2C_2). In the holoenzyme conformation, the kinase is inactive. The PKA catalytic subunit (PKAC) is usually trapped in the R_2C_2 holoenzyme in a fully active conformation. Two phosphorylation sites are crucial for this activity, Thr197 in the activation loop and S338 on the C-terminal tail. The activation loop is a conserved structure amongst AGC kinases and phosphorylation of Thr197 is crucial for kinase activity and stability (Taylor et al., 2012b). During recombinant expression in *E. coli* Thr197 phosphorylation of PKAC is an autophosphorylation event (Shoji et al., 1979; Steinberg et al., 1993; Yonemoto et al., 1993). *In vivo*, PDK1 typically catalyzes the activation loop phosphorylation of AGC kinases after PDK1 interaction with the AGC kinase C-terminal tail. In the context of PKA, it was demonstrated that phosphorylation of S338 on the C-terminal tail is required for this interaction (Romano et al., 2009). To dissociate the PKA holoenzyme and release the catalytic subunits, binding of cyclic adenosine monophosphate (cAMP) to the regulatory subunit is required. Each regulatory subunit possesses two cyclic nucleotide binding domains (CNBs), which need to bind cAMP for PKA activation. Upon increasing concentrations, this molecule binds to the CNBs and causes a series of conformational changes that lead to R-C dissociation and downstream phosphorylation of PKA substrates (Taylor et al., 2008). The increase of cAMP levels is usually triggered by a cascade starting at the activation of G-protein coupled receptors (GPCR), which trigger the activation of an adenylate cyclase (AC) and result in cAMP synthesis. After PKA is activated, the signal is terminated again by cAMP degradation via phosphodiesterases (PDE). Together these components constitute the canonical cAMP/PKA signaling pathway (Figure 6A). In kinetoplastids, like *T. brucei* we observe some deviations from this well-conserved

pathway. First, the *T. brucei* genome does not encode for any GPCRs, except for the unconventional GPR89, which is an oligopeptide transporter involved in stumpy formation (Rojas et al., 2019). However, the genome does encode a family of ACs with transmembrane domains. It was proposed that the ACs could directly serve as receptors and circumvent the need for specific GPCRs (reviewed in (Salmon, 2018)). Secondly, the holoenzyme in *T. brucei* only consist of a heterodimer of one regulatory and one catalytic subunit (Bachmaier et al., 2019; Bubis et al., 2018). The heterodimeric structure is also conserved in some other species like, *Dictyostelium*, *Amphipidinium* and *Plasmodium* (Bandje et al., 2016; Haste et al., 2012; Leighfield et al., 2002; Mutzel et al., 1987). More importantly, the *T. brucei* PKA regulatory subunit (PKAR) does not respond to cAMP (Bachmaier, 2008; 2015; Kramer, 2004; Schulte zu Sodingen, 2000; Shalaby et al., 2001). Differences in the CNB caused a shift from cAMP to nucleoside

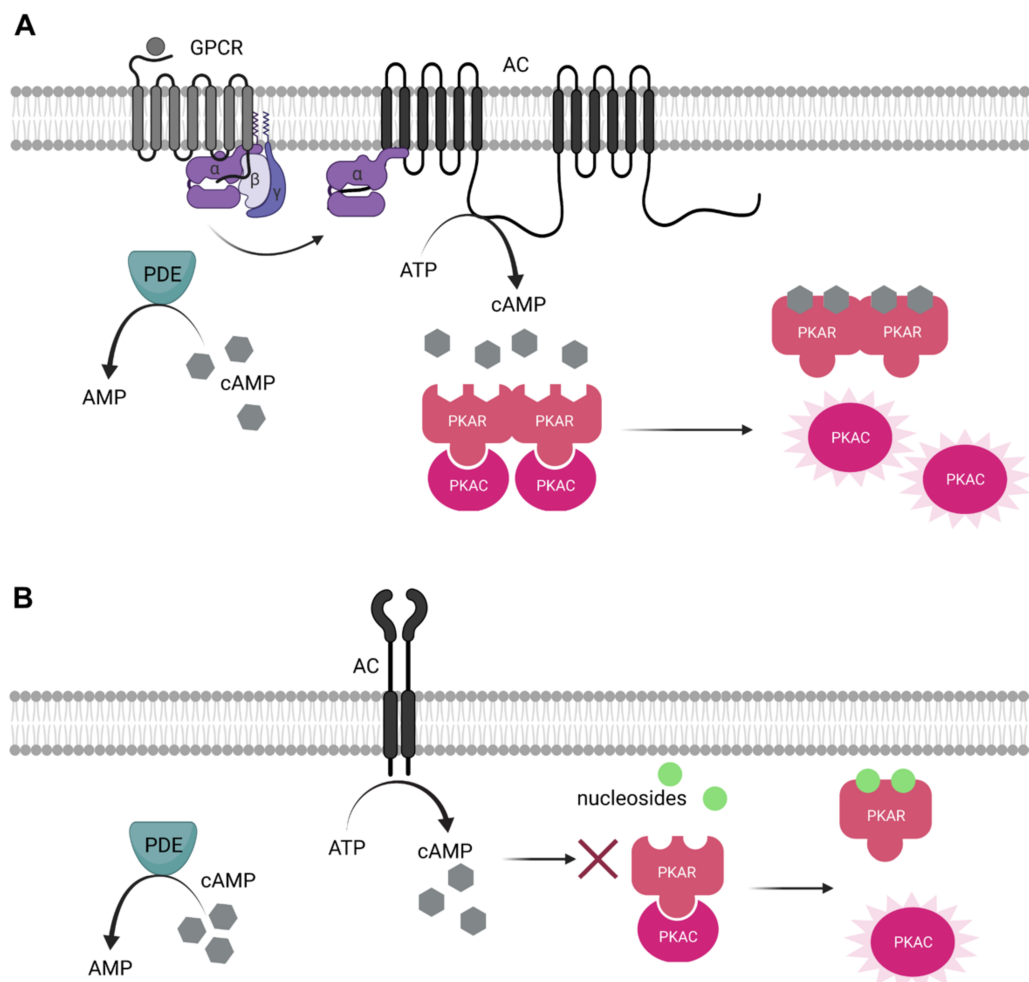


Figure 6: PKA signaling pathways. A: In the mammalian system, adenylate cyclases (AC) are stimulated by the $G\alpha$ -subunit of a heterotrimeric G-protein coupled to a G-protein coupled receptor (GPCR). The AC synthesizes cAMP from ATP, which can bind to the heterotetrameric PKA complex, leading to R-C dissociation. The signal is terminated by cAMP degradation by phosphodiesterases (PDE). **B:** *T. brucei* lacks GPCRs but expresses ACs and PDEs. Even though cAMP signaling is important in *T. brucei*, it is decoupled from PKA. The PKAR subunit does not bind cAMP, but nucleosides. Figure was created with Bio-Render.com.

binding (Bachmaier *et al.*, 2019; Githure, 2014) (Figure 6B). The changes in the CNB pockets were also identified in other kinetoplastid species and binding of nucleosides to PKAR subunits of *T. cruzi* and *Leishmania donovani* could be demonstrated *in vitro* (Ober, 2021). The binding of nucleosides and analogs was shown to trigger dissociation and phosphorylation of downstream substrates at a nanomolar range (Bachmaier *et al.*, 2019; Wu, 2021). This indicates a decoupling of cAMP and PKA pathways in kinetoplastids. Upstream regulatory elements of this pathway have not yet been identified and it is unclear how PKA activation by nucleosides is regulated *in vivo*.

1.3.1.2 How is subunit specificity conferred?

The genomes of most organisms encode for multiple subunits of PKAR and PKAC and in most organisms PKA has pleiotropic functions (Peng *et al.*, 2015; Shabb, 2001). Under the assumption that specific subunits/holoenzymes have specific functions, there is a need for mechanisms to ensure that the correct subunits are activated in the correct place and time to trigger the desired downstream response. Spatial and temporal regulation is often achieved by compartmentalization through A kinase anchoring proteins (AKAPs) (reviewed in (Calejo and Tasken, 2015)). These proteins interact with the PKAR subunits via the N-terminal dimerization/docking (DD) domain (reviewed in (Taylor *et al.*, 2012a)) and target PKA to a specific site of action. This can be either a specific compartment, membrane, or cellular structure (reviewed in (Calejo and Tasken, 2015)). There are different classes of AKAPs in the mammalian system, forming interactions with either one of the two regulatory subunits or both (reviewed in (Welch *et al.*, 2010)). This means the holoenzyme specificity is conferred via the regulatory subunit. The *T. brucei* genome only encodes one regulatory subunit and there are no canonical AKAPs either. In *Saccharomyces cerevisiae*, the situation is quite similar. The genome encodes for one regulatory subunit (Bcy1) and three catalytic isoforms (Tpk1, Tpk2, Tpk3) (Toda *et al.*, 1987). Here, the localization of the different subunits is dynamic and responds to environmental fluctuations, like glucose starvation or heat (Griffioen *et al.*, 2000; Tudisca *et al.*, 2010). The regulatory subunit Bcy1 was demonstrated to form protein interactions which are important for subcellular localization (Galello *et al.*, 2014; Griffioen *et al.*, 2001). Interaction of Bcy1 with Zds1 leads to enhanced cytoplasmic localization, a downstream effect of glucose-starvation. The interaction with Zds1 can be enhanced via phosphorylation of serine clusters in the N-terminus of Bcy1 (Galello *et al.*, 2014). Other interaction partners were shown to tether Bcy1 to the mitochondria or the Ras complex (Galello *et al.*, 2014).

Recent findings indicate the presence of catalytic kinase anchoring proteins (C-KAPs) as well, which are described as proteins binding to the catalytic PKA subunits. These proteins include substrates and pseudosubstrates and can influence localization and activity of the kinase (reviewed in (Soberg and Skalhegg, 2018)). In most reports, the interaction sites of PKAC with the C-KAPs are not mapped. One exception is the interaction of mammalian PKAC α 1 with AKIP1. Here, interaction takes place on the N-terminal residues 15-30 (Sastri *et al.*, 2005). In general, most interactions of the PKA catalytic subunits are mediated through the N- and C-termini, which are also the most variable regions of the protein (Kannan *et al.*, 2007; Sastri *et al.*, 2005). The C-terminal tail is a conserved structure in AGC kinases in general and is usually phosphorylated on several sites. Structural analyses have shown that the C-tail of AGC kinases interacts with the catalytic core and influences kinase activity (Kannan *et al.*, 2007). Therefore, subunit-specific phosphorylations in this region could influence the activity and confer specificity. On the N-terminus, post translational modifications (PTMs) seem to influence localization, activity, and interactions (Tholey *et al.*, 2001). The N-terminus of mammalian PKAC is usually disordered and becomes ordered upon myristoylation of Gly1. Some splice variants lack this myristoylation site, which was hypothesized to alter activity and localization (Breitenlechner *et al.*, 2004; Cembran *et al.*, 2012; Zheng *et al.*, 1993). PTMs on the N-terminus of yeast Tpk2 were shown to affect nuclear and cytoplasmic localization (Haesendonckx *et al.*, 2012; Solari *et al.*, 2014). On Tpk2, the catalytic domain and intrinsically disordered regions play a role in the localization to cytoplasmic foci and a prion-like domain on the N-terminus is responsible for localization (Barraza *et al.*, 2017; Barraza *et al.*, 2021; Tudisca *et al.*, 2012). In *T. brucei* PKA, the catalytic cores are conserved, and the major differences between the three isoforms lie on the termini. The N-terminal myristoylation sites known from mammalian PKA are missing, but there are many phosphorylation sites, especially on PKAC1, which could contribute to subunit-specific features.

1.3.1.3 PKA subunits in *T. brucei*

The *T. brucei* genome encodes one regulatory PKA subunit (PKAR (Schulte zu Sodingen, 2000)) and three catalytic isoforms (PKAC1/2/3 (Bachmaier and Boshart, 2013; Klöckner, 1996)). All catalytic isoforms have been shown to interact with PKAR in immunoprecipitation experiments (Bachmaier *et al.*, 2019; Kramer, 2004). Expression of the PKA subunits is partially developmentally regulated. PKAR is expressed in BSF and approximately twofold downregulated in PCF (Bachmaier, 2015; Schulte zu Sodingen, 2000). PKAC1 is exclusively expressed in BSF, while PKAC2 is predominant in the procyclic stage. Interestingly, these two subunits share over 90% sequence

identity and cannot be distinguished by an antibody generated against PKAC1. Therefore, they are often referred to as PKAC1/2. The differences between these two subunits are located mainly on the extreme N- and C-terminus (Bachmaier and Boshart, 2013). PKAC3 shares only approximately 55% sequence homology with PKAC1/2 and is expressed throughout the *T. brucei* life cycle (Bachmaier, 2015; Kramer, 2004). All *T. brucei* PKA subunits have been shown to localize preferentially to the flagellum ((Krumbholz, 2006), tryptag.org). The N-terminus of PKAR is significantly longer than the mammalian orthologues (Schulte zu Sodingen, 2000), which is a kinetoplastid specific feature. By a series of truncations, it was shown that the N-terminus was necessary and sufficient to target the kinase to the flagellum, where it interacts with the paraflagellar rod (PFR), a structural component of the flagellum (Krumbholz, 2006). This localization might also explain the altered motility observed in PKAR RNAi and knockout lines (Krumbholz, 2006) in BSF. This motility defect was also observed after depletion of PKAC1/2 by RNAi. Reverse genetic analyses in BSF cells showed that RNAi against PKAR is lethal (Bachmaier, 2015; Kramer, 2004). However, it was possible to generate a PKAR null mutant that only shows a mild growth phenotype (Bachmaier, 2015; Pepperl, 2007). A possible explanation for this discrepancy could be the difference in kinetics. RNAi leads to rapid gene depletion. In contrast, the knockout was generated by depletion of one allele first, which might lead to adaptation processes that allow survival after removal of the second allele. Further, the PKAR knockout initially showed a slender to stumpy differentiation phenotype, which was lost shortly after successful cell line generation (Bachmaier, personal communication), indicating quick adaptation processes. In BSF, the absence of PKAR leads to the downregulation of PKAC1/2, while levels of PKAC3 remain unchanged (Bachmaier, 2015; Pepperl, 2007). Attempts to generate a PKAC1 knockout were not successful and RNAi-mediated knock-down led to severe growth phenotypes (Bachmaier, 2015; Kramer, 2004). RNAi mediated knock-down of PKAC1/2 in BSF resulted in a mild differentiation phenotype from stumpy to PCF (Bachmaier, 2015). A comprehensive RNAi and knockout series of all PKA subunits by (Kramer, 2004) showed a failure in the last step of cytokinesis. These observed phenotypes of motility and cytokinesis are perfectly in line with the flagellar localization of PKA. The flagellum is essential for cellular motility, as shown by knock-down of structural components (Bastin et al., 1998). Additionally, in BSF impaired motility results in a cytokinesis phenotype that is characterized by the failure of cell segregation in the final step of cytokinesis, which is lethal in BSF (Broadhead et al., 2006; Ralston et al., 2006). This is exactly the same phenotype we observe for PKA genetic disruption. Based on this, we hypothesize that the cytokinesis phenotype is a consequence of the impaired motility in BSF trypanosomes. This

hypothesis is supported by the less severe phenotypes observed in strains that are cultured in a viscous matrix of methylcellulose. Here, wild type trypanosomes exhibit a directional swimming behavior that is enabled by the physical properties and the resistance provided by the matrix. A full list of all PKA phenotypes can be found in Table 1. In summary, PKA is involved in cell motility and cytokinesis in the BSF stage. Depletion of PKAR and PKAC1 is not well tolerated and causes growth phenotypes. The only available knockouts in PCF are Δ PKAR and Δ PKAC3, which have no obvious phenotypes. Knockout of PKAC3 in PCF only caused a mild growth phenotype which was lost after prolonged time in culture. There was no effect on expression of any other PKA subunits or on cytokinesis (Schulte zu Sodingen, 2000).

Several environmental activation cues have been identified for PKA in BSF, which result in downstream phosphorylation of a PKA reporter substrate (Kramer, 2004). The most prominent one was activation by low temperatures, termed *cold shock*. Further investigations showed that cold shock activation was dependent on PKAR and PKAC1 (Bachmaier, 2008; 2015; Pepperl, 2007). Other environmental conditions that increased substrate phosphorylation were hypotonic conditions and mild acidic pH (Kramer 2004). Both of these triggers were independent of PKAR and appeared to work via PKAC3 (Bachmaier, 2008; Malenica, 2016). The effects were abolished by inclusion of the PKA-specific inhibitor peptide PKI (Cheng et al., 1986), indicating that the effects were dependent on PKA. So far, all known PKA activators, including nucleoside analogs and environmental stimuli, have only increased detectable substrate phosphorylation in the bloodstream form stage. PKAC1/2-specific triggers (nucleosides and cold shock) have no effect in the procyclic stage (Bachmaier, 2015). Effects of pH fluctuations and changes in osmolarity were not investigated in much detail. In fact, up to now, no PKA activators have been identified in PCF that cause downstream substrate phosphorylation.

Table 1: Summary of PKA phenotypes observed in reverse genetic experiments in BSF.

Subunit	Reference	<i>T. brucei</i> strain	Gene manipulation	Phenotype
PKAR	(Krumbholz, 2006)	MITat 1.2	$\Delta pkar/\Delta pkar$	Motility: old and new flagellum not beating in parallel → tumbling instead of swimming
	Bachmaier, pers. communication	AnTat 1.1 Munich (cultured in matrix)	$\Delta pkar/\Delta pkar$	Motility: same as in MITat 1.2 Growth: increase in PDT Cytokinesis: not observed Differentiation: impaired SS/PCF differentiation, no PAD1 marker expression → phenotype lost after prolonged culturing
	(Schulte zu Sodingen, 2000)	MITat 1.2	PKAR overexpression (pLEW82 vector, very mild OE)	Growth: increase in PDT
	(Schulte zu Sodingen, 2000)	Antat 1.1 (cultured in matrix)	PKAR overexpression (pHD547 vector, very mild OE)	No growth phenotype
	(Kramer, 2004)	MITat 1.2	RNAi (p2T7TA Blue vector, 90% knock-down efficiency)	Growth arrest, downregulation of PKAC1/2 to 10%, downregulation of PKAC3 to 50% Cytokinesis: accumulation of 2K2N and multinucleated cells*, increase in kinetoplast distance upon RNAi induction
	(Alsford et al., 2011)	MITat 1.2	Genome wide RIT screen	Decreased fitness

PKAC1	(Kramer, 2004)	MITat 1.2	$\Delta pkac1/PKAC1$	Growth: increase in PDT Cytokinesis: accumulation of 2K2N and multinucleated cells*, no effect on kinetoplast distance
	(Kramer, 2004)	MITat 1.2	$\Delta pkac1/\Delta pkac1$	Could not be generated → appeared essential
	(Wu, 2021)	AnTat 1.1 Paris	$\Delta pkac1/\Delta pkac1$ TY-PKAC2 ^{Ti}	Could be obtained when PKAC2 or PKAC1/2 chimeras were tetracycline-inducibly expressed during knockout, termination of expression showed no phenotypes upon tetracycline removal
PKAC2	(Kramer, 2004)	MITat 1.2	$\Delta pkac2/\Delta pkac2$	Growth: increase in PDT, lost after prolonged time in culture Cytokinesis: accumulation of 2K2N and multinucleated cells*, no effect on kinetoplast distance
	This work	AnTat 1.1 90-13	$\Delta pkac2/\Delta pkac2$	Growth: mild increase in PDT, lost when selection antibiotics were omitted Differentiation: elevated PAD1 levels compared to parental line, PAD1 expression detectable in low density slender cultures
PKAC1/2	(Kramer, 2004)	MITat 1.2	RNAi (p2T7TA Blue vector), 80-90% knock-down efficiency	Growth: arrest after 4h, lethal after 2 days Cytokinesis: accumulation of 2K2N and multinucleated cells*, no effect on kinetoplast distance Motility: same phenotype as in $\Delta PKAR$
	(Bachmaier, 2015)	AnTat 1.1 Munich (cultured in matrix)	RNAi (pHD615 vector, >90% efficiency)	Growth: mild increase in PDT Cytokinesis: no cytokinesis phenotype Motility: same phenotype as in $\Delta PKAR$ Differentiation: outgrowth as PCF impaired when differentiation is performed ≤ 0.06 mM CA, PAD1 levels are not altered

	(Alsford <i>et al.</i> , 2011)	MITat 1.2	Genome wide RIT screen	Decreased fitness
	(Jones <i>et al.</i> , 2014)	2T1	Kinome wide RNAi screen	Decreased fitness Cytokinesis: as described by (Kramer, 2004)
PKAC3	(Kramer, 2004)	MITat 1.2	RNAi (p2T7TA Blue vector), 80-90% knock-down efficiency	Growth: increase in PDT No co-regulation of other PKA subunits Cytokinesis: accumulation of 2K2N and multinucleated cells*, postulated function in kinetoplast segregation, but could not be confirmed
	(Rieck, 2001)	MITat 1.2	RNAi (p2T7TA Blue vector)	Accumulation of 1K2N cells with 1 large kinetoplast
	(Schulte zu Sodingen, 2000)	MITat 1.2	PKAC3 OE (pHD615 vector)	Approx. 3x increase in kinase activity No effect on growth Slight downregulation of PKAC1/2 and PKAR
	(Githure, 2014)	MITat 1.2	$\Delta pkac3/\Delta pkac3$	Growth: increase in PDT, lost after prolonged time in culture No other phenotypes were reported (morphology, motility)
*Cytokinesis phenotype: cells that are exclusively connected at the extreme posterior pole were characterized as 2K2N cells and multinucleated				

1.3.1.4 Known and potential functions of PKA in single cellular parasites

In multicellular organisms, PKA has pleiotropic functions, which are often tissue specific. PKA is involved in regulation of gene expression by phosphorylation of transcription factors, like cAMP response element binding proteins (CREBs) (reviewed in (Moody, 2019; Ortega-Prieto and Postic, 2019)). It is also known to regulate metabolism. In hepatocytes, PKA regulates glycolysis and gluconeogenesis by phosphorylation of a carbohydrate response element binding protein and phosphofructokinase amongst other enzymes involved in these pathways (Ortega-Prieto and Postic, 2019; Pilkis et al., 1988). In addition, it promotes glycogen breakdown to glucose-6-phosphate by activation of glycogen phosphorylase via phosphorylase kinase and inhibition of glycogen synthase (Han et al., 2016). Besides carbohydrate metabolism, it regulates lipolysis in adipocytes (reviewed in (London et al., 2020)).

In yeast, PKA is involved in the glucose repression pathway (introduced in 1.2). In parasitic single cellular organisms, PKA was often associated with differentiation. In the pathogen *Giardia lamblia*, inhibition of PKA activity by the PKA-specific inhibitor peptide PKI (Cheng et al., 1986; Scott et al., 1986), resulted in impaired differentiation from the dormant cyst stage to the active trophozoite (Abel et al., 2001). In *Toxoplasma gondii*, TgPKAC3 was shown to be involved in differentiation from replicative tachyzoites to quiescent bradyzoites (Sugi et al., 2016). In *Leishmania donovani*, the phosphorylation level of LdPKAR3 changes during promastigote to amastigote differentiation (Tsigankov et al., 2014; Tsigankov et al., 2013) and is accompanied by a rapid dephosphorylation of RXXS/T substrates, re-phosphorylation only occurs during promastigote maturation (Bachmaier et al., 2016). Moreover, inhibition of LdPKA by PKI reduced macrophage infection rates (Malki-Feldman and Jaffe, 2009). Additionally, the unconventional LdPKAR3-LdPKAC3 holoenzyme was shown to bind the subpellicular microtubules at the cell cortex and is important to maintain elongated cell shape in promastigotes (Fischer Weinberger et al., 2021). Furthermore, starvation conditions, a trigger for metacyclogenesis, were shown to cause upregulation of LdPKAR1, suggesting a function in this process. LdPKAR1 overexpression accelerated autophagy, a process necessary for metacyclogenesis (Bhattacharya et al., 2012). Recently, LdPKAC1 was demonstrated to be involved in the arginine deprivation response pathway (ADR) (Zilberstein and Myler, 2021). Under arginine depletion, a high affinity arginine transporter is upregulated (Darlyuk et al., 2009). The ADR is essential for virulence *in vivo* (Goldman-Pinkovich et al., 2020) and involves LdTOR kinase for regulation (Madan et al., 2021). In *Leishmania mexicana*, LmPKAC1 deletion was not successful, indicating

that it is an essential gene (as in *T. brucei*) and the localization was cell-cycle dependent (Baker et al., 2021). It was further demonstrated that LmPKAC3 is required for survival as amastigotes *in vivo* and *in vitro* (Baker et al., 2021). In plenty of intracellular parasites, PKA is involved in host invasion or egress. The *T. cruzi* TcPKAC was demonstrated to interact with and phosphorylate multiple members of the trans-sliadase superfamily, a group of proteins involved in adherence and invasion of host cells (Bao et al., 2010). In *Plasmodium falciparum*, conditional knockout of PfPKAC1 resulted in reduced growth and a deficiency in host invasion (Wilde et al., 2019). This is mediated by abolishing of phosphorylation of the apical membrane protein 1 (PfAMA1), a crucial event for successful invasion (Leykauf et al., 2010; Prinz et al., 2016). In *Toxoplasma gondii*, TgPKAC1 is involved in the regulation of host cell egress together with Protein kinase G (Jia et al., 2017; Uboldi et al., 2018).

1.4 Aims of the thesis

The main topic of this thesis is the identification of downstream functions of PKA in procyclic *T. brucei*. A special focus is put on the regulation of metabolism and nutrient sensing. One of the catalytic subunits (PKAC2) was reported in the high confidence glycosomal proteome (Guther et al., 2014). This observation led us to hypothesize that TbPKA might play a role in carbohydrate metabolism, as was shown in yeast or mammalian hepatocytes (see chapter 1.2, 1.3.1.4). Responding to changes in nutrient availability is mainly important during differentiation from bloodstream form to procyclic cells and in the PCF stage where a variety of carbon sources can be used for energy generation (depicted in Figure 3). Further, (Guevara et al., 2019) recently reported that glucose-deprivation activates PKA in *Trypanosoma equiperdum*, a closely related species, thus strengthening our hypothesis.

Besides investigating the suspected role in metabolism, we also used unbiased approaches to search for downstream targets and substrates of the kinase and potentially propose some functions of TbPKA. For this purpose, we employed BioID for the identification of proteins interacting with the different subunits in BSF and PCF. By including all subunits expressed in the respective life cycle stage as bait proteins we were hoping to further address the question of redundancy amongst the catalytic subunits. Why are there three isoforms? Do they have specialized functions? Will we observe a big overlap in BioID interactomes or subunit-specific sets of proteins? Can we draw conclusions from these datasets in terms of functions? Moreover, a special focus was set on the comparison of PKAC1 and PKAC2, two subunits sharing extremely high degrees of homology, yet a life-cycle-dependent expression profile.

2 MATERIALS AND METHODS

2.1 Materials

2.1.1 Oligonucleotides

Oligo ID	Name	Sequence	Gene	Origin
KM001	BamHI_PKAC1_f	TGGTAGGATCCATGAC-GACAACCTCCCACTGGT	PKAC1	This thesis
-	PKAC1 rev NotI	ACTATGCAA-TAGTTTAGCGGCCGCCTAAAAACCA CGGAATGCAAC	PKAC1	G. Githure
KM002	BamHI_PKAC3_f	TGGTAGGATCCATGAAGTCG-GATGGGTGCCT	PKAC3	S. Kramer
-	PKAC3 rev NotI	ACTATGCAA-TAGTTTAGCGGCCGCCTAAAAACCAC-GGAATGCAAC	PKAC3	G. Githure
KM018	BamHI-PKAC2_fwd	TGGTAGGATCCATGCCTGTAGCCAC-GTCGACG	PKAC2	This thesis
KM019	PKAC2-NotI_rev	GAAGATGCGGCCGCCTAAAACCCAC-GGAACCTCAATTGT	PKAC2	This thesis
KM073	NcoI-PKAC3_fwd	GGTGTCCATGGTGAAGTCG-GATGGGTGC	PKAC3	This thesis
KM124	XbaI-pETM11-SUMO-C3_fwd	TCCTTTCTAGAAATAATTTTGAT-TTAACTTTAAGAAGGAGATATAC-CATGAAGTCGGATGGGTGCCT	PKAC3	This thesis
KM009	BsaI(XbaI)-GS-PKAC1_f	AGCGCAGAGAA-GCTCGAGGGTCTCTCTAGAG-GATCAGGATCTGGATCAGGATCGGG-TAGTATGACGACAACTCCCAC	PKAC1	This thesis
-	PKAC1-BamHI.l.	CTAAGGATCCCTAAAACCCAC-GGAATGC	PKAC1	S. Kramer
KM013	BsaI(XbaI)-GS-PKAC2_f	AGCGCAGAGAA-GCTCGAGGGTCTCTCTAGAG-GATCAGGATCTGGATCAGGATCGGG-TAGTATGCCTGTAGCCACGTCG	PKAC2	This thesis
KM014	PKAC2-BamHI_r	TCTAACGGATCCCTAAAACCCAC-GGAACCTCAA	PKAC2	This thesis
KM005	XbaI-GS-PKAC3_f	AGCGCAGAGAAGCTCGAGTCTAGAG-GATCAGGATCTGGATCAGGATCGGG-TAGTATGAAGTCGGATGGGTGC	PKAC3	This thesis
-	PKAC3-BamHI.l.	CTGGGGATCCTCAGATCCTCGTG-TATTC	PKAC3	S. Kramer
KM125	SpeI-BLE_fwd	GTCTCCACTAGTgATGGCCAAGTT-GACCAGT	phleomycin resistance gene	This thesis
KM129	BLE-StuI_rev	GTTGGTAGGCCTTCAG-TCCTGCTCCTCGG	phleomycin resistance gene	This thesis
KM127	SpeI-BSD_fwd	CTTCTTACTAGTgATGGCCAA-GCCTTTGTCT	blasticidin-S-deaminase	This thesis
KM130	BSD-StuI_rev	GGTT-GTAGGCCTTTAGCCCTCCCACACATA	blasticidin-S-deaminase	This thesis
KM169	SpeI-puro_fwd	GTGTCCACTAGTATGACCGAGTACAA-GCCCAC	puromycin-N-acetyltransferase	This thesis

KM170	puro_rev	TCAGGCACCGGGCTTGCG	<i>puromycin</i> -N-acetyl-transferase	This thesis
KM077	C2 UTR_rev_C2 KO.Seq	atgcgcaatgccgaacccaaatt	PKAC2 3'UTR	This thesis
KM080	PKAC2_fwd2_C2 KO	TGCAAACGGATCACACGAAAC	PKAC2	This thesis
-	pBlas_up	CTTCTCGATCTGCATCCTGG	blasticidin-S-deaminase	M. Panzer
KM120	Phleo_fwd	GTGCACTTCGTGGCCGAG	phleomycin resistance gene	This thesis
-	puro_upper	AGCAACAGATGGAAGGCCTC	<i>puromycin</i> -N-acetyl-transferase	M. Hahn
KM179	PKAC1_2-ACT5'_fwd_CRI SPR repair	GGTGACTGATTTTGGTTTTGCTAA-GAAGGTGACGGATCGTACCTATAC-GTGGGCACAG-CAAGGTCTTCTGAAATT	Actin UTR	This thesis
KM180	ACT 3'-PKAC1_2_rev_CRISPR repair	GTCCTTTGCTCTGAATTAC-CTCAGGTGCAAGA-TACTCAGGTGTCCACATAATACTG-CATAGATAACAAACGCAT	Actin UTR	This thesis
KM171	pPOT tagging_PKAC2_fwd	TTTTGTTGCATACGTAAGTC-TACATTTATTTATACATTATTCTTTTT-GACAGAGCTTGAG-CAGGACTGGTAGTGCGGAGTATAATGCAGACCTGCTGC	pPOTv4	This thesis
KM172	pPOT tagging_PKAC2_rev	AAGTCAC-TCAGCTCCATCCCGATGTGTCAGGT TTGGTAAACACATACGTTT-GCGGTTCCGTCGACGTGGC-TACAGGCATACCTGAC-GACCCTCCACC	pPOTv4	This thesis
KM038	XhoI-Ty1-eGFP_fwd	CTCGAGCCGCCAC-CATGGAGGTCCATACTAACCAG-GACCCACTTGACAGCAAGGGCGAG-GAGCT	eGFP	This thesis
KM027	eGFP-GS-HindIII (rev)	CCTCTCAAGCTTGAGAACCAC-CTCCCCCTTGTAGAGCTCGTCCAT	eGFP	This thesis
KM177	HindIII-PEX14_fwd	GCTGTTAAGCTTccATGTCTTT-GCTGCTGTCG	PEX14	This thesis
KM178	PEX14-KpnI_rev	TGTTGGGGTACCCGGAT-TTCATAAGGCGAA	PEX14	This thesis
KM181	Bsal-(PA)PEX14_rev	AGAGAAGGTCTcGTAAAgcAGcGTGACGCCGGGATTG	PEX14	This thesis
KM182	Bsal-(PM)PEX14_rev	AGAGAAGGTCTcGTAAAttcttcGTGAC-GCCGGGATTG	PEX14	This thesis
KM183	Bsal-PEX14_L124_fwd	AGAGAAGGTCTCTTTACTTTAC-GCGCCACAAG	PEX14	This thesis
KM184	PEX14*-KpnI_rev	GTTTGTGGTACCTCAA-GCTGCCTCGCCGCC	PEX14	This thesis
KM189	PEX14 (nt456-476)_rev	CCGCCAATCACGGCAGCACC	PEX14	This thesis
KM190	PEX14 (nt276-296)_fwd	CCGAATAGCCAGCACATGAC	PEX14	This thesis

2.1.2 Plasmids

Plasmids for bacterial PKA expression

pKM001	pETM11-SUMO3-PKAC1
Description	IPTG-inducible expression of 6xHis-SUMO3-tagged PKAC1 in <i>E. coli</i>
Construction	PKAC1 ORF was PCR amplified using primers KM001 and PKAC1 rev NotI (G. Githure) and ligated into pETM11-SUMO3-eGFP (EMBL) using BamHI and NotI restriction sites
Made by	K. Malenica
Linearization	-
Selection markers	34 µg/ ml kanamycin

pKM003	pETM11-SUMO3-PKAC3
Description	IPTG-inducible expression of 6xHis-SUMO3-tagged PKAC3 in <i>E. coli</i>
Construction	PKAC3 ORF was PCR amplified using primers KM002 and PKAC3 rev NotI (G. Githure) and ligated into pETM11-SUMO3-eGFP (EMBL) using BamHI and NotI restriction sites
Made by	K. Malenica
Linearization	-
Selection markers	34 µg/ ml kanamycin

pKM015	pETM11-SUMO3-PKAC2
Description	IPTG-inducible expression of 6xHis-SUMO3-tagged PKAC2 in <i>E. coli</i>
Construction	PKAC2 ORF was PCR amplified using primers KM018 and KM019 and ligated into pETM11-SUMO3-eGFP (EMBL) using BamHI and NotI restriction sites
Made by	K. Malenica
Linearization	-
Selection markers	34 µg/ ml kanamycin

pKM051	pETM11-6xHis-PKAC3
Description	IPTG-inducible expression of 6xHis-PKAC2 in <i>E. coli</i> , used for anti-PKAC3 antibody generation
Construction	PKAC3 ORF was PCR amplified using the primers KM073 and PKAC3 rev NotI (G. Githure), the ORF was ligated into pETM11-SUMO3-eGFP (EMBL) using the NcoI and NotI restriction sites
Made by	K. Malenica
Linearization	-
Selection markers	34 µg/ ml kanamycin

	pETDUET 6xHisTEV-PKAR
Description	IPTG-inducible expression of 6xHisTEV-PKAR in <i>E. coli</i>
Construction	-
Made by	G. Githure
Linearization	-
Selection markers	100 µg/ml ampicillin

pKM057	pETM11_PKAC3 (tag-free)
Description	IPTG-inducible expression of untagged PKAC3, used for affinity purification of PKAC3 antibody
Construction	PKAC3 ORF was PCR amplified using the primers KM124 and PKAC3 rev NotI (G. Githure), the ORF was ligated into pETM11-SUMO3-eGFP (EMBL) using the XbaI and NotI restriction sites
Made by	K. Malenica
Linearization	-
Selection markers	34 µg/ml kanamycin

Plasmids for BioID

pKM005	pLEW100.v5b1d_TY-BirA*-PKAC1
Description	Tetracycline-inducible expression of TY-BirA*-tagged PKAC1 in <i>T. brucei</i> for BioID
Construction	PCR amplification of PKAC1 (KM009 & BamHI-PKAC1 from S. Kramer) from pETDUET strep-PKAC1, cloning into the backbone using BamHI & XbaI (Insert XbaI overhang was produced by BsaI digestion)
Made by	K. Malenica
Linearization	NotI
Selection markers	100 µg/ml ampicillin (<i>E. coli</i>), 5 µg/ml phleomycin (<i>T. brucei</i> BSF)

pKM006	pLEW100.v5b1d_TY-BirA*-PKAC2
Description	Tetracycline-inducible expression of TY-BirA*-tagged PKAC2 in <i>T. brucei</i> for BioID
Construction	PCR amplification of PKAC1 (KM013 & KM014) from genomic DNA (Mitat 1.2 wt, prepped by Q. Wu), cloning into the backbone using BamHI & XbaI (Insert XbaI overhang was produced by BsaI digestion)
Made by	K. Malenica
Linearization	NotI
Selection markers	100 µg/ml ampicillin (<i>E. coli</i>), 5 µg/ml phleomycin (<i>T. brucei</i> PCF)

pKM007	pLEW100.v5b1d_TY-BirA*-PKAC3
Description	Tetracycline-inducible expression of TY-BirA*-tagged PKAC3 in <i>T. brucei</i> for BioID
Construction	PCR amplification of PKAC1 (KM005 & BamHI-PKAC3 from S. Kramer) from pETDUET strep-PKAC3 (G. Githure), cloning into the backbone using BamHI & XbaI
Made by	K. Malenica
Linearization	NotI
Selection markers	100 µg/ml ampicillin (<i>E. coli</i>), 5 µg/ml phleomycin (<i>T. brucei</i> BSF and PCF)

PKA reverse genetics constructs

pKM058	pΔPKAC2 phleo
Description	Replacement of PKAC2 ORF with resistance marker
Construction	PCR amplification of resistance cassette from pΔPKAC1 phleo using KM125 und KM129. Ligation into pΔPKAC2 hygro (P. Hassan) using StuI & SpeI.
Made by	K. Malenica
Linearization	XmnI + XcmI
Selection markers	100 µg/ml ampicillin (<i>E. coli</i>), 5 µg/ml phleomycin (<i>T. brucei</i> BSF and PCF)

pKM059		pΔPKAC2 blas	
Description		Replacement of PKAC2 ORF with resistance marker	
Construction		PCR amplification of resistance cassette from pΔPKAC1 blas using KM127 und KM130, ligation into pΔPKAC2 hygro using Stul & SpeI	
Made by		K. Malenica	
Linearization		XmnI + XcmI	
Selection markers		100 µg/ml ampicillin (<i>E. coli</i>), 2 µg/ml phleomycin (<i>T. brucei</i> BSF)/10 µg/ml (<i>T. brucei</i> PCF)	
pKM088		pΔPKAC2 puro	
Description		Replacement of PKAC2 ORF with resistance marker	
Construction		puro resistance marker was PCR amplified from pHD615 TY-C2 (puro) using the primer KM169 & KM170 and ligated into the pΔC2 backbone using SpeI and EcoRV sites	
Made by		K. Malenica	
Linearization		XmnI and XcmI	
Selection markers		100 µg/ml ampicillin (<i>E. coli</i>), 1 µg/ml puromycin (<i>T. brucei</i> PCF)	
pKM071		pLEW82.v4_TY-PKAC2 (puro)	
Description		Tetracycline-inducible expression of TY-PKAC2 in <i>T. brucei</i> , high expression level, but leakiness	
Construction		First, the puro resistance cassette was cut out from pHD615 TY-PKAC2 (Q. Wu) using SnaBI and ligated into pLEW82.v4.luc (phleo) backbone (G. Cross lab, Addgene #24009). The TY-PKAC2 ORF was cut out from pHD615 TY-PKAC2 and ligated into the pLEW82.v4.luc (puro) backbone using BamHI and HindIII.	
Made by		K. Malenica	
Linearization		EcoRV	
Selection markers		100 µg/ml ampicillin (<i>E. coli</i>), 0.1 µg/ml puromycin (<i>T. brucei</i> BSF)/1 µg/ml (<i>T. brucei</i> PCF)	
pKM075		pLEW82.v4_TY-PKAC1 (puro)	
Description		Tetracycline-inducible expression of TY-PKAC1 in <i>T. brucei</i> , high expression level, but leakiness	
Construction		The TY-PKAC1 ORF was cut out from pHD615 TY-PKAC1 (Q. Wu) and ligated into pKM071 using BamHI and HindIII restriction sites.	
Made by		K. Malenica	
Linearization		EcoRV	
Selection markers		100 µg/ml ampicillin (<i>E. coli</i>), 0.1 µg/ml puromycin (<i>T. brucei</i> BSF)/1 µg/ml (<i>T. brucei</i> PCF)	
pHD615 PKAC1 3'UTR RNAi			
Description		Tetracycline-inducible knock-down of PKAC1 using a PKAC1-specific fragment of the 3' UTR	
Construction		described in (Bachmaier, 2008)	
Made by		S. Bachmaier	
Linearization		NotI	
Selection markers		100 µg/ml ampicillin (<i>E. coli</i>), 0.1 µg/ml (<i>T. brucei</i> BSF)/1 µg/ml (<i>T. brucei</i> PCF) puromycin	

PKA endogenous tagging

pPOTv4_eGFP-Linker-blast-blast

Description	Vector for amplification of resistance marker and TY-GFP-tag for endogenous tagging of genes
Construction	-
Made by	J. Street
Linearization	-
Selection markers	100 µg/ml ampicillin (<i>E. coli</i>), 2 (<i>T. brucei</i> BSF)/10 (<i>T. brucei</i> PCF) blas

PEX14 project

pKM091 p2675_TY-eGFP-PEX14

Description	Endogenous tagging of PEX14 on the N-terminus with TY-eGFP-tag
Construction	TY-eGFP was PCR-amplified from pETM11-SUMO3-eGFP using KM038 and KM027 and ligated into p2675 (Kelly et al., 2007) using the XhoI and HindIII restriction sites. Subsequently, PEX14 was amplified using KM177 and KM178 and ligated into the resulting vector using the HindIII and KpnI restriction sites
Made by	K. Malenica
Linearization	SpeI
Selection markers	100 µg/ml ampicillin (<i>E. coli</i>), 0.1 µg/ml (<i>T. brucei</i> BSF)/1 µg/ml (<i>T. brucei</i> PCF) puromycin

pKM096 p2675_TY-eGFP-PEX14 (S122A/T123A)

Description	Endogenous tagging of PEX14 on the N-terminus with TY-eGFP-tag
Construction	The mutation was introduced in the PEX14 ORF by 2 PCR amplifications using KM177 & KM181 primers (digested with HindIII + BsaI) and KM183 & KM184 (digested with BsaI + KpnI), respectively. Both products were ligated into pKM091 using HindIII and KpnI restriction sites.
Made by	K. Malenica
Linearization	used as PCR template for CRISPR/Cas repair construct
Selection markers	100 µg/ml ampicillin (<i>E. coli</i>), 0.1 µg/ml (<i>T. brucei</i> BSF)/1 µg/ml (<i>T. brucei</i> PCF) puromycin

pKM097 p2675_TY-eGFP-PEX14 (S122E/T123E)

Description	Endogenous tagging of PEX14 on the N-terminus with TY-eGFP-tag
Construction	The mutation was introduced in the PEX14 ORF by 2 PCR amplifications using KM177 & KM182 primers (digested with HindIII + BsaI) and KM183 & KM184 (digested with BsaI + KpnI), respectively. Both products were ligated into pKM091 using HindIII and KpnI restriction sites.
Made by	K. Malenica
Linearization	used as PCR template for CRISPR/Cas repair construct
Selection markers	100 µg/ml ampicillin (<i>E. coli</i>), 0.1 µg/ml (<i>T. brucei</i> BSF)/1 µg/ml (<i>T. brucei</i> PCF) puromycin

Purine Response Element Project

pGR108 (blas)

Description	Plasmid used for purine response reporter assay. Expression of firefly luciferase is regulated by a wild type actin 3'UTR.
Construction	The puromycin resistance cassette was cut out from pGR12 (kind gift of A. Estevez) using XbaI and ScaI and ligated into pGR108 (puro) (kind gift of A. Estevez) using SpeI and ScaI restriction sites.
Made by	T. Thanner

Linearization	NotI
Selection markers	100 µg/ml ampicillin (<i>E. coli</i>), 2 µg/ml blasticidin (<i>T. brucei</i> BSF and PCF)

pGR292 (blas)

Description	Plasmid used for purine response reporter assay. Expression of firefly luciferase is regulated by an actin 3'UTR containing the purine response element (Fernandez-Moya et al., 2014).
Construction	The puromycin resistance cassette was cut out from pGR12 (kind gift of A. Estevez) using XbaI and ScaI and ligated into pGR292 (puro) (kind gift of A. Estevez) using SpeI and ScaI restriction sites.
Made by	T. Thanner
Linearization	NotI
Selection markers	100 µg/ml ampicillin (<i>E. coli</i>), 2 µg/ml blasticidin (<i>T. brucei</i> BSF and PCF)

pGR108 (blas)

Description	Plasmid used for purine response reporter assay. Expression of firefly luciferase is regulated by a wild type actin 3'UTR.
Construction	The puromycin resistance cassette was cut out from pGR12 (kind gift of A. Estevez) using XbaI and ScaI and ligated into pGR108 (puro) (kind gift of A. Estevez) using SpeI and ScaI restriction sites.
Made by	T. Thanner
Linearization	NotI
Selection markers	100 µg/ml ampicillin (<i>E. coli</i>), 2 µg/ml blasticidin (<i>T. brucei</i> BSF and PCF)

pGR292 (blas)

Description	Plasmid used for purine response reporter assay. Expression of firefly luciferase is regulated by an actin 3'UTR containing the purine response element (Fernandez-Moya et al., 2014).
Construction	The puromycin resistance cassette was cut out from pGR12 (kind gift of A. Estevez) using XbaI and ScaI and ligated into pGR292 (puro) (kind gift of A. Estevez) using SpeI and ScaI restriction sites.
Made by	T. Thanner
Linearization	NotI
Selection markers	100 µg/ml ampicillin (<i>E. coli</i>), 2 µg/ml blasticidin (<i>T. brucei</i> BSF and PCF)

2.1.3 *E. coli* strains

Strain	Genotype	Usage	origin
<i>E. coli</i> Rosetta™ (DE3)	F- ompT hsdSB(rB- mB-) gal dcm (DE3) pRARE (CamR)	Protein expression	Novagen
<i>E. coli</i> XL10-Gold®	F' proA+B+ lacI ^q Δ(lacZ)M15 zcf::Tn10 (Tet ^R) / Δ(ara-leu) 7697 araD139 fhuA ΔlacX74 galK16 galE15 e14- Φ80dlacZΔM15 recA1 relA1 endA1 nupG rpsL (Str ^R) rph spoT1 Δ(mrr-hsdRMS-mcrBC)	Cloning and plasmid propagation	Stratagene
<i>E. coli</i> TOP10	F-mcrA Δ(mrr-hsdRMS-mcrBC) φ80lacZΔM15 ΔlacX74 recA1 araD139 Δ(ara-leu)7697 galU galK rpsL (Str ^R) endA1 nupG	Cloning and plasmid propagation	Invitrogen

2.1.4 *Trypanosoma brucei* cell lines

Parental/wild-type cell lines

Nomenclature according to (Clayton et al., 1998)

AnTat 1.1 Munich

Origin	(Delauw et al., 1985)
Description	Pleomorphic wild type cell line, matrix-dependent, for more information see (Bachmaier et al., 2020)

AnTat 1.1 Paris

Origin	(Delauw et al., 1985)
Description	Pleomorphic wild type cell line, cultured in the lab of B. Rotureau and gained matrix-independence, for more information see (Bachmaier et al., 2020)

AnTat 1.1 90-13

Genotype	T7POL NEO, TETR HYG
Made by	(Engstler and Boshart, 2004)
Constructs	pLEW13, pLEW90
Selection markers	4 µg/ml (BSF)/25 µg/ml (PCF) hygromycin, 2 µg/ml (BSF)/15 µg/ml (PCF) neomycin, G418
Description	Expression of T7 polymerase and Tetracycline repressor, pleomorphic cell line that became matrix-independent

EATRO 1125 T7T

Genotype	T7POL NEO, TETR HYG
Made by	(Bringaud et al., 2000)
Constructs	pLEW13, pLEW90
Selection markers	25 µg/ml hygromycin, 15 µg/ml neomycin, G418
Description	Expression of T7 polymerase and Tetracycline repressor

MITat 1.2 single maker

Genotype	T7POL, TETR NEO
Made by	(Wirtz et al., 1999)
Constructs	single marker construct
Selection markers	2 µg/ml neomycin, G418
Description	Expression of T7 polymerase and Tetracycline repressor

Cell lines used/generated in this thesis

TbKM041	AnTat 1.1 90-13 ΔPKAC2
Genotype	T7POL NEO, TETR HYG, Δ pkac2::BSD/ Δ pkac2::BLE
Clone used	p2b2, p1b6
Made by	K. Malenica
Constructs	pLEW13, pLEW90, p Δ PKAC2 phleo (pKM058)/p Δ PKAC2 blas (pKM059)
Selection markers	4 µg/ml (BSF)/ 25 µg/ml (PCF) hygromycin, 2 µg/ml (BSF)/ 15 µg/ml (PCF) neomycin, G418, 2 µg/ml (BSF & PCF) phleomycin, 2 µg/ml (BSF & PCF) blasticidin
Description	Homozygous PKAC2 null mutant generated in pleomorphic BSF cell line with Tet-inducible system

TbKM056	AnTat 1.1 90-13 ΔPKAC2 PKAC1 3'UTR^{Ti}
Genotype	T7POL NEO, TETR HYG, Δ pkac2::BSD/ Δ pkac2::BLE, C1 3'UTR RNAi ^{Ti} PAC
Clone used	clone 1, 3
Made by	K. Malenica
Con-structs	pLEW13, pLEW90, p Δ PKAC2 phleo (pKM058)/p Δ PKAC2 blas (pKM059), pHD615 C1 3'UTR RNAi (S. Bachmaier)
Selection markers	4 μ g/ml (BSF)/ 25 μ g/ml (PCF) hygromycin, 2 μ g/ml (BSF)/ 15 μ g/ml (PCF) neomycin, G418, 2 μ g/ml (BSF & PCF) phleomycin, 2 μ g/ml (BSF & PCF) blasticidin, 0.1 μ g/ml (BSF)/ 1 μ g/ml (PCF) puromycin
Description	Homozygous PKAC2 null mutant with Tet-inducible PKAC1-specific RNAi, generated in BSF and differentiated to PCF

TbKM073	AnTat 1.1 90-13 ΔPKAC1/2
Genotype	T7POL NEO, TETR HYG, Δ pkac1::PAC/ Δ pkac1::PAC, Δ pkac2::PAC/ Δ pkac2::PAC
Clone used	C6 (C4)
Made by	K. Malenica
Con-structs	pLEW13, pLEW90, PCR repair template generated using primers KM179 + KM180 to amplify puromycin resistance cassette, including actin UTRs from pKM075
Selection markers	25 μ g/ml hygromycin, 15 μ g/ml neomycin, G418, 1 μ g/ml puromycin
Description	Homozygous PKAC1/2 null mutant generated in PCF using CRISPR/Cas9, ORFs were disrupted by insertion of a puromycin resistance cassette.

AnTat 1.1 Munich Δ PKAC3

Genotype	Δ pkac3::BLE/ Δ pkac3::NEO
Clone used	A2
Made by	(Schulte zu Sodingen, 2000)
Con-structs	PKA γ -neo-k.o, PKA γ -phleo-k.o.
Selection markers	never added after thawing
Description	Homozygous PKAC3 null mutant, generated in PCF by ORF replacement with antibiotic resistance cassette.

TbKM080 AnTat 1.1 Munich Δ PKAC1/2/3

Genotype	Δ pkac3::PHLEO/ Δ pkac3::NEO, Δ pkac1::PAC/ Δ pkac1::PAC, Δ pkac2::PAC/ Δ pkac2::PAC
Clone used	F12, G12
Made by	K. Malenica
Con-structs	PKA γ -neo-k.o, PKA γ -phleo-k.o., PCR repair template generated using primers KM179 + KM180 to amplify puromycin resistance cassette, including actin UTRs from pKM075
Selection markers	1 μ g/ml puromycin
Description	Homozygous PKAC1/2/3 null mutant generated in PCF using CRISPR/Cas9 by disruption of PKAC1 and PKAC2 ORFs by insertion of a puromycin resistance cassette in the Δ PKAC3 cell line (Schulte zu Sodingen, 2000)

AnTat 1.1 Munich Δ PKAR

Genotype	Δ pkar::BLE/ Δ pkar::PAC
Clone used	8 (PCF)
Made by	S. Bachmaier
Con-structs	pBSK[PAC]Rko, pBSK[BLE]Rko
Selection markers	never added after thawing

Description	Homozygous PKAR null mutant generated in pleomorphic BSF and differentiated to PCF.
EATRO 1125 T7T RBP6^{Ti}	
Genotype	T7POL NEO, TETR HYG, RBP6 ^{Ti} BLE
Clone used	Pool
Made by	S. Allmann
Constructs	pHD328, pLEW114, pLEW100v5b1d RBP6 (S. Allmann)
Selection markers	25 µg/ml hygromycin, 10 µg/ml neomycin, G418, 5 µg/ml phleomycin
Description	Inducible overexpression of RBP6 to induce metacyclogenesis <i>in vitro</i> .
TbKM068 EATRO 1125 T7T RBP6^{Ti} ΔPKAC2	
Genotype	T7POL NEO, TETR HYG, RBP6 ^{Ti} BLE, Δ <i>pkac2</i> ::BSD/Δ <i>pkac2</i> ::PAC
Clone used	b2p2, b3p1
Made by	K. Malenica
Constructs	pHD328, pLEW114, pLEW100v5b1d RBP6
Selection markers	25 µg/ml hygromycin, 10 µg/ml neomycin, G418, 5 µg/ml phleomycin, 10 µg/ml blasticidin (omitted after successful selection), 1 µg/ml puromycin (omitted after successful selection)
Description	Homozygous PKAC2 null mutant generated in PCF to analyze metacyclogenesis.
TbKM077 EATRO 1125 T7T RBP6^{Ti} ΔPKAC1/2	
Genotype	T7POL NEO, TETR HYG, RBP6 ^{Ti} BLE, ^Δ <i>pkac1</i> ::PAC/ ^Δ <i>pkac1</i> ::PAC, ^Δ <i>pkac2</i> ::PAC/ ^Δ <i>pkac2</i> ::PAC
Clone used	A3, A5
Made by	K. Malenica
Constructs	pHD328, pLEW114, pLEW100v5b1d RBP6, PCR repair template generated using primers KM179 + KM180 to amplify puromycin resistance cassette, including actin UTRs from pKM075
Selection markers	25 µg/ml hygromycin, 15 µg/ml neomycin, G418, 5 µg/ml phleomycin, 1 µg/ml puromycin
Description	Homozygous PKAC1/2 null mutant generated in RBP6 OE background using CRISPR/Cas9, ORFs were disrupted by insertion of a puromycin resistance cassette to analyze metacyclogenesis.
TbKM066 AnTat 1.1 90-13 TY-GFP-PKAC2	
Genotype	T7POL NEO, TETR HYG, TY-GFP::PKAC2 BSD
Clone used	2
Made by	K. Malenica
Constructs	pLEW13, pLEW90, PCR product amplified from pPOTv4_eGFP-Linker-blast-blast using primers KM171 and KM172
Selection markers	4 µg/ml (BSF)/ 25 µg/ml (PCF) hygromycin, 2 µg/ml (BSF)/ 15 µg/ml (PCF) neomycin, G418, 2 µg/ml (BSF & PCF) blasticidin
Description	Endogenous tagging of PKAC2 with TY-GFP based on tagging method from (Dean et al., 2015)
TbKM001 MITat 1.2 SM TY-BirA*-PKAC1^{Ti}	
Genotype	T7POL TETR NEO, TY-BirA*-PKAC1 ^{Ti}
Clone used	1
Made by	K. Malenica

Con-structs	single marker construct, pKM005
Selection markers	2 µg/ml neomycin, G418, 5 µg/ml phleomycin
Description	Tet-inducible overexpression of TY-BirA*-tagged PKAC1 for BioID
TbKM002	MITat 1.2 SM TY-BirA*-PKAC3^{Ti}
Genotype	T7POL TETR NEO, TY-BirA*-PKAC3 ^{Ti}
Clone used	2
Made by	K. Malenica
Con-structs	single marker construct, pKM007
Selection markers	2 µg/ml neomycin, G418, 5 µg/ml phleomycin
Description	Tet-inducible overexpression of TY-BirA*-tagged PKAC3 for BioID
TbKM005	EATRO 1125 T7T TY-BirA*-PKAC2^{Ti}
Genotype	T7POL NEO, TETR HYG, TY-BirA*::PKAC2 ^{Ti} BLE
Clone used	2
Made by	K. Malenica
Con-structs	pHD328, pLEW114, pKM006
Selection markers	25 µg/ml hygromycin, 15 µg/ml neomycin, G418, 5 µg/ml phleomycin
Description	Tet-inducible overexpression of TY-BirA*-tagged PKAC2 for BioID
TbKM006	EATRO 1125 T7T TY-BirA*-PKAC3^{Ti}
Genotype	T7POL NEO, TETR HYG, TY-BirA*::PKAC3 ^{Ti} BLE
Clone used	2
Made by	K. Malenica
Con-structs	pHD328, pLEW114, pKM007
Selection markers	25 µg/ml hygromycin, 15 µg/ml neomycin, G418, 5 µg/ml phleomycin
Description	Tet-inducible overexpression of TY-BirA*-tagged PKAC3 for BioID
TbGW060	AnTat 1.1 90-13 TY-PKAC1^{Ti}
Genotype	T7POL NEO, TETR HYG, TY-PKAC1 ^{Ti} PAC
Clone used	1
Made by	G. Wagner, bachelor thesis
Con-structs	pLEW90, pLEW13, pKM075
Selection markers	25 µg/ml hygromycin, 15 µg/ml neomycin, G418, 1 µg/ml puromycin
Description	Tet-inducible overexpression of TY-PKAC1 in PCF, leaky expression
TbGW061	AnTat 1.1 90-13 TY-PKAC2^{Ti}
Genotype	T7POL NEO, TETR HYG, TY-PKAC2 ^{Ti} PAC
Clone used	3
Made by	G. Wagner, bachelor thesis

Con-structs	pLEW90, pLEW13, pKM071
Selection markers	25 µg/ml hygromycin, 15 µg/ml neomycin, G418, 1 µg/ml puromycin
Description	Tet-inducible overexpression of TY-PKAC2 in PCF, leaky expression
TbKM071 AnTat 1.1 90-13 TY-GFP-PEX14	
Genotype	T7POL NEO, TETR HYG, TY-GFP::PEX14 PAC
Clone used	only obtained 1 clone
Made by	K. Malenica
Con-structs	pLEW90, pLEW13, pKM091
Selection markers	4 µg/ml (BSF)/ 25 µg/ml (PCF) hygromycin, 2 µg/ml (BSF)/ 15 µg/ml (PCF) neomycin, G418, 0.1 µg/ml (BSF)/ 1 µg/ml (PCF) puromycin
Description	Endogenous TY-GFP-tagging of PEX14 in BSF and differentiation to PCF.
TbKM074 AnTat 1.1 90-13 ΔPKAC2 TY-GFP-PEX14	
Genotype	T7POL NEO, TETR HYG, Δ <i>pkac2</i> ::BSD/Δ <i>pkac2</i> ::BLE, TY-GFP::PEX14
Clone used	1
Made by	K. Malenica
Con-structs	pLEW90, pLEW13
Selection markers	25 µg/ml (PCF) hygromycin, 15 µg/ml (PCF) neomycin, G418, 1 µg/ml puromycin, 2 µg/ml phleomycin (omitted), 2 µg/ml blasticidin (omitted)
Description	Endogenous TY-GFP-tagging of PEX14 in BSF and differentiation to PCF.
TbKM083 AnTat 90-13 PEX14 S122A/T123A	
Genotype	T7POL NEO, TETR HYG, pex14(S122A/T123A)/ pex14(S122A/T123A)
Clone used	B4
Made by	K. Malenica
Con-structs	pLEW90, pLEW13, PCR repair template generated using primers KM189 and KM190 from pKM096
Selection markers	25 µg/ml hygromycin, 15 µg/ml neomycin, G418
Description	Scar-free replacement of pex14 phosphosites by alanine to generate homozygous phosphoablative mutant by CRISPR/Cas9 transfection in PCF.
TbKM084 AnTat 90-13 PEX14 S122E/T123E	
Genotype	T7POL NEO, TETR HYG, pex14(S122E/T123E)/ pex14(S122E/T123E)
Clone used	A3
Made by	K. Malenica
Con-structs	pLEW90, pLEW13, PCR repair template generated using primers KM189 and KM190 from pKM097
Selection markers	25 µg/ml hygromycin, 15 µg/ml neomycin, G418
Description	Scar-free replacement of pex14 phosphosites by glutamate to generate homozygous phosphomimetic mutant by CRISPR/Cas9 transfection in PCF.
AnTat 1.1 Munich pGR108	
Genotype	LUC-ACT 3'UTR BSD
Clone used	3
Made by	T. Thanner

Con-structs	pGR108 (blas)
Selection markers	2 µg/ml blasticidin (BSF and PCF)
Description	Expression of firefly luciferase under the control of an actin 3'UTR, used as a control for purine response experiments.

AnTat 1.1 Munich pGR292

Genotype	LUC-ACT 3'UTR_PuRE BSD
Clone used	4
Made by	T. Thanner
Con-structs	pGR292 (blas)
Selection markers	2 µg/ml blasticidin (BSF and PCF)
Description	Expression of firefly luciferase under the control of an actin 3'UTR containing the Purine response element. Expression of the luciferase is regulated by purine levels (Fernandez-Moya <i>et al.</i> , 2014)

AnTat 1.1 Munich ΔPKAR pGR108

Genotype	$\Delta pkar::BLE/\Delta pkar::PAC$, LUC-ACT 3'UTR BSD
Clone used	2
Made by	T. Thanner
Con-structs	pBSK[PAC]Rko, pBSK[BLE]Rko, pGR108 (blas)
Selection markers	2 µg/ml blasticidin (BSF and PCF), PKAR KO selection omitted
Description	Expression of firefly luciferase under the control of an actin 3'UTR in ΔPKAR background, used as a control for purine response experiments.

AnTat 1.1 Munich ΔPKAR pGR292

Genotype	$\Delta pkar::BLE/\Delta pkar::PAC$, LUC-ACT 3'UTR_PuRE BSD
Clone used	3
Made by	T. Thanner
Con-structs	pBSK[PAC]Rko, pBSK[BLE]Rko, pGR292 (blas)
Selection markers	2 µg/ml blasticidin (BSF and PCF), PKAR KO selection omitted
Description	Expression of firefly luciferase under the control of an actin 3'UTR containing the Purine response element in the ΔPKAR background. Expression of the luciferase is regulated by purine levels (Fernandez-Moya <i>et al.</i> , 2014)

2.1.5 Antibodies

Primary antibodies

Name	organism	origin	dilution	Buffer system	Primary antibody incubation
Anti-PKAC1/2	Rabbit	Recombinantly expressed and purified PKAC1 (G. Githure) was sent to Pineda Antikörper-Service (Berlin) for rabbit immunization up to 210 days. Antibody was affinity purified as described in 2.2.4.3	1:1,000	PBS	1% milk

Anti-PKAR	Rabbit	Recombinantly expressed and purified PKAR (G. Githure) was sent to Pineda Antikörper-Service (Berlin) for rabbit immunization up to 210 days. Antibody was affinity purified as described in 2.2.4.3	1:500 - 1,000	PBS	1% milk
Anti-His	Mouse	BioRad MCA1396	1:1,000	PBS	1% milk
Anti-strep	Mouse	Qiagen, 1023944	1:1,000	PBS	1% milk
Anti-Ty1 (BB2)	Mouse	(Bastin et al., 1996)	1:2,000	PBS	1% milk
Anti-PFR (L13D6)	Mouse	(Kohl et al., 1999)	1:2,000	PBS	1% milk
RXXS*/T*	Rabbit	Phospho (Ser/Thr) PKA substrate Antibody, Cell signaling #9621	1:1,000	TBS	Odyssey blocking buffer
PKAC3	Rabbit	this thesis	1:250	PBS	1% milk
RBP6	Rabbit	(Kolev et al., 2012), kind gift from F. Bringaud	1:1,000	PBS	1% milk
PPDK	Rabbit	(Bringaud et al., 1998), kind gift of F. Bringaud	1:5,000	PBS	1% milk
BIP	Rabbit	(Bangs et al., 1993), kind gift of S. Kramer	1:100,000	PBS	1% milk
Enolase	Rabbit	(Hannaert et al., 2003), kind gift of F. Bringaud	1:10,000	PBS	1% milk
HSP60	Mouse	(Bringaud et al., 1995), kind gift of F. Bringaud	1:10,000	PBS	1% milk
PEX14	Rabbit	(Moyersoen et al., 2003), kind gift of F. Bringaud	1:1,000	PBS	1% milk
AMPKα	Rabbit	Phospho-AMPK α (Thr172) rabbit, Cell signaling, #2535	1:1,000	TBS	Odyssey blocking buffer

Secondary antibodies

Name	Type	Dilution	Usage	Origin
IRDye800CW	Goat anti-mouse	1:5,000	Western Blot	LI-COR (#926-32210)
IRDye680LT	Goat anti-rabbit	1:50,000	Western Blot	LI-COR (#926-68021)
IRDye800CW Streptavidin	IRDye-coupled streptavidin	1:5,000	Western Blot	LI-COR (#926-32230)

2.1.6 Antibiotic stock solutions

Antibiotic (stock concentration)	Concentration used	Supplier
Ampicillin (100 mg/ml in H₂O)	100 μ g/ml	Sigma (Cat.# A9518)
Chloramphenicol (50 mg/ml in H₂O)	50 μ g/ml	Sigma (Cat.# C0378)
Kanamycin (34 mg/ml in H₂O)	34 μ g/ml	Merck (Cat.# K21420677)
Hygromycin (10 mg/ml in H₂O)	4 μ g/ml (BSF)/25 μ g/ml (PCF)	Sigma (Cat.# H3274)
Neomycin, G418 (10 mg/ml in H₂O)	2 μ g/ml (BSF)/15 μ g/ml (PCF)	Capricorn (Cat.# G418-Q)
Phleomycin (10 mg/ml in H₂O <i>T. brucei</i>)	2 μ g/ml (BSF)/ 5 μ g/ml (PCF)	InvivoGen (Cat.# ant-ph-5p)
Puromycin (10 mg/ml in H₂O)	0.1 μ g/ml (BSF)/1 μ g/ml (PCF)	Sigma (Cat.# P8830)
Blasticidin (10 mg/ml in H₂O)	2 μ g/ml (BSF)/5-15 μ g/ml (PCF)	Capricorn (Cat.# BLA-1X)
Tetracycline (10 mg/ml in 50% ethanol)	1 – 10 μ g/ml (BSF, PCF)	Roth (Cat.# HP63.1)

2.2 Methods

2.2.1 *Trypanosoma brucei*

2.2.1.1 Cultivation of BSF trypanosomes

Different strains of BSF trypanosomes are available in the laboratory. The most commonly used ones are the so-called *monomorphic* strains (e.g., MITat 1.2). These strains can be cultured as BSF but have lost their differentiation ability to PCF. In contrast to that *pleomorphic* cells (e.g., AnTat 1.1) are still able to fulfill the complete life cycle. To successfully culture pleomorphic cells, they need to be grown in presence of methylcellulose as a *matrix*. Some subtypes of the AnTat 1.1 strain exist that remain pleomorphic but became matrix independent (AnTat 1.1 *Paris* and AnTat 1.1 90-13). For more information, see (Bachmaier *et al.*, 2020).

2.2.1.1.1 Matrix-independent BSF

HMI-9	Supplements
Iscoves modified medium (IMDM) powder (+ L-glutamine, - NaHCO ₃), pH 7.4, sterilized through 0.2 µm filter	3.024 g/l NaHCO ₃ , 136 mg/l hypoxanthine, 28.2 mg/l bathocuproine sulfonate, 0.2 mM β- mercaptoethanol, 100000 U/l penicillin, 100 mg/l streptomycin, 182 mg/l cysteine, 10 % (v/v) heat- inactivated fetal calf serum (FCS)

Monomorphic BSF and matrix-independent pleomorphic strains AnTat 1.1 Munich 90-13 and AnTat 1.1 Paris were cultured in liquid HMI-9 at 37°C, 5% CO₂ in vented culture flasks in a humidified incubator. The cells were regularly counted using a Neubauer counting chamber and kept below a density of 10⁶ cells/ml.

2.2.1.1.2 Matrix-dependent BSF

Methylcellulose (Bachmaier <i>et al.</i> , 2020; Vassella and Boshart, 1996)	HMI-9	Supplements
Iscoves modified medium (IMDM) powder (+ L-glutamine, - NaHCO ₃), pH 7.4, sterilized through 0.2 µm filter		11g/l methylcellulose (Sigma Methocel #94378), 3.024 g/l NaHCO ₃ , 136 mg/l hypoxanthine, 28.2 mg/l bathocuproine sulfonate, 0.2 mM β- mercaptoethanol, 100000 U/l penicillin, 100 mg/l streptomycin, 182 mg/l cysteine, 15 % (v/v) heat- inactivated fetal calf serum (FCS)

Matrix-dependent cells (AnTat 1.1 Munich) were cultured in methylcellulose HMI-9 at 37°C, 5% CO₂ in vented culture flasks in a humidified incubator. Cultures were always thoroughly mixed before counting and after dilution. The cells were counted using a Neubauer counting chamber and the density was kept below 10⁶ to avoid differentiation. To recover cells from methylcellulose HMI-9, the cultures were mixed with 5 volumes of PBS + 10 mM glucose and mixed by inversion. The diluted cultures were filtered through a folded paper filter, which collects the methylcellulose while the cells pass through. Cells were recovered by centrifugation at 1,400 g, for 10 min.

2.2.1.2 Cultivation of PCF trypanosomes

SDM79	Supplements
SDM79 basic medium (+/+), prepared as described by (Brun and Schönenberger, 1979), pH 7.3, sterilized through 0.2 µm filter	91 mM sodium pyruvate, 50 mM l-threonine, 265 µM l-proline, 200 mM l-glutamine, 2.6 mM NaHCO ₃ , 7.5 mg/l hemin, 100000 U/l penicillin, 100 mg/l streptomycin, 10 mM glycerol, 10 mM glucose, 10 % heat-inactivated FCS
SDM79 -/- (free of glycolytic carbon sources)	91 mM sodium pyruvate, 50 mM l-threonine, 265 µM l-proline, 200 mM l-glutamine, 2.6 mM NaHCO ₃ , 7.5 mg/l hemin, 100000 U/l penicillin, 100 mg/l streptomycin, 50 mM N-acetylglucosamine, 10 % heat-inactivated FCS
SDM79 +/- (glucose-free)	91 mM sodium pyruvate, 50 mM l-threonine, 265 µM l-proline, 200 mM l-glutamine, 2.6 mM NaHCO ₃ , 7.5 mg/l hemin, 100000 U/l penicillin, 100 mg/l streptomycin, 50 mM N-acetylglucosamine, 10 mM glycerol, 10 % heat-inactivated FCS

CASY-ton	135.7 mM NaCl; 1.3 mM EDTA; 5.35 mM KCl; 1.37 mM Na ₂ HPO ₄ / 5.44 mM NaH ₂ PO ₄ ; 7.14 NaF
-----------------	---

Procyclic cells were cultured in standard SDM79 medium (+/+), if not indicated otherwise, at 27°C in sealed-cap culture flasks. The cell density was determined using the CASY model TT cell counter (Innovatis) and kept in a range of 10⁶ – 2*10⁷ cell/ml.

2.2.1.3 Freezing and thawing of stabilates

<i>T. brucei</i> freezing medium	Fully complemented HMI-9 (BSF)/SDM79 (PCF), supplemented with 10 % FCS and 10% (v/v) glycerol → sterilized through 0.2 µm filter
---	--

For each stabilate 1-6 *10⁶ (BSF)/~5*10⁷ (PCF) cells were harvested by centrifugation at 1,400 g (BSF)/ 900 g (PCF), 4°C for 10 min. The supernatant was removed quantitatively, and the cells resuspended in 500 µl freezing medium/stabilate. The cells were transferred to 1.5 ml cryotubes and frozen at -80°C in a precooled stratacooler.

Frozen trypanosomes were thawed quickly in a 37°C (BSF)/27°C (PCF) waterbath and transferred to 9 ml of the respective medium. The cells were centrifuged once to remove glycerol from the freezing buffer and resuspended in 10 ml fresh medium. After a few hours of recovery, the appropriate selection antibiotics were added, and the cells diluted if necessary.

2.2.1.4 Generation of transgenic Trypanosoma lines

2.2.1.4.1 Preparation of DNA for transfection

2.2.1.4.1.1 Isopropanol precipitation

For stable transfection of trypanosomes, 10 µg plasmid/transfection were linearized overnight with the enzymes indicated in the table under 2.1.2. Successful linearization was confirmed by agarose gel electrophoresis as described in 2.2.3.1.1. The linearized DNA was purified by isopropanol precipitation. Briefly, 1/10 volume of 3 M sodium acetate pH 7.0 was added to the DNA and vortexed briefly. DNA was precipitated by

addition of 1 volume isopropanol and inverted a few times. The DNA was pelleted at 20,000 g, 4°C for 20 min, washed twice with 70% ethanol and centrifuged at 20,000 g, 4°C for 10 min. After the second wash step, the ethanol was removed under sterile conditions, the pellet air-dried under the sterile bench and solved in sterile H₂O at a concentration of 1 µg/µl.

2.2.1.4.1.2 Phenol-chloroform extraction

PCR products amplified for transfection were purified by phenol-chloroform extraction. 200 µl PCR product were mixed with 200 µl phenol/chloroform/isoamyl alcohol in a 1.5 ml reaction tube (tube 1) and vortexed vigorously for 1 min. The aqueous and organic phase were separated by centrifugation at 20,000 g, RT for 5 min. The upper aqueous phase was removed and transferred to a new 1.5 ml reaction tube (tube 2). 200 µl elution buffer (10 mM Tris/Cl pH 8.5) were added to the lower organic phase (tube 1) and the vortex and centrifugation steps were repeated. The upper phase was removed and added to the aqueous phase in tube 2. An equal volume of phenol/chloroform/isoamyl alcohol was added to the pooled aqueous phases in tube 2 and the vortex and centrifugation steps were repeated one more time. The resulting aqueous phase was transferred to a new 1.5 ml reaction tube, 1/10 volume of 3 M sodium acetate pH 7.0 were added and briefly vortexed. DNA was precipitated by addition of 3 volumes 100% ice-cold ethanol and frozen for 1h to overnight at -80°C. The DNA was centrifuged at 20,000 g, 4°C for 20 min and washed twice with 70% ethanol. After the second wash step, the ethanol was removed under sterile conditions, the pellet air-dried under the sterile bench and solved in sterile H₂O at a concentration of 1 µg/µl.

2.2.1.4.2 Transfection of BSF cells (Amaxa)

Transfection buffer (Burkard et al., 2007)	90 mM sodium phosphate, 5 mM potassium chloride, 0.15 mM calcium chloride, 50 mM HEPES, pH 7.3
--	--

Transfection of BSF trypanosomes was performed as described by (Burkard *et al.*, 2007). Briefly, 1-2*10⁷ cells were harvested by centrifugation at 1,400 g, 37°C for 10 min. The supernatant was discarded, the cells resuspended in the remaining liquid and transferred to a 1.5 ml reaction tube. After a second centrifugation (1,400 g; RT; 10 min) the supernatant was removed quantitatively and the cells resuspended in 100 µl transfection buffer. They were transferred to a 2 mm gap electroporation cuvette (BTX #45-0125) and mixed with 10 µg linearized DNA. Cells were transfected once in the Amaxa Nucleofector® IIb using the program CD4+ T cells X-001. Afterwards, they were transferred to 30 ml HMI-9 and a 1:10 and 1:100 dilution was prepared. For each dilution, a 24-well plate was prepared with 1 ml aliquots of the cell suspension. The

plates were incubated at 37°C, 5% CO₂ in a humidified incubator. After 6-12 h, 1 ml of HMI-9 containing the 2x antibiotics concentration was added to each well. Resistant clones could be detected after 5-7 days.

2.2.1.4.3 Transfection of PCF cells (BTX)

Based on (Merritt and Stuart, 2013), modified by S. Allmann

Cytomix	25 mM HEPES (pH 7.6); 10 mM K ₂ HPO ₄ /KH ₂ PO ₄ ; 2 mM EGTA; 120 mM KCl; 150 μM CaCl ₂ ; 5 mM MgCl ₂ ; 1 mM hypoxanthine; 0.5 % glucose; 100 μg/ml BSA
----------------	---

For each transfection 1-2*10⁷ cells were harvested by centrifugation (900 g; RT; 10 min) and washed once in cold (4°C) cytomix. Afterwards the cells were resuspended in 400 μl cytomix and transferred to a 2 mm gap electroporation cuvette (BTX #45-0125) containing 10 μg of linearized DNA. The cells were transfected once in the BTX Electro Cell Manipulator 630 (1.2kV; 25 μF; 186 Ω; electrode distance = 0.2 cm) and subsequently transferred to a flask containing 10 ml SDM79 + 20% FCS. 200 μl of the cell suspension were transferred to the top row of a 96-well plate and a 1:1 serial dilution was performed by pipetting 100 μl to the row below containing 100 μl medium. The remaining cell suspension was kept as a pool in a sealed cap culture flask. After one doubling time (12-20h, depending on the cell line) 100 μl of medium containing the doubled concentration of antibiotics was added. Depending on the population doubling time of the strain, resistant clones could be detected after 10-20 days.

2.2.1.4.4 Genetic manipulation using CRISPR/Cas9

(Protocol provided by Emmanuel Tetaud, Bordeaux, unpublished)

Transfection buffer (Burkard <i>et al.</i> , 2007)	90 mM sodium phosphate, 5 mM potassium chloride, 0.15 mM calcium chloride, 50 mM HEPES, pH 7.3
--	--

The gRNA was designed using the online tool from EuPaGDT (<http://grna.ctegd.uga.edu/>). A 20 nt gRNA for SpCas9 with 3' NGG PAM motif, which showed high efficiency but no off-targets was selected. For the PKAC1/ double knock-out, a gRNA in the active site was chosen, which is redundant for PKAC1 and PKAC2. For generation of PEX14 phosphomutants, a gRNA as close as possible to the phosphosite was chosen. All necessary components for transfection were ordered from Integrated DNA technologies (IDT):

Product	Catalog #	Sequence
Alt-R CRISPR-Cas9 crRNA pkac1/2	Custom made	GATCGTACCTATACGTTATG (ordering without PAM)
Alt-R CRISPR-Cas9 crRNA pex14	Custom made	AAAGTAAACTAGTGTGACGC (ordering without PAM)
Alt-R CRISPR-Cas9 tracrRNA	1072533	Universal, not stated at IDT
Alt-R CRISPR S.p. Cas9 Nuclease V3	1081059	-

RNAs were solubilized to final concentration of 200 μ M in the buffer provided by IDT. The complex was assembled *in vitro* prior to transfection by mixing 2.5 μ l crRNA and 2.5 μ l tracrRNA in an RNase-free 1.5 ml reaction tube. The mixture was heated at 95°C for 5 min and subsequently cooled down to RT for 15 min. Afterwards, 3 μ l Cas9 nuclease were added and incubated at RT for 20 min. In the meantime, 2×10^6 cells were harvested by centrifugation (900 g; RT; 10 min) and washed once in PBS. Cells were resuspended in 100 μ l transfection buffer and mixed with the annealed crRNA-tracrRNA/Cas9 complex. Additionally, 5 μ g of repair template were added. Construction of repair templates is described in the cell line specifications in 2.1.4. The mixture of cells, CRISPR-Cas9 complex and repair template was transferred to a 2 mm gap transfection cuvette (BTX #45-0125) and transfected once using the Amaxa Nucleofector® IIb, program CD4+ T cells X-001. Afterwards, the cells were transferred to a culture flask containing 5 ml SDM79 + 20% FCS and incubated at 27°C overnight. After 16-20 h, selection antibiotics were added, and the cells were plated by 1:1 serial dilution: 100 μ l of transfected cells were pipetted into the top row of a 96-well plate and 50 μ l of medium was pipetted in the remaining rows. 50 μ l of cells were transferred to the row below, mixed and transferred to the next row until the end of the plate. Depending on the population doubling time of the strain, resistant clones could be detected after 10-20 days and were tested by gDNA extraction (described in 2.2.3.2), followed by ORF PCR. In the case of PKAC1/2 double knock-out, successfully modified clones would show no endogenous PKAC1 or PKAC2 ORF, but a disrupted one, which is increased in size by integration of the puromycin cassette. For the pex14 phosphomutants, successful modification removes an S_{pel} site and was therefore screened by PCR and enzymatic digestion. Promising clones were subjected to sequencing.

2.2.1.5 Differentiation of trypanosomes

2.2.1.5.1 BSF to PCF differentiation of pleomorphic cells

DTM (Vassella and Boshart, 1996; Ziegelbauer et al., 1990)	Supplements
33.3 mM HEPES, 116.4 mM NaCl, 5.4 mM KCl, 2.4 mM CaCl ₂ , 1 mM NaH ₂ PO ₄ , 811.5 μ M MgSO ₄ , 9.2 mM L-glutamine, 1.6 mM glutamate, 5.5 mM proline, 999.6 μ M sodium pyruvate, 4.1 μ M biotin, 9.9 mM glycerol, 10 mg/l phenol red, 1x MEM amino acid solution (Invitrogen/Gibco #11130), 1x MEM non-essential amino acids (Invitrogen/Gibco #11140), 1x MEM vitamin solution (Invitrogen/Gibco #11120) → pH set to 7.5, sterile filtered	100000 U/l penicillin, 100 mg/l streptomycin, 28.2 mg/l bathocuproine, 14 mg/l hypoxanthine, 182 mg/l hypoxanthin, 7.5 mg/l hemin, 15% (v/v) heat-inactivated FCS

To obtain short stumpy cells, BSF cultures were grown to a density of 5×10^5 cells/ml and afterwards incubated for another 36-40 h at 37°C, 5% CO₂ without further dilution.

The stumpy cells were harvested by centrifugation (1,400 g; RT; 10 min), resuspended in 5 ml DTM medium supplemented with 6 mM cis-aconitate, transferred to a sealed cap culture flask and shifted to 27°C. Differentiation into Procyclic cells occurred within 48-72 h, at this point the cells were transferred to SDM79 medium.

2.2.1.5.2 *In vitro* PCF to metacyclic differentiation by RBP6 overexpression

Differentiation from procyclics to metacyclics (*metacyclogenesis*) can be initiated *in vitro* by RBP6 overexpression (Kolev *et al.*, 2012). For metacyclogenesis, cells were adapted to glucose and glycerol-free SDM79 (-/-) for at least 4 days. Differentiation was initiated by RBP6 overexpression using 10 µg/ml tetracycline. Cultures were diluted on days 2 and 4 post-induction by mixing 6 ml culture with 4 ml fresh medium. Sampling was performed every 2 days over 8 days, including growth documentation, western blot sampling and methanol-fixation for DAPI staining. On days 0 and 4 post-induction, samples were taken for PFA-fixation and calflagin staining.

2.2.2 *E. coli*

2.2.2.1 Cultivation

LB medium	10 g/l tryptone, 10g/l NaCl, 5g/l yeast extract → autoclave for sterility
LB agarose plates	For agarose plates equal volumes of 2x autoclaved LB-medium were mixed with a melted 2x autoclaved agarose (30g/l) and ca. 30 ml aliquoted per plate

E. coli cells were generally grown in LB-medium supplemented with the appropriate antibiotics at 37°C.

2.2.2.2 Preparation of competent cells

Variant of (Hanahan *et al.*, 1991)

CCMB80 buffer	10 mM KOAc pH 7.0, 80 mM CaCl ₂ , 20 mM MnCl ₂ , 10 mM MgCl ₂ , 10% glycerol → sterile filtered and stored at 4°C
----------------------	--

Bacteria were picked from a glycerol stock, spread on an agarose plate, and inoculated at 37°C overnight to allow recovery and promote growth. The next evening 250 ml LB medium were inoculated with bacteria from that plate and allowed to grow to an OD₆₀₀ ~0.3 at 20°C. Cells were harvested at 3,000 g; 4°C for 10 min and resuspended in 80 ml CCMB80 buffer. After 20 min incubation on ice, the cells were centrifuged again at 3,000 g; 4°C for 10 min and resuspended in 10 ml CCMB80 buffer. The OD₆₀₀ of a 1:5 dilution was measured and diluted to OD₆₀₀ 1.0-1.5, if necessary. After 20 min incubation on ice, the cells were transferred to pre-chilled 1.5 ml microcentrifuge tubes in aliquots of 100 µl. Competent cells were frozen in liquid nitrogen and stored at -80°C.

2.2.2.3 Transformation

For transformation, 50 µl competent cells were used per reaction. They were thawed on ice and mixed with plasmid DNA (12-25 ng for ligations, 1 µl of plasmid preparation for re-transformation). The mixture was incubated on ice for 20 min and subjected to a 45 s heat-shock at 42°C. The cells were placed back on ice for 2 min. In the case of ampicillin selection (100 µg/ml), the cells were directly spread on agarose plates. In case of kanamycin selection (34 µg/ml), 950 µl LB-medium were added and the cells were incubated for 45 min at 37°C before plating.

2.2.3 Nucleic acids

2.2.3.1 Standard cloning procedures

2.2.3.1.1 Agarose gel electrophoresis

TAE buffer	40 mM Tris-acetate pH 8.3, 1 mM EDTA
-------------------	--------------------------------------

For most purposes, 1% agarose gels were prepared by melting the agarose powder in TAE buffer the microwave until completely dissolved. After the mixture was cooled down, 1 µg/ml ethidium bromide were added for DNA staining. Gels were run at 80 V for 15-30 min, depending on the necessary separation and visualized by UV illumination in the BioRad Geldoc 2000.

2.2.3.1.2 DNA amplification by PCR

If the PCR product was intended for use in a downstream application (cloning, transfection), PCR was performed using the Q5 High-Fidelity DNA Polymerase (NEB #M0491) according to the manufacturer's instructions. Annealing temperature was always calculated using NEB's Tm calculator (<https://tmcalculator.neb.com/>). PCR products for cloning were purified using High Yield PCR Clean-up/Gel extraction kit (SLG #30 HYDF300) according to the manufacturer's instructions. PCR products for transfection were purified by phenol-chloroform extraction (described in 2.2.1.4.1.2).

When the PCR product was only generated for analytical purposes (integration PCR, colony PCR), the reaction was performed using the GoTaq DNA Polymerase (Promega #M3001) according to the manufacturer's instructions.

2.2.3.1.3 DNA modification

Restriction digests were performed using NEB restriction enzymes according to the manufacturer's instructions. Digests were planned using NEB's online tool: <https://nebcloner.neb.com/#!/redigest>, paying attention to buffer requirements, incubation temperature and specificities of the respective enzymes.

When plasmid backbones were digested for cloning purposes, a simultaneous dephosphorylation was performed using Shrimp Alkaline Phosphatase (NEB, #M0371).

2.2.3.1.4 DNA extraction from agarose gel

Digested and dephosphorylated backbone fragments were separated by agarose gel electrophoresis (described in 2.2.3.1.1) and illuminated on a UV table with low intensity illumination. The required fragment was cut out of the gel using a scalpel and transferred to a 1.5 ml reaction tube. DNA extraction was performed with the High Yield PCR Clean-up/Gel extraction kit (SLG #30 HYDF300) according to the manufacturer's instructions.

2.2.3.1.5 Ligation

DNA fragments were ligated using the NEB T4 DNA ligase (NEB #M0202) according to the manufacturer's instructions. Usually, a vector to insert ratio of 1:3 was used, and the necessary amounts of DNA were calculated using the NEB online ligation calculator: <https://nebiocalculator.neb.com/#!/ligation>.

2.2.3.1.6 Isolation of plasmid DNA

Plasmids were usually isolated from *E. coli* cells by plasmid isolation kits (Promega PureYield™ Plasmid Miniprep (#A1223) or Midiprep (#A2492) system, depending on amount of DNA needed) according to the manufacturer's instructions.

If a lot of plasmids were isolated from small culture volumes at the same time, an alkaline lysis was performed (Green and Sambrook, 2016):

P1	50 mM Tris/Cl pH 8.0, 10 mM EDTA, 100 µg/ml RNase, store at 4°C
P2	0.1 M NaOH, 1% SDS
P3	1.5 M KOAc, 5% formic acid

2 ml of a dense overnight culture were harvested at 13,000 g for 1 min, the pellet was resuspended in 300 µl P1 buffer. Cells were lysed by addition of 300 µl P2 buffer and inverted about 6 times. Afterwards, 300 µl neutralization buffer were added and the mixture was inverted a few times. The precipitates were removed by centrifugation at 13,000 g for 3 min at RT and the supernatant transferred to a new 1.5 ml reaction tube. DNA was precipitated by addition of 630 µl isopropanol and inverted a few times. The precipitated DNA was pelleted at 13,000 g for 15 min and subsequently washed once with 1 ml 70% ethanol. DNA pellets were air-dried at 55 – 65°C in a heating block and resuspended in 50 µl H₂O.

2.2.3.1.7 Sequencing

Sequencing reactions were performed in-house in the sequencing service of the faculty of biology (<http://www.gi.bio.lmu.de/sequencing>) using the cycle, clean & run BigDye 3.1 protocol. The submitted samples were prepared according to the sequencing service's instructions.

2.2.3.2 Isolation of gDNA from *T. brucei*

Lysis buffer	50 mM Tris/Cl pH 8.0, 10 mM EDTA, 2% SDS
Precipitation buffer	8 M KOAc

For genomic DNA (gDNA) extraction, $1-2 \cdot 10^7$ cells were harvested by quick centrifugation at 8,000 g, RT for 30s. The pellet was resuspended in 200 μ l lysis buffer and incubated in a heating block at 65°C for 10 min. Afterwards, proteins were precipitated by addition of 40 μ l precipitation buffer, vortexed thoroughly and placed on ice for 3-5 min. Precipitates were removed by centrifugation at 11,000 g; RT for 5 min and the supernatant transferred to a new 1.5 ml reaction tube. DNA was precipitated by addition of 160 μ l isopropanol, followed by inversion of the tube. The DNA was pelleted at 14,100 g, RT for 2 min and washed once with 1 ml 70% ethanol. Pellets were dried at 65°C and the DNA solved in 50 μ l H₂O.

2.2.4 Proteins

2.2.4.1 Recombinant protein expression in *E. coli*

Terrific broth (TB)	12g/l tryptone, 24g/l yeast extract, 5g/l glycerol → autoclave → complete with 10% 10x TB salts
10x TB salts	0.17 M KH ₂ PO ₄ , 0.72 M K ₂ HPO ₄ , autoclaved

Plasmids were transformed in *E. coli* Rosetta on LB-agarose plates containing appropriate selection antibiotics and 50 μ g/ml chloramphenicol. A single colony was used to inoculate a 20 ml TB-medium and grown overnight at 37°C. The next morning, the OD₆₀₀ was measured, and the culture diluted to OD₆₀₀ = 0.0125 in 400 ml TB-medium. Cells were grown to a density of OD₆₀₀ ~0.8 at 37°C. After that, the temperature was lowered to 18°C and the culture was cooled down for 30 min. Recombinant protein expression was induced with 0.5 – 1 mM IPTG overnight. The cells were then harvested at 4,000 g; 4°C for 10 min and either directly subjected to protein purification or the pellets frozen at -80°C

2.2.4.2 Purification of recombinant proteins

2.2.4.2.1 PKAC subunits from *E. coli* inclusion bodies

(Adapted from application note of amersham pharmacia)

Lysis buffer	20 mM Tris/Cl pH 8.0, 0.1 µg/ml DNase, 1 mM PMSF (DNase and PMSF added fresh)
Wash buffer	20 mM Tris/Cl pH 8.0, 0.5 M NaCl, 2 M urea, 2% Triton X-100
Extraction buffer	20 mM Tris/Cl pH 8.0, 0.5 M NaCl, 6 M guanidinium hydrochloride, 1 M β-mercaptoethanol
Storage buffer	20 mM Tris/Cl pH 8.0, 0.5 M NaCl, 6 M urea, 1 mM β-mercaptoethanol

The pellet from a 400 ml culture was resuspended in 30 ml lysis buffer and lysed by passing through the French press twice at a maximum pressure of 1,500 psi. The lysate was incubated on ice for 10 min to allow DNA degradation by DNase. Afterwards, the lysate was cleared by centrifugation at 10,000 g; 4°C for 10 min. The pellet containing the inclusion bodies and hence the recombinant protein, was washed twice in 10 ml wash buffer by gentle resuspending and sonication (Diagenode Bioruptor, 1-2x 30s on ice). Finally, the inclusion bodies were solubilized in 5-10 ml extraction buffer, depending on the size of the pellet. Solubilization was promoted by 1h incubation at RT with gentle agitation. The final preparation was cleared by centrifugation at 15,000 g; 4°C for 10 min and passed through a 0.45 µm filter. Since guanidinium hydrochloride precipitates in the presence of SDS and therefore interferes with SDS-PAGE, a buffer exchange was performed using a PD10 column as described by the manufacturer's instructions. Alternatively, the samples were diluted 1:10 prior to SDS-PAGE.

2.2.4.2.2 Purification of PKAR from *E. coli* by His-trap column

Binding/washing buffer	250 mM NaH ₂ PO ₄ , 300 mM NaCl, 40 mM imidazole, pH 8.0
Lysis buffer	250 mM NaH ₂ PO ₄ , 300 mM NaCl, 40 mM imidazole, pH 8.0, 1 mM PMSF, 10 µg/ml DNase
Elution buffer	250 mM NaH ₂ PO ₄ , 300 mM NaCl, 250 mM imidazole, pH 8.0

The pellet from a 400 ml culture was resuspended in 30 ml lysis buffer and passed twice through French press at a maximum pressure of 1,500 psi. The lysate was cleared by centrifugation at 10,000 g; 4°C for 10 min. A gravity flow Ni-NTA column was prepared by packing with 2 ml of bead slurry (PureCube Ni-NTA agarose from Cube-Biotech) and equilibrated with 10 ml of binding/washing buffer. The lysate was added to the column and incubated for 10 min before collecting the flow-through. The column was washed with 60 ml binding/washing buffer and PKAR was eluted in 6x 1 ml elution buffer. Elutions were stored at 4°C until further use.

2.2.4.3 Affinity purification of antibodies

Based on (Olmsted, 1981)

Staining solution	1% PonceauS in 1% acetic acids
Blocking solution	5% skimmed milk powder in PBS
Elution buffer	0.2 M glycine, 1 mM EGTA, pH 2.2

Affinity purification of PKA antibodies is performed to improve specificity on whole cell lysate detection. 300 µg recombinant protein containing the antibodies antigen were loaded onto a single-well SDS gel. After successful separation (described in 2.2.4.8), the protein was blotted onto a PVDF membrane (described in 2.2.4.10) and stained with 1% PonceauS in 1% acetic acid. The protein band was carefully cut out, transferred to a 15 ml centrifuge tube and destained with H₂O. The stripe was blocked with 5% milk in PBS for 1h at RT. Afterwards, the stripe was rinsed thrice with PBS, followed by 3 washes of 5 min. For the affinity purification, 1-2 ml of antisera were added to the protein stripe and incubated either for 4h at RT or at 4°C overnight. The stripe was washed again as described before and the antibody eluted in 1 ml elution buffer for 10 min. The eluted antibody was transferred to a new 1.5 ml reaction tube, the pH was neutralized by addition of 200 µl 1M tris/Cl pH 8.0 and 200 µg BSA were added for stabilization of the antibody. The purified antibody was dialyzed against PBS overnight, exchanging the buffer thrice. After dialysis, NaN₃ was added at a final concentration of 0.02% for preservation and the antibodies stored at 4°C.

2.2.4.4 Generation of anti-PKAC3 antibody

For generation of a new PKAC3 antibody, a 6x-his-tagged version of the full-length protein was expressed from pETM11-6xHis-TEV-PKAC3 (pKM051) (described in 2.2.4.1) and purified from inclusion bodies as described in 2.2.4.2.1. The protein concentration was estimated by nanodrop measurement and diluted to 2 mg/ml. To refold the protein, a buffer exchange was performed against 50 mM Tris pH 6.0, 9.6 mM NaCl, 0.4 mM KCl, 1 mM EDTA, 0.4 M sucrose, 0.75 M guanidinium chloride, 0.1 % Triton X-100 by dialysis overnight, including three buffer exchanges. Protein preparations from three purifications were pooled and precipitates were removed by centrifugation at 15,000 g; 4°C for 10 min. Concentration of the dialyzed protein was determined by Bradford assay as described in 2.2.4.5.3. A total of 2.2 mg at a concentration of 0.65 mg/ml was sent for immunization to ProteoGenix, France. The protein was used to immunize two rabbits for 51 days.

2.2.4.5 Protein quantification

2.2.4.5.1 Nanodrop

For quick protein estimation of highly concentrated samples, the nanodrop ND-1000 was used and concentration was determined based on A₂₈₀ absorbance.

2.2.4.5.2 On SDS-gel

For determination of low protein concentrations or proteins with impurities, a BSA standard was prepared and amounts of 100 – 1,000 ng were loaded on an SDS-gel

along with the protein, whose concentration should be determined. The proteins were separated (described in 2.2.4.8) and the gel stained with colloidal Coomassie as described in 2.2.4.9. The gel was scanned in the LI-COR Odyssey® CLx and the bands of BSA and the protein of interest were quantified. The intensities of BSA were plotted against the protein amount in a linear standard curve. The protein concentration of the protein of interest was determined using the standard curve's formula.

2.2.4.5.3 Bradford assay

For determination of low protein concentrations or complex protein mixtures (cell lysates, cell fractionations) a Bradford assay was chosen. A BSA standard was prepared and performed in 1 ml photometer cuvettes. The standard was usually prepared in the range of 100 – 1,500 ng BSA/cuvette in a volume of 800 µl H₂O, along with samples for protein quantification. Here between 1-10 µl were used, depending on the expected concentration. Afterwards, 200 µl Bradford reagent (Sigma Cat.# B6916) were added to each cuvette and mixed by pipetting up and down. Samples were incubated for 5-60 min and absorbance was measured at OD₅₉₅. The absorbance of BSA was plotted against the protein amount in a linear standard curve. The protein concentration of the protein of interest was determined using the standard curve's formula.

2.2.4.5.4 BCA assay

The BCA assay (Pierce™ Cat. #23225) was used for protein quantification before (phospho-) proteomics. The assay was performed as described by the manufacturer.

2.2.4.6 Absolute quantification of PKA subunits in *T. brucei* lysates

For absolute quantification of PKA amounts in *T. brucei*, recombinant PKAC1, PKAC3 and PKAR were expressed and purified as described in 2.2.4.2.1 and 2.2.4.2.2, respectively. Protein concentration in the final elution was determined in quadruplicate using a BSA standard on SDS-PAGE as described in 2.2.4.5.3. The recombinant protein was used to generate a subunit-specific protein standard curve ranging from 2-50 ng (PKAR/PKAC1) and 0.2-5 ng (PKAC3). The different protein amounts were loaded on an SDS-gel along with 2×10^6 cells from BSF and PCF trypanosomes. After western blotting, the proteins were stained with PKA-specific antibodies, scanned in the LI-COR Odyssey® CLx and quantified using LI-Cor Image StudioLite. The standard curve was converted from ng to molecule numbers using the formula: molecules = $NA \cdot ((ng/10^9)/M)$, NA being the Avogadro constant and M the molecular weight of the recombinant proteins including the tags. Molecule numbers of PKAR, PKAC1 and PKAC3 were determined from the standard curve and divided by the cell number to

obtain molecules/cell. The western blots and quantifications were performed in triplicate and plotted as average \pm stdev.

2.2.4.7 Preparation of *T. brucei* lysates for SDS-PAGE

6x SDS loading buffer (Laemmli buffer)	350 mM Tris/HCl pH 6.8, 30 % (v/v) glycerol, 10 % (w/v) SDS, 0.6 M DTT, 0.06 % (w/v) bromphenolblue
---	---

For each sample, 10^7 cells were harvested by centrifugation (1,400g BSF/900g PCF; 10 min; RT), washed once in PBS and transferred to a 1.5 ml reaction tube. The cells were harvested by centrifugation (8,000g; 30s; RT) and the supernatant was removed quantitatively. The cell pellet was resuspended in 33 μ l 1.5 x SDS loading buffer.

2.2.4.8 SDS-PAGE

6x SDS loading buffer (Laemmli buffer)	350 mM Tris/HCl pH 6.8, 30 % (v/v) glycerol, 10 % (w/v) SDS, 0.6 M DTT, 0.06 % (w/v) bromphenolblue
Separating gel (10%)	1.5 ml separating gel buffer (1.5 M Tris/HCl pH 8.8, 0.4 % (w/v) SDS), 2 ml acrylamide/bisacrylamide 37, 5:1, 2.5 ml H ₂ O, 20 μ l 10% (w/v) APS, 4 μ l TEMED
Separating gel (12%)	1.5 ml separating gel buffer (1.5 M Tris/HCl pH 8.8, 0.4 % (w/v) SDS), 2.4 ml acrylamide/bisacrylamide 37, 5:1, 1.9 ml H ₂ O, 20 μ l 10% (w/v) APS, 4 μ l TEMED
Stacking gel	0.75 ml stacking gel buffer (0.5 M Tris/HCl pH 6.8, 0.4 % (w/v) SDS), 0.39 ml acrylamide/bisacrylamide 37, 5:1, 1.85 ml H ₂ O; 22.5 μ l 10 % (w/v) APS, 4.5 μ l TEMED
10x electrophoresis running buffer	0.25 M Tris, 1.96 M glycine, 1 % (w/v) SDS \rightarrow diluted to 1x before use

Protein samples and cell lysates were mixed with 6x SDS loading buffer and denatured for 5 min at 95°C prior to SDS-gel loading. Gels were usually cast freshly before use. Proteins and size marker (NEB #P7706 or NEB #P7718) were separated at 30 mA/gel in Biorad Mini-PROTEAN Tetra vertical electrophoresis chambers.

2.2.4.9 Coomassie staining of SDS gels

Colloidal Coomassie	75 mM aluminium sulfate (18) hydrate, 10% EtOH, 0.02% Coomassie brilliant Blue G250, 2.35% orthophosphoric acid
----------------------------	---

Proteins were separated as described in 2.2.4.8. The gels were washed in H₂O for 10 min with gently agitation. Protein bands were stained with Colloidal Coomassie overnight and gels were destained with H₂O until the background became clear.

2.2.4.10 Western blot analysis

10x PBS	1.37 M NaCl; 27 mM KCl; 43 mM Na ₂ HPO ₄ /14 mM KH ₂ PO ₄ \rightarrow dilute stocks to 1x before use
10x TBS	200 mM Tris/Cl pH 7.6, 1.37 M NaCl \rightarrow dilute stocks to 1x before use
Anode buffer	300 mM Tris HCl (pH 10.4); 20 % (v/v) MeOH
Cathode buffer	25 mM Tris HCl (pH 7.6); 40 mM ϵ -aminop cypronic acid; 20 % (v/v) MeOH

Proteins separated by SDS-PAGE were transferred to a PVDF membrane (Immobilon-FL #IPFL00010) by semi-dry western blotting. The membrane was activated by 30s

incubation in 100% methanol and afterwards equilibrated in H₂O. The blotting “sandwich” was assembled as follows (bottom to top): three whatman papers (Machery Nagel #742118) soaked in anode buffer, PVFD membrane, SDS-gel, two whatman papers soaked in cathode buffer. Air bubbles and excess buffer were removed by rolling over the assembly with light pressure. The transfer was performed at 0.1 A for 70 min in BioRad’s Trans-Blot Turbo system. After blotting, the membrane was transferred to a 50 ml centrifuge tube with the protein side facing inwards. The membrane was blocked for 1h in 5% milk in PBS for standard antibodies and 5% milk in TBS for phosphoantibodies. Afterwards the membrane was incubated with the primary antibody in 1% milk in 0.1% (v/v) PBS-Tween (exceptions are listed in table 2.1.5) for either 1h at RT or 4°C overnight. Unspecifically bound antibody was washed away during 4 washes of 5 min with 0.2% (v/v) PBS-Tween. Secondary antibody incubation was performed in 1% milk in 0.1% PBS-Tween, 0.02% (w/v) SDS for 1h in the dark. After 4 x 5 min washes in 0.2% PBS-Tween, the membrane was briefly rinsed in H₂O and dried between two whatman papers. The signal was detected using the LI-COR Odyssey® CLx. Blots were quantified in the LI-COR Image Studio Lite software. The background was subtracted around the respective band using the median method.

2.2.4.11 Immunoprecipitation by GFP-trap

Adapted from Chromotek

RIPA buffer	10 mM Tris/Cl pH 7.4, 150 mM NaCl, 0.5 mM EDTA, 0.1% SDS, 1% NP40, 1% SDC
Dilution buffer	10 mM Tris/Cl pH 7.5, 150 mM NaCl, 0.5 mM EDTA
Wash buffer	10 mM Tris/Cl pH 7.5, 150 mM NaCl, 0.5 mM EDTA, 0.4% NP40

For each pull-down, 2×10^8 cells were harvested by centrifugation (900 g; 10 min; RT) and washed twice with serum-free SDM79. During the second wash, the cells were transferred to a 1.5 ml reaction tube and spun down at 8,000 g for 30s. The pellet was resuspended in 400 µl RIPA buffer supplemented with cOmplete EDTA-free protease inhibitor cocktail (Roche #4693132001) and PhosStop (Roche #4906845001). Cells were incubated on ice for 30 min and afterwards sonicated on ice for 2x 30s in the Diagenode Bioruptor. The lysate was cleared by centrifugation at 20,000 g; 4°C for 10 min. The cleared lysate was diluted with 600 µl dilution buffer supplemented with protease and phosphatase inhibitors. Magnetic GFP-trap agarose beads (Chromotek #gtma-10) were equilibrated in 3 x 500 µl dilution buffer. 25 µl beads were added to the lysate per immunoprecipitation reaction and incubated at 4°C for 1h in an overhead rotator. Unbound proteins were separated using a magnetic stand. The beads were washed 4 x in 500 µl wash buffer, followed by 4 washes in 500 µl dilution buffer. During the last step, beads were transferred to a new 1.5 ml reaction tube to prevent elution

of proteins sticking to the tube. Finally, proteins were resuspended in 80 μ l 2x SDS loading buffer (=12.5x compared to input) and eluted for 10 min at 95°C.

2.2.5 Cell fractionations

STE buffer	250 mM sucrose, 25 mM Tris/Cl pH 7.4, 1 mM EDTA
6x SDS loading buffer (Laemmli buffer)	350 mM Tris/HCl pH 6.8, 30 % (v/v) glycerol, 10 % (w/v) SDS, 0.6 M DTT, 0.06 % (w/v) bromphenolblue

2.2.5.1 Glycosome enrichment by differential centrifugation

(Protocol kindly provided by F. Bringaud and slightly modified)

For glycosome enrichment, $4 \cdot 10^9 - 10^{10}$ cells were harvested by centrifugation (900 g; 10 min; RT) and washed once in STE buffer. The pellet (~1 g wet weight) was resuspended in ca. 500 μ l STE buffer supplemented with protease inhibitor cocktail (Roche #4693132001) and transferred to a mortar. Cells were ground in the mortar with 0.5 g silicon carbide/g cell pellet until ca. 90 % of cells were lysed. The mixture was resuspended in 7 ml STE buffer containing protease inhibitor and subjected to differential centrifugation. The first centrifugation step (1.000 g; 4°C; 10 min) removed intact cells and nuclei. The supernatant was transferred in a fresh tube and the mitochondria were removed at 5.000 g; 4°C; 10 min. The supernatant of the second step was transferred again in a fresh tube and the glycosomes were enriched in the pellet at 42.000 g; 4°C; 10 min. This pellet was washed once in 1 ml STE buffer and the glycosomes finally resuspended in 200 μ l STE buffer. This method enriches mainly for glycosomes, but the final preparation also contains flagella and traces of mitochondria and the endoplasmic reticulum (ER). Due to that, additional purification steps were employed, depending on the scientific question.

2.2.5.2 Glycosome purification by Optiprep density gradient

Ultracentrifugation through an Optiprep density gradient was used to separate glycosomes and flagella from such contaminants as mitochondria and ER. Therefore, the differential centrifugation was performed as described in the previous paragraph with the following exceptions: Cells were resuspended in 2 ml STE buffer supplemented with protease inhibitor cocktail and the protocol was only employed until the 5.000 g centrifugation step. In the meantime, the discontinuous Optiprep density gradient was prepared in a polypropylene ultracentrifuge tube (Beckman Coulter #331374) by layering 2 ml of a 50%, 40%, 34% and 28% (bottom to top) Optiprep (Nycomed pharma #1030061) in STE. The 5.000 g supernatant was loaded on top of the gradient and ultracentrifuged for 12h at 150.000 g (34.500 rpm); 4°C; ACCEL 8; DECEL 8 in the TH-641 rotor of the UC WX Ultra90 Sorval ultracentrifuge. After centrifugation, two

bands were distinguishable. The upper band contains cellular contaminants, while the lower band contains pure glycosomes and flagella. The lower band was aspirated with a syringe by puncturing the centrifuge tube and transferred to a 1.5 ml reaction tube. If the material was needed for protease protection assay, the glycosomes and flagella were centrifuged at maximum speed, 4°C for 15 min in a microcentrifuge and resuspended in 50-100 µl STE buffer.

2.2.5.3 Glycosome purification by sucrose density gradient

Two methods were used to separate glycosomes from flagella following the Optiprep density gradient. The first method was a second density gradient using sucrose. For that, the recovered Optiprep band corresponding to glycosomes and flagella was loaded on a discontinuous sucrose density gradient. The density gradient was prepared by layering of 2 ml of a 2M, 1.85M, 1.75M and 1.7M sucrose in STE solution in a polypropylene ultracentrifuge tube (Beckman Coulter #331374) and the barriers of the layers were marked on the tube. Centrifugation was performed at 150.000 g (34.500 rpm) at 4°C; ACCEL 8; DECEL 8 for 12 h in the TH-641 rotor in the UC WX Ultra90 Sorval ultracentrifuge. Afterwards, samples of all interfaces were collected by aspiration with a syringe. The fractions were concentrated by methanol precipitation: 400 µl fraction were transferred to 1.600 µl cold methanol in a 2 ml reaction tube and vortexed. Proteins were precipitated at 4°C for at least 4 h or overnight. Precipitated proteins were centrifuged at 13.000 g; 4°C for 15 min and the supernatant discarded. The pellets were air dried under the fume hood and resuspended in 40 µl 1.5 x SDS loading buffer (= 10x concentrated). Migration pattern of the protein of interest was compared to that of glycosomal and flagellar marker proteins.

2.2.5.4 Protease protection assay of glycosome enriched fractions

Based on (Francisco et al., 2017)

Another way of separating glycosomes from flagella was by protease digestion. While glycosomal proteins are protected within the organelle from protease digestion, flagellar proteins are quickly degraded. Glycosomal preparations were diluted to 1 µg/µl in STE buffer. A control without proteinase K (-PK) was used as a reference for undigested proteins. Triton X-100 was added to solubilize organelles and control for digestibility of the protein of interest. The reaction was assembled on ice as described in the following table:

Reagent	Final concentration	-PK	+PK	+PK +TX-100
Organelles	50 µl/reaction (ca. 50 µg)	50 µl	50 µl	50 µl
20% Triton X-100	1%	-	-	2.5 µl
10 mg/ml Proteinase K	100 µg/ml	-	0.5 µl	0.5 µl

The reaction was incubated on ice up to 6h, depending on the experiment. Afterwards, 50 µl samples were collected and transferred to tubes containing 0.5 µl PMSF (50 mg/ml in EtOH) to inactivate proteinase K and incubated on ice for 2 min. Proteins were precipitated by addition of 5.5 µl 100% (w/v) TCA, vortexed and incubated on ice for at least 30 min. Afterwards, samples were centrifuged at 11.300 g; 4°C for 15 min and the pellets washed in 1 ml 100% acetone. The acetone was removed quantitatively, and the pellets dried at 37°C. They were resuspended in 50 µl 1.5 x SDS loading buffer and 20 µl was used for western blot analysis.

2.2.5.5 Preparation of glycosome enriched fractions for proteomics

MS-buffer	100 mM Tris/Cl pH 7.8, 2% SDS, 50 mM DTT
------------------	--

For proteomic analysis 10^9 cells were harvested by centrifugation (15 min; 900g; 4°C) and subsequently washed once in STE buffer (+/- glycerol). The pellets were resuspended in approx. 500 µl lysis buffer (STE supplemented with protease inhibitor cocktail) and transferred to a mortar. Cells were ground in the mortar with 0.2-0.3 g silicon carbide (SiC) until 90% were lysed. Lysates were transferred to a 2 ml reaction tube in a final volume of 2 ml. Unlysed cells, nuclei and SiC were removed at 1,000g; 10 min; 4°C. The supernatant was transferred to a fresh tube and centrifuged for 10 min at 5,000g; 4°C to remove the mitochondrial fraction. The resulting supernatant was centrifuged at maximum speed (20,627g); 4°C for 10 min to obtain a glycosome enriched fraction. This pellet was washed once in 1 ml STE buffer (+/- glycerol) and resuspended in 50 µl MS- buffer. Samples were denatured at 95°C for 5 min followed by 5 min sonication (30s on/off cycles). Protein concentration was determined by Bradford assay (2.2.4.5.3) and 10 µg protein were submitted for proteomic analysis by the Proteomics core facility of the LMU biocentre.

MaxQuant Analysis

(done by Ignasi Forne, LMU biocenter, Proteomics Core facility)

Protein identification and label-free quantification (LFQ) was performed using MaxQuant 2.0.1.0 (Tyanova et al., 2016a) against the TriTrypDB-56_Tbrucei TREU927_AnnotatedProteins database obtained from tritrypdb.org including the following parameters: MS tol 20 ppm, MS/MS tol 0.5 Da, peptide FDR 0.01, protein FDR 0.01, Min. peptide length 7, variable modifications Oxidation (M), Acetyl (Protein N-term), fixed modification Carbamidomethyl (C), Trypsin/P digestion, max 2 missed cleavages, Peptides for protein quantification razor and unique, Min. peptides 1, Min. peptide count 1.

Perseus statistical analysis

The proteingroups.txt file was loaded into Perseus version 1.6.2.3 with LFQ intensities as main columns. Sequences were filtered for reverse sequences, contaminants and proteins only identified by site. Groups were defined for wild type and PEX14 phosphomutants cultured in presence or absence of glycerol. The data was log₂ transformed and filtered based on valid values (at least 3 of 4 replicates within one group). Missing values were imputed from normal distribution using the default parameters. Afterwards, we filtered for glycosomal proteins using the consensus of a predefined list obtained from Frederic Bringauid (Bordeaux) and the (Guther *et al.*, 2014) glycosomal proteome. Sample groups were compared using a student's t-test with the FDR = 0.05 and $S_0 = 0.5$. Normalization by Z-score was performed before clustering analyses. Only proteins with a fold-change of at least 1.5 were considered as potentially interesting.

2.2.6 Microscopy

2.2.6.1 Methanol fixation

For methanol-fixation, 10^7 cells were harvested by centrifugation (900 g; 10 min; RT) and resuspended in 50 μ l PBS. A drop of 10 μ l was placed on the edge of a microscope slide and spread using a second slide. The slides were air dried and afterwards placed in 100% ice-cold methanol at -20°C for up to 10 days. This method was used for DAPI DNA staining and subsequent Trypanosome staging.

2.2.6.2 PFA-fixation

For fixation in paraformaldehyde, 10^7 cells were harvested by centrifugation (900 g; 10 min; RT) and resuspended in 200 μ l PBS. The same volume of 4% PFA in PBS was added to the cells and they were incubated for 5 min at RT. Afterwards, the fixed cells were washed 3 times in 1 ml PBS and finally resuspended in 50 μ l. This method was used for imaging of fluorophore tagged lines and immunofluorescence stainings.

2.2.6.3 Trypanosoma staging (RBP6)

Mounting dium	me-	4% n-propyl-gallate in 90% glycerol in PBS
----------------------	------------	--

After induction of metacyclogenesis by RBP6 overexpression, trypanosomes were categorized into procyclic, epimastigote and metacyclic based on morphology and kinetoplast positioning. Therefore, methanol-fixed samples were rehydrated in PBS for 15 min and afterwards stained with 0.1 ng/ μ l DAPI in PBS for 5 min. The slides were washed 3x in PBS and rinsed in H₂O. Finally, a drop of mounting medium was placed on the slide, covered with a cover slip and sealed with nail polish. Images of each slide

were taken using the Leica DM750 microscope and Leica Application Suite V4 Software. For each time-point, 100-300 cells were staged: in procyclic cells the kinetoplast is positioned posterior to the nucleus, in epimastigotes it is positioned either on top or anterior to the nucleus. In metacyclic cells, the kinetoplast is positioned at the extreme posterior pole of the cell.

2.2.6.4 Imaging of GFP-tagged lines

For microscopic analysis of GFP-tagged protein localization, 5×10^6 – 10^7 cells were fixed with PFA as described in 2.2.6.2. Stacks were imaged with the DeltaVision using the “green” filter set with an illumination of 100% for 0.15-0.2 s exposure time and afterwards assembles using Fiji. For fluorescent channels and POL, the option “max intensity” and “average” was chosen, respectively.

2.2.7 *In vivo* cellular assays

2.2.7.1 Glycerol-depletion assay

SDM79 -/- (free of glycolytic carbon sources)	91 mM sodium pyruvate, 50 mM l-threonine, 265 μ M l-proline, 200 mM l-glutamine, 2.6 mM NaHCO ₃ , 7.5 mg/l hemin, 100000 U/l penicillin, 100 mg/l streptomycin, 50 mM N-acetylglucosamine, 10 % heat-inactivated FCS
SDM79 +/- (glucose-free)	91 mM sodium pyruvate, 50 mM l-threonine, 265 μ M l-proline, 200 mM l-glutamine, 2.6 mM NaHCO ₃ , 7.5 mg/l hemin, 100000 U/l penicillin, 100 mg/l streptomycin, 50 mM N-acetylglucosamine, 10 mM glycerol, 10 % heat-inactivated FCS
6x SDS loading buffer	350 mM Tris/HCl pH 6.8, 30 % (v/v) glycerol, 10 % (w/v) SDS, 0.6 M DTT, 0.06 % (w/v) bromphenolblue

Cells were cultured in SDM79 supplemented with 10 mM glycerol and 50 mM N-acetylglucosamine for at least three days prior to the assay. The cell density was kept below 8×10^6 cells/ml before the assay to avoid density-dependent glycerol-depletion. For each sample, 10^7 cells were harvested by centrifugation (900 g; 10 min; RT) and washed once in either 1 ml SDM79 + glycerol or SDM79 -glycerol. After the wash, cells were harvested at 8,000g; RT for 30s and resuspended in 100 μ l SDM79 +/- glycerol. Cells were incubated at 27°C for 1h. Afterwards, they were harvested by centrifugation (8,000g; RT; 30s) and resuspended in 33 μ l 1x SDS loading buffer. Samples were denatured at 95°C for 5 min and sonicated for 5 min (30s on/off cycles, Diagenode Bioruptor). For each sample, 6×10^6 cells were loaded and RXXS*/T* phosphorylation was detected by western blot using the anti-PKA substrate antibody (CST #9621).

2.2.7.2 Glycerol-depletion phosphoproteome

The phosphoproteomic experiment described here resulted in multiple useful datasets (Figure 7). Comparison of wild-type and Δ PKAC2 sites before and after glycerol-depletion yielded phosphorylation sites regulated by glycerol. By comparison of these two lists, PKAC2-dependent phosphorylations can be extracted. This data is described in

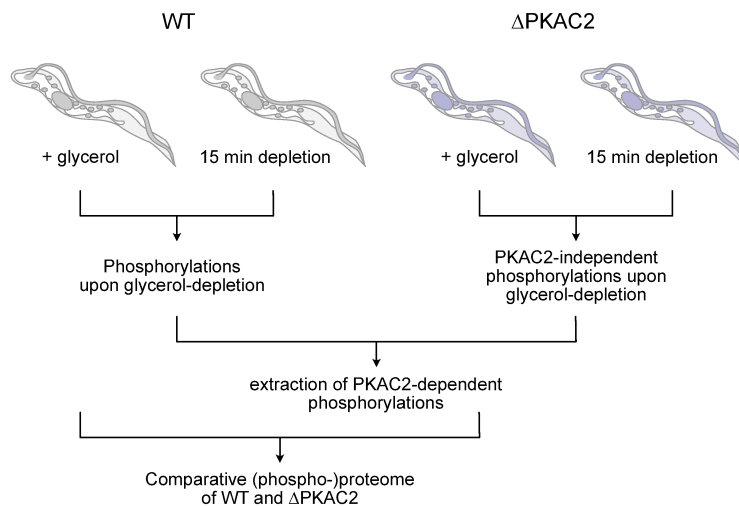


Figure 7: Data sets obtained from glycerol-depletion (phospho-) proteome. 15-minute glycerol-depletion was performed in wildtype and PKAC2 knockout. Comparison of +/- glycerol samples will yield phosphorylation sites regulated by glycerol in both cell lines. Comparison of these sites shows PKAC2-dependent sites. Comparison of wildtype and PKAC2 knockout under + glycerol gives a comparative proteome and phosphoproteome.

chapter 3.4.2.2.3. Furthermore, comparison wild-type and Δ PKAC2 proteome and phosphoproteome can give insight into PKAC2 targets and functions and is described in chapters 3.3.1 and 3.3.2.

2.2.7.2.1 Assay

SDM79 -/- (free of glycolytic carbon sources)	91 mM sodium pyruvate, 50 mM l-threonine, 265 μ M l-proline, 200 mM l-glutamine, 2.6 mM NaHCO_3 , 7.5 mg/l hemin, 100000 U/l penicillin, 100 mg/l streptomycin, 50 mM N-acetylglucosamine, 10 % heat-inactivated FCS
SDM79 +/- (glucose-free)	91 mM sodium pyruvate, 50 mM l-threonine, 265 μ M l-proline, 200 mM l-glutamine, 2.6 mM NaHCO_3 , 7.5 mg/l hemin, 100000 U/l penicillin, 100 mg/l streptomycin, 50 mM N-acetylglucosamine, 10 mM glycerol, 10 % heat-inactivated FCS
SDC buffer	4% Sodium deoxycholate, 100 mM Tris/Cl pH 8.5 (prepared fresh)
6x SDS loading buffer	350 mM Tris/HCl pH 6.8, 30 % (v/v) glycerol, 10 % (w/v) SDS, 0.6 M DTT, 0.06 % (w/v) bromphenolblue
Urea buffer	8 M urea, 100 mM Tris/Cl pH 8.5

Cells were grown in SDM79 +/- to a density of $1-2 \times 10^7$ cells/ml in 4 individual cultures. For each sample, 2.5×10^8 cells were harvested by centrifugation (900g; 27°C; 10 min) and washed once in either FCS-free SDM79 +/- (control) or FCS-free SDM79 -/- (depletion). The cells were transferred to a 1.5 ml reaction tube, centrifuged at 8,000g; RT for 20s and resuspended in 1 ml FCS-free SDM79 +/- or -/-. Samples were incubated at 27°C for 15 min. An 80 μ l sample was taken for western blot analysis, harvested by centrifugation (8,000g; RT; 20s) and resuspended in 66 μ l 1.5x SDS loading buffer, 40 μ l were incubated for 1h and processed identically with the exception that they were resuspended in 33 μ l 1.5 x SDS loading buffer. For mass-spectrometry, 850 μ l were

harvested by centrifugation (8,000g; RT; 20s) and resuspended in 300 µl SDC buffer. The samples were immediately boiled at 95°C for 5 minutes and subsequently sonicated for 5 min on ice (30s on/off cycle in Diagenode Bioruptor). 275 µl were transferred to a fresh tube and frozen at -80°C until further use. For protein quantification, 10 µl were transferred to 190 µl urea buffer and quantified using the Pierce™ BCA Protein assay kit (Thermo Scientific #23227) according to manufacturer's instructions. All samples were diluted to the same concentration in 270 µl SDC buffer prior to sample preparation for mass spectrometry.

2.2.7.2.2 Sample preparation for mass spectrometry

Reduction/alkylation buffer	100 mM Tris(2-carboxyethyl)phosphine hydrochloride TCEP, 400 mM 2-chloroacetamide pH 7-8 adjusted with KOH
EP (EasyPhos) loading buffer	6 % (v/v) Trifluoroacetic acid (TFA), 80 % (v/v) acetonitrile (ACN)
EP enrichment buffer	48 % (v/v) TFA, 8 mM KH ₂ PO ₄
EP wash buffer	5 % (v/v) TFA, 60 % (v/v) isopropanol (ISO)
EP transfer buffer	0.1 % (v/v) TFA, 60 % (v/v) ISO
EP elution buffer	200 µl ammonia solution (NH ₄ OH) to 400 µl 40 % (v/v) ACN (prepared fresh)
SDB-RPS loading buffer	1 % (v/v) TFA in ISO
SDB-RPS wash buffer 1	1 % (v/v) TFA in ISO
SDB-RPS wash buffer 2	0.2 % (v/v) TFA in 60 % (v/v) ACN
SDB-RPS elution buffer	20 µl ammonia (NH ₄ OH) to 4 ml 60 % (v/v) ACN (prepared fresh)
MS loading buffer	0.3 % (v/v) TFA, 2 % (v/v) ACN

Phosphopeptide enrichment was performed as described in (Humphrey et al., 2018). Briefly, samples of 2.6 mg/ml protein (700 µg in total) were reduced and alkylated for 5 min at 45°C, 1,500 rpm and subsequently digested overnight at 37°C with LysC and trypsin at an enzyme to protein ratio of 1:100. For Phosphopeptide enrichment, samples were thoroughly mixed with 400 µl ISO. After addition of 100 µl EP buffer, precipitates were removed at 2,000 g; RT; 15 min. Phosphopeptides were enriched using 5 mg TiO₂ beads resuspended in 5 µl EP loading buffer for 5 min at 40°C; 2,000 rpm. Beads were washed 5x in 1 ml EP wash buffer and pelleted at 2,000 g; RT for 1 min. Finally, they were resuspended in 75 µl EP elution buffer, transferred to a C8 stage tip and eluted in 2 x 30 µl EP elution buffer. Phosphopeptides were dried in a SpeedVac at 45°C to a volume of ~15 µl.

Afterwards the enriched phosphopeptides as well as the proteome samples were de-salted: 100 µl SDB-RPS loading buffer was added, samples transferred to an SDB-RPS stage tip and centrifuged at 1,500 g; RT to dryness (ca. 8 min). The stage tips were washed with 100 µl SDB-RPS wash buffer 1 and subsequently with SDB-RPS wash buffer 2 and centrifuged to dryness at 1,500 g; RT. The (phospho-)peptides were eluted in 60 µl SDB-RPS elution buffer and concentrated to dryness at 40°C in a

SpeedVac. Samples were resuspended in 15 μ l MS loading buffer and submitted to the Proteomics core facility in the LMU biomedical center.

2.2.7.2.3 MS data analysis

MaxQuant

(Done by Ignasi Forne, proteomics core facility, LMU BMC)

Protein identification and label-free quantification (LFQ) was performed using MaxQuant 1.6.14.0 (Tyanova *et al.*, 2016a) against the TriTrypDB-46_Tbrucei TREU927_AnnotatedProteins database obtained from tritrypdb.org including the following parameters: MS tol 10 ppm, MS/MS tol 0.5 Da, peptide FDR 0.01, protein FDR 0.01, Min. peptide length 7, variable modifications Oxidation (M), Phosphorylation (STY), Acetyl (Protein N-term), fixed modification Carbamidomethyl (C), Trypsin/P digestion, max 2 missed cleavages, Peptides for protein quantification razor and unique, Min. peptides 1, Min. peptide count 2.

Perseus analysis of phosphoproteome data

The phospho(STY)Sites.txt file was loaded into Perseus version 1.6.7.0 (Tyanova *et al.*, 2016b) with LFQ intensities as main columns according to the MaxQuant summer school tutorials (<http://www.coxdocs.org/doku.php?id=:perseus:start>). Briefly, sequences were filtered for reverse sequences, contaminants and localization probability of >0.75 . After expanding the site tables, groups were defined for wild type, Δ PKAC2 and +/- glycerol. The data was log₂ transformed and filtered based on valid values (at least 3 of 4 replicates within one group). Missing values were imputed from normal distribution using the default parameters. Phosphoproteomes of +/- glycerol conditions were compared using a student's t-test with the FDR = 0.1 and $S_0 = 0.1$. Phosphoproteomes of wild type and Δ PKAC2 were compared at steady-state levels (+ glycerol) using an FDR = 0.1 and $S_0 = 0.5$. The function *add linear kinase motifs* was used to add annotations of kinases known to phosphorylate the identified motif and later screened for the annotation "*PKA kinase substrate motif*". Enrichment analysis of GO terms was performed using REVIGO (Supek *et al.*, 2011) implemented in tritrypdb.org. Normalization by Z-score was performed before clustering analyses.

Perseus analysis of proteome data

The proteingroups.txt file was loaded into Perseus version 1.6.7.0 with LFQ intensities as main columns. Sequences were filtered for reverse sequences, contaminants and proteins only identified by site. Groups were defined for wild type and Δ PKAC2. The data was log₂ transformed and filtered based on valid values (at least 3 of 4 replicates

within one group). Missing values were imputed from normal distribution using the default parameters. Proteomes were compared using a student's t-test with the FDR = 0.05 and $S_0 = 0.1$. Normalization by Z-score was performed before clustering analyses.

2.2.7.3 Alamar Blue assay

Alamar blue assay was used to test cytotoxicity of the PEX14 inhibitor MABNH₂ (#5 from (Dawidowski *et al.*, 2017)) in wild-type and PEX14 phosphomutant cell lines. Individual stock solutions of the compound were prepared in SDM79 (+/- glycerol) in the range of 100 nM – 6 μ M. 100 μ l of each concentration were aliquoted on a 96-well plate in technical triplicates for each cell line, including a background control. Cells were diluted to 2×10^6 /ml and 100 μ l were added to each well, except the background control. Here, only medium was added. The plates were incubated at 27°C, 5% CO₂ for 48h. After incubation, 20 μ l of 0.5 mM resazurin in PBS were added to each well and the plates were incubated for another 2h at 27°C, 5% CO₂. Fluorescence was measured in the TECAN Infinite 200 Pro plate reader at 538 nm excitation and 590 nm emission. The fluorescence intensity of the technical replicates was averaged and the background subtracted from this value. A dose-response curve was generated from 3 individual replicates using the non-linear regression curve fitting in GraphPad Prism.

2.2.7.4 Purine response assays in pleomorphic cells

HMI-9 purine-depleted	Supplements
Iscoves modified medium (IMDM) powder (+ L-glutamine, - NaHCO ₃), pH 7.4, sterilized through 0.2 μ M filter	3.024 g/l NaHCO ₃ , 28.2 mg/l bathocuproine sulfonate, 0.2 mM β -mercaptoethanol, 100000 U/l penicillin, 100 mg/l streptomycin, 182 mg/l cysteine, 2 % (v/v) heat- inactivated fetal calf serum (FCS)

Cells were grown in methylcellulose HMI-9 and harvested by mixing with 4-5V PBS + 10 mM glucose and passing through a folded paper filter. They were centrifuged at 1,400g; 37°C for 15 min and washed twice in purine-depleted HMI-9. Cells were re-suspended to a density of 8×10^5 cells/ml in purine-depleted HMI-9. The culture was split in two and one was supplemented with 100 μ M hypoxanthine as a purine source. Both cultures were split in two again and one was supplemented with 3 μ M 7-cyano-7-deaza-inosine for PKA-activation. All cultures were incubated at 37°C, 5% CO₂ for 8h. After the incubation, 4×10^5 cells per sample were harvested, resuspended in 80 μ l PBS + 10 mM glucose and transferred to a white flat-bottom 96- well plate. 80 μ l of ONE Glo™ EX Luciferase Assay system (Promega #E8110) was added to each well and the plate was incubated for 5 min at RT. The luminescence of each well was measured in quadruplicates with 1,000 ms integration time using the TECAN Infinite 200 Pro plate reader. The mean value of the four measurements was calculated and

used for further analysis. The experiment was performed in biological triplicates and the mean values and standard deviations were calculated.

2.2.7.5 NMR

1 M proline	115 mg in 1 ml H ₂ O → sterile filtered
1 M glucose	180.2 mg in 1 ml H ₂ O → sterile filtered
1 M glycerol	73 µl in 927 µl H ₂ O → sterile filtered
1 M C¹³ glucose	186.11 mg in 1 ml H ₂ O → sterile filtered
1 M C¹³ glycerol	75.2 µl in 924.8 µl H ₂ O → sterile filtered
PBS	12 mM Na ₂ HPO ₄ , 3 mM KH ₂ PO ₄ , 150 mM NaCl, pH 7.4 + 5 g/l NaHCO ₃

Bloodstream form AnTat 1.1 Munich was freshly differentiated into procyclics and transferred to SDM79 supplemented with glucose, glycerol, both or neither (glucose-free medium contained 50 mM GlcNAc to prohibit glucose uptake from serum). $3.5 \cdot 10^7$ cells were harvested per sample (900g; 10 min; RT), washed once in sterile PBS and resuspended in PBS at a final density of $2 \cdot 10^7$ cell/ml. 1 ml was transferred into 1.5 ml reaction tubes already containing 0.5 ml PBS + 4 mM of the respective carbon source. The cells were incubated for 6h at 27°C and viability was confirmed microscopically every hour. Afterwards, the cells were centrifuged at 2,000 g; RT for 10 min and the supernatants transferred to a new 1.5 ml reaction tube. Supernatants were frozen in liquid nitrogen and shipped on dry ice to Frederic Bringaud, (Bordeaux/France) where the proton NMR was performed as described in (Mantilla *et al.*, 2017).

2.2.7.6 BioID

Lysis buffer	50 mM Tris/Cl pH 7.4, 500 mM NaCl, 0.4% SDS, 5 mM EDTA, 1 mM DTT, 1x complete protease inhibitor (Roche #4693132001)
Equilibration buffer	50 mM Tris/Cl pH 7.4, 250 mM NaCl, 0.2 % SDS, 2.5 mM EDTA, 0.5 mM DTT, 1% Triton X-100
10x PBS	1.37 M NaCl; 27 mM KCl; 43 mM Na ₂ HPO ₄ /14 mM KH ₂ PO ₄ → dilute stocks to 1x before use

BioID pulldown

Expression of BirA*-PKA was induced with 1 µg/ml tetracycline for 24h. Biotinylation of proteins in close proximity was induced simultaneously by addition of 50 mM biotin to the culture medium. For each replicate, $4 \cdot 10^8$ cells were harvested by centrifugation (1,400g; 37°C for BSF/900g; 27°C for PCF). The cells were washed three times in PBS, resuspended in 0.5 ml lysis buffer and sonicated on ice for 2x 30s in the Diagenode Bioruptor. Triton X-100 was added at a final concentration of 2% and the lysate sonicated again for 2 x 30s on ice. Afterwards, 0.5 ml 50 mM Tris/Cl pH 7.4 were added and the lysate was sonicated one more time as described before. The lysate was cleared by centrifugation at 15,000g; 4°C for 15 min. The buffer was exchanged for equilibration buffer using a PD10 column (GE Healthcare # 17-0851-01) as described by the manufacturer. The resulting eluate was concentrated to ca 1 ml using a Spin-X

UF 6 concentrator column (Corning # CLS431478) according to manufacturer's instructions. The precipitation of biotinylated proteins was performed using 50 μ l magnetic Dynabeads™ MyOne™ Streptavidin C1 (Thermo Fisher #65001) per reaction equilibrated in PBS. Binding was performed overnight at 4°C in a head over head rotator. Unbound proteins were separated, and the beads washed in PBS for 5 x 5 min. Finally, the beads were resuspended in 40 μ l Tris/Cl pH 7.5 and submitted for mass spectrometry to Michael Stadelmaier, AG Carell at the faculty of chemistry.

Mass spectrometry

(performed by Michael Stadelmaier, AG Carell at the faculty of chemistry)

The supernatant was removed, and the beads resuspended in 27 μ l digest buffer (50 mM TEAB pH 8.5, 1 mM MgCl₂). The beads were supplemented with 1.2 μ l 100 mM DTT and incubated at 750 rpm, RT for 30 min. Afterwards, 1.8 μ l 100 mM IAA were added and the beads incubated for another 10 min at 750 rpm, RT in the dark. Another 20 μ l of digest buffer were added and the proteins digested on-bead using 0.5 μ g trypsin in 50 mM AcOH at 37°C, 650 rpm overnight. Afterwards, the supernatant was removed, and the beads washed in 20 μ l digest buffer. Both supernatants were pooled and digested with 0.25 μ g trypsin for another 3.5h at 37°C, 350 rpm. Peptides were purified via stage-tips using standard methods and solved in 6 μ l MS solvent (0.1% formic acid, 2% MeCN). 3.5 μ l were used for MS² on Orbitrap (Thermo Fischer).

MS analysis by MaxQuant and Perseus

Protein identification and LFQ-quantification was performed using MaxQuant version 1.6.0.16 TriTrypDB-33_Tbrucei_TREU927_AnnotatedProteins database obtained from tritrypdb.org with default settings (Tyanova *et al.*, 2016a), except for max. allowed missed cleavages =3.

Statistical analysis was performed as described for the Glycerol proteome. Valid values were filtered for at least 3 (BSF)/4 (PCF) in at least one group (all replicates). BirA*-tagged lines were compared to the wild-type cell line using a student's t-test with the FDR = 0.01 and S₀ = 2.

3 RESULTS

The aim of the following experiments was to investigate the downstream function of PKA in the procyclic life cycle stage with a special focus on a possible role in metabolism. For that purpose, we first established a set of tools for analysis, including recombinant proteins and a series of PKA knockouts. Afterwards, we proceeded to the functional analysis which includes an unbiased multi-omics approach to screen for possible downstream targets of the kinase. Finally, we addressed the question whether *T. brucei* PKA is involved in metabolic adaptation as seen in other single cellular organisms.

3.1 Tools for TbPKA analysis

3.1.1 Purification of recombinant PKA subunits from *E. coli*

Mammalian PKA, both regulatory and catalytic subunit, can easily be expressed and purified from *E. coli* (Herberg and Taylor, 1993; Slice and Taylor, 1989; Steichen et al., 2012). Here, the regulatory subunit was expressed in *E. coli Rosetta*, a strain optimized for protein expression and purified by Ni-NTA affinity purification from the soluble fraction as described in 2.2.4.2.2 (Figure 8). Previous attempts to purify *T. brucei* PKAC in

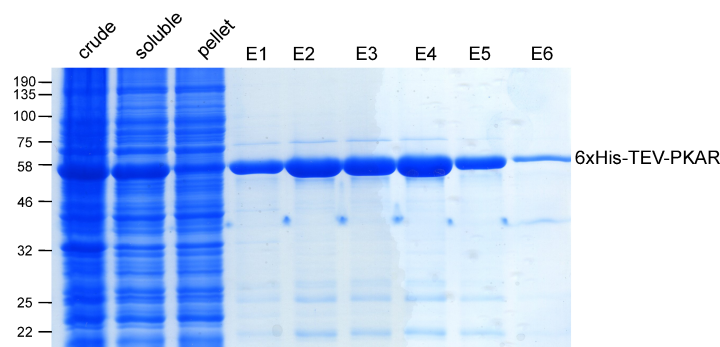


Figure 8: Purification profile of 6xHis-PKAR. The PKAR subunit was expressed and purified as described in 2.2.4.2.2. Equivalent amounts of each fraction were loaded on SDS-PAGE for analysis. E = elution.

our lab resulted in low yields and poor activity, indicating that eukaryotic expression is required for activity (Githure, 2014). The SUMO-tag is known to enable production of high yields of soluble protein (Peroutka lii et al., 2011) and was therefore chosen here as an alternative to the widely-used his-tag. All three catalytic subunits were cloned and expressed in *E. coli Rosetta*. Even though the SUMO-tag is reported to increase solubility, we observed the opposite for *T. brucei* PKAC. All subunits could be expressed at extremely high yields, but they remained completely insoluble (Figure 9). Since mammalian PKAC can easily be purified from soluble fractions, we tested whether using that same expression and purification protocol would increase the yield of soluble protein of *T. brucei* PKAC as well (Steichen et al., 2012). However, using

the mammalian protocol did not lead to changes in solubility. Numerous attempts were made to increase solubility, including variation of expression times and temperature,

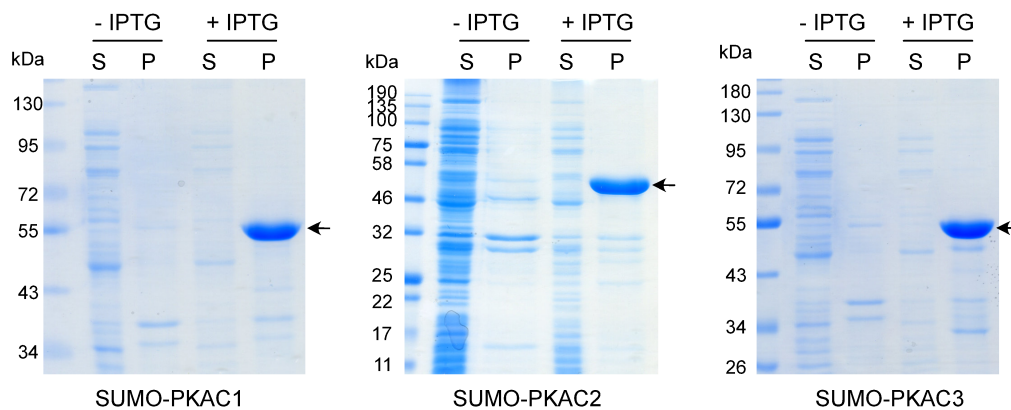


Figure 9: Expression of PKA catalytic subunits in *E. coli*. 6xHis-SUMO-tagged versions of PKAC1, PKAC2 and PKAC3 were expressed in *E. coli Rosetta* overnight at 18°C after induction with 1 mM IPTG. Soluble (S) and pellet fractions (P) were analyzed on SDS-PAGE. The arrows indicate the recombinant protein at the expected sizes.

IPTG concentrations or the use of different expression strains. None of this increased solubility. Interestingly, it should be noted, that the purification protocol of mammalian PKAC varies between publications, indicating that, in contrast to *T. brucei* PKAC, the purification conditions are not critical for the mammalian orthologues.

Despite the lack of solubility, the expression level of SUMO-tagged PKAC was extremely high, so we tested whether we could purify the insoluble protein from inclusion bodies. We adapted the inclusion body purification protocol from GE healthcare (now Cytiva, described in 2.2.4.2.1) and tested purification of all three PKAC subunits. As described before, all three subunits were detected in the insoluble fraction (Figure 10). The inclusion bodies were washed twice with a buffer containing sub-denaturing concentrations of urea (2M) and finally the protein was extracted from the inclusion bodies with 6M guanidinium hydrochloride. Equivalent amounts of each fraction were loaded

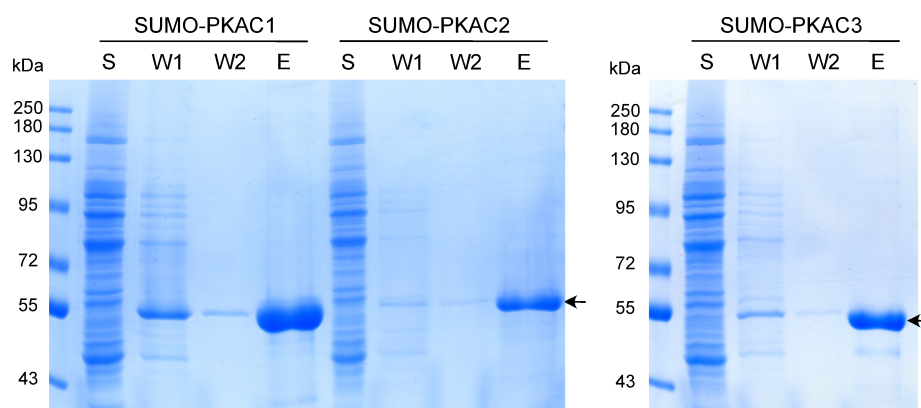


Figure 10: Purification of PKAC from inclusion bodies. The inclusion body pellets were washed twice (W1, W2) with sub-denaturing amounts of urea (2M) and extracted in 6 M guanidinium hydrochloride (E). Equivalent amounts of each fraction were analyzed by SDS-PAGE.

on SDS-PAGE and show extremely high protein yield (in this purification: ~48 mg PKAC1, 20 mg PKAC2 and 26 mg PKAC from 200 ml of culture) and purity. Further affinity purification by tags is not necessary. For most of the following applications, the denatured protein was sufficient. For generation of the anti-PKAC3 antibody, we employed a subsequent refold procedure (described in 2.2.4.4).

3.1.2 Generation of an anti-PKAC3 antibody

Our α -PKAC3 antibody showed quite low sensitivity and more importantly, some cross-reactivity with PKAC1/2. Since we had established a protocol to produce plenty of

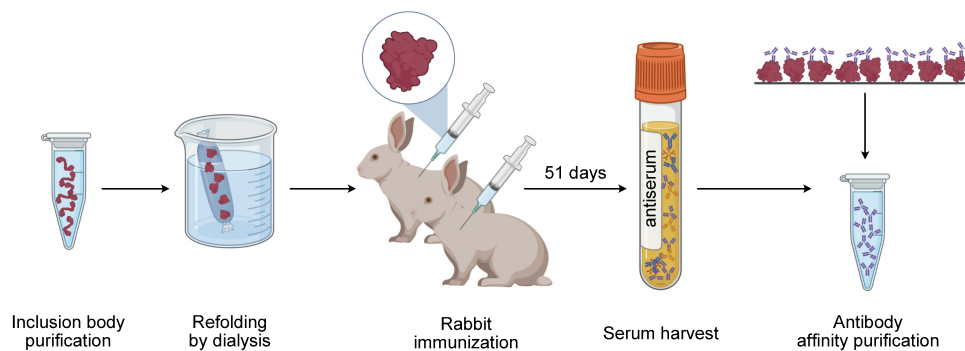


Figure 11: Generation of PKAC3 antibody. 6xHis-tagged PKAC3 was purified from inclusion bodies and refolded by dialysis. The soluble fraction after refolding was sent to Proteogenix (France) for immunization of two rabbits for 51 days. After immunization, the sera were harvested and returned. Antibodies were affinity purified using a non-tagged PKAC3 protein before use. Figure was created with BioRender.com.

PKAC3, we used this protein for generation of a new α -PKAC3 antiserum (Figure 11).

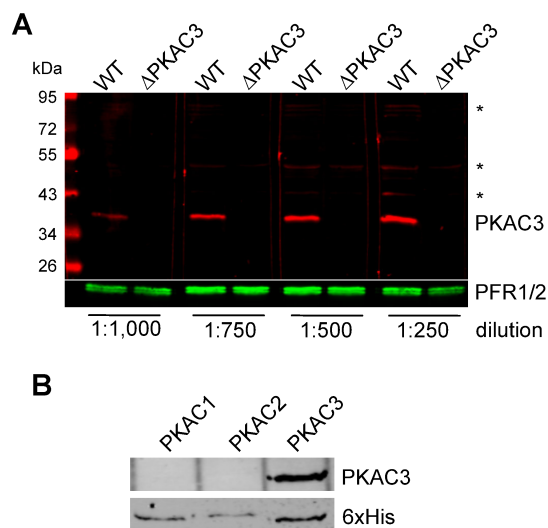


Figure 12: Sensitivity and specificity test of new PKAC3 antibody. **A:** Different dilutions of the affinity-purified serum were tested on wild-type and Δ PKAC3 PCF cell lysates. Asterisks (*) indicate unspecific bands. PFR was used as a loading control. **B:** Antibody specificity was tested on approx. 5 ng recombinant PKAC1, PKAC2 and PKAC3 protein, α -His was used as a loading control.

For this purpose, we exchanged the His-SUMO for a simple his-tag, purified the protein from inclusion bodies and then refolded by dialysis (described in 2.2.4.4). The soluble protein was afterwards sent to Proteogenix (France) for immunization of two rabbits. We decided to use soluble material to generate an antibody that also detects folded PKAC3 and could potentially be used in immunofluorescence or pulldown experiments. After 51 days, the antisera were harvested and delivered. Using the sera without further purification led to a lot of unspecific background staining. Therefore, the antisera were subjected to

affinity purification using a tag-free PKAC3 subunit to avoid co-purification of antibodies specific to the his-tag (described in 2.2.4.3). After purification, the antibody was tested for sensitivity and specificity (Figure 12). Four different dilutions were tested in western blot on *T. brucei* wild-type and PKAC3 knockout (Δ PKAC3, cell line specifications can be found in 2.1.4) whole cell lysates. In each condition, only one very prominent band is visible at the appropriate size of approximately 40 kDa and band intensity increases with increasing antibody concentration. A few larger bands can still be detected (indicated by the asterisk in the western blot) but appear as very faint signals in PCF. No band is detected in the Δ PKAC3 cell line indicating a high specificity for PKAC3. This specificity was further confirmed using the recombinant PKAC subunits purified in 3.1.1 (Figure 12B).

3.1.3 Quantification of absolute PKA amounts in *T. brucei* lysates

From previous work (Bachmaier, 2015; Kramer, 2004; Schulte zu Sodingen, 2000), we know the life cycle-dependent expression profiles for each PKA subunit, but some im-

portant questions remained open: How abundant is PKA in *T. brucei*? Are the subunits expressed at similar levels? Is there a balance between PKAR and PKAC? To address these questions, we used the recombinant subunits purified in 3.1.1 and determined the concentration as precisely as possible. For that we generated a BSA protein standard and subjected it to SDS-PAGE along with the recombinant PKA subunits (described in 2.2.4.5.2).

This method allowed to quantify the protein of interest exclusively without any potential impurities. The quantification was done in quadruplicate and the average value used for further calculations. Figure 13 shows a typical standard curve and the

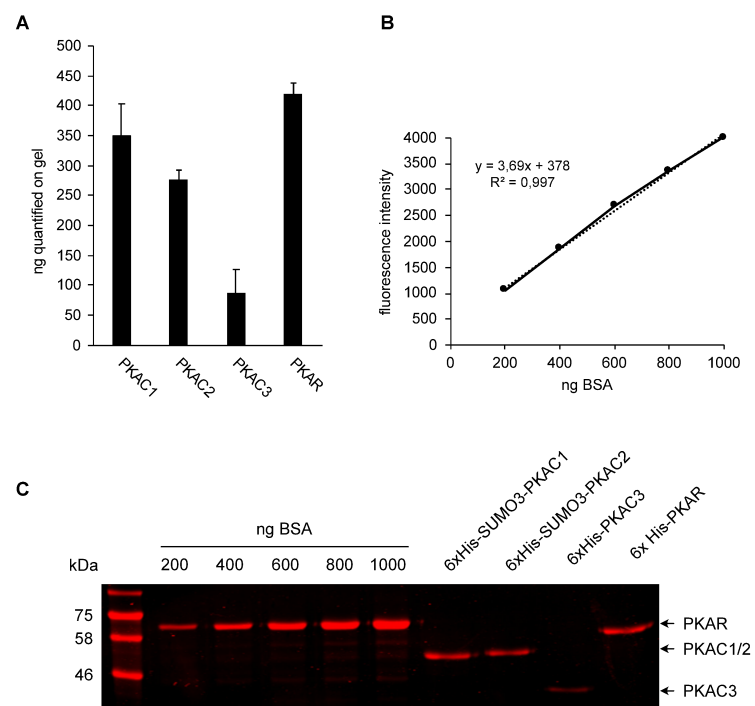


Figure 13: Quantification of recombinant PKA subunits for absolute quantification. **A:** Protein concentration was determined in quadruplicate on Coomassie stained SDS-gels in comparison to a BSA protein standard. Plotted here are mean \pm stdev. **B:** Example of BSA standard curve used for quantification. **C:** Example of Coomassie stained SDS-gel after electrophoresis. Gels were imaged using LI-COR Odyssey Clx.

corresponding SDS gel. Even though the standard curve shows a good linear fit, the quantification has a certain variance which is indicated by the error bars in Figure 13A. The next step for absolute quantification was preparation of protein standards using the PKA subunits and their quantification on western blot along with lysates of a defined cell number. These blots were performed in triplicates and the downstream analysis included conversion of protein mass to molecule number and subsequent calculation of molecules/cell (described in 2.2.4.6). Two strains of each life cycle stage were used for comparison (Figure 14). In this case, the subunit ratios are more important than accurate molecule numbers. Figure 14A shows a reduction of PKAR protein levels in PCF to roughly half compared to BSF. PKAC1/2 levels are reduced around 10-fold in PCF, while levels of PKAC3 remain unchanged. All of this is perfectly in line with previous data from our laboratory (Bachmaier, 2015) and detection is specific as seen in the corresponding western blots (Figure 14C). In Figure 14B we addressed the

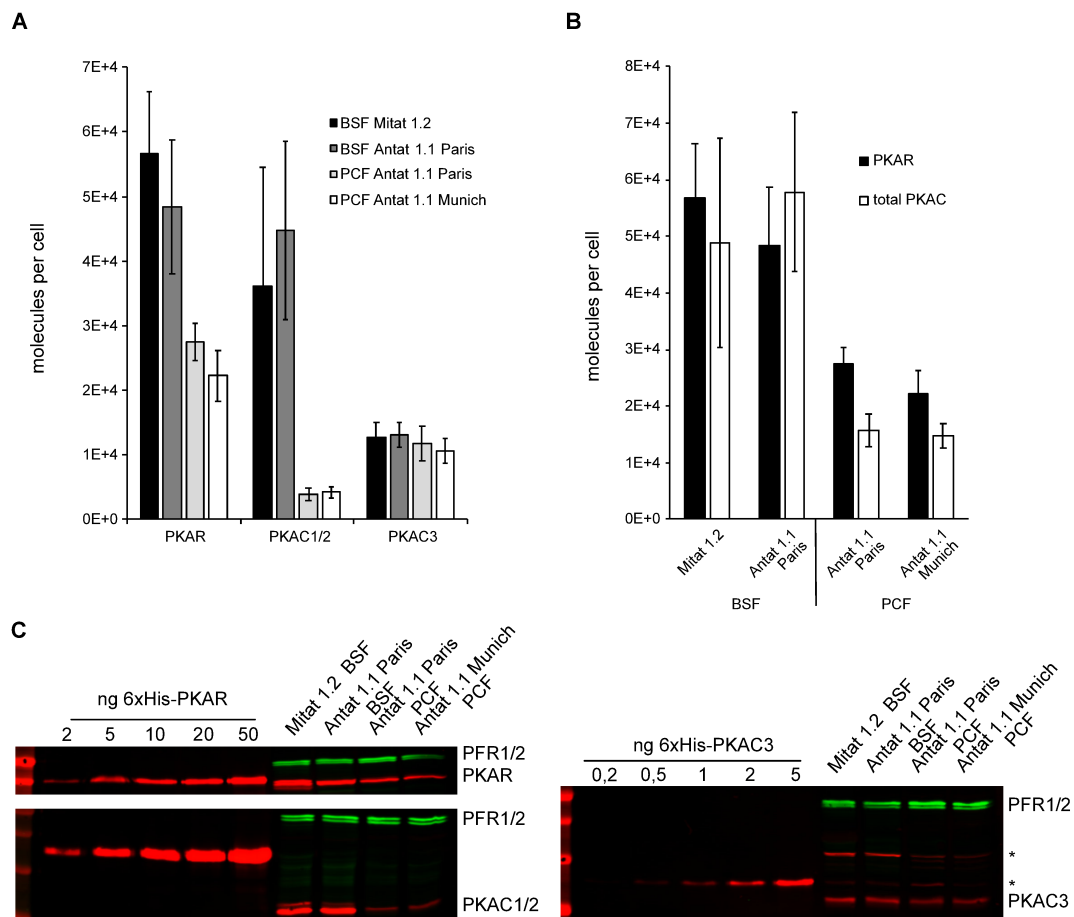


Figure 14: Absolute quantification of PKA molecules in different life cycle stages. 2×10^6 cells of PCF and BSF strains were loaded along with a PKA standard using the recombinant proteins ($n=3$, example in **C**. PFR was used as a loading control.). Masses were converted to molecule numbers using the formula: $\text{molecules} = \text{NA} \cdot (\text{ng}/10^9)/\text{M}$, NA being the Avogadro constant and M the molecular weight of the recombinant proteins including the tags. **A:** Absolute molecule numbers determined for PKAR; PKAC1/2 and PKAC3 in the different strains. Plot shows average \pm stdev. **B:** Illustration of PKAR and combined PKAC molecule numbers in the different strains, plot shows average \pm stdev.

question whether there is a balance between regulatory and catalytic subunits. Indeed, we found similar levels in both, BSF and PCF indicating that potentially all PKAC subunits can be bound in a holoenzyme in BSF. Here the PKAR to PKAC ratio seems 1:1, while we quantified an excess of PKAR in the PCF stage.

We quantified molecule numbers in the range of $X \cdot 10^4$ /cell. Assuming that a cell contains $3 \cdot 10^6$ proteins/ μm^3 (Milo, 2013) and a *T. brucei* BSF cells has a volume of roughly $67 \mu\text{m}^3$ (Jung, 2015) that would result in $\sim 2 \cdot 10^8$ protein molecules/cell. Kinases compose 2% (ca. 180 genes) of the *T. brucei* coding genome (Parsons et al., 2005). Under the assumption of equal expression levels among all genes, that would result in $4 \cdot 10^6$ kinases/cell. Assuming they are expressed in equal numbers, this leaves $2,2 \cdot 10^4$ of each PKA subunit/cell, which is perfectly in line with the observation reported for PKA. However, this calculation is strongly dependent on the estimation of the total protein number/cell, which will vary between different references. Additionally, proteins are not expressed equally, e.g., structural proteins will always be more abundant than signaling proteins. Based on that, we would conclude that it is not a very high abundance protein in general, but it could be high abundance amongst protein kinases.

3.2 Generation of a PKAC knockout series

Previous work in BSF showed essentiality of PKAC1 (Bachmaier, 2015; Kramer, 2004). Since most of this laboratory's work had focused on BSF, we had no information on PKA essentiality in the PCF life cycle stage so far. The only PKA subunit null mutants available in PCF were ΔPKAR and ΔPKAC3 (cell line specification in 2.1.4), both of which were not essential for cell survival. Therefore, we aimed for a comprehensive analysis of PKAC null mutants from single to double and finally triple knockouts in terms of growth and differentiation potential.

3.2.1 Generation of Δ PKAC2

Our starting point was a single knockout of PKAC2. This null mutant was generated in pleomorphic BSF in order to evaluate differentiation ability from slender to stumpy to procyclic as well as essentiality in PCF. The same knockout-constructs were used as described by (Kramer, 2004) for the monomorphic Δ PKAC2 line and the ORFs replaced by antibiotic resistance cassettes. Proper replacement was confirmed by PCR (Figure 15A/B) and expression levels of the remaining PKA subunits analyzed by west-

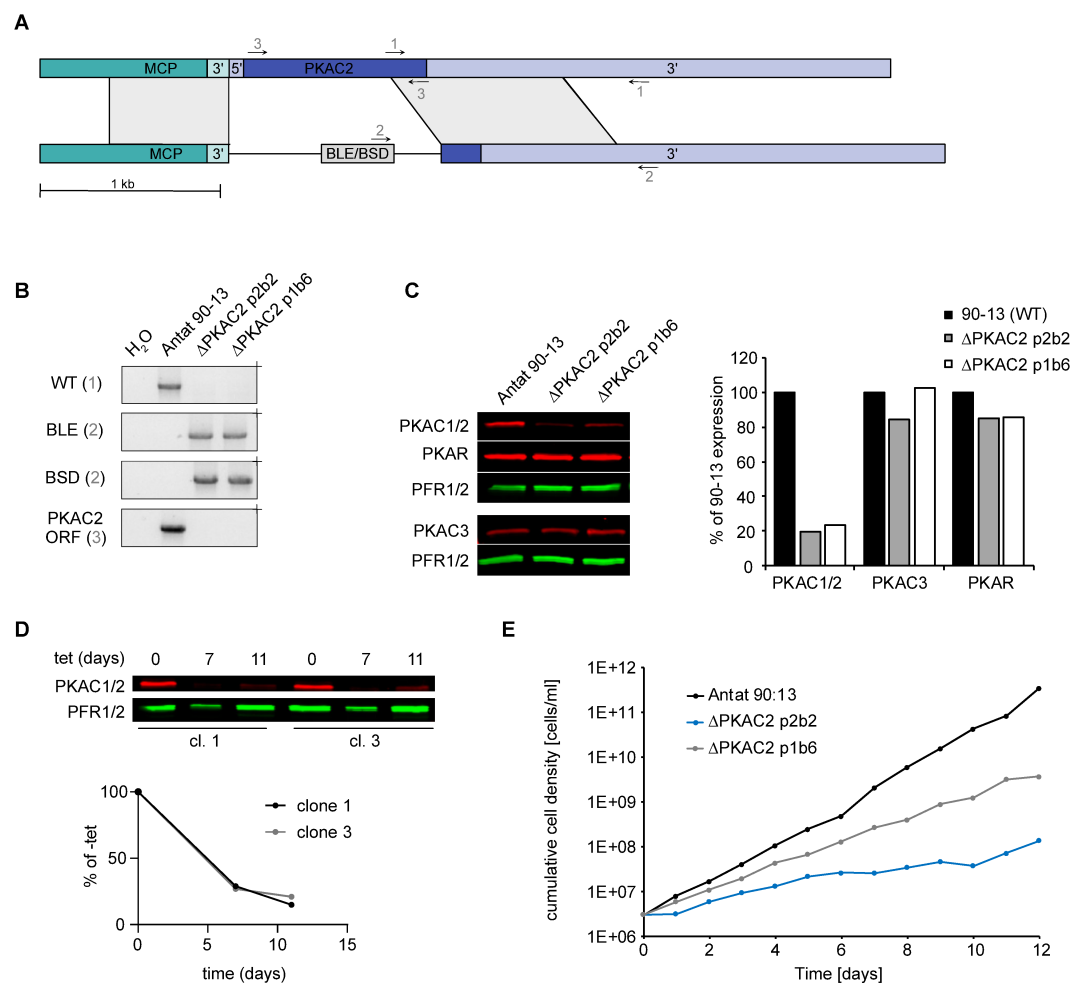


Figure 15: Generation and confirmation of Δ PKAC2 cell line. **A:** PKAC2 knockout was generated by ORF replacement with a resistance cassette by two consecutive transfections. **B:** Proper integration of the marker was confirmed by integration PCR using the primer pairs indicated in **A** for two independent clones. **C:** Analysis of PKA expression levels of two independent clones in PCF shows barely affected PKAR and PKAC3 levels and a strong reduction in PKAC1/2 protein levels compared to the parental cell line. PFR was used as a loading control. **D:** Further knock-down of PKAC1 using a subunit-specific RNAi shows elimination of the residual PKAC1/2 signal. PFR was used as a loading control. **E:** Growth analysis of two independent Δ PKAC2 clones compared to wild type shortly after differentiation from BSF to PCF.

ern blot in PCF. The western blots in BSF showed no difference compared to the parental cell line (data not shown), which can be explained by extremely low expression levels of PKAC2 in BSF (Bachmaier, 2015). In procyclic cell lysates, levels of PKAR and PKAC3 remained unchanged, while we still detected levels of PKAC1/2 above the

limits of detection (due to high sequence similarity, the antibody does not distinguish PKAC1 and PKAC2), indicating the presence of PKAC1 (Figure 15C). Further RNAi-mediated specific knock-down of PKAC1 (cell line specificities described in 2.1.4) confirmed that the remaining signal can be attributed to this subunit (Figure 15D). Previous data indicated that PKAC1 is usually completely downregulated in PCF on protein level (Bachmaier, 2015), which would suggest an upregulation of PKAC1 in response to PKAC2 knockout. Alternatively, there could always be a low expression of PKAC1 in PCF and we simply couldn't detect it so far due to low sensitivity of the methods used before and the issue of antibody cross-reactivity on western blot. After confirmation, two independent clones of Δ PKAC2 were analyzed in the following experiments. Both clones successfully differentiated to stumpy and later to procyclics without any problems. Growth as PCF cells was slightly impaired after differentiation (Figure 15E) but recovered after prolonged time in culture (data not shown).

Finally, we analyzed differentiation from procyclic to metacyclic cells (*metacyclogenesis*) using the RBP6 differentiation system established in this laboratory (Allmann, 2014; Wargnies *et al.*, 2018; Ziebart, 2016). Overexpression of the RNA binding protein RBP6 induces differentiation from PCF to epimastigotes and later on metacyclics (Kolev *et al.*, 2012). The initial attempt to transfect the RBP6 expression construct on top of the knockout was not successful as no viable cells were obtained, neither in the

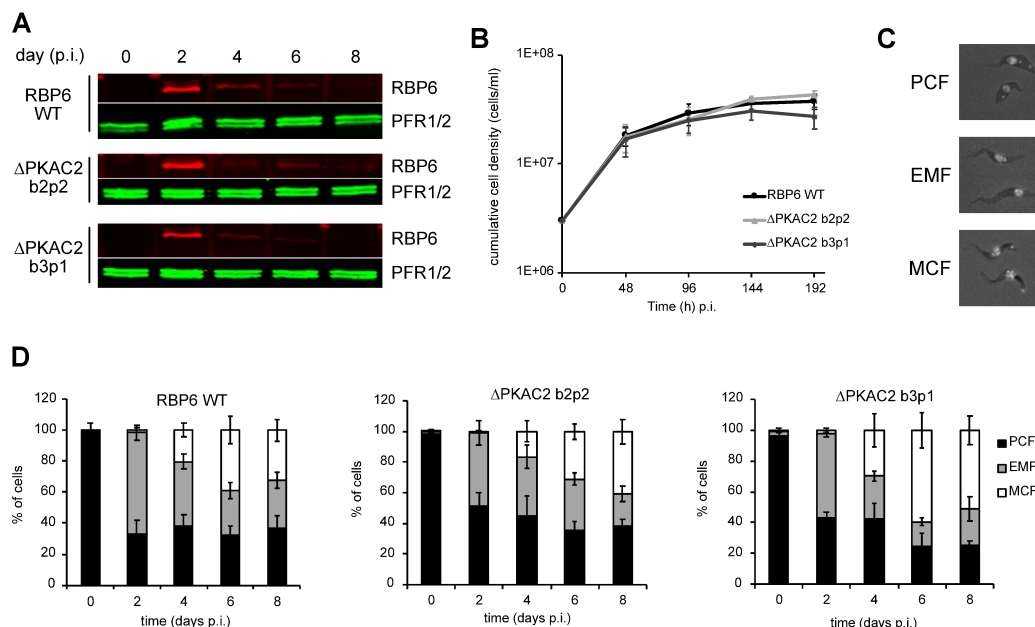


Figure 16: Analysis of metacyclogenesis in two independent Δ PKAC2 clones. *In vitro* differentiation was induced by RBP6 overexpression and analyzed for 8 days (n=3). **A:** Expression levels of RBP6 are highest at day 2 post-induction. **B:** Growth curve showing the growth arrest upon RBP6 induction. **C:** Examples of Procyclic (PCF), epimastigote (EMF) and metacyclic (MCF) cells in DAPI staining of nucleus and kinetoplast. Kinetoplasts of PCF are positioned posterior to the nucleus and dividing cells can be observed. In EMF, the kinetoplast is positioned on top or anterior to the nucleus. Metacyclic cells show a distinct shape and a kinetoplast on the extreme posterior pole of the cell. **D:** Categorization of cell populations into PCF, EMF and MCF throughout the course of RBP6 induction based on the examples given in **C**.

knockout nor the parental line (Antat 1.1 90-13). Consequently, we knocked out PKAC2 in the EATRO 1125 T7T RBP6 cell line and confirmed as described before (Supplementary Figure 1). Overexpression of RBP6 was induced by tetracycline addition and successful metacyclogenesis monitored by growth arrest and morphological evaluation of cell shape and kinetoplast repositioning. All cell lines showed highest RBP6 expression after 2 days post-induction (p.i.) and a growth arrest after 96 h p.i. (Figure 16). Samples were taken every second day and subjected to DAPI staining. The cells were afterwards categorized into procyclic, epimastigotes (EMF) and metacyclic (MCF) according to the example given in Figure 16C. In PCF cells the kinetoplast is positioned posterior to the nucleus, in epimastigotes forms the kinetoplast is positioned anterior of or on top of the nucleus and in metacyclics it is positioned at the extreme posterior pole. Both Δ PKAC2 clones showed a similar distribution of the different forms compared to the parental cell line (Figure 16D). We also analyzed PKA expression levels during metacyclogenesis and RXXS*/T* substrate site phosphorylation (Figure 17). RXXS*/T* (* indicates phosphorylated residue) is the main PKA consensus motif and phosphorylation of the serine/threonine residue can be detected with a specific phosphoantibody (see 2.1.5). A clear increase of the PKAC1/2 signal can be

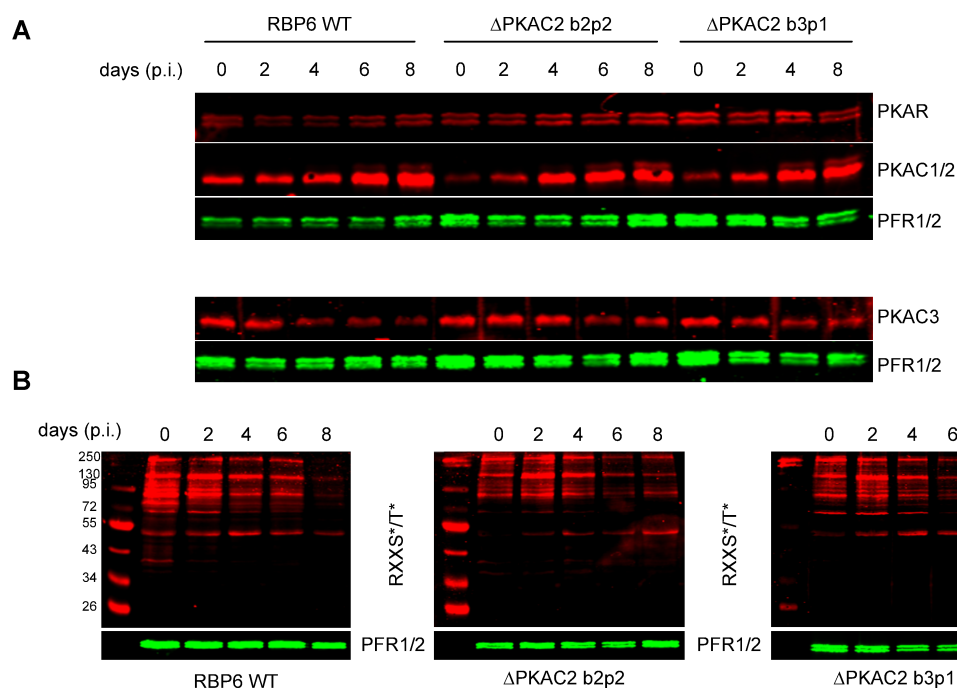


Figure 17: RXXS*/T* phosphorylation and PKA expression levels throughout RBP6 induced metacyclogenesis. **A:** Phosphorylation levels of RXXS*/T* sites were analyzed by western blot using the Phospho-(Ser/Thr) PKA substrate antibody. **B:** Expression levels of PKA were analyzed by western blot. Levels of PKAR and PKAC3 do not seem to change, while PKAC1 is upregulated.

detected in the parental as well as in the Δ PKAC2 lines, indicating that PKAC1 is up-regulated during metacyclogenesis. This observation could also be confirmed by other

lab members (S. Bachmaier, personal communication). Meanwhile, PKAC3 appears to be downregulated, but this could not be observed in a second replicate (Supplementary Figure 2). However, the upregulation of PKAC1 is not correlated with any increase in RXXS*/T* phosphorylation levels. In fact, they even seem to decrease indicating a level of regulation of kinase activity that is independent of kinase abundance. One explanation could be that PKAC1 in metacyclics is not (yet) active. Alternatively, other RXXS*/T* phosphorylating kinases and phosphatases might be down- or upregulated, respectively.

In conclusion, PKAC2 can easily be knocked-out in BSF and differentiated to procyclics, where the cells exhibit a mild growth phenotype freshly after differentiation. Further differentiation into metacyclics is not affected, but an upregulation of PKAC1 can be observed.

3.2.2 Generation of Δ PKAC1/2

After PKAC2 knockout, we could still observe the presence of PKAC1. Given their overall high similarity, it is not clear whether there are functional redundancies which would have masked potential phenotypes in PCF. So far, we were not able to properly investigate this with classical gene replacement methods due to a shortage of available

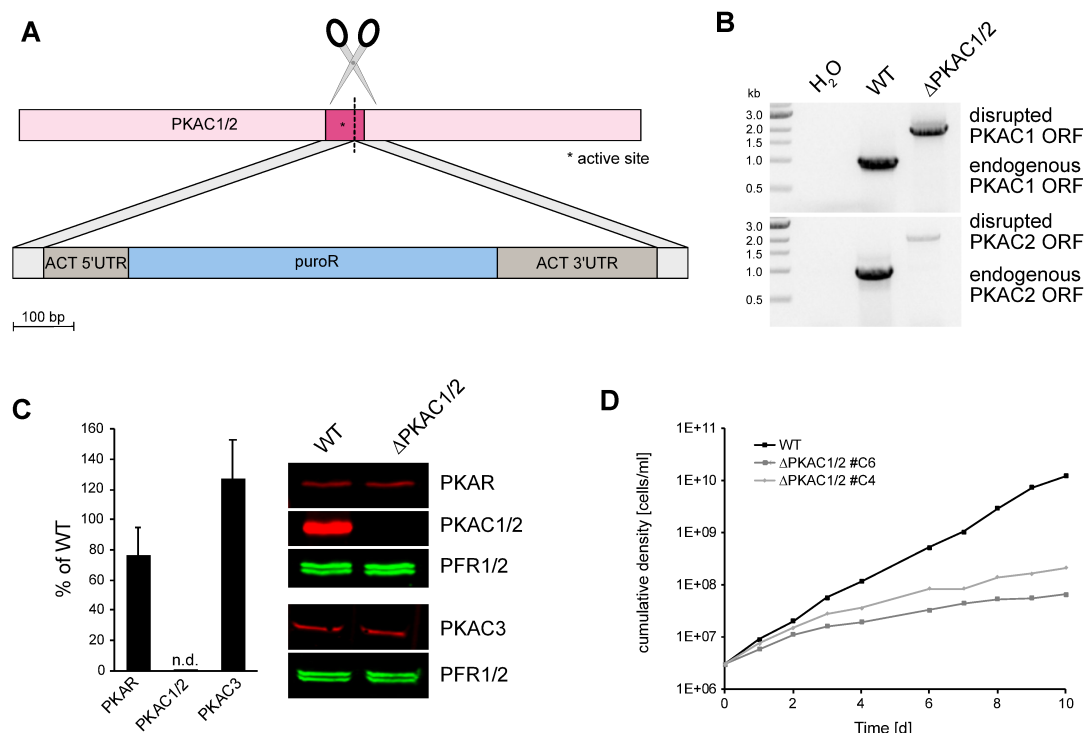


Figure 18: Generation and confirmation of PKAC1/2 double knock-out in PCF. **A:** CRISPR/Cas9-mediated cut in the active site of PKAC1 and PKAC2 was replaced by a puromycin resistance cassette supplied as the repair template. Proper modification can be monitored by size shift of the resulting ORF and was confirmed by PCR (**B**). **C:** Analysis of PKA expression levels shows no significant difference in PKAR and PKAC3 levels (n=3) and clear elimination of PKAC1 and PKAC2. PFR was used as a loading control. **D:** Growth analysis showed a mild phenotype shortly after transfection compared to the parental cell line.

selection markers. Luckily, recent advances in CRISPR/Cas9 technology solved this issue. We were able to obtain a highly efficient CRISPR/Cas9 protocol from our collaboration partners (E. Tetaud, Bordeaux, unpublished). Their protocol describes the transfection of the whole CRISPR/Cas9 complex without the necessity to generate a designated CRISPR cell line. To generate a PKAC1 and PKAC2 double knockout, we designed a gRNA targeting the conserved region in the active sites and provided an antibiotic resistance cassette as repair template that is inserted in the ORF (Figure 18A). This way, we managed to successfully disrupt both alleles of PKAC1 and PKAC2 with only one transfection as can be seen in Figure 18B. The following western blot analysis further confirms a complete knockout of both catalytic subunits. Additionally,

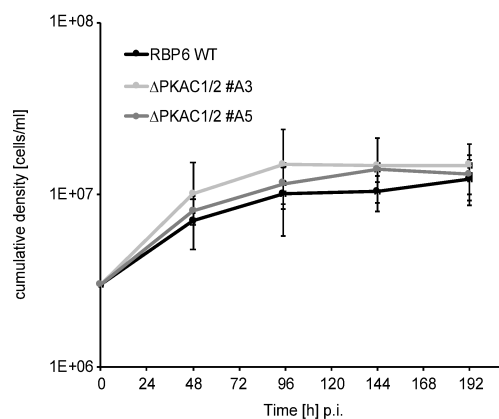


Figure 19: Growth arrest of Δ PKAC1/2 in response to RBP6 overexpression (n=3) using two independent clones. Experiments performed by lab rotation student (T. Linner-Horn, 2021).

we could not observe any major co-regulation of PKAR or PKAC3 in response to the knockout (Figure 18C). Growth analysis only showed a mild phenotype shortly after transfection (Figure 18D). However, this is also lost after prolonged culture time as seen in the Δ PKAC2 single knockout (Figure 15E). The strong upregulation of PKAC1 in the RBP6 differentiation system described in the previous paragraph was raising the question whether this subunit was relevant for metacyclogenesis. To test

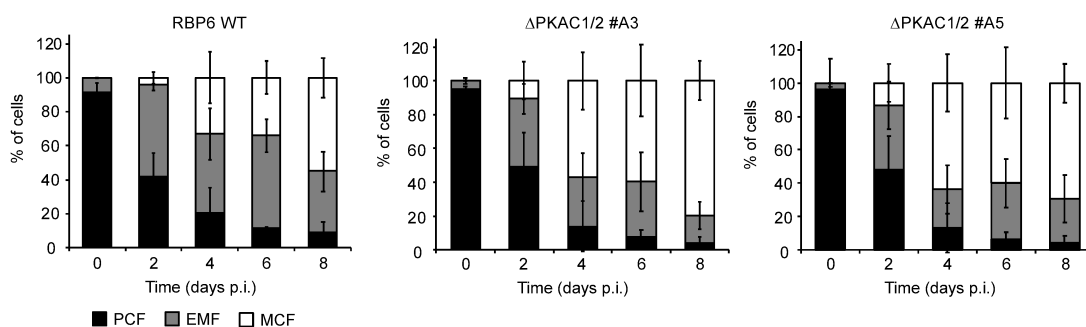


Figure 20: Categorization of different fly-stages upon RBP6 overexpression in Δ PKAC1/2. Cells were categorized into PCF, EMF and MCF based on kinetoplast to nucleus positioning (n=3, experiment performed by T. Linner-Horn, lab rotation 2021)

this hypothesis, the double knockout was also carried out in the RBP6^{Ti} background (T. Linner-Horn, lab rotation 2021). Two independent Δ PKAC1/2 knockout clones were tested, and both showed growth arrest upon RBP6 overexpression (Figure 19) and high levels of epimastigote and metacyclic parasites (Figure 20). We had the impression that metacyclogenesis was even more efficient in the Δ PKAC1/2 line, but the

reciprocal experiment using PKAC1 and PKAC2 overexpression showed no difference in growth behavior and also led to generation of morphologically metacyclic cells (Supplementary Figure 3). In conclusion, PKAC1 and PKAC2 activities are not important for RBP6-driven differentiation and metacyclogenesis in culture.

3.2.3 Generation of Δ PKAC1/2/3

The last step in this reverse genetic analysis was the generation of a PKAC1/2/3 triple-knockout. Here, we again made use of the new CRISPR/Cas9 system and knocked-out PKAC1 and PKAC2 on top of a PKAC3 knockout (Schulte zu Sodingen, 2000) using the same strategy as described for the Δ PKAC1/2 line. PCR showed successful disruption of both PKAC1 and PKAC2 ORFs and proper knockout could be confirmed by western blot (Figure 21). Interestingly, growth analysis of two independent clones

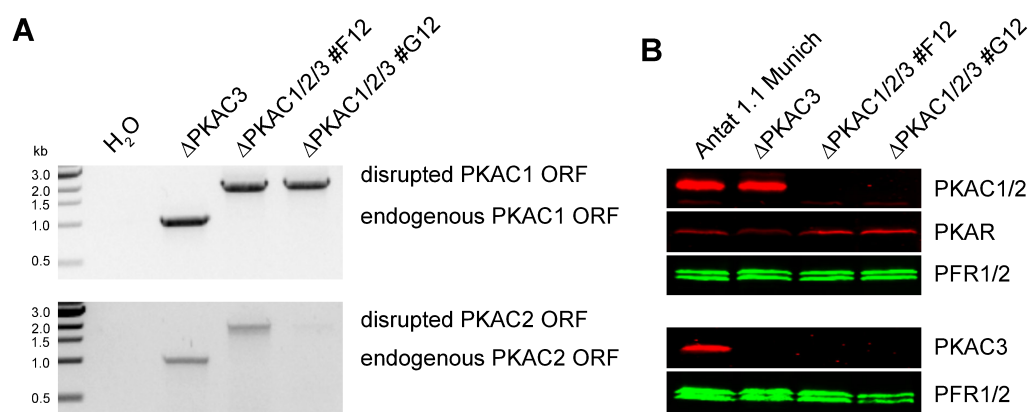


Figure 21: Validation of Δ PKAC1/2/3 triple knockout. **A:** PCR of PKAC1/2 ORF, disrupted loci can be distinguished by size shift. **B:** Western blot analysis of PKA expression levels in Δ PKAC1/2/3 compared to wild-type and parental (Δ PKAC3) cell line. PFR was used as a loading control.

did not show any phenotype at all compared to the wild-type or parental cell line (Δ PKAC3, Figure 22). Since both, the Δ PKAC2 and Δ PKAC1/2 knockout showed a

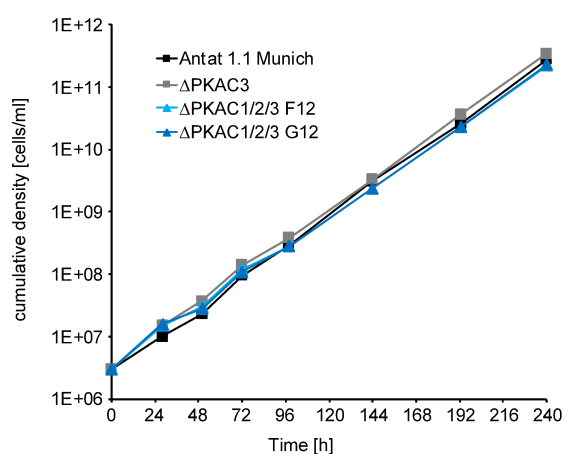


Figure 22: Growth curve of PKAC triple knockout over the course of two weeks comparing two independent clones to wild-type and Δ PKAC3 parental cell line.

slight growth phenotype compared to their parental cell line, it is surprising to see no effect at all in combination with Δ PKAC3. One explanation could be that the PKAC3 knockout was generated a long time ago directly in PCF cells and can therefore be considered a long-term PCF strain. In contrast, the Δ PKAC2 single and Δ PKAC1/2 double knockouts were generated

in relatively freshly differentiated cells. It could be possible that the mild growth phenotypes we have initially observed are only detectable in early procyclics. The flagellar localization of PKA could suggest a motility defect in the knockouts. In neither of the cell lines generated here, we observed any obvious abnormalities in cell motility. Therefore, this was not analyzed in a quantitative manner.

In conclusion, the series of PKAC knockouts generated here clearly shows that PKA catalytic activity is not essential for cellular survival and basic functions under standard culturing conditions *in vitro*. In addition, we conclude that the absence of phenotypes is not due to PKAC isoform redundancy. However, this will be beneficial to study specific phenotypes, e.g., in metabolism without the issue of impaired overall cell fitness.

3.2.4 Comparison of RXXS*/T* phosphorylation in PKA knockouts

With the full set of PKA null mutants, we finally compared global effects of PKA subunits on steady-state RXXS*/T* phosphorylation using the phospho-specific substrate antibody (Figure 23). Western blot analysis showed comparable levels between the two parental strains AnTat 1.1 Munich and AnTat 1.1 90-13, as well as in the Δ PKAR

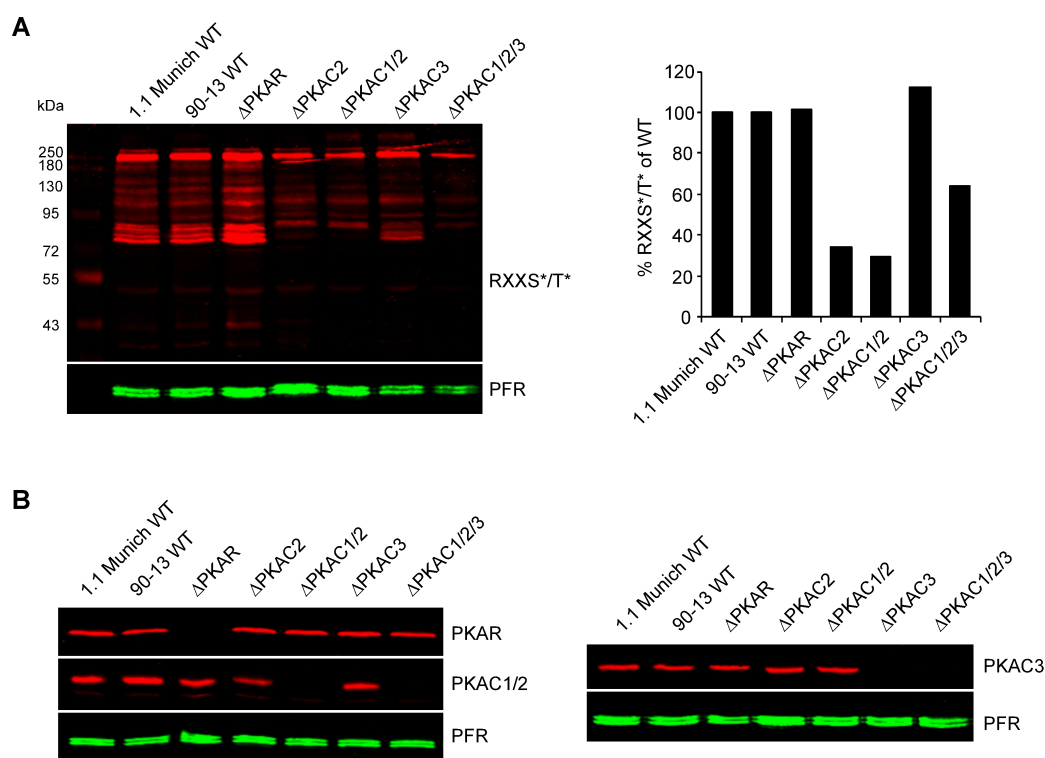


Figure 23: Comparison of steady-state RXXS*/T* phosphorylation in PKA null mutants. **A:** Equivalent amounts of each PKA knockout line were loaded for western blot analysis of RXXS*/T* substrates using the Phospho (Ser/Thr) PKA substrate antibody. Right panel shows the quantification of RXXS*/T* signal (*phosphorylation) to the PFR loading control. **B:** Confirmation of the knockouts used in **A**.

knockout. Knockout of PKAC2 alone or PKAC1/2 showed a very similar pattern and mainly leads to the loss of some bands in the range of 70 – 95 kDa and slightly less

overall intensity. Deletion of PKAC3 doesn't seem to cause any major differences in phosphorylation pattern and knockout of all three catalytic subunits causes a similar pattern to that of Δ PKAC2 and Δ PKAC1/2. The quantification of RXXS*/T* signal in the PKAC1/2/3 triple knockout suggests a higher degree of phosphorylation, but this appears to be due to a blotting issue of the loading control (PFR in Figure 23A). One very prominent band at ca. 200 kDa is preserved throughout all PKA null mutants.

In conclusion, this would suggest that the majority of PKA-regulated RXXS*/T* phosphorylations in PCF are mediated by PKAC2. However, there are still bands detected even in the triple knockout indicating the presence of other kinases with RXXS*/T* motif specificity. This would not be surprising, RXXS*/T* is the main PKA consensus motif but is shared with other AGC kinases (Bradley and Beltrao, 2019; Pearson and Kemp, 1991).

3.3 Identification of possible PKA targets in PCF using a multi-omics approach

After successful establishment of analytical tools and PKA knockouts, we proceeded to the functional analysis of PKA focusing on the PCF life cycle stage. We were interested in downstream targets as well as interaction partners. Since PKAC2 appeared to be responsible for the majority of RXXS*/T* phosphorylations (3.2.4), we put a special focus on PKAC2.

3.3.1 Δ PKAC2 proteome

In the proteome dataset we identified 3,177 proteins in total, of which 177 are significantly regulated (FDR = 0.05, $S_0 = 0.1$) between WT and Δ PKAC2 (Figure 24A, Supplementary table 1). We find 94 significantly downregulated and 83 upregulated proteins in abundance compared to the wild type. Of these proteins, 63 were regulated at

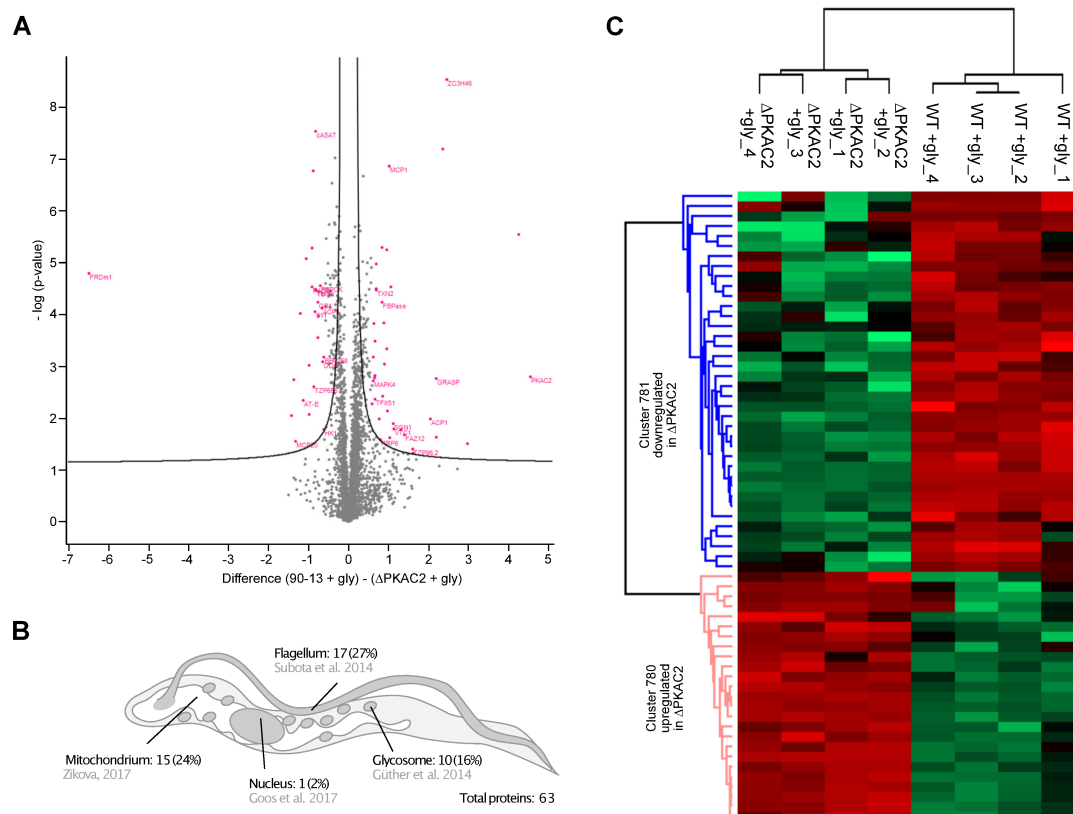


Figure 24: Comparative proteome of wild-type and Δ PKAC2. **A:** Volcano plot showing significantly (FDR=0.05, $S_0=0.1$) regulated proteins between wildtype and Δ PKAC2, proteins with a fold-change of at least 1.5x are considered for localization and clustering analysis and marked in pink. **B:** Localization of regulated proteins as assessed by published subcellular proteomes. **C:** Clustering analysis of identified proteins, divided into up- and downregulated in Δ PKAC2.

least 1.5-fold and considered in the following workflow (marked in pink in Figure 24A). Most of these proteins are localized to the flagellum, but even more (40%) of the regulated proteins localize to the metabolically active compartments: glycosomes and the mitochondrion (Figure 24B). For the proteome, GO enrichment analysis showed numerous annotations with metabolic functions in both, the up- and downregulated protein clusters (Figure 25). When these differentially expressed enzymes are mapped on

the carbohydrate pathways, it appears like PKAC2 deletion promotes glycolysis while inhibiting gluconeogenesis and parts of the TCA cycle (Figure 26).

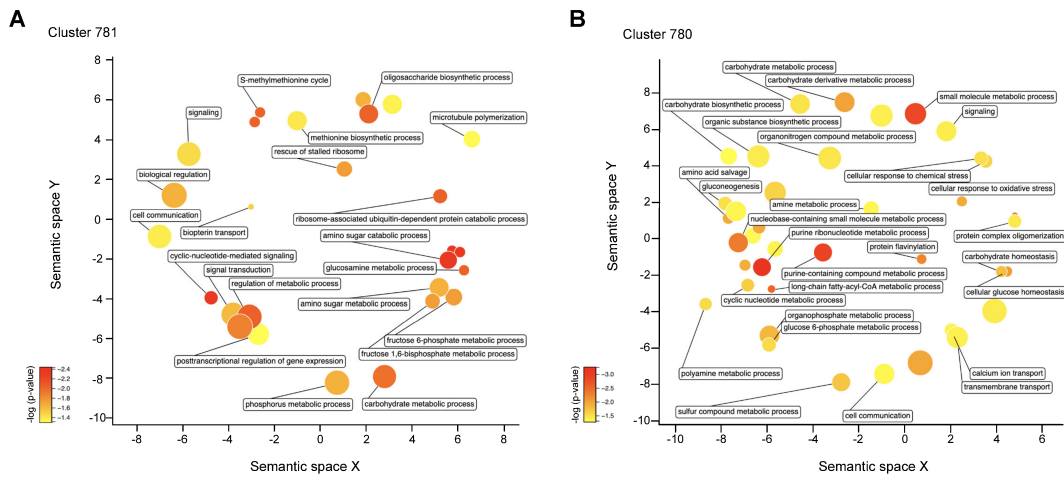


Figure 25: GO enrichment analysis using REVIGO (Supek et al., 2011) of cellular processes of significantly regulated proteins between wild-type and Δ PKAC2. **A:** Annotations of proteins less abundant in PKAC2 knockout. **B:** Annotations of proteins more abundant in the PKAC2 knockout.

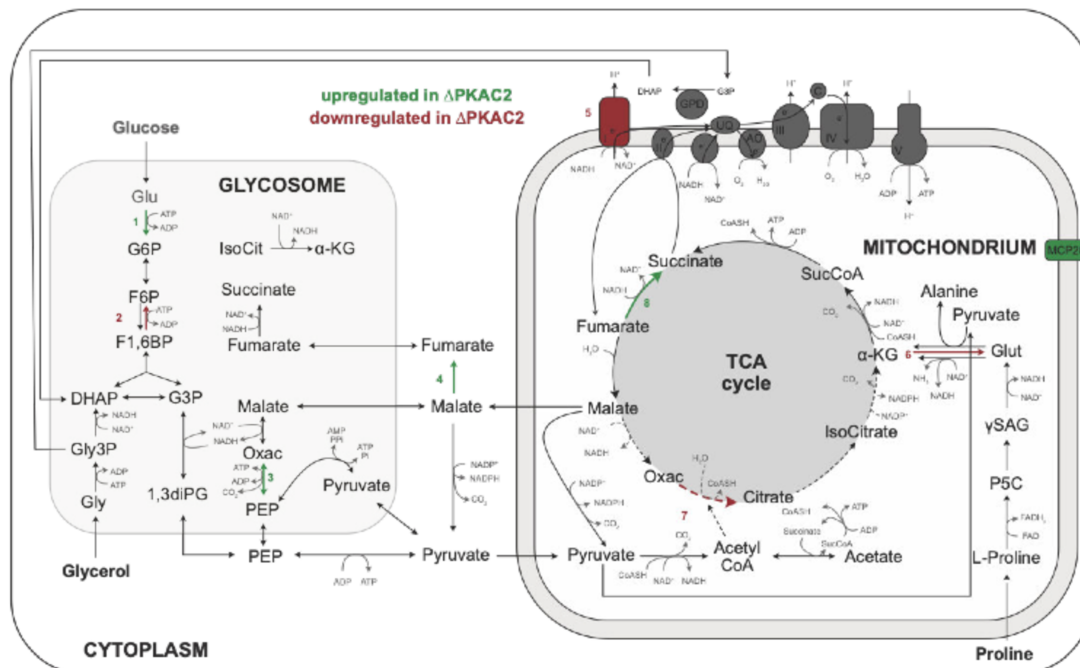


Figure 26: Differences in metabolic enzyme levels between PKAC2 knockout and wild type under + glycerol culture conditions. Upregulated enzymes are indicated in green, downregulated enzymes are indicated in red. 1: hexokinase, 2: fructose-1,6-bisphosphatase, 3: phosphoenolpyruvate carboxykinase, 4: fumarase, 5: NADH dehydrogenase, 6: aspartate transaminase, 7: citrate synthase, 8: fumarate reductase.

3.3.2 Δ PKAC2 phosphoproteome

In the previous chapter, we observed that PKAC2 knockout causes differences in metabolic enzyme expression levels. Now, we wanted to focus on the comparison between wild-type and PKAC2 knockout in the phosphoproteome to analyze the primary targets of PKAC2. In the complete dataset we identified 10,924 phosphosites on 1,932 proteins. Of these, 194 sites were significantly regulated between WT and Δ PKAC2 on 105 proteins (Figure 27A, Supplementary Table 2). They can be divided into two clusters of up- or downregulation in Δ PKAC2. We find 27 significantly upregulated and 167 downregulated (FDR = 0.1, $S_0 = 0.1$) phosphosites in the KO (Figure 27C). This can be expected upon knockout of a kinase. Most of these potential substrates are localized in the flagellum (Subota et al., 2014). That is also expected, since this is the major localization of PKAC2. We also identified some glycosomal (Guther et al., 2014), mi-

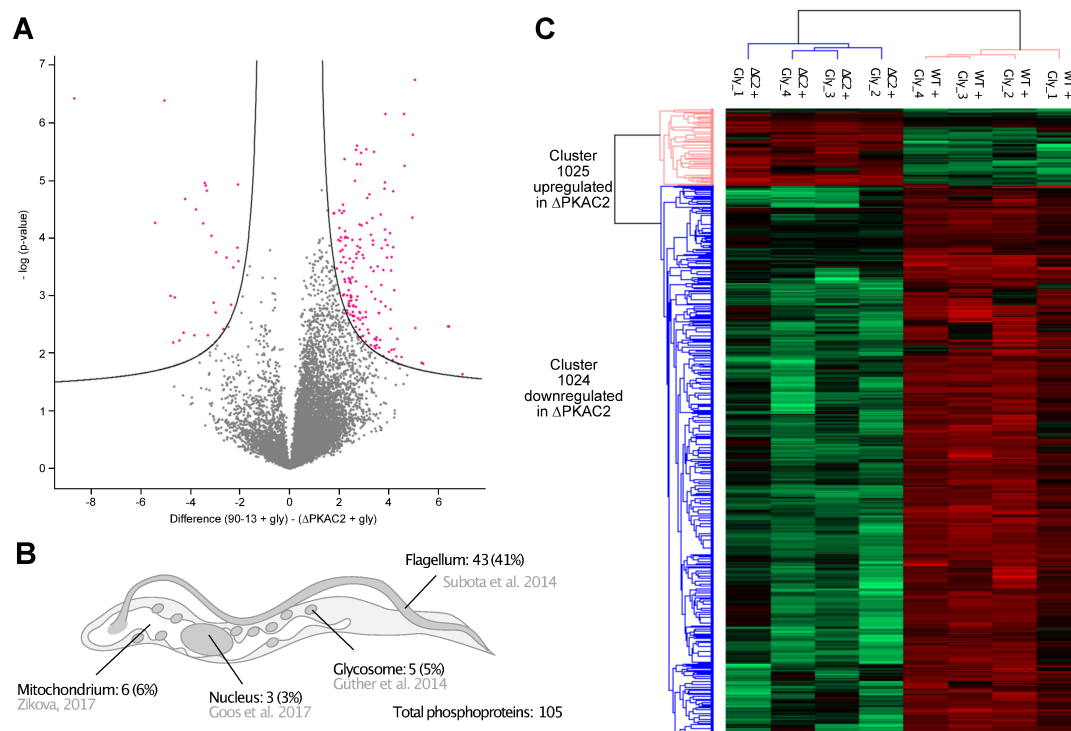


Figure 27: Comparative phosphoproteome of wild-type and Δ PKAC2. **A:** Volcano plot showing significantly (FDR=0.1, $S_0=0.5$) regulated phosphorylation sites (pink) of at least 1.5-fold between wildtype and PKAC2 knockout. **B:** Localization of the phosphoproteins assessed by published subcellular proteomes. **C:** Clustering analysis of identified phosphosites, divided into up- and downregulated in Δ PKAC2.

tochondrial (Zikova et al., 2017) and nuclear (Goos et al., 2017) proteins. Most identified proteins were not identified in any subcellular proteome and are thus most likely cytoplasmic (Figure 27B). Analysis of the phosphorylation motif of the regulated phosphosites showed a clear enrichment for (R)RXS* and S*P motifs (Figure 28A). The S*P motif is very common in the CMGC superfamily of proline-directed protein kinases (Melo-Braga et al., 2014; Pinna and Ruzzene, 1996). This group of kinases is

overrepresented in kinetoplasts and composes the biggest kinase group in *T. brucei* (Parsons *et al.*, 2005). Enrichment of this motif might indicate that PKAC2 is involved in a signaling cascade with CMGC kinases. Amongst the 65 regulated sites which were annotated as PKA sites by Phosphosite.org, (R)RXS* appears to be the most prominent consensus motif (Figure 28B).

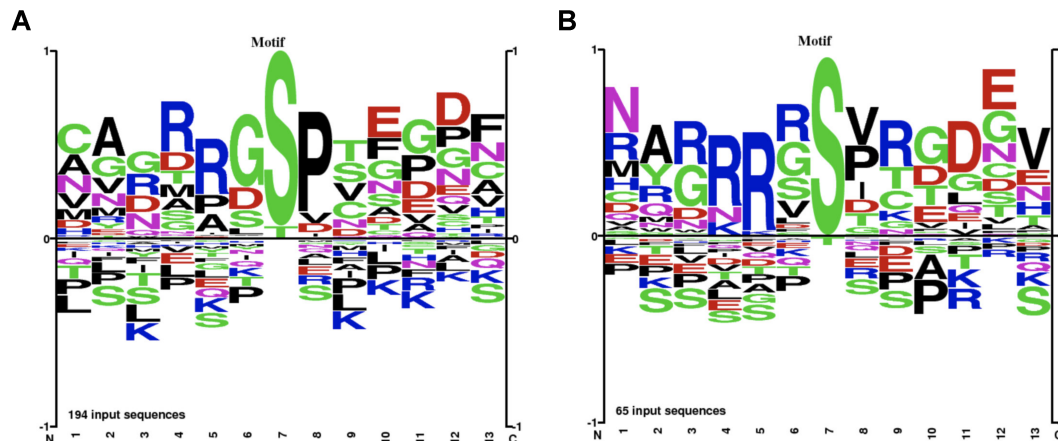


Figure 28: Consensus motif analysis of phosphosites regulated between wild type and Δ PKAC2. Motif and sequence logo analysis of 13 amino acid peptides (phosphoresidue on position 7) was performed with the sequence logo analysis tool available at Phosphosite.org using Phospho Ser as background. X-axis represents the position of the amino acid; y-axis shows which amino acids are over- or underrepresented at each position. **A:** Motif analysis of all significantly regulated phosphosites. **B:** Motif analysis of all phosphosites downregulated in Δ PKAC2 and annotated as PKA sites during Perseus analysis (kinase annotations obtained from Phosphosite.org)

GO enrichment analysis of cellular processes in both clusters mainly showed annotations for regulatory functions (Figure 29).

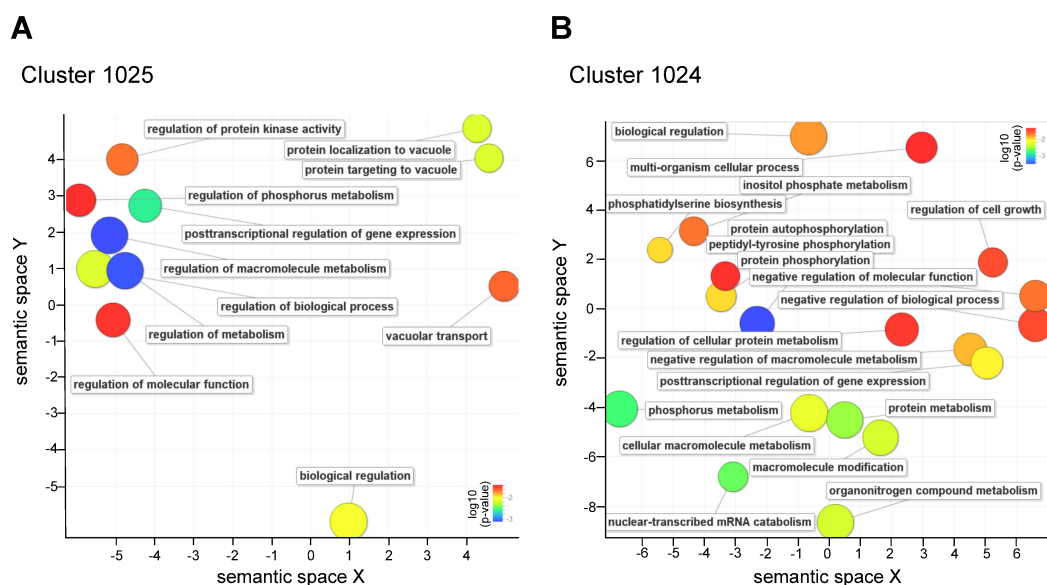


Figure 29: GO enrichment analysis of cellular processes of WT and Δ PKAC2 phosphoproteome using REVIGO (Supek *et al.*, 2011). **A:** Annotations of proteins with phosphosites upregulated in PKAC2 knockout. **B:** Annotations of proteins with phosphosites downregulated in the PKAC2 knockout.

Taken together, this would suggest that most substrates of PKAC2 are involved in the regulation of cellular processes, such as gene expression or signaling. But the consequence of PKAC2 removal are changes in different metabolic enzyme levels, indicating that PKAC2 might affect metabolic enzymes at the level of gene expression.

3.3.3 Interactome by BioID

In this chapter we wanted to explore interactions of the PKA catalytic subunit with other proteins using BioID. The BioID method was already established in our laboratory (M. Gould) and used to identify interaction partners of the PKA regulatory subunit in both life cycle stages (Reith, 2016). By performing a BioID screen using the catalytic subunit as a bait, we aimed to identify some interaction partners of the catalytic subunit and compare them with the interactome of the PKAR subunit. This way, we could distinguish between interaction partners of the holoenzyme and interaction partners of the active catalytic subunit, such as substrates. The advantage of using BioID is the high sensitivity for detection of transient interactions. This type of interaction is expected between a kinase and their substrate. We were hoping to be able to draw some conclusions on PKA function based on the localization and functional annotations of the putative interaction partners likely to be substrates. Further, we wanted to explore the possibility of alternative regulatory components in PCF, since PKAR-dependent activation by nucleosides or cold shock have no effect on PKA substrate phosphorylation in PCF (Bachmaier, 2015; Wu, 2021). We chose to do a comprehensive analysis involving all catalytic subunits expressed in their respective life cycle stage to additionally address the question of PKAC substrate specificity. Initially, N- and C-terminal fusion proteins of PKA and BirA* were generated, but C-terminal fusions were difficult to obtain and showed low expression levels. Additionally, C-terminal tags on PKA catalytic subunits were not well tolerated in *T. brucei* in the past. Hence, experiments were performed with the N-terminal BirA*-PKAC fusions only.

3.3.3.1 Bloodstream forms

First, we generated BirA*-tagged lines for PKAC1 and PKAC3 in BSF. BirA* is a small biotin-ligase from *E. coli*, optimized for BioID experiments (Roux et al., 2012). Fusion of BirA* to a bait-protein will lead to biotin-tagging of proteins in close proximity (approx. 10 nm) upon biotin addition. These biotinylated proteins can afterwards be purified using streptavidin-coupled beads and identified by mass spectrometry (Kim and Roux, 2016). We did not analyze PKAC2 in BSF due to very low expression levels in this life cycle stage (Bachmaier, 2015). After generation of the BSF cell lines we tested for expression of the fusion protein and biotinylation efficiency. In both cases, the fusion proteins were expressed at the expected size and induction of biotinylation for 24h showed a clear increase of biotinylated proteins, including self-biotinylation of the bait (Figure 30A). In general, using PKAC3 as a bait appears to result in overall less biotinylation and a slightly different pattern compared to PKAC1. Biotinylated proteins were purified using streptavidin beads and sent for identification via mass-spectrometry (M. Stadlmaier, faculty of chemistry). Figure 30B shows successful solubilization and capture of almost all biotinylated protein bands by the beads. Downstream analysis using

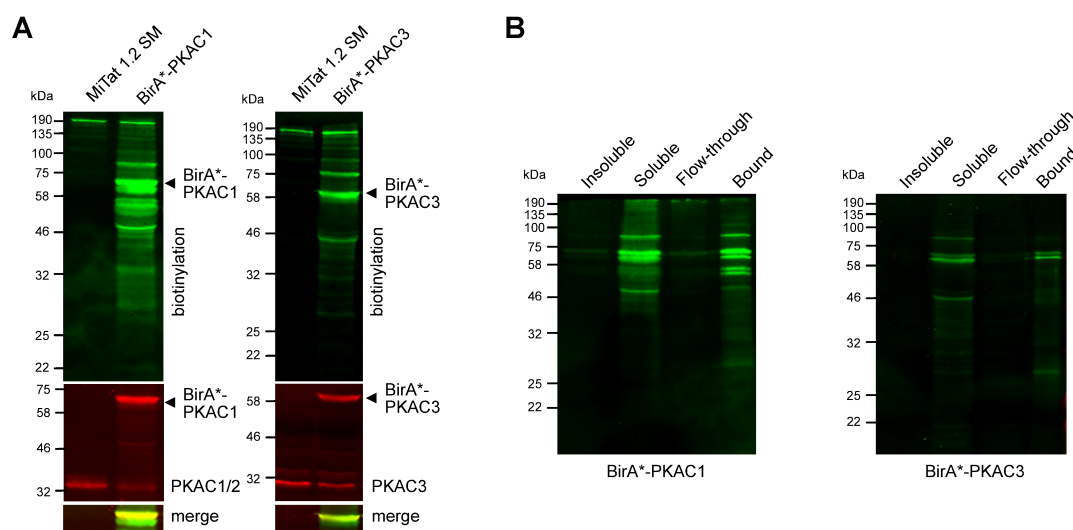


Figure 30: Generation of BSF BioID cell lines and MS pulldown. **A:** Expression of BirA*-PKAC was induced for 24h with 1 μ g/ml tetracycline. Biotinylation was induced simultaneously by addition of 50 mM biotin. Biotinylation was monitored by western blot using streptavidin-coupled IRDye800 (LI-COR). Expression of the BirA*-fusion proteins was confirmed using PKAC-specific antibodies. **B:** Examples of pulldown profiles of biotinylated proteins after BirA*-PKAC1 or BirA*-PKAC3 induction.

MaxQuant and Perseus (Tyanova and Cox, 2018; Tyanova et al., 2016a; Tyanova et al., 2016b) (described in 2.2.7.6) showed 159 significantly enriched proteins for PKAC1 and 155 for PKAC3 by Student's t-test (FDR = 0.01, $S_0 = 2$). The hits that were identified as enriched in the wild-type control (negative difference, left side of the volcano plot) were excluded from further analysis. As expected, the bait proteins were always one of the most enriched hits (Figure 31, Supplementary tables 3, 4). In both cases,

most of these proteins localize to the flagellum (Oberholzer *et al.*, 2011), which is not surprising given the predominantly flagellar localization of PKA. We did find a few pu-

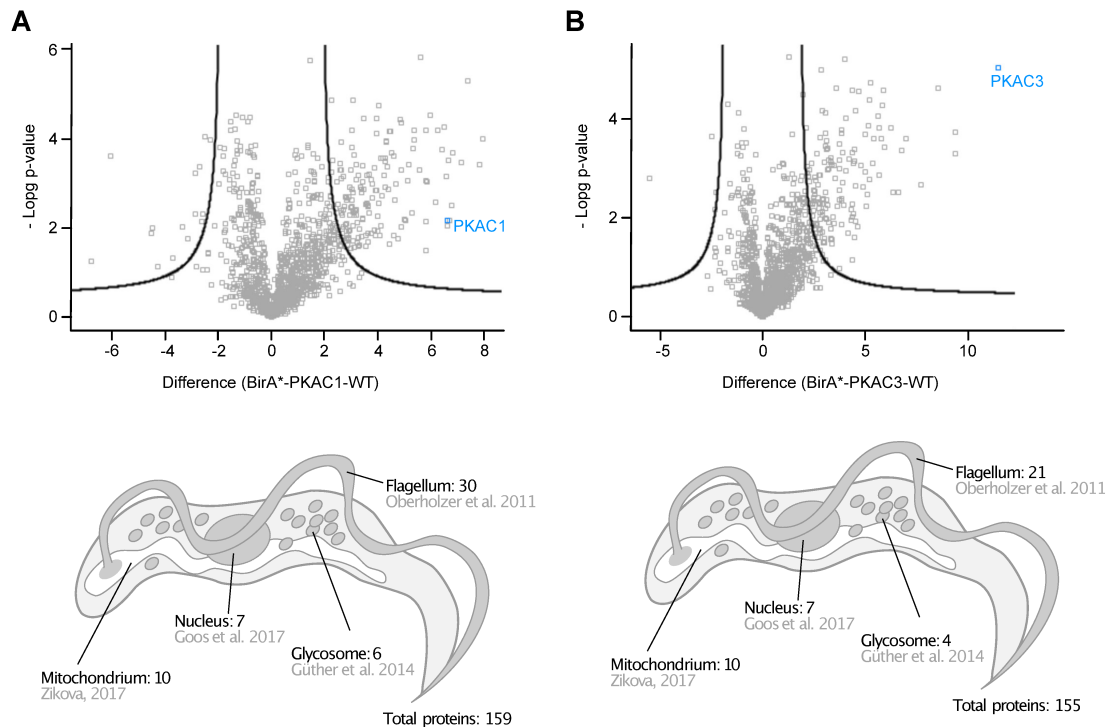


Figure 31: Significantly enriched proteins after BioID pull-down in comparison to wild-type control in BSF using PKAC1 and PKAC3 as bait. **A:** Upper panel shows volcano plot of significantly ($\text{FDR}=0.01$, $S_0=2$) enriched proteins using PKAC1 as bait. The lower panel gives an overview of the localization of identified proteins. **B:** Upper panel shows volcano plot of significantly ($\text{FDR}=0.01$, $S_0=2$) enriched proteins using PKAC3 as bait. The lower panel gives an overview of the localization of identified proteins.

tative interaction partners with mitochondrial (Zikova *et al.*, 2017), nuclear (Goos *et al.*, 2017) and glycosomal (Güther *et al.*, 2014) localization. However, the vast majority of identified hits has not been reported in any of the subcellular proteomes and therefore probably localizes to the cytoplasm. Comparison with the PKAR BioID experiment showed an overlap of 13 proteins with PKAC1 and 8 proteins with PKAC3 BioID. In general, the number of identified proteins is relatively high for a pull-down experiment, which might be due to the MS sample preparation. Instead of protein elution from the beads, an on bead-digest was performed to avoid elution problems due to the strong interaction of biotin and streptavidin. This protocol was tested beforehand in comparison to a classical elution and showed much higher reproducibility between replicates (data not shown).

3.3.3.2 Procyclics

We repeated the same experiment in procyclic trypanosomes using PKAC2 and PKAC3 as bait in this case. PKAC1 was considered irrelevant for this life cycle stage due to the downregulation in PCF and therefore omitted. Similar to the data from the BSF pulldown, we could confirm expression of the BirA*-fusion proteins and biotinylation of various proteins 24h post-induction with tetracycline. Fusion of BirA* to PKAC2

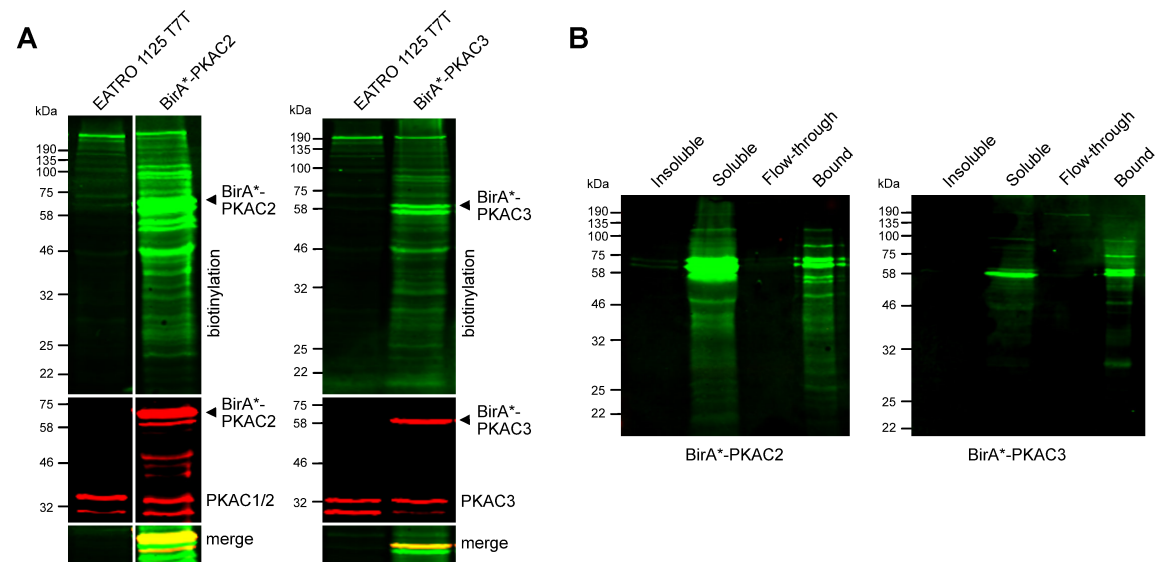


Figure 32: Western blot analysis of BiD pull-down in PCF. **A:** Expression of BirA*-PKAC was induced for 24h with 1 μ g/ml tetracycline. Biotinylation was induced simultaneously by addition of 50 mM biotin. Biotinylation was monitored by western blot using streptavidin-coupled IRDye800 (LI-COR). Expression of the BirA*-fusion proteins was confirmed using PKAC-specific antibodies. **B:** Examples of pulldown profiles of biotinylated proteins after BirA*-PKAC2 or BirA*-PKAC3 induction

leads to a slightly different band pattern compared to PKAC3 and also appears to have an overall higher biotinylation efficiency. Also, in this case self-biotinylation of the BirA*-PKAC3 fusion-protein could be detected (Figure 32A). Successful precipitation of most biotinylated proteins could be demonstrated in Figure 32B.

Downstream analysis showed 165 putative interaction partners for PKAC2 and 112 for PKAC3 (Student's t-test, FDR = 0.01, $S_0 = 2$) with the bait proteins being the most prominent hits (Figure 33, supplementary tables 5, 6). Again, most proteins localize to the flagellum (Subota *et al.*, 2014) or were not associated with any of the investigated subcellular proteomes.

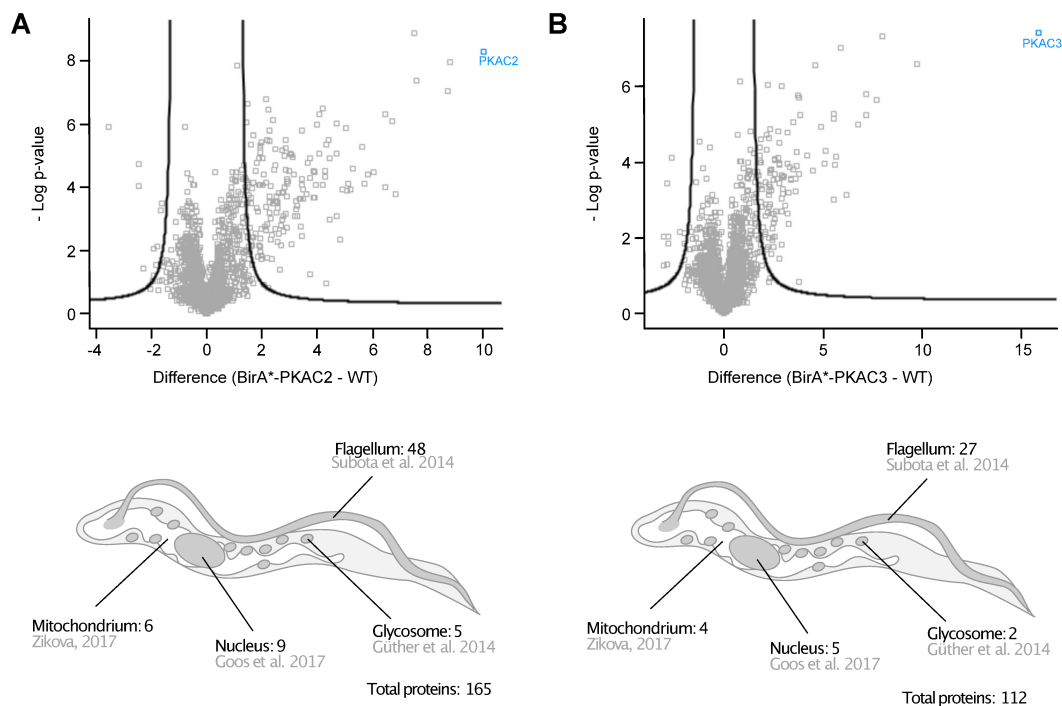


Figure 33: Significantly enriched proteins from BioID pulldowns in PCF. **A:** Upper panel shows volcano plot of significantly (FDR=0.01, $S_0=2$) enriched proteins using PKAC2 as bait. The lower panel gives an overview of the localization of identified proteins. **B:** Upper panel shows volcano plot of significantly (FDR=0.01, $S_0=2$) enriched proteins using PKAC3 as bait. The lower panel gives an overview of the localization of identified proteins.

3.3.3.3 Data exploration

First, we had a closer look at the proteins that we found in every PKA BioID experiment. Running a GO analysis using the REVIGO online tool implemented in tritrypdb.org (Supek *et al.*, 2011) results in annotations concerning protein stability and folding. Given that each protein needs to be folded, sorted and transported to its final destination, this group of hits seems to be rather unspecific and most of these would probably be found using any random bait. Comparison of PKAC1 and PKAR common hits leaves 4 flagellar proteins in BSF and 8 in PCF, when excluding PKAR itself from the list. Analysis of the associated GO terms shows mainly structural components and annotations for motility (Figure 34A/B). Comparison of BSF PKAC3 and PKAR yields no overlapping hits in PCF and only one common protein in BSF: microtubule-associated-repetitive protein 2 (MARP2), which localizes to the basal body. In general, the holoenzyme-specific hits for both life cycle stages are very few. This can be explained by the rather short hitlist for PKAR which is most likely due to the protein elution after pulldown instead of the on-bead digest. In addition to the technical differences, we expect the catalytic subunits to form more transient interactions due to substrate phosphorylation. These reactions do not necessarily have to take place in close proximity to the PKAR subunit or even in the flagellum at all. In contrast to the catalytic subunit,

PKAR is anchored to the PFR and cannot freely diffuse (Fort et al., 2016; Krumbholz, 2006), which would also lead to less transient interactions.

Overlaps between PKAC1 and PKAC3 pulldowns in BSF and PKAC2 and PKAC3 in PCF show a majority of common hits, but also numerous subunit-specific proteins (Figure 34A/B). GO enrichment analysis for biological processes shows mostly very similar annotations, mainly for regulation of gene expression and phosphorylation. Enrichment analysis for PKAC1-specific genes (BSF) mainly yields regulation of gene expression, metabolic process and cytokinesis, and cell cycle. For PKAC3 in BSF we find enrichment for protein phosphorylation and regulation of gene expression and metabolic processes. In PCF, PKAC2-specific annotations include phosphorylation, cell division and

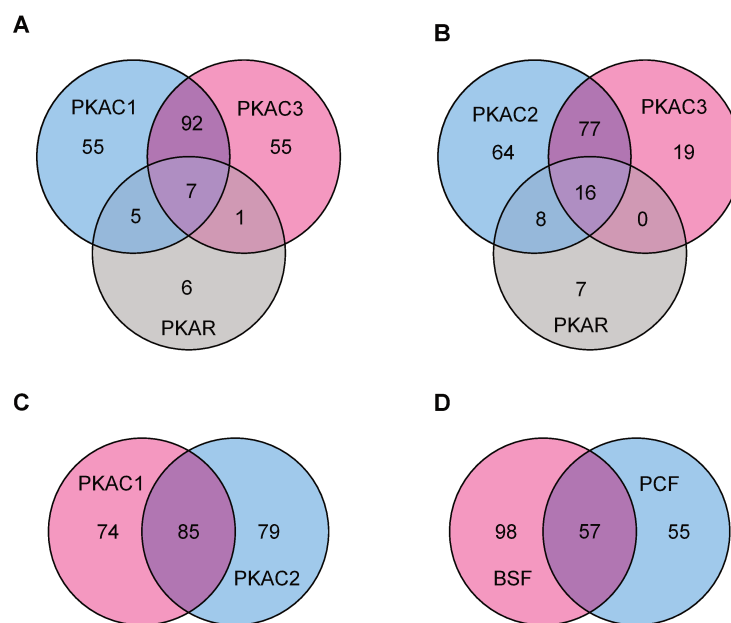


Figure 34: Venn diagrams showing common and subunit-specific hits of PKA BioID experiments. **A:** Comparison of PKA BioID experiments in BSF. **B:** Comparison of PKA BioID experiments in PCF. **C:** Comparison of hits from PKAC1 (BSF) and PKAC2 (PCF) BioID experiments. **D:** Comparison of PKAC3 BioID experiments in BSF and PCF.

nucleoside metabolism, while the PKAC3-specifics mainly focus on cell cycle and cell division.

Comparison of PKAC3 between BSF and PCF show a lot of common proteins (Figure 34D) with annotations for phosphorylation, cytokinesis and regulation of gene expression and metabolism. The BSF-specific ones focus on regulation of gene expression and structural

parts of the cell, like microtubules, cytoskeleton and the flagellar attachment zone (FAZ). Amongst the PCF-specific annotations we find regulation of protein folding, organization of cell structures and multi-cellular signaling.

Comparison of PKAC1 (BSF) and PKAC2 (PCF) showed more similarities than differences in terms of putative interaction partners (Figure 34C). GO enrichment analysis of the common hits shows nucleoside metabolism, protein phosphorylation, motility, signaling and regulation of gene expression and metabolism. Focusing on PKAC1-specific genes shows quite similar annotations: regulation of gene expression, signaling and regulation of cytokinesis. For PKAC2-specific proteins we find annotations for nucleoside metabolism, cytokinesis, motility and phosphorylation.

Since we were specifically interested in kinase-substrate interactions, we compared our interactomes with available PKA phosphoproteomes. For PKAC2, we checked for proteins that were also identified as regulated between wild-type and Δ PKAC2 (see chapter 3.3.2). In this comparison we only found 10 proteins, which were identified in BioID and differentially phosphorylated between wild-type and Δ PKAC2. For PKAC1, we compared the differentially phosphorylated proteins in response to 7-CN-7-C-inosine (= jaspamycin) treatment, a potent PKA activator which mainly activates PKAC1 in BSF (Bachmaier *et al.*, 2019). Here we found 38 common hits, which are highly likely to be PKAC1 substrates.

Next, we wanted to investigate whether the PKAC1 (BSF) and PKAC2 (PCF) specific interactions could be simply explained by life cycle regulated expression of these genes. The same was investigated for BSF- and PCF-specific interaction partners of PKAC3. For this purpose, we extracted a list of proteins from the PCF/BSF comparative proteome (Urbaniak *et al.*, 2012) which are upregulated at least 2-fold in BSF or PCF, depending on the comparison. These lists were compared with our interaction partners identified in BioID. We found that the majority of hits is not regulated between BSF and PCF using the parameters of at least a two-fold difference (Figure 35).

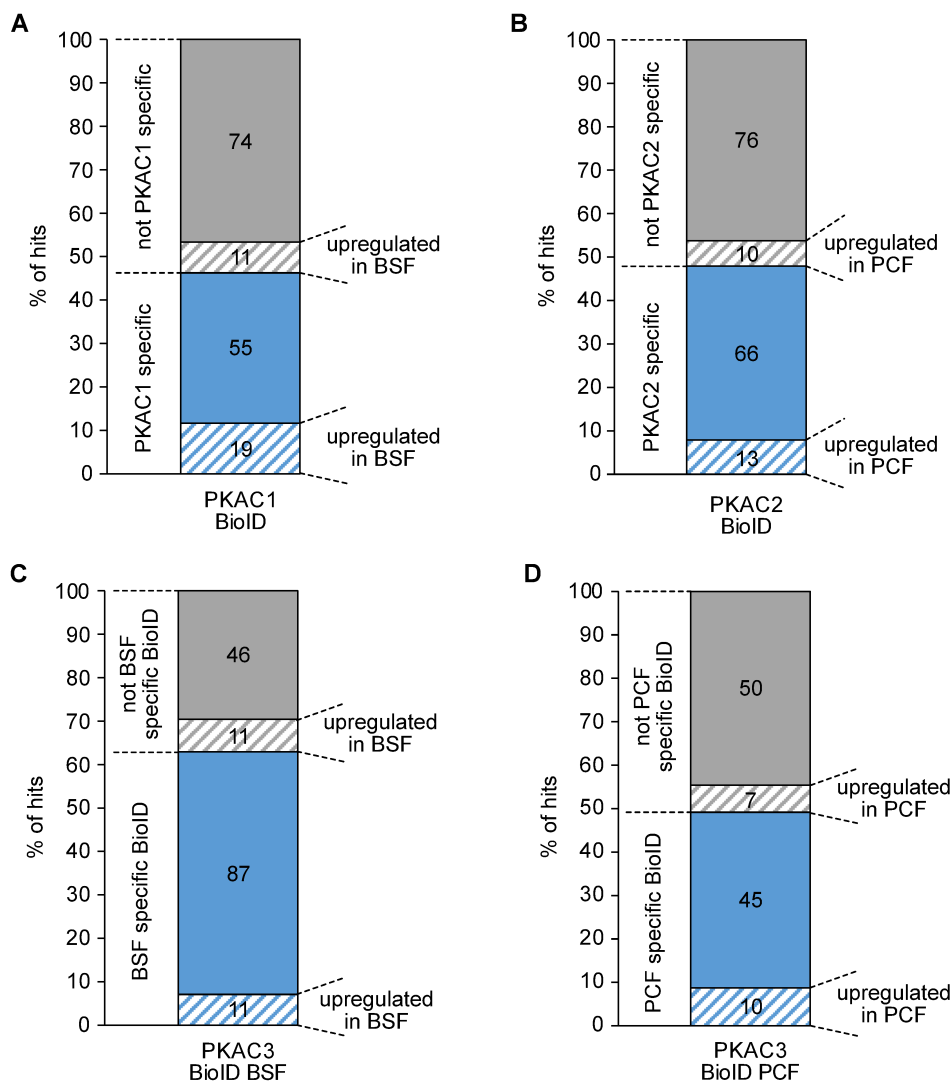


Figure 35: Comparison of BioID hits with (Urbaniak et al., 2012) PCF/BSF comparative proteome. Up-regulation in BSF was defined as at least 2x by filtering for \log_2 fold change ≤ -1 . Up-regulation in PCF was defined as at least 2x by filtering for \log_2 fold change ≥ 1 . **A:** PKAC1 BioID in BSF. **B:** PKAC2 BioID in PCF. **C:** PKC3 BioID in BSF. **D:** PKAC3 BioID in PCF. Color code: blue = subunit-/stage-specific hits, grey= interactors identified for both subunits/life cycle stages, pattern fill in respective color indicates up-regulation in BSF/PCF. Numbers represent absolute number of hits in each category, while the y-axis shows the percentage.

In summary, the overlap between the different BioID experiments shows only very few PKAR-PKAC holoenzyme-specific protein interactions. They are all localized in the flagellum and almost exclusively found with PKAC1/2 subunits. Comparison of the datasets from all PKAC subunits also shows a certain redundancy between the different catalytic subunits, but still roughly 20-50% of the hits remain subunit-specific. These specificities are unlikely due to life-cycle stage dependent expression of the putative interaction partners. In terms of function, the same GO annotations are reoccurring: regulation of gene expression, phosphorylation and signaling, cytokinesis, motility, nucleoside metabolism.

3.3.4 Structural modeling of PKAC1 and PKAC2

The *T. brucei* genome encodes three PKA catalytic subunits, of which PKAC1 and PKAC2 share an extremely high similarity but are still differentially regulated throughout the life cycle. PKAC1 and PKAC2 only differ in 19 amino acids, which are mostly located on the N- and C-terminus of the proteins. These two PKA subunits are not essential as shown before but may have specialized functions under specific conditions. So far, known activators like nucleoside analogs or cold shock were shown to be mediated by PKAC1 (Bachmaier, 2015). However, none of these activators induce PKA activities in PCF, as measured by downstream substrate phosphorylation. In the PCF stage, PKAC2 is predominant. Additionally, we found subunit-specific interaction partners in the BioID interactome analysis. The majority of these interactors are not expressed in a life-cycle-dependent manner indicating that there is a subunit-specific subset of interactors. The question now is how this specificity is conferred. In this paragraph, we want to focus on the few key differences in amino acids between PKAC1 and PKAC2 by structural modeling and hypothesize potential consequences of these differences. The structural modeling was performed using the Phyre2 server (Kelley et al., 2015). A model with high confidence and sequence coverage for both subunits was chosen for structural comparison. Both structures were superimposed and the differences highlighted. Figure 36A shows the linear protein structure where the important domains and differences between the subunits are highlighted. As mentioned before, most of them are located on the extreme N-terminus or the C-terminal AGC-kinase domain. Unfortunately, the extreme N-terminus could not be modeled by the software and therefore not be analyzed here. The differences of the amino acids are highlighted in the protein surface model in Figure 36B. Interestingly, the only modeled N-terminal difference (1) seems to structurally contribute to the AGC-kinase C-terminal domain once the protein is folded. The L237 in PKAC1 and F239 in PKAC2 (2) appear structurally quite similar. Due to its aromatic properties, phenylalanine (F) can potentially contribute to protein-protein interactions, but is also buried within the structure, most likely not causing any major impact on functionality. The serine on position 247 in PKAC2 (3) is a phosphorylatable amino acid and should be highly similar to the glutamate (phosphomimetic amino acid) on PKAC1 on that position, when phosphorylated. However, this residue is to date not reported as phosphorylated in any of the phosphoproteomes. On position (4/5) PKAC2 has acquired two aromatic residues, which seem bulkier compared to PKAC1. R321 on PKAC2 (6) also appears bulkier compared to the small glycine in PKAC1. Right next to it, PKAC1 harbors a serine residue, which is also reported to be phosphorylated. The next difference is T324 on PKAC1 (7), also

known as the stumpy-specific phosphorylation (Kramer, 2004). Phosphorylation of this amino acid is upregulated in stumpy forms and is PKAC1-specific. The differences marked as positions (6) and (7) are in close proximity to the catalytic site and could be important for catalytic activity or substrate specificity. And finally, the last difference is composed of L331 and E332 in PKAC2 and V329 and A330 in PKAC1 (8). Both differences seem to result in a bulkier overall protein surface in PKAC2.

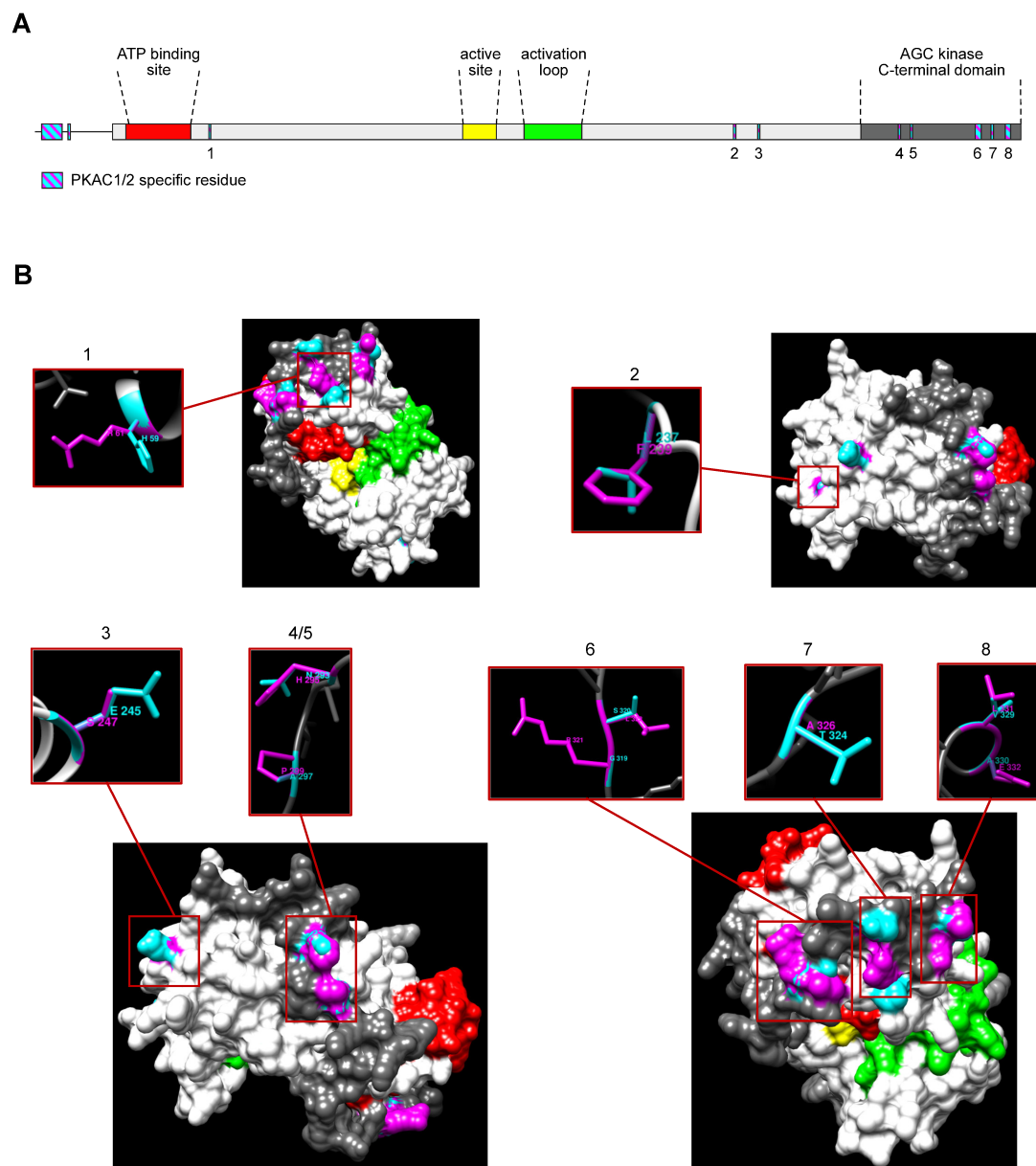


Figure 36: Structural modeling of PKAC1 and PKAC2. **A:** Linear structure of PKAC1/2, indicating protein domains and differences between the subunits. **B:** Superimposed models of PKAC1 and PKAC2 generated using UCF Chimera. Domains and Differences are colored as indicated in **A**.

The N- and C-terminus are also regions with plenty of differences in phosphorylation reported in phosphoproteomic analyses (Nett *et al.*, 2009; Urbaniak *et al.*, 2013; Zhang *et al.*, 2020). The residue color code represents in which dataset the phosphosites

were discovered (Figure 37). The phosphorylation sites in the activation loop appear to be conserved, however this region is in fact too similar to be distinguished by MS after tryptic digest. These phosphosites were not identified in the available phosphoproteomes from PCF datasets (Urbaniak *et al.*, 2013). This could indicate that these phosphosites are either PKAC1-specific or only phosphorylated on PKAC2 in BSF.

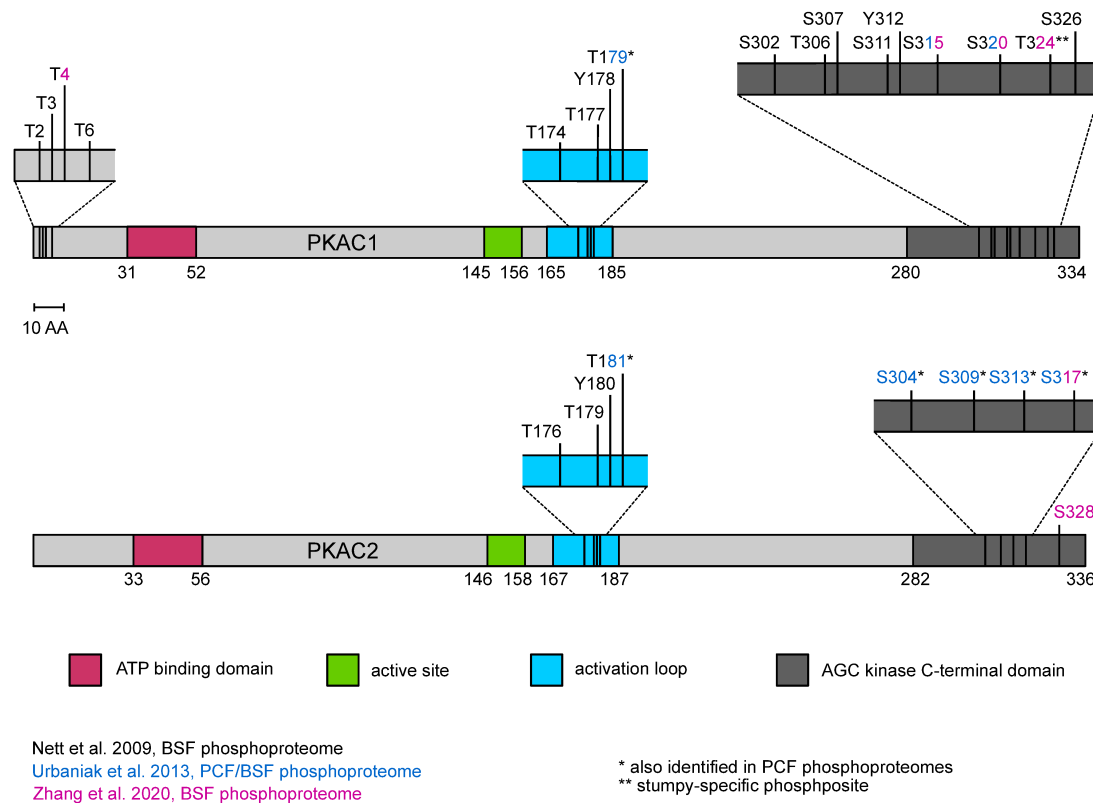


Figure 37: Phosphorylation sites identified on PKAC1 and PKAC2. Schematic representation of all phosphosites identified on PKAC1 and PKAC2 in phosphoproteomic analyses of (Nett *et al.*, 2009; Urbaniak *et al.*, 2013; Zhang *et al.*, 2020). Phosphosites are color coded based on the datasets in which they were found.

Additionally, in the phosphoproteome described in chapter 3.3.2, we could only identify the activation loop phosphorylation (T179/T181) and one additional C-terminal phosphorylation on S315 (PKAC1)/S317 (PKAC2). Numerous differences are located on the N-terminus. Here, PKAC1 is heavily phosphorylated while some of these amino acids are not even phosphorylatable in PKAC2. For both subunits, multiple phosphorylation sites were identified on the C-terminus, but to a higher extent for PKAC1. In general, PKAC1 appears to be phosphorylated at a higher extent compared to PKAC2, which could also lead to different properties.

In conclusion, most differences which could be modeled here are surface exposed and at least structurally located on the C-terminus. In this region, PKAC1 and PKAC2 appear to have a different surface topology which could result in differences of protein-

protein interaction. Moreover, this C-terminal region is located close to the catalytic site and could influence substrate binding specificities.

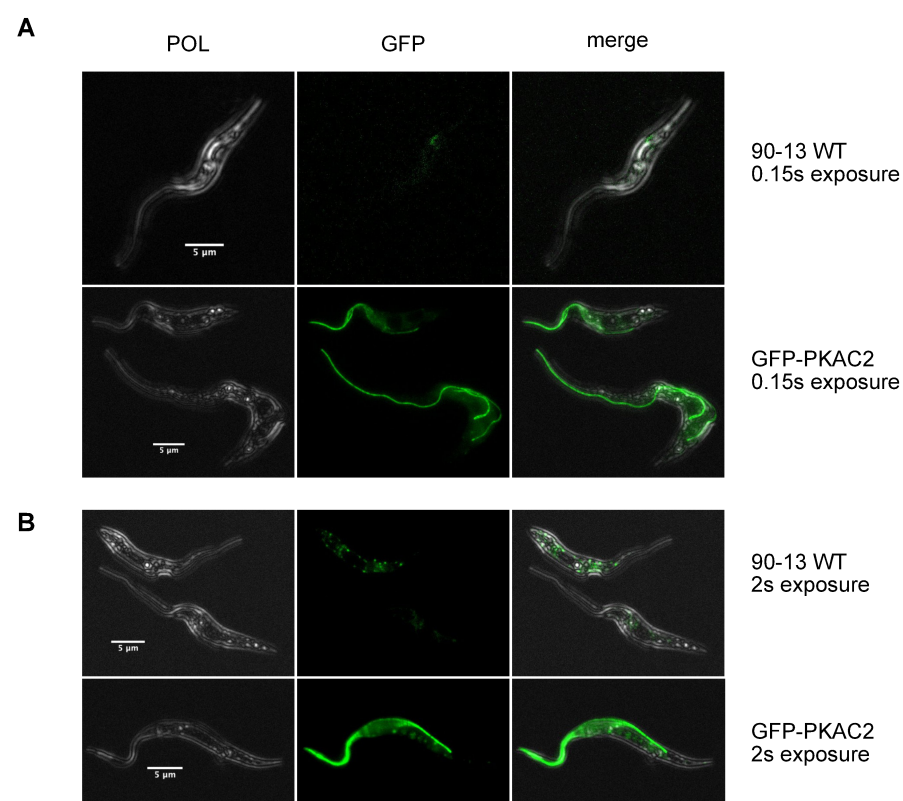
3.4 Possible role of PKAC2 in the regulation of metabolism

3.4.1 Glycosomal localization of PKAC2

The flagellar localization of all PKA subunits in both life cycle stages has been known for a while now (Fort *et al.*, 2016; Krumbholz, 2006; Oberholzer *et al.*, 2011). The PKAC2 subunit was the only one reported in the high confidence glycosomal proteome as a second location (Guther *et al.*, 2014). Additionally, the results of the multi-omics approach in the previous chapter indicate a function of PKAC2 in metabolism. The imaging data from tryptag.org (Dean *et al.*, 2017) for PKAC2 shows a flagellar and a punctuated pattern which would be compatible with glycosomes. Since this was not reported for BSF, we hypothesized this could be one functional difference between PKAC1 and PKAC2. Therefore, we tried to confirm this additional localization and explore whether PKAC1 also had the potential to localize to glycosomes or if this was a PKAC2-specific feature, possible due to some of the key differences highlighted in chapter 3.3.4.

3.4.1.1 Fluorescence microscopy of GFP-PKAC2

Initially, we tried to reproduce the imaging data from tryptag.org and used the same *in-situ* tagging strategy (Dean *et al.*, 2015) (Cell line specification are described in 2.1.4). Using a low exposure time that gives no background fluorescence in wild-type cells only resulted in flagellar fluorescence signal with some cytoplasmic background (Figure 38A). If the exposure time was increased, we could see a punctuated pattern that resembled glycosomes, but it also resulted in a very similar pattern in wild-type cells (Figure 38B). This background fluorescence could be attributed to auto-fluorescent proteins, like glycosomal fumarate reductase for example (Schenk *et al.*, 2021). Unfortunately, this background fluorescence doesn't allow to draw any conclusions on glycosomal localization of PKAC2.



3.4.1.2 Glycosome purification

Since imaging of GFP-tagged PKAC2 was not conclusive, we aimed to answer the question using biochemical methods and established a repertoire of glycosome enrichment and purification methods in our laboratory.

3.4.1.2.1 Glycosomal localization of endogenous PKAC2

The first question to answer was whether PKAC2 truly localizes to glycosomes in PCF cells. We used a differential centrifugation protocol (kindly provided by F. Bringaud) to enrich a glycosomal fraction (Figure 39A). We were aiming to analyze localization to a metabolically important compartment. Since we did not know whether import would be regulated by metabolic state, we performed the purification on cells grown in two met-

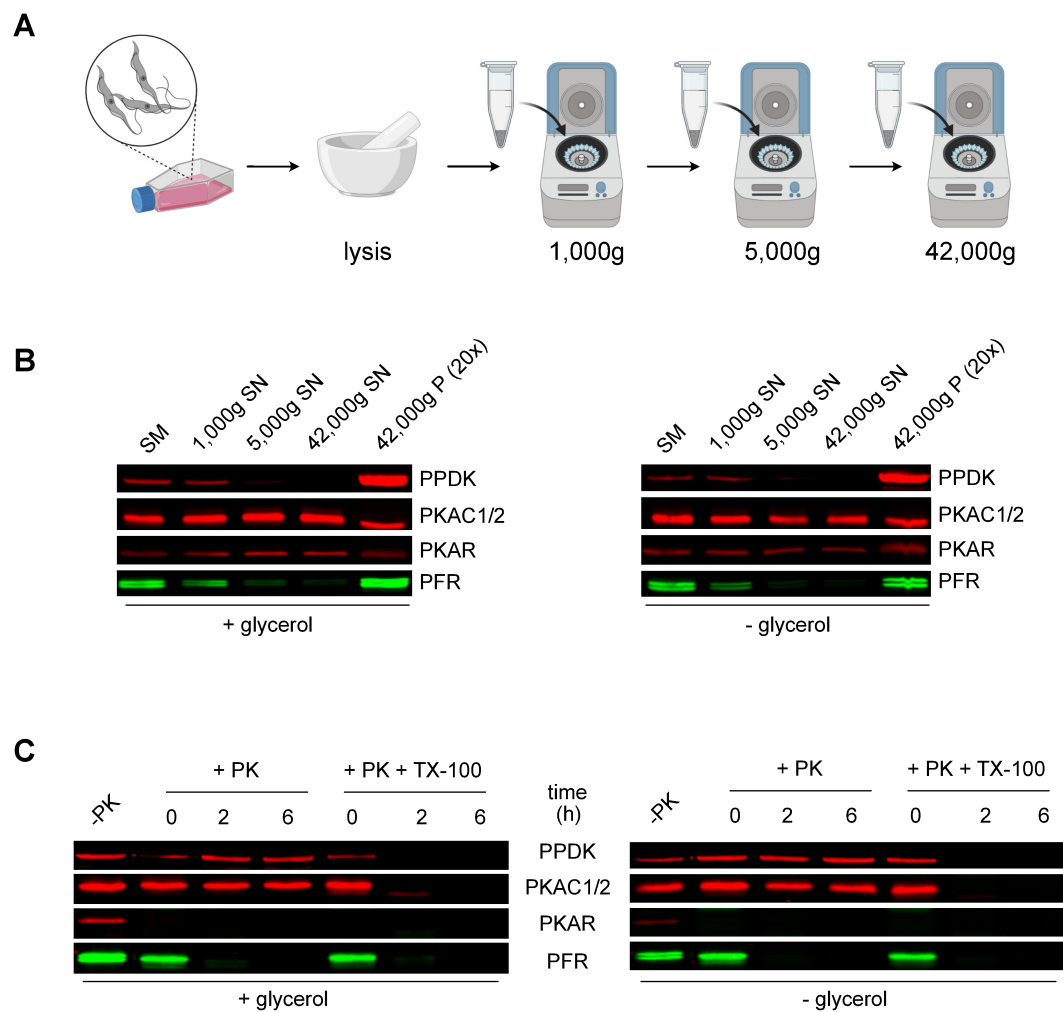


Figure 39: Confirmation of PKAC2 glycosomal localization by glycosome enrichment. **A:** Overview of the purification workflow. Cells were harvested and mechanically lysed in a mortar. At 1,000g cell ghosts and nuclei were removed, the supernatant transferred to a fresh tube. At 5,000g the mitochondria were removed and at 42,000g the glycosomes were pelleted. Created with Biorender.com. **B:** Profiles of PKAC1/2, PKAR, glycosomal (PPDK) and flagellar (PFR) makers throughout the purification process. Equivalent amounts of each fraction were loaded, except for 42,000g enriched organelles. **C:** Protease protection assay of the 42,000g enriched organelles. 10 μ g of enriched organelles were incubated with proteinase K (PK) for up to 6h. Addition of Triton X-100 (TX-100) served as control for protein digestibility. Protection of PKAR and PKAC1/2 was analyzed by western blot and compared to glycosomal and flagellar marker proteins.

abolically different conditions (+/- glycerol). In both cases, we could detect a strong enrichment for the glycosomal marker (PPDK) as well as PKAC1/2 and PKAR in the final preparation. Unfortunately, we could also detect an enrichment for the flagellar marker (PFR) (Figure 39B). The fact that PKA localizes mainly to the flagellum meant

we needed an additional way to separate glycosomes from flagella. Further incubation of the glycosomal preparation with proteinase K (PK) led to efficient degradation of flagellar proteins, while glycosomal contents remained protected (Figure 39C). Susceptibility to proteinase K digestion of all analyzed proteins was controlled by prior permeabilization of glycosomes with Triton X-100. In both metabolic conditions, we observed protection of PKAC2 while PKAR was completely degraded, confirming the glycosomal localization of PKAC2.

3.4.1.2.2 Glycosomal localization of ectopic TY-PKAC1 and TY-PKAC2

Finally, we were interested in the question whether PKAC1 could potentially be imported in glycosomes as well. Alternatively, this could be one functional difference conferred by the different N- and C-termini of PKAC1 and PKAC2 for example. Therefore, we generated TY-tagged overexpression lines of PKAC1 and PKAC2 in PCF (cell lines generated by G. Wagner, bachelor thesis 2020) and investigated glycosomal localization by glycosome purification. We used TY-tagged fusions to be able to distinguish TY-PKAC1/TY-PKAC2 from endogenous PKAC2. During the course of this project, we noticed that the differential centrifugation used for the initial purification in the previous chapter, not just enriched glycosomes and flagella, but also some other membrane-bound vesicles, like the endoplasmic reticulum (ER). Therefore, we optimized the purification procedure to remove as many contaminating compartments as possible by an additional ultracentrifugation step through a discontinuous optiprep density gradient (Figure 40). This gradient resulted in two bands, the upper one contained mitochon-

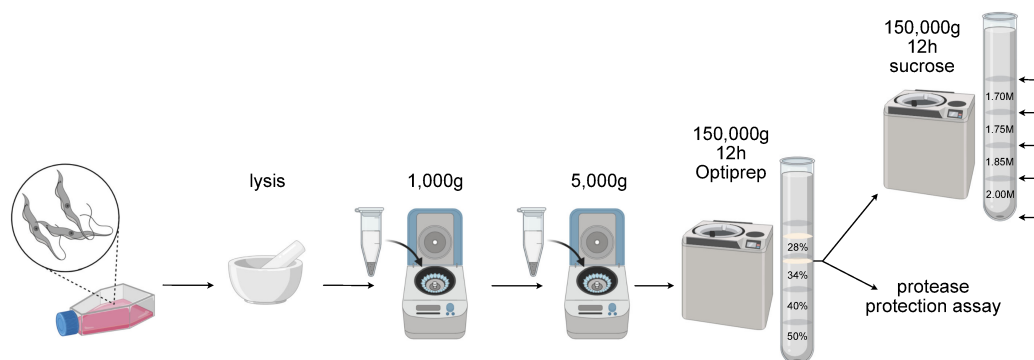


Figure 40: Purification procedure for clean glycosome preparations. Cells were mechanically lysed in a mortar and subjected to differential centrifugation at 1,000g and 5,000g. The 5,000g supernatant was subjected to ultracentrifugation through a discontinuous optiprep gradient, resulting in two distinct bands. The upper band contains cytoplasm, endoplasmic reticulum and mitochondria. In the lower band we detect glycosomes and flagella. The lower band was extracted and subjected to either protease protection assay or a second ultracentrifugation step through a discontinuous sucrose-gradient. Figure was created using BioRender.com

drial, ER and cytoplasmic proteins, while we only detected glycosomes and flagella in the lower band (*band 2*) (Figure 41A). This band was extracted and subjected to either a discontinuous sucrose gradient or protease protection assay. Each interface of the

sucrose gradient was sampled and we profiled glycosomal and flagellar markers as well as PKA. We could observe a quite similar profile for TY-PKAC1 and TY-PKAC2 resembling the glycosomal marker protein (Figure 41B). Proteinase K digestion further confirmed protection of both subunits within the glycosomes (Figure 41C).

In summary, both PKAC1 and PKAC2 can be imported into PCF glycosomes as long as they are expressed.

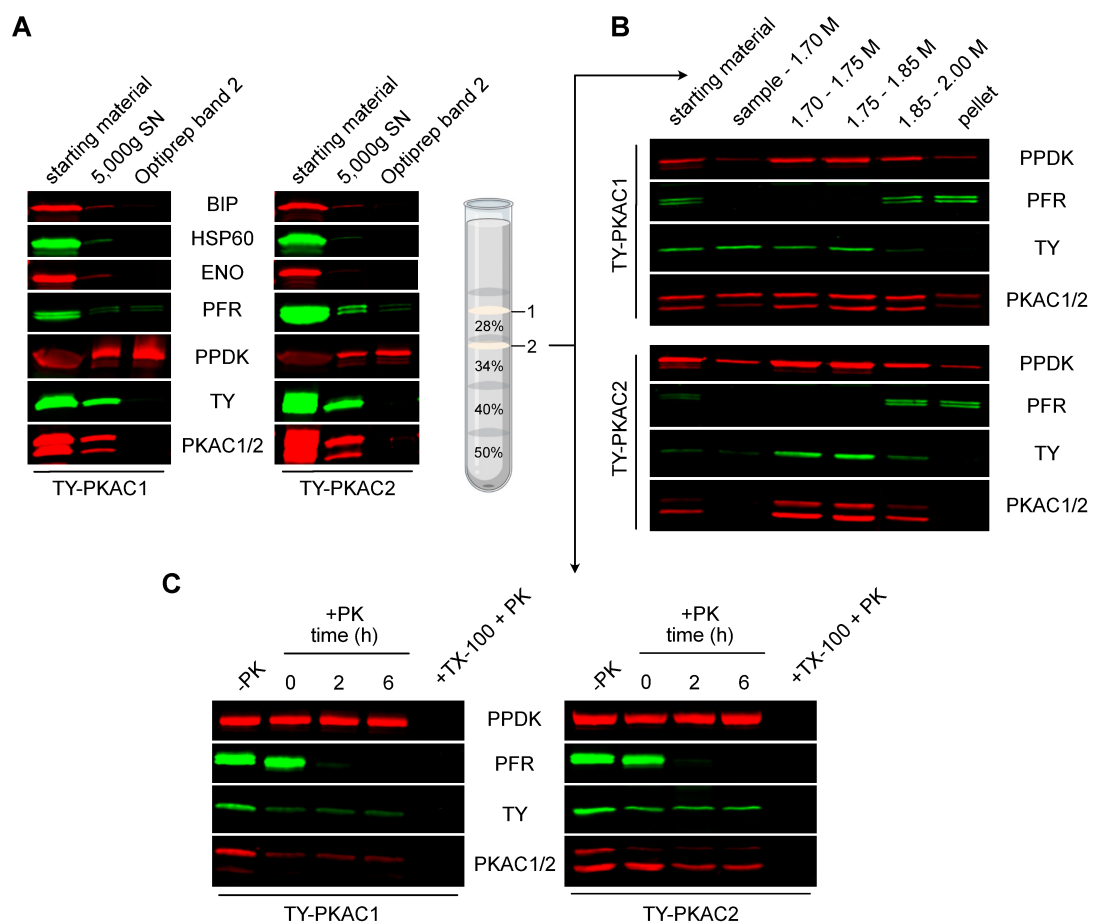


Figure 41: Analysis of glycosomal localization of TY-PKAC1 and TY-PKAC2. **A:** Assessment of organelle composition in the band recovered from Optiprep gradient using organellar markers (BIP = ER, HSP60=mitochondria, PFR=flagella, PPKD=glycosomes). **B:** Profiles of TY-PKAC1 and TY-PKAC2 through sucrose density gradient compared to glycosomal and flagellar marker distribution. **C:** Protease protection assay of Optiprep band.

3.4.2 Regulation of carbohydrate metabolism

The glycosomal localization of PKAC which we could confirm in the previous chapter led us to hypothesize that PKA could be involved in carbon source-mediated signaling processes. In contrast to BSF, procyclic trypanosomes have a more sophisticated repertoire of metabolic pathways and can utilize multiple carbon sources for energy generation. Here we can distinguish between glycolytic carbon sources which are degraded in glycosomes and amino acids which are metabolized in mitochondria. We wanted to explore whether switching the carbon source would first of all lead to any

changes in RXXS*/T* substrate phosphorylation and if so, whether these changes are PKA-dependent.

3.4.2.1 Growth analysis under different carbon sources

Standard SDM79 medium is rich in glucose, glycerol and proline amongst other amino acids. Initially, we aimed to analyze the switch from glucose to proline metabolism. However, we found that when PCF cells (AnTat 1.1 90-13) are supplemented with glucose only, they go into growth arrest and eventually die off (Figure 42A). The matrix-

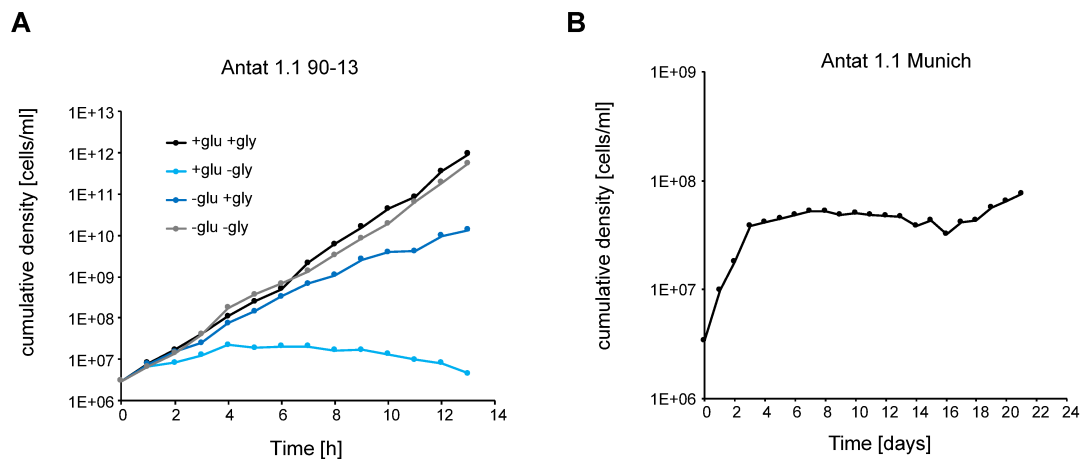


Figure 42: Growth analysis of AnTat wild-type strains in different carbon sources. **A:** Growth behavior of AnTat 1.1 90-13 under different carbon sources. Glucose as sole glycolytic carbon source in SDM79 medium leads to growth arrest and eventual cell death. **B:** Growth analysis of AnTat 1.1 Munich (=parental cell line of AnTat 1.1 90-13) in SDM79 supplemented with glucose only. Here we observe a transient growth arrest over two weeks.

dependent parental cell line (for more information on strain specificities see 2.1.4) of this strain shows a transient growth arrest, too (Figure 42B). During this time, the cells change shape and look extremely unhealthy. This observation was one reason for the decision to use glycerol as a glycolytic carbon source for the following experiments. In addition to that, we believe that glycerol has a higher physiological relevance in the procyclic life cycle stage. Glucose-depletion is an event that occurs shortly after transmission, but glycerol might be available after each blood meal of the tsetse fly once the cell membranes of the erythrocytes are broken down.

3.4.2.2 Role of PKA in carbon source metabolism

3.4.2.2.1 Glycerol depletion changes RXXS*/T* phosphorylation pattern

To address our initial question of whether PKAC2 is involved in carbon-source signaling, we performed glycerol-depletion on procyclic cells for 1h and analyzed the resulting band pattern of phosphorylated RXXS*/T* substrates. We could detect slight changes in the pattern in wild-type cells, most prominently a band of ~50 kDa (Figure

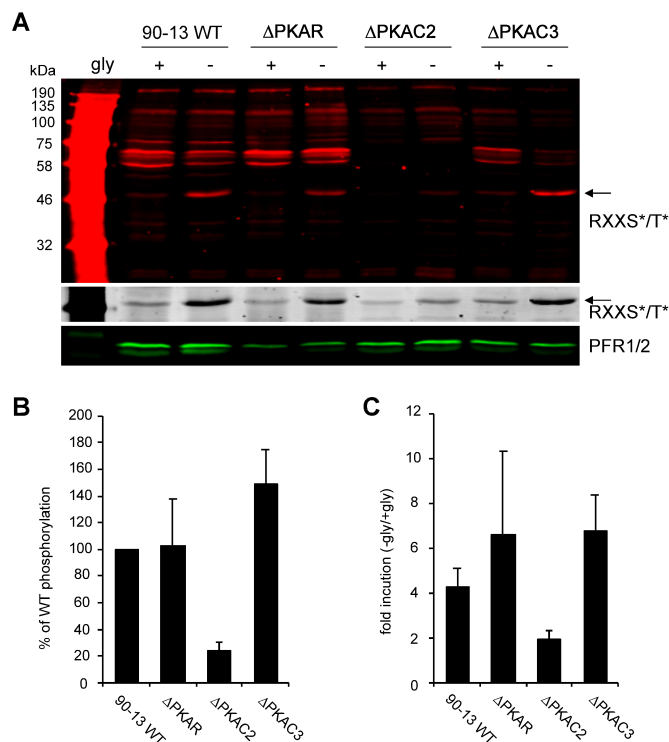


Figure 43: Effects of glycerol-depletion on RXXS*/T* phosphorylation in WT and PKA null mutants. PCF cells were cultured in glucose-free medium containing glycerol as a glycolytic carbon source. They were washed once and resuspended in glucose and glycerol-free medium and incubated for 1h at 27°C. Finally, samples were taken and subjected to western blot analysis using Phospho (Ser/Thr) PKA substrate antibody (representative blot in **A**). PFR was used as a loading control, arrow indicates a strongly regulated phosphoband. This phosphoband is additionally presented in greyscale with higher contrast. **B:** Quantification of phosphorylation after 1h of glycerol-depletion. Wildtype was set to 100% (n=4), bars represent average \pm stdev. **C:** Changes in phosphorylation level upon glycerol-depletion in the different cell lines.

43A). The optimal depletion time was determined by a previous time course (Supplementary Figure 4). We proceeded to analyze this phosphorylation event in the available PKA null mutants (note: the Δ PKAC1/2 double knockout was generated after these data were acquired, which is why we use the Δ PKAC2 single knockout here). The phosphorylation or abundance of this band/these bands (it cannot be excluded that the band represents multiple proteins of similar size) was severely reduced in Δ PKAC2 (~20%), but not affected in any of the other PKA knockouts (Figure 43A/B). The fold-change in band intensity in Δ PKAC2 is not completely reduced to 1 (Figure 43C). This could be

due to some residual PKAC1 activity. We performed the same experiment as in Figure 43 also with glucose-depletion instead of glycerol-depletion and it led to the same regulation of band phosphorylation (Supplementary Figure 5). For further confirmation of PKAC2-dependency, we repeated the glycerol-depletion experiment with a second,

independent knockout clone. With the second clone, we saw the same PKAC2 dependency of glycerol-regulated phosphorylation (Figure 44).

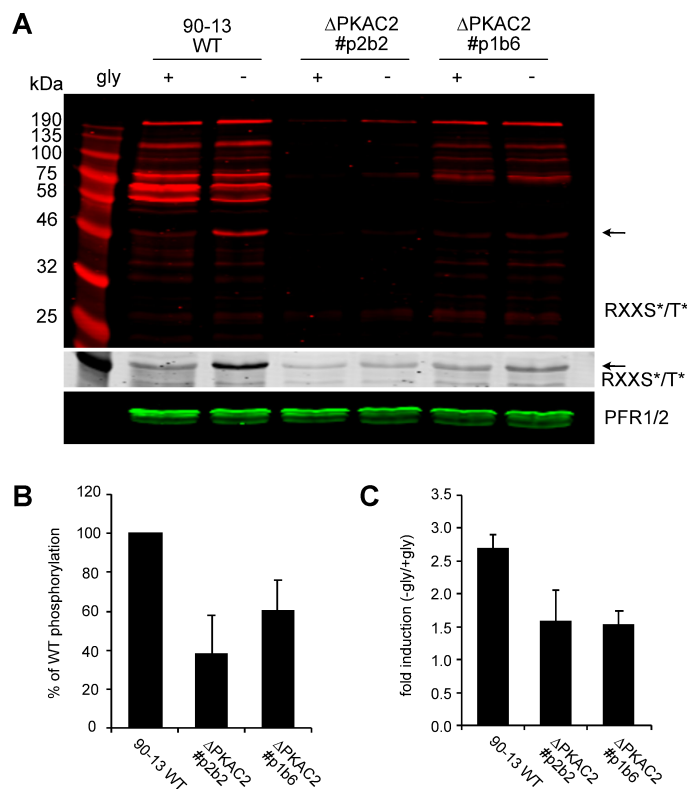


Figure 44: Effects of glycerol-depletion on RXXS*/T* phosphorylation in ΔPKAC2 cells. PCF cells were cultured in glucose-free medium containing glycerol as a glycolytic carbon source. They were washed once and resuspended in glucose and glycerol-free medium and incubated for 1h at 27°C. Finally, samples were taken and subjected to western blot analysis using Phospho (Ser/Thr) PKA substrate antibody (representative blot in **A**). PFR was used as a loading control. The 50 kDa band is additionally presented in greyscale with higher contrast. **B:** Quantification of phosphorylation after 1h of glycerol-depletion. Wildtype was set to 100% (n=4), bars represent average ± stdev. **C:** Changes in phosphorylation level upon glycerol-depletion in the different cell lines.

To summarize, we found a change in RXXS*/T* phosphorylation pattern induced by depletion of glycolytic carbon sources (glycerol/glucose). Phosphorylation intensity of this band was severely reduced in ΔPKAC2, but not affected in ΔPKAR.

3.4.2.2.2 The glycerol-regulated RXXS*/T* band is glycosome associated

Combining the observations that glycerol-depletion leads to PKAC2-dependent changes in RXXS*/T* phosphorylation and the confirmation of glycosomal PKAC2, we hypothesized that this substrate band might be a glycosomal protein as well. To test this, we employed the same purification method as for confirmation of glycosomal PKAC2 by density gradient centrifugation and protease protection assay. Using an Optiprep gradient we could successfully separate flagella and glycosomes from other contaminating organelles. In this preparation, two RXXS*/T* bands are enriched. Further purification by sucrose density-gradient revealed a very similar purification profile of the upper band to the flagellar marker (PFR). This band will therefore be referred to as *flagellum-associated* band. On the contrary, the profile of the lower (50 kDa), glycerol-regulated band shows a clear correlation with the glycosomal marker (PPDK) and will be referred to as *glycosome-associated* band (Figure 45A). Interestingly, when we

subjected the organelle preparation from the Optiprep gradient to proteinase K digestion, both bands completely disappeared (Figure 45B).

Taken together, this would suggest that the glycerol-regulated RXXS*/T* band is a glycosomal protein, that is not protected inside the organelle. This could either be a membrane associated protein or a membrane protein with the RXXS*/T* phosphosite facing towards the cytoplasm.

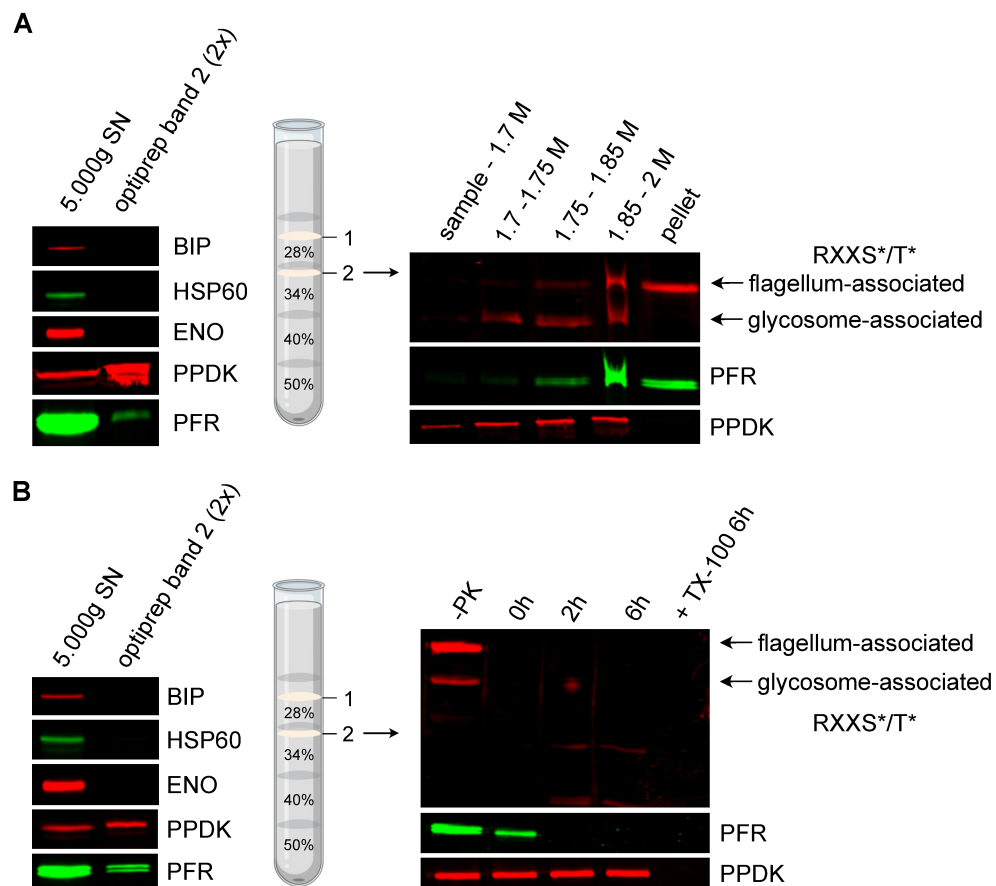


Figure 45: Subcellular localization of glycerol regulated RXXS*/T* band after glycosome enrichment by differential centrifugation and ultracentrifugation through Optiprep density gradient. **A:** Migration profile of flagellum- and glycosome-associated RXXS*/T* bands through a discontinuous sucrose gradient. **B:** Protease protection assay of organelle fraction recovered from Optiprep gradient.

3.4.2.2.3 Glycerol-depletion phosphoproteome

We decided to investigate this further by performing a glycerol-depletion (Phospho-) proteome in wild-type and Δ PKAC2 to answer the following questions. Which phosphorylation events take place upon glycerol-depletion? Are these phosphorylation events mediated by PKAC2? Signaling events usually take place within minutes and are eventually terminated again, which is why we reduced the glycerol-depletion time for the phosphoproteome to 15 minutes. This way we also wanted to avoid inducing changes in protein levels that could complicate evaluation of changes in phosphorylation levels. Western blot analysis confirmed that the same phosphorylation pattern is observed after 15 minutes already as it is after 60 minutes and that phosphorylation of the prominent 50 kDa band is clearly reduced in Δ PKAC2 (Figure 46A). Comparison

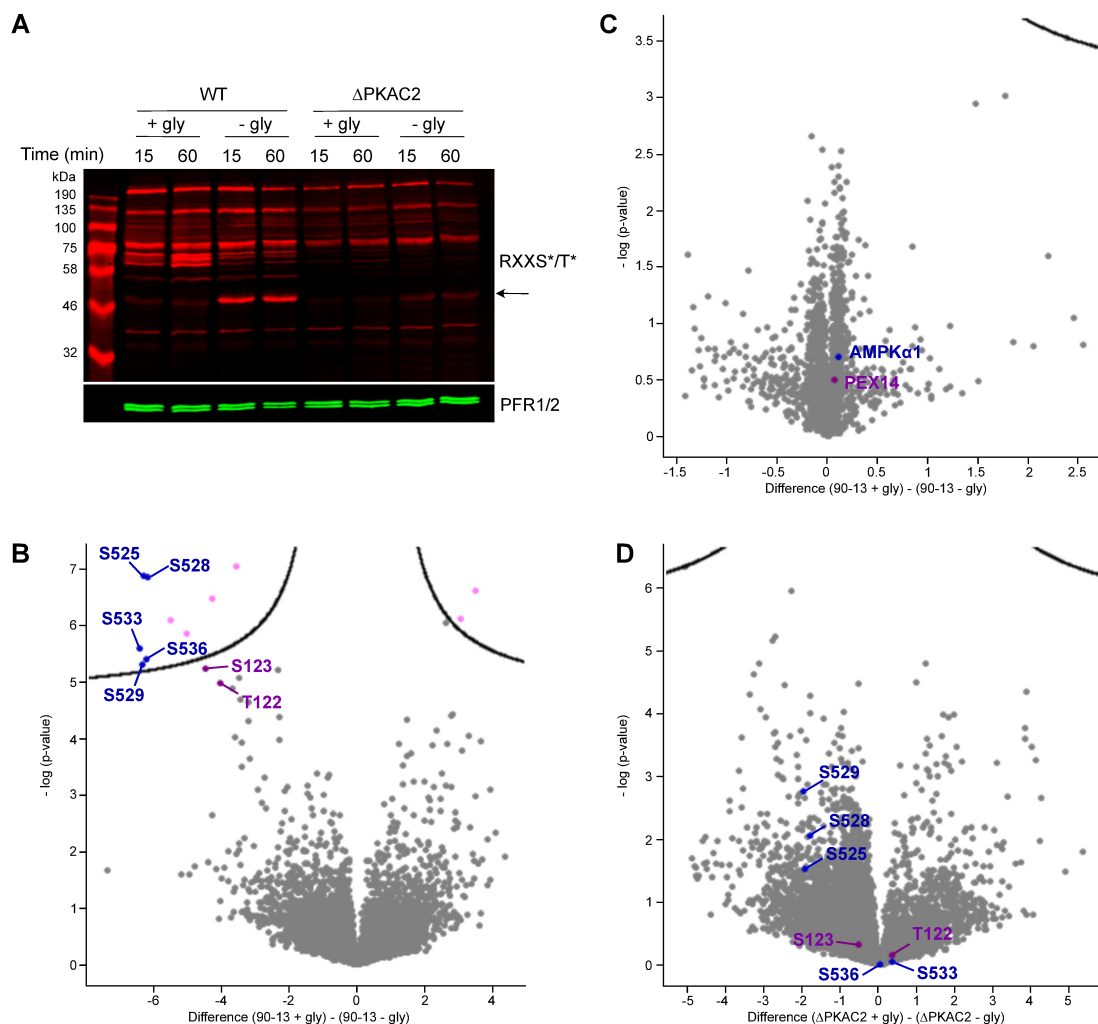


Figure 46: Phosphoproteome analysis of glycerol-depletion in wildtype and Δ PKAC2. **A:** Representative western blot of RXXS*/T* phosphorylation, arrow indicates glycerol-regulated phosphoband. AMPK α 1 was colored in blue and PEX14 was colored in purple in the following volcano plots. **B:** Volcano plot showing significantly (FDR=0.1, S_0 =0.1) regulated (pink) phosphorylations after 15-minute glycerol-depletion. **C:** Volcano plot showing no significantly (FDR=0.05, S_0 =0.1) regulated changes in protein expression level after 15-minute glycerol-depletion in wildtype cells. **D:** Volcano plot showing no significantly (FDR=0.1, S_0 =0.1) regulated phosphosites in Δ PKAC2 after 15-minute glycerol-depletion.

of +/- glycerol conditions in the wild-type revealed 11 significantly (FDR = 0.1, $S_0 = 0.1$) regulated phosphosites on 6 proteins (Figure 46B, Table 2). Using the same significance cut-offs, we found no significantly regulated phosphorylations in the PKAC2 knockout (Figure 46D). No proteins were significantly regulated on proteome level between +/- glycerol in the wild-type (FDR = 0.05, $S_0 = 0.1$, Figure 46C). The most prominent hit in this experiment was AMPK α 1, the catalytic subunit of AMP-activated protein kinase. This protein was phosphorylated on 5 residues in the S/T loop, but only one of these phosphosites was actually in a PKA substrate motif (S533). Interestingly, the most prominent and visible ~50 kDa band on RXXS*/T* western blot (Figure 46A) could not be attributed to any of the proteins in the list of significantly regulated sites. However, we found a candidate slightly below the set significance cut-off that met all the criteria of the phosphoband, which are a molecular weight of ~50 kDa and glycosomal membrane association: PEX14.

Table 2: Phosphosites regulated upon 15-minute glycerol-depletion in wildtype cells.

GeneID	Gene Name or Symbol	Product Description	Significant	-LOG (P-value)	Difference	Position	PKA motif	Mol. Weight [kDa]
Tb927.10.5310	AMPK α 1	AMP-activated protein kinase alpha	+	5.6	-6.4	S533	RXS	80,6
Tb927.10.5310	AMPK α 1	AMP-activated protein kinase alpha	+	5.3	-6.3	S529		80,6
Tb927.10.5310	AMPK α 1	AMP-activated protein kinase alpha	+	6.9	-6.3	S525		80,6
Tb927.10.5310	AMPK α 1	AMP-activated protein kinase alpha	+	5.4	-6.2	S536		80,6
Tb927.10.5310	AMPK α 1	AMP-activated protein kinase alpha	+	6.8	-6.2	S528		80,6
Tb927.6.3540	N/A	zinc-finger protein, conserved	+	6.1	-5.5	S105	RXS	41,6
Tb927.7.7210	POMP37	Present in the outer mitochondrial membrane proteome 37	+	5.9	-5.0	S62		77,5
Tb927.3.1670	N/A	hypothetical protein, conserved	+	6.5	-4.3	S114		112,6
Tb927.11.1820	N/A	translation initiation factor eIF2B delta subunit, putative	+	7.0	-3.6	S315	RXS	68,6
Tb927.7.2650	CAP51V	hypothetical protein, conserved	+	6.1	3.1	S147		62,2
Tb927.7.2650	CAP51V	hypothetical protein, conserved	+	6.6	3.5	S150		62,2
Tb927.10.240	PEX14	peroxin 14, putative		5.2	-4.5	S123	RXXS	39,9
Tb927.10.240	PEX14	peroxin 14, putative		5.0	-4.0	T122	RRXT	39,9

PEX14 is a 40 kDa protein and part of the glycosomal import machinery. It localizes to the glycosomal membrane, where it interacts with the cytoplasmic cargo receptors and mediates protein translocation through the membrane. Two phosphorylations upon glycerol-depletion were identified on RXXS*/T* sites.

3.4.2.2.4 AMPK α activity changes upon glycerol-depletion

AMPK α 1 was the most differentially phosphorylated protein upon glycerol-depletion. All of these phosphosites clustered in the S/T loop, a region in which phosphorylations are reported to inhibit activity in mammalian cells (Trefts and Shaw, 2021). AMPK activity can be monitored by Thr172 (mammalian) phosphorylation, a residue located within the activation loop. Using a phospho-specific antibody, we analyzed if glycerol-depletion had any effect on AMPK activity. We used the samples from the phospho-proteome (Figure 46) to analyze activity by western blot. Both AMPK α subunits could

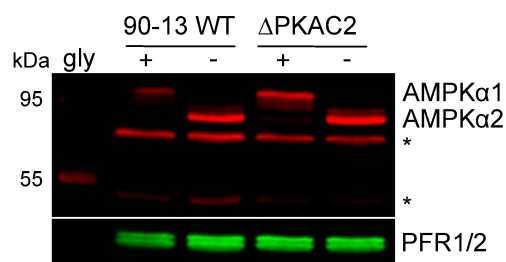


Figure 47: Effects of glycerol-depletion on AMPK active state. Samples shown in Figure 46A were probed with AMPK phospho-Thr172 antibody (Cell Signaling #2535). Asterisks mark unspecific bands also identified in *T. cruzi* (Sternlieb et al., 2021; Zhang et al., 2020).

be detected at the appropriate sizes, along with two unspecific bands, which are also detected in *T. cruzi* (indicated by asterisks (Sternlieb et al., 2021)). In these samples, we could indeed observe changes in active AMPK α (Figure 47).

The amount of active AMPK α 1 is strongly reduced, while active AMPK α 2 increases. We cannot distinguish between activity and abundance using this antibody, but the 15-minute depletion and proteomic

comparison shown in Figure 46C argue against the latter (AMPK α 2 was not detected in the (phospho-)proteome and can thus not be highlighted). We observe the same pattern in Δ PKAC2 as well. This is not surprising, given that only one of the regulated phosphosites was actually on a PKA motif. It is possible that PKAC2 is involved in this regulatory process, but not essential. In addition to that, AMPK α is an already known and well-studied regulator of cellular metabolism. Therefore, we decided to focus on PEX14, a novel and potentially interesting mechanism for metabolic regulation.

3.4.2.2.5 PEX14 is RXXS*/T* phosphorylated upon glycerol-depletion

Luckily, we were able to obtain an α -PEX14 antibody (kind gift of F. Bringaud, originally from (Moyersoen *et al.*, 2003)) and first analyzed whether PEX14 protein levels are affected by glycerol-depletion and if the protein size would match that of the RXXS*/T* band. A glycerol-depletion assay was performed and after blotting, the membrane was first incubated with the anti-RXXS*/T* phosphoantibody. Subsequently, the blots were re-incubated with α -PEX14 and both scans were finally superimposed (Figure 48). This way, we could confirm that PEX14 expression levels are not affected within 60 min of glycerol-depletion and that the size perfectly matches that of the RXXS*/T* substrate band. For further validation, we tagged the gene with a TY-GFP-tag in wild-type and Δ PKAC2 to facilitate downstream analysis. Successful tagging was confirmed by in-

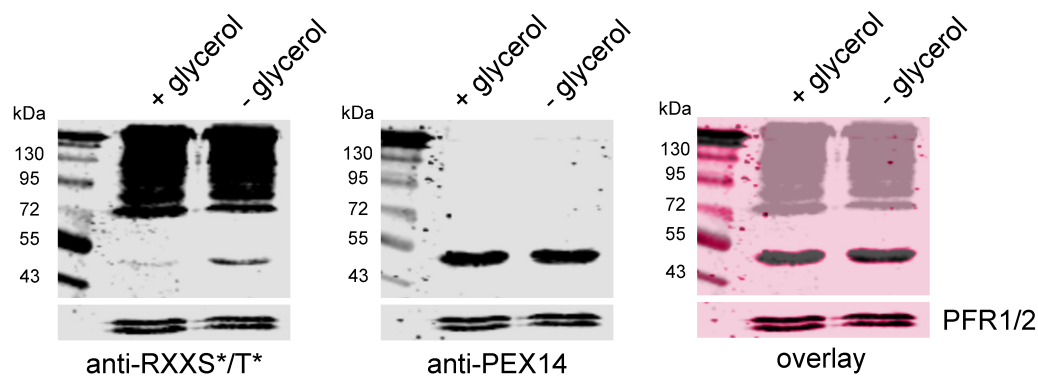


Figure 48: Glycerol-depletion assay of wildtype cells. Blots were first probed with Phospho (Ser/Thr) PKA substrate antibody and afterwards re-incubated with α -PEX14 antibody. On the right, both blots were superimposed. Anti-PEX14 incubation was colored in pink. PFR was used as a loading control.

gel fluorescence of the GFP and western blot against the TY-tag (Figure 49A/B). Here we noticed, that the α -PEX14 antibody does not detect the fusion protein. This could be explained by the fact that the antibody was generated using an N-terminal peptide of the protein and that an N-terminal tag simply interferes with the binding. Correct localization was also confirmed by fluorescence microscopy of the GFP-tag (Figure 49C). This TY-GFP-PEX14 wild-type line was subjected to glycerol-depletion assay and we analyzed RXXS*/T* phosphorylation by western blot. Thorough comparison of +/- glycerol samples indeed showed the appearance of an RXXS*/T* band at the same

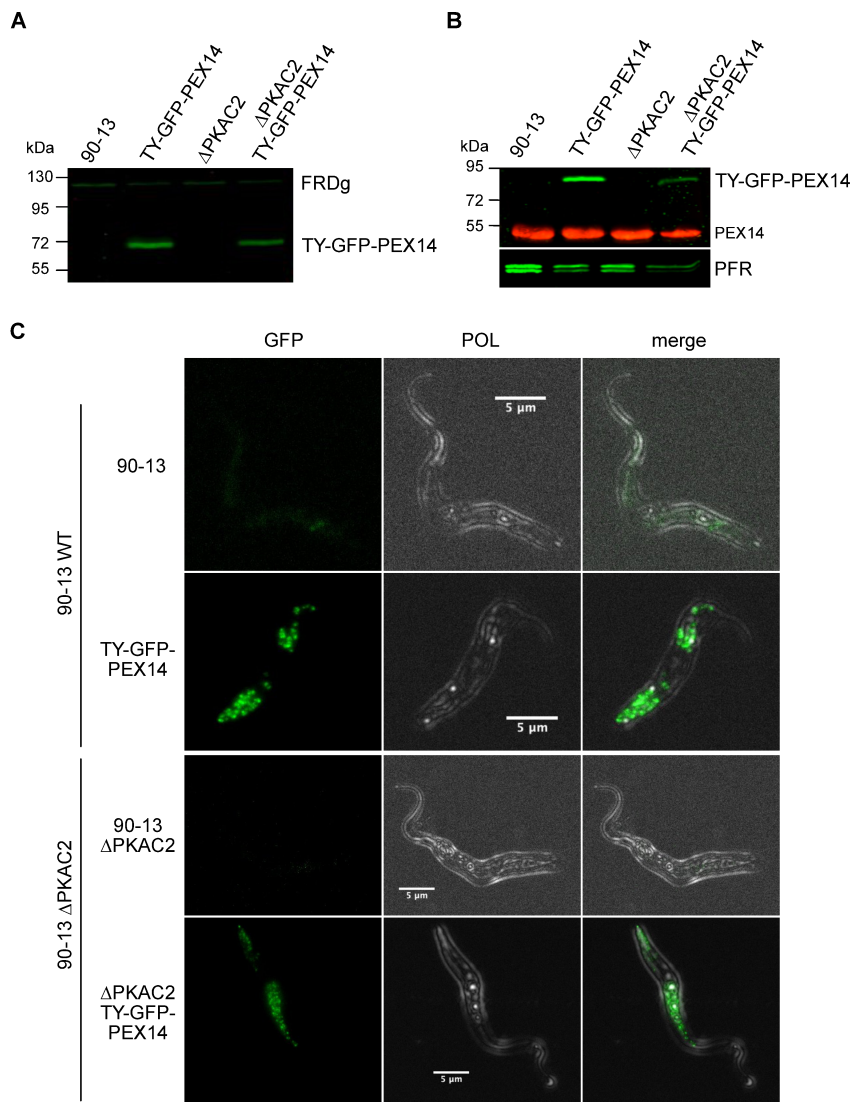


Figure 49: TY-GFP-tagging of PEX14. **A:** In-gel fluorescence analysis after SDS-PAGE. **B:** Western blot confirmation of TY-GFP-tagging using α -TY (BB2) and α -PEX14. PFR was used as a loading control. **C:** Fluorescence microscopy of tagged cell lines using 100% intensity at 0.15s exposure in DeltaVision microscope. Stacks were imaged and assembled in Fiji.

size as the fusion protein (Figure 50). This band was not observed in the wild-type control. Due to high background phosphorylation in whole cell lysates in the size range of the fusion protein, we enriched the TY-GFP-tagged PEX14 by GFP-trap pulldown from cells grown in presence or absence of glycerol. We analyzed RXXS*/T* phos-

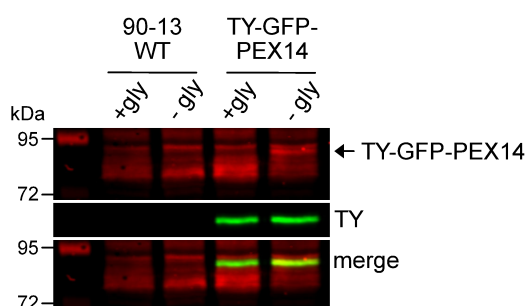


Figure 50: Glycerol-depletion assay of TY-GFP-PEX14 cell line. Cells were cultured in glucose-free medium containing glycerol. For the assay, cells were washed once with and resuspended in glucose and glycerol-free medium. After 1h incubation at 27°C, samples were taken for western blot analysis of RXXS*/T* phosphorylation. TY-GFP-PEX14 was detected using α -TY (BB2) antibody, arrow indicates phosphorylation of the fusion protein under - glycerol conditions in the tagged line.

phorylation as well as protein abundance by TY-tag. In the WT background, we observed 3-9x higher phosphorylation in absence of glycerol, depending on the individual experiment. In the Δ PKAC2 background, we could not detect any RXXS*/T*

phosphorylation of the fusion protein at all (Figure 51). Normalization of RXXS*/T* to the TY-tag could confirm that indeed the ratio of PEX14 phosphorylation increases and not simply protein abundance.

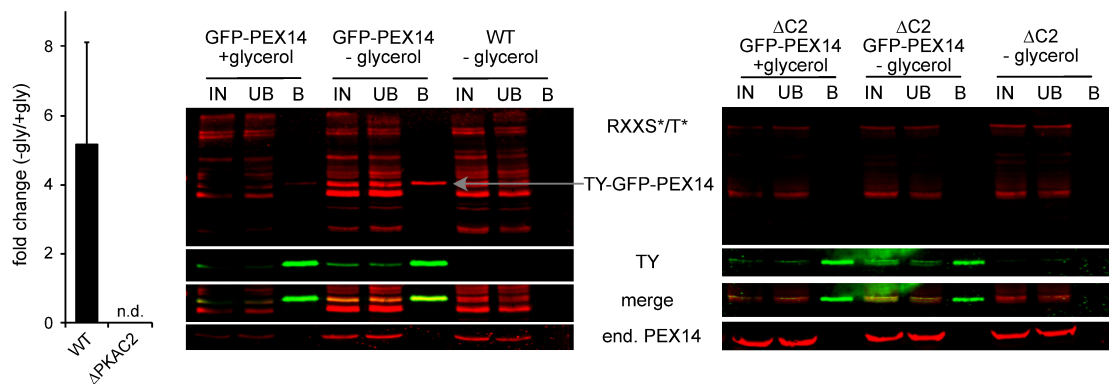


Figure 51: GFP-trap purification of TY-GFP-PEX14 from wildtype and Δ PKAC2 cells grown in presence or absence of glycerol. Bar chart represents fold-change in phosphorylation level between + and – glycerol normalized to the TY-tag (n=3, average \pm stdev). n.d. = not determined due to lack of signal. Western blots show representative purification profiles from wildtype (left) and Δ PKAC2 (right). IN=input, UB=unbound, B=bound.

3.4.2.2.6 Investigation of physiological relevance of PEX14 phosphorylation

After confirmation of PKAC2-dependent PEX14 phosphorylation upon glycerol-depletion, we wanted to investigate the physiological relevance of this phosphorylation event. Given that PEX14 is part of the glycosomal import machinery, we hypothesized that phosphorylation in response to glycerol-depletion might have an effect on import of glycosomal proteins. This could either affect import in general, a specific subset (e.g., PTS1 or PTS2 cargo) or only individual proteins. PEX14 phosphorylations were reported in the literature of some other organisms (Johnson et al., 2001; Komori et al., 1999; Yamashita et al., 2020). Some of them could be shown to affect import of specific proteins, like catalase or citrate synthase (Okumoto et al., 2020; Schummer et al., 2020). In other cases, the consequences are unclear. The phosphosites we identified here as glycerol-regulated (T122 and S123) are located in the PEX14 conserved region (Pfam). We also indicated all known phosphorylation sites identified in (Urbaniak et al., 2013; Zhang et al., 2020) in the linear scheme in Figure 52A. All of these sites were identified in our phosphoproteome as well (chapter 3.3.2), except for S317. Additionally, we identified a cluster of new phosphosites on the C-terminus of PEX14 that were only identified in Δ PKAC2 (S329 was identified but not categorized as significantly upregulated after imputation of missing values). The glycerol-regulated phosphosites (T122 and S123) are not annotated in tritrypdb.org but were identified in BSF *T. brucei* and *T. evansi* phosphoproteomes of (Zhang et al., 2020). Only the N-terminal region of TbPEX14 has been solved by solution NMR (Dawidowski et al., 2017). A

structure prediction of the whole protein is available from the AlphaFold2 database (Wheeler, 2021), available at <http://wheelerlab.net/alphafold/>. However, the location of

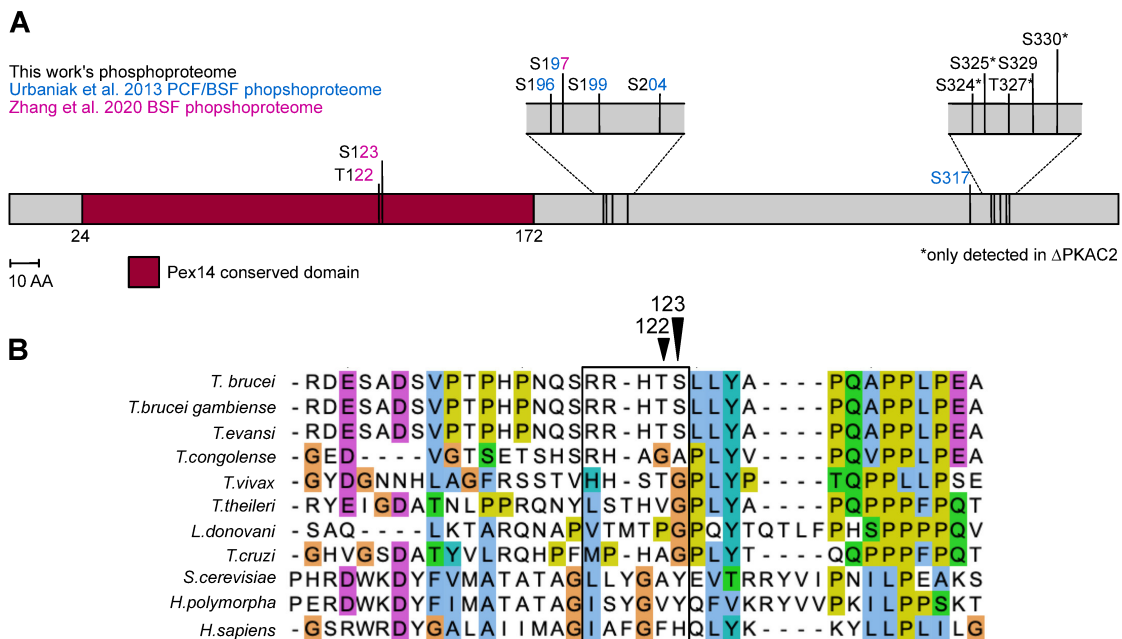


Figure 52: Phosphorylations on PEX14 and conservation of glycerol-regulated sites. **A:** Schematic representation of PEX14 phosphorylation previously reported (Nett et al., 2009; Urbaniak et al., 2013) and newly identified phosphorylation sites. All previously described sites, except S317 were identified in this phosphoproteome as well. New sites include S324, S325, T327, S330 which are only detected in Δ PKAC2, and S329, which was identified, but not statistically significantly regulated. **B:** PEX14 sequence alignment created using MUSCLE 3.8 and visualized using Jalview and focused on region including glycerol regulated PKA phosphosites. RXXS*/T* sites are only conserved in *T. brucei gambiense* and *T. evansi*, two very closely related trypanosoma species.

the glycerol-regulated phosphosites appears to be in a disordered region without any functional annotations. Protein alignments of PEX14 from different species show that these RXXS*/T* sites are not conserved at all. Only in closely related kinetoplastid species we observe a gradually increasing sequence similarity. The threonine residue is conserved in *L. donovani* and *T. vivax*, but not the RXXS*/T* motif. Conservation of the RXXS*/T* sites is only observed in *T. evansi*. Since there is no conservation of these sites, we could not rely on previous knowledge from the literature in terms of physiological relevance. Therefore, we generated a phosphomimetic (T122E, S123E) and phosphoablative (T122A, S123A) mutant of both sites. We used the CRISPR/Cas9 system to generate a homozygous mutant without further modifications of the locus by placing the cut next to the phosphosite and supplying a short repair template with the desired mutation (Figure 53A). Correct modification was confirmed by PCR of the locus and subsequent sequencing (Figure 53B). First, we analyzed whether the mutations had an effect on growth in medium with or without glycerol. Under culture conditions, we did not observe any effect on the growth behavior (Figure 53C). Since this phosphorylation event is dependent on the availability of glycolytic carbon sources, we hypothesized that the phosphorylation might be involved in modification of glycosomal

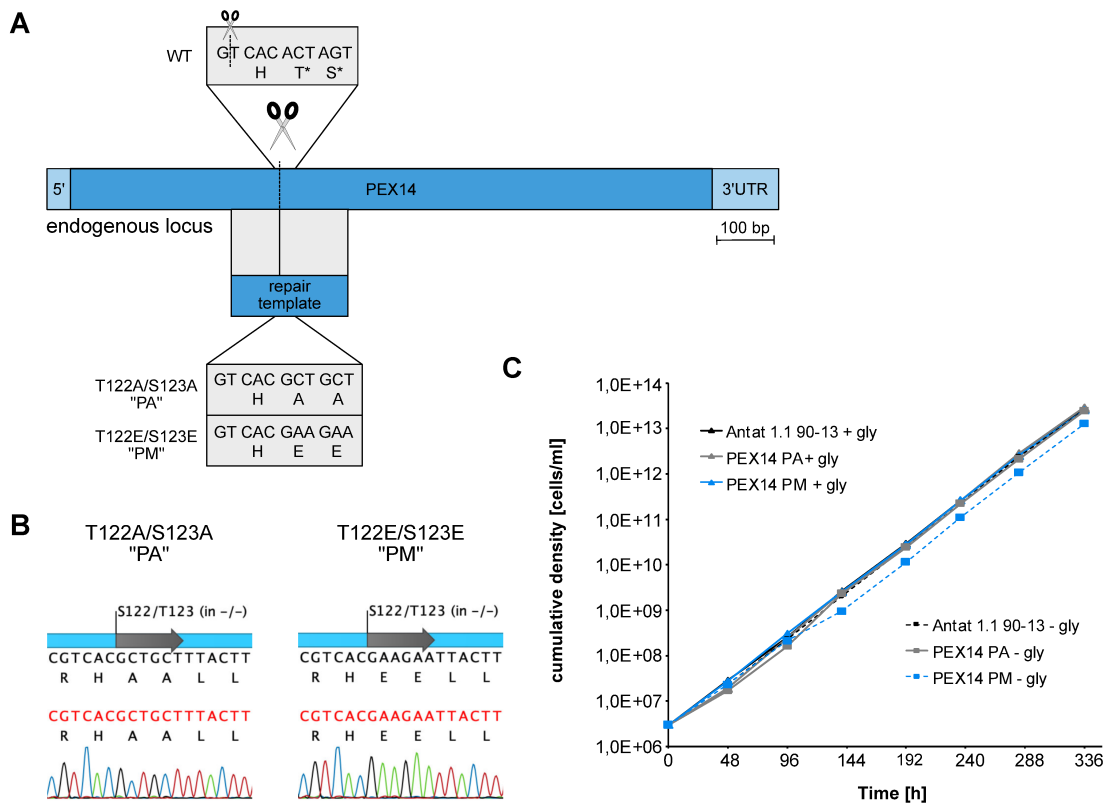


Figure 53: Generation of PEX14 phosphomutants. A: CRISPR/Cas9 strategy for scar-free mutagenesis. The gRNA was designed as closely as possible to the site of mutation (indicated by dashed line) and a repair template containing either phosphoablative (PA) or phosphomimetic (PM) amino acid codons was added as repair template. B: Validation of correct modification by sequencing. C: Growth analysis of the PEX14 phosphomutants in SDM79 +/- glycerol.

protein import. To test this, we first used a drug known to inhibit glycosomal import in *T. brucei* by inhibition of PEX5/PEX14 interaction, eventually resulting in cell death (Dawidowski *et al.*, 2017). We tested for synthetic cytotoxicity of this compound to the

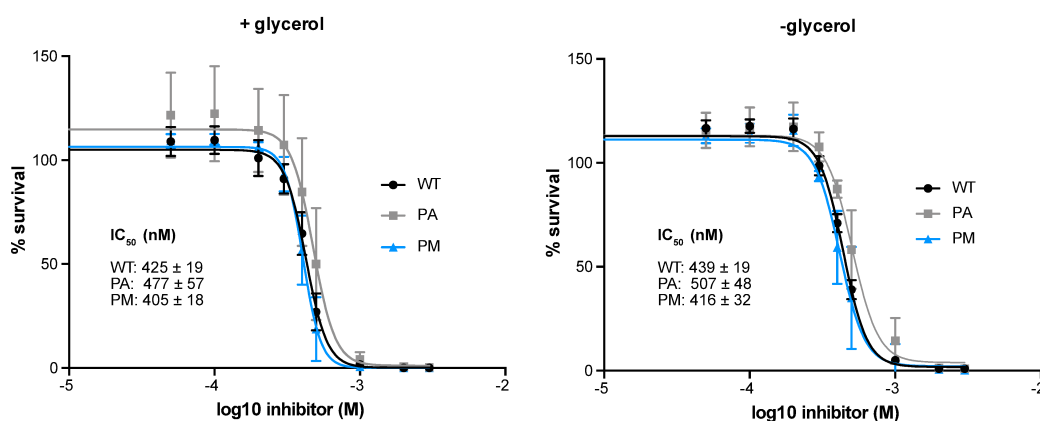


Figure 54: Alamar blue assay of PEX14 phosphomutants. Cells were treated with indicated concentrations of MABNH₂ (Dawidowski *et al.*, 2017) as described in 2.2.7.3. Curves were fitted by non-linear regression using GraphPad Prism (n=3, average ± stdev).

phosphomutants using an alamar blue assay (described in 2.2.7.3) under the assumption of an effect of the phosphosites on general protein import. The cells were treated

with different concentrations of the inhibitor and a dose-response curve was derived. Since the PEX14 phosphorylation event is regulated by glycerol-availability, we performed the assay in presence or absence of glycerol. We observed no major difference in terms of drug sensitivity between the PEX14 phosphomutants and the wild type (Figure 54). This observation together with the fact that growth behavior of the mutant lines is not affected either, leads us to the conclusion that the PEX14 phosphorylation is not likely to affect glycosomal import in general. In most cases where PEX14 phosphorylations were analyzed, they were regulating import of specific proteins (Okumoto *et al.*, 2020; Schummer *et al.*, 2020). To investigate whether this is the case here, we compared the glycosomal proteomes of the PEX14 phosphomutants grown in presence or absence of glycerol and used the wild type as a reference. For this purpose, we enriched glycosomal fractions by differential centrifugation (described in 2.2.5.5) and submitted them for proteomic analysis (Figure 55A). We could identify a total of 3,299 proteins across all samples. The overall high number of identified proteins can be explained by an enrichment of membrane bound organelles in general by the

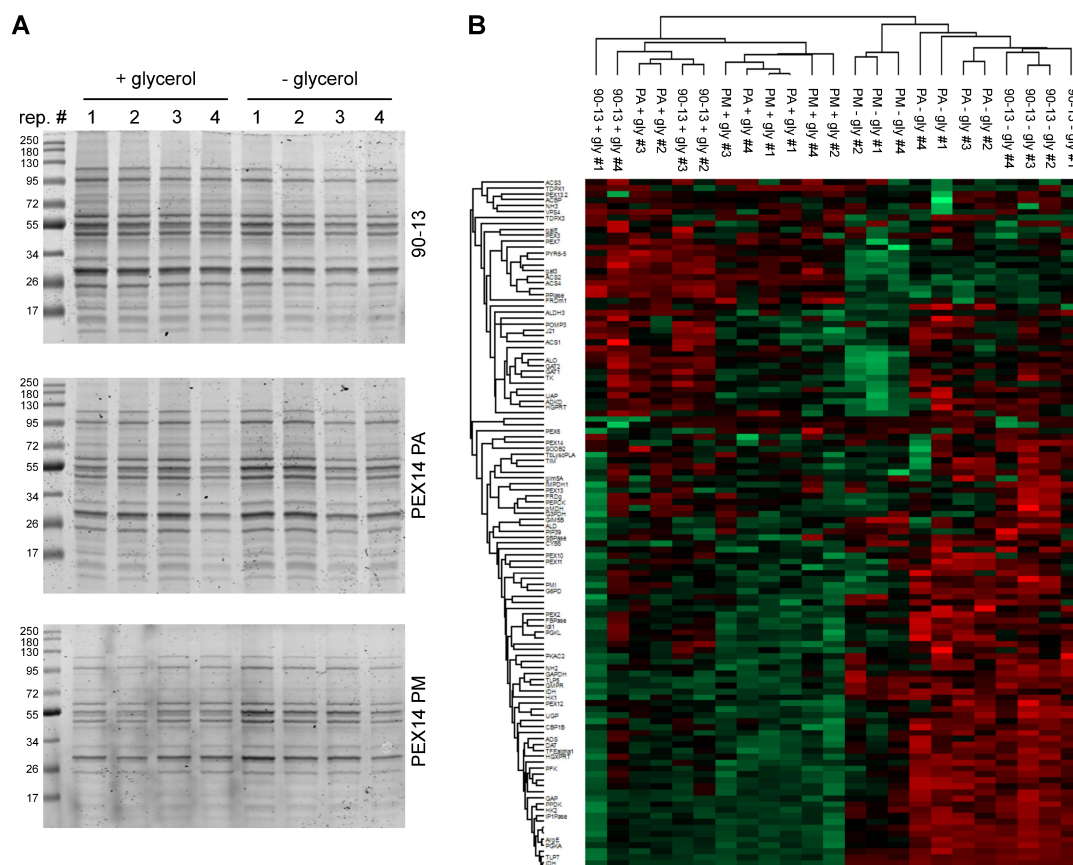


Figure 55: Glycosomal proteome quality controls. Glycosomes from wild type (90-13) and PEX14 phosphoablative (PA) and phosphomimetic (PM) cells grown in presence or absence of glycerol were enriched by differential centrifugation. **A:** SDS-PAGE analysis of 5 μ l all samples sent for mass spectrometry. Gels were stained with colloidal Coomassie and imaged using the LI-COR Odyssey. Samples were diluted to the same concentration prior to MS. **B:** Hierarchical clustering analysis of high confidence glycosomal proteins after normalization by Z-score using Perseus.

differential centrifugation. For mass spectrometry, we still preferred the glycosome enrichment method over the optimized protocols described in 3.4.1.2 because the simpler workflow ensures higher reproducibility between samples and less potential for protein contaminations. We filtered the list of identified proteins for glycosomal ones and obtained 117 high confidence glycosomal proteins which we compared in abundance. The first thing we compared was glycosomal protein composition in presence or absence of glycerol for each cell line. Hierarchical clustering analysis showed a clear separation between glycosomal protein abundance of cells cultured in presence or absence of glycerol (Figure 55B). We identified 22 significantly regulated proteins in the wild type using a Student's t-test with a cut-off of FDR = 0.05, S0 = 0.5 and a fold-change of at least 1.5x (= Difference \pm 0.585). Of the 16 proteins upregulated in absence of glycerol most were involved in early steps of glycolysis, gluconeogenesis or nucleotide metabolism. Of the 6 proteins downregulated in absence of glycerol there was no clear enrichment for specific functions. However, the number of proteins is too low for a proper enrichment analysis (Figure 56A). Regulation of these hits by glycerol is in line with a previous proteome experiment where whole cell proteomes of cells grown in different carbon sources were analyzed (Ziebart, 2016). Not all of the proteins identified here were identified in the whole cell proteome, which is most likely due to higher sample complexity and different sample preparation for mass spectrometry. Additionally, for most of these proteins, PEX14-dependent import could be demonstrated by (Peikert et al., 2017) (Table 3).

Table 3: Glycosomal proteins regulated by glycerol availability in AnTat 1.1 90-13 wild type cells. Fold-change can be calculated by $2^{\text{Difference}}$. Annotations include whether the protein was regulated by glycerol in the PEX14 phosphoablative (PA) or phosphomimetic (PM) mutants, if the protein was significantly regulated in the whole cell proteome of (Ziebart, 2016) and whether glycosomal import was disturbed by PEX14 RNAi (Peikert *et al.*, 2017). Highlighted in green are the proteins whose glycerol-dependent import regulation as lost in at least one of the PEX14 phosphomutants. n.i.= not identified, n.s. = not significant.

GeneID	-LOG(P-value)	Difference (+gly)-(-gly)	regulated in PA	regulated in PM	Difference (+ gly)- (-gly) in proteome (Ziebart, 2016)	PEX14-dependent import (Peikert et al., 2017)	Product Description	Gene Name or Symbol	functional tag(s)
Tb927.11.900	4.0	-1.8	+	+	-1.7	-	isocitrate dehydrogenase, putative	IDH	citrate metabolism
Tb927.7.5680	3.0	-1.0	+	+	-1.6	+	deoxyribose-phosphate aldolase, putative		nucleotide metabolism
Tb927.1.3830	4.9	-1.1	+	+	-1.0	n.s.	glucose-6-phosphate isomerase, glycosomal	PGI	glycolysis, gluconeogenesis
Tb927.7.4770	2.6	0.9	+	+	0.6	-	cyclophilin-type peptidyl-prolyl cis-trans isomerase, putative	PPlase	protein folding

Tb927.5.300	4.2	-1.2	+	+	n.i.	n.i.	thymine-7-hydroxylase, putative	TLP5	nucleotide metabolism
Tb927.7.7500	3.6	-1.1	+	+	n.i.	+	thymine-7-hydroxylase, putative	TLP7	nucleotide metabolism
Tb927.11.3850	3.2	0.9	+	+	n.i.	+	AMP deaminase, putative		nucleotide metabolism
Tb927.9.4200	2.5	1.4	+	+	n.i.	n.i.	fatty acyl CoA synthetase 2	ACS2	fatty acid synthesis
Tb927.10.6880	3.7	-1.3	+	+	n.s.	-	glyceraldehyde 3-phosphate dehydrogenase, cytosolic	GAP	glycolysis
Tb927.8.7410	3.1	0.9	+	+	n.s.	-	calreticulin, putative		protein folding
Tb927.9.6090	3.4	-0.8	+	-	-1.9	n.i.	PTP1-interacting protein, 39 kDa	PIP39	signaling
Tb927.8.1910	3.3	-0.9	+	-	n.i.	n.i.	metallo-peptidase, Clan MH, Family M18	ArgE	protease
Tb927.4.1360	1.7	-0.6	+	-	n.s.	+	Glucose-6-phosphate 1-epimerase, putative		glycolysis, gluconeogenesis
Tb927.10.2010	1.7	-0.7	-	+	n.i.	-	hexokinase	HK1	glycolysis
Tb927.7.1140	0.6	0.9	-	+	n.i.	n.i.	trypanothione/trypanothione dependent peroxidase 3	TDPX3	trypanothion
Tb927.5.940	2.7	0.8	-	+	n.s.	+	NADH-dependent fumarate reductase, putative	FRD	succinate metabolism
Tb927.10.2020	3.1	-0.6	-	-	-2.3	+	hexokinase	HK2	glycolysis
Tb927.8.7170	3.1	-0.7	-	-	-0.9	+	inositol polyphosphate 1-phosphatase, putative	IP1Pase	signaling
Tb927.4.4070	2.3	-0.6	-	-	-0.7	+	mevalonate kinase, putative		isoprenoid synthesis
Tb927.8.3280	3.5	-0.7	-	-	n.i.	n.i.	Beta-lactamase superfamily domain containing protein, putative		unknown
Tb927.9.6100	1.6	-0.6	-	-	n.i.	n.i.	PTP1-interacting protein, 39 kDa	PIP39	signaling
Tb927.5.2080	3.7	-0.6	-	-	n.s.	+	GMP reductase	GMPR	nucleotide metabolism

The same comparison in the PEX14 phosphomutant cell lines returned 26 and 21 significantly regulated proteins for the phosphoablative and phosphomimetic mutants, respectively (Figure 56B-C, Supplementary Tables 7,8). Comparison of the significantly regulated hits in all three cell lines shows 10 proteins which are still regulated irrespective of the PEX14 phosphosites and 3 proteins which were regulated in at least two of the cell lines and 5-10 proteins which are only regulated in individual cell lines. We

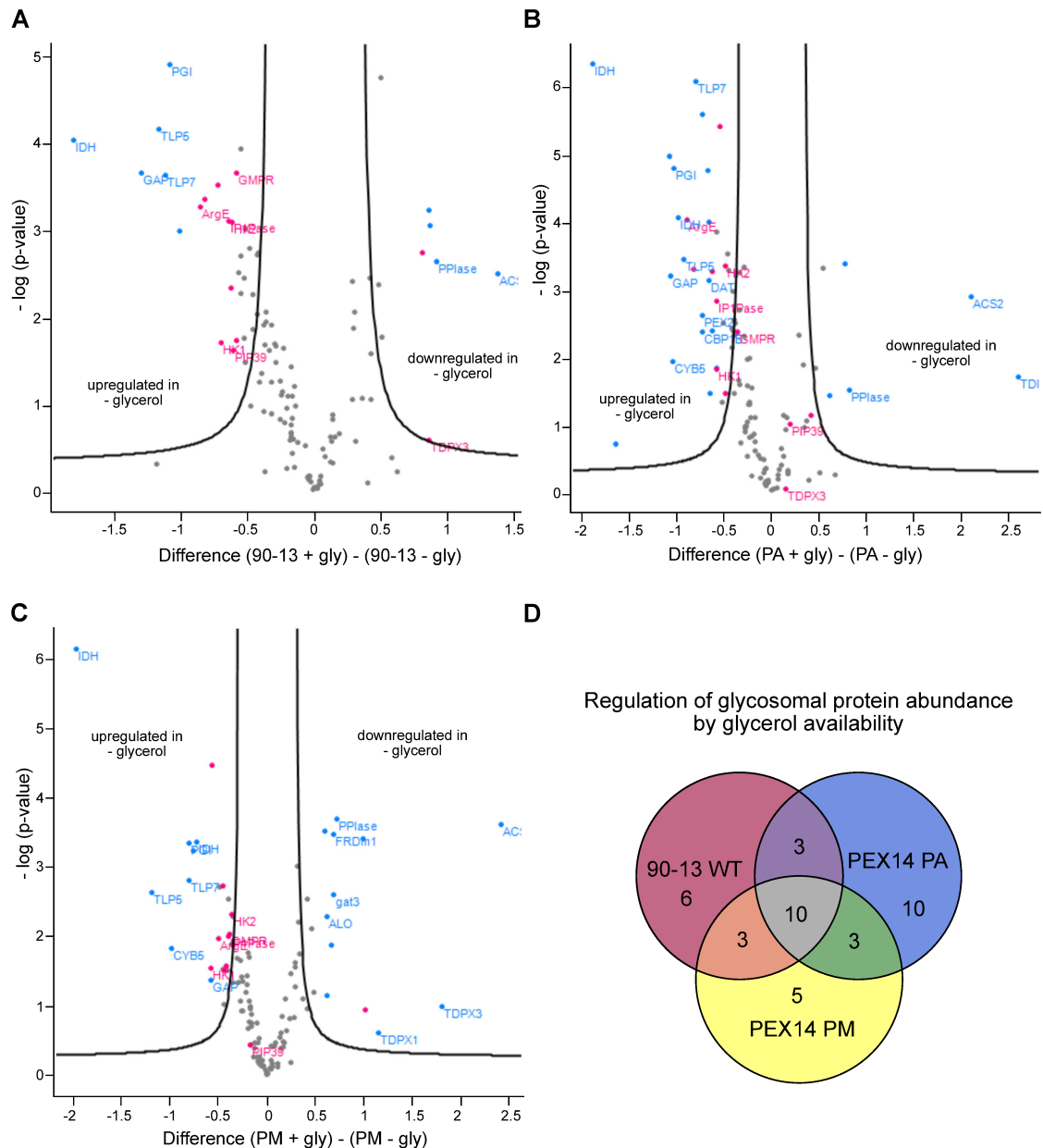


Figure 56: Glycosomal proteome analysis wild type and PEX14 phosphomutants. Comparison of Glycosomal protein composition of wild type cells (**A**), PEX14 phosphoablative (PA, **B**) or PEX14 phosphomimetic (PM, **C**) cells cultured in the presence or absence of glycerol. Protein abundance was compared using a Student's t-test with an FDR = 0.05 and $S_0 = 0.5$. Proteins which were regulated by at least 1.5-fold were indicated in blue. Proteins highlighted in pink have lost regulation by glycerol in at least one of the PEX14 phosphomutants compared to the wild type. These proteins have been highlighted in green in Table 3. Fold-change of protein abundance can be calculated by $2^{(\text{Difference})}$. **D:** Venn diagram showing the distribution of proteins regulated by glycerol in either one, two or all three cell lines. The 6 proteins whose regulation in response to glycerol is lost in both PEX14 phosphomutants (red section) were considered of highest interest, followed by the 6 proteins whose regulation was lost in at least one of the mutants (purple and orange sections).

considered the loss of regulation by glycerol in at least one of the mutants as the most interesting category to hypothesize potential physiological relevance of this phosphorylation event (Figure 56D). This category yields 12 proteins which are highlighted in green in Table 3 and in pink in Figure 56A-C. For most of these proteins, import regulation was not completely abolished, but rather reduced to a very low threshold (< 1.5 fold-change = difference ± 0.585). They were still statistically significant though (outside the borders of the volcano plots in Figure 56B-C). The only proteins that lost statistically significant regulation by glycerol were PIP39, GMP reductase and TDPX3 for the phosphoablative mutant and PIP39 and FRDm2 in the phosphomimetic mutant (inside the borders of the volcano plots). TDPX3 showed very high variation between individual replicates and FRDm2 is a mitochondrial protein, which is usually not expressed (Wargnies et al., 2021). However, FRDm2 and FRDg share a 483 amino acid core that is perfectly conserved between these two isoforms. The peptides identified here might be a mixture of both FRD isoforms. This only leaves PIP39 as a candidate where glycerol-dependent import regulation was completely lost (statistically non-significant change) in both PEX14 phosphomutants. Additionally, comparison of the individual cell lines with one another was performed but did not return any significant differences with the selected cut-offs (Supplementary Figure 6). Furthermore, in all cell lines, PKAC2 appears slightly enriched in the glycosomal fractions from cells grown in absence of glycerol, but the effect is not statistically significant. However, only a small fraction of PKAC2 localizes to glycosomes, while the flagellum is the predominant subcellular localization. The glycosome enrichment method used here also enriches for flagella. The flagellar PKAC2 fraction could mask potential differences in glycosomal import of PKAC2 leading to a loss of statistical significance.

In summary, we observe loss of import regulation by glycerol for some proteins, of which PIP39, a Ser/Thr phosphatase involved in stumpy to PCF differentiation, is extracted as the most promising target based on the statistical analysis. Due to the overall low fold-changes, this needs experimental validation before further downstream analysis.

3.4.2.3 Carbon source preferences of early PCF by NMR

Even though the decision to use glycerol-withdrawal instead of glucose-withdrawal for the metabolic adaptation analysis in previous sections was made, we were still wondering why the AnTat strain cannot grow on glucose alone. Together with our collaboration partners (F. Bringaud, Bordeaux), we investigated whether freshly differentiated (= *early*) procyclics can metabolize glucose using proton-NMR. We started the experiment with BSF AnTat 1.1 Munich and differentiated them into procyclics. After expansion of cultures, we split them into the four different conditions: + glucose and glycerol, + glucose or glycerol and without both. After 24h adaptation, the cells were resuspended in PBS containing proline and either ^{13}C -glucose or ^{13}C -glycerol. Unlabeled glucose or glycerol was added as an alternative carbon source as indicated in Figure 57. After 6h incubation, the supernatants were sent for NMR analysis of excretion products. The excreted metabolites were quantified and plotted grouped by carbon sources added during the NMR experiment (Figure 58). Based on the isotope label, it can be distinguished whether a metabolite was derived from the labeled or unlabeled source.

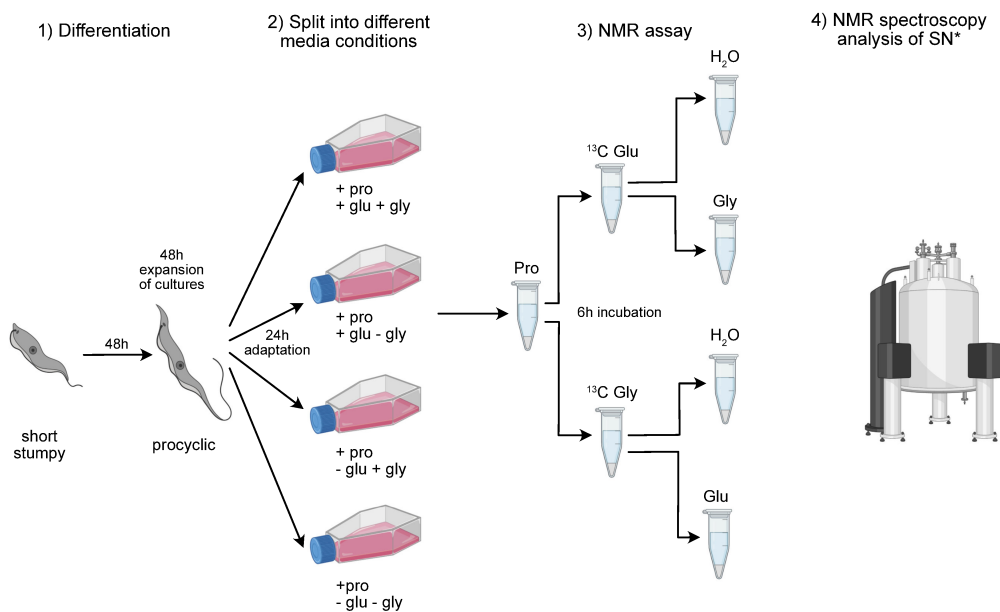


Figure 57: Experimental workflow of Antat 1.1 Munich NMR analysis. Cells were freshly differentiated from BSF short stumps to procyclics. After culture expansion, cells were split into different carbon-source containing media and adapted for 24h. For the NMR assay, cells were resuspended in PCS containing the indicated labeled and unlabeled carbon sources and incubated for 6h. The supernatants were sent for proton-NMR. Figure was created using BioRender.com.

When glucose and proline were added, both were metabolized. We even observe more metabolites derived from glucose than from proline (Figure 58A). This observation actually confirms previous data suggesting that glucose represses proline consumption (Lamour *et al.*, 2005). However, previous data were generated using the EATRO 1125 strain, which is a long-term laboratory PCF strain and does not show any growth phenotype in medium containing glucose but no glycerol. The culturing conditions prior to

the assay had a mild effect on total metabolite excretion in all four groups. Cells which were cultured exclusively in proline beforehand showed lowest metabolic activity. In contrast, cells which were cultured beforehand in glucose without glycerol showed highest metabolic activity in all cases. Addition of ^{13}C Glycerol led to the highest overall metabolic flux measured here (Figure 58B). This can be explained by the high activity and abundance of glycerol-kinase which leads to rapid degradation of glycerol (Allmann *et al.*, 2021). Addition of glycerol to ^{13}C glucose labeled cells resulted in higher overall metabolic flux compared to ^{13}C glucose alone, but less glucose-derived

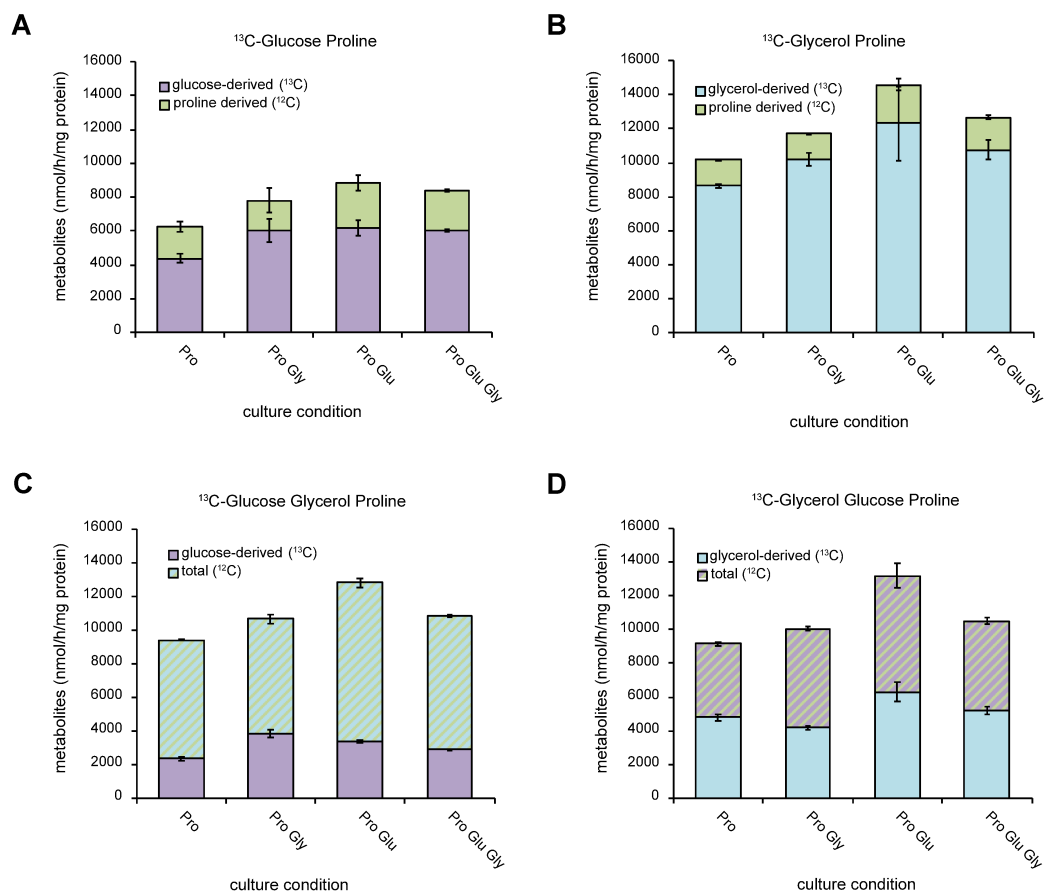


Figure 58: NMR analysis of freshly differentiated AnTat 1.1 Munich. Bar charts represent total excreted metabolites during the 6h incubation grouped by different (^{13}C -labeled) carbon sources added during the assay ($n=3$, average \pm stdev). **A:** Supplementation with Proline and ^{13}C -Glucose. **B:** Supplementation with Proline and ^{13}C -Glycerol. **C:** Supplementation with Proline, ^{13}C -Glucose and Glycerol. **D:** Supplementation with Proline, ^{13}C -Glycerol and Glucose.

products compared to Figure 58A. This can also be explained by competition of the highly active glycerol-kinase with hexokinase (Allmann *et al.*, 2021). Addition of unlabeled glucose to ^{13}C glycerol (Figure 58D) led to similar levels of excretion products as Figure 58C, which is expected since we are using the same carbon sources just with swapped labels. However, we do see higher levels of glycerol-derived metabolites than

we did for ^{13}C glucose, which is again explainable by competition and the higher glycerol-kinase activity.

In conclusion, this experiment confirmed the preferences in carbon source consumption already known from experiments with the EATRO 1125 T7T PCF strain. We do not see major differences in freshly differentiated cells at the time point of measurement. To answer the initial question: Yes, early procyclics can metabolize glucose and they even prefer it over proline. Therefore, the severe growth phenotype on medium containing glucose and no glycerol (Figure 42) should not be a result of energy starvation. However, the cells were measured only 24h after the transfer to the new medium. At this time, the cells still appear healthy and motile. It is not excluded that there are differences later on, when the glucose-only phenotype is becoming apparent. Measuring this time-point is technically challenging because the cells are obviously unhealthy and results would probably not be interpretable.

3.4.3 Regulation of purine metabolism

Previous work in this laboratory showed purine nucleosides and nucleoside analogs to be potent *T. brucei* PKA ligands (Bachmaier, 2015; Bachmaier *et al.*, 2019; Githure, 2014). In BSF, low concentrations of cell permeable nucleoside analogs, like toyocamycin or 7-cyano-7-deaza-inosine (7-CN) were able to dissociate the PKAR-PKAC complex (Wu, 2021) and induce phosphorylation of downstream targets (VASP reporter protein, RXXS*/T* substrates in general (Bachmaier, 2015; Bachmaier *et al.*, 2019)). In PCF however, these nucleoside analogs do not lead to increases in substrate phosphorylation (Bachmaier, 2015), even though nucleosides can dissociate the complex (Wu, 2021). Uptake of purine nucleosides and nucleobases is essential in trypanosomes since they cannot synthesize them *de novo*. Recent work of the Estevez laboratory showed that purine abundance causes the repression of the nucleobase transporter NT8 in PCF (termed *Purine Response*). This response is mediated by a regulatory element in the 3'UTR of the NT8 gene. When fused to firefly luciferase, this regulatory element is sufficient to confer regulation of luciferase expression in response to purines (Fernandez-Moya *et al.*, 2014). When they used this regulatory element as a bait in a pulldown experiment, they identified two RNA binding proteins, Purine Response Element Binding Protein 1/2 (PuREBP1/2, (Rico-Jimenez *et al.*, 2021)). RNAi-mediated knock-down of either PuREBP resulted in reduced/abolished repression of luciferase expression. PuREBP1 was identified as a PKA substrate in the 7-CN phosphoproteome (Bachmaier *et al.*, 2019) and PuREBP2 was found in the PCF BioID pulldowns (3.3.3.2). These observations led to the question whether PKA could be involved in purine response signaling and was approached in collaboration

with the Estevez laboratory (Granada, Spain). Purine response reporter cell lines were generated in pleomorphic BSF wild type and Δ PKAR cells, differentiated into PCF and analyzed for purine response regulation (T. Thanner, unpublished). We could reproduce the purine-dependent regulation, but there were no differences between wild-type and Δ PKAR (T. Thanner, unpublished). Therefore, we proceeded to test purine response in BSF, the life cycle stage where we actually observe PKA activation by nucleosides that results in enhanced substrate phosphorylation. In this experiment, we investigated whether purine response also takes place in BSF, if it is affected in Δ PKAR and whether simultaneous PKA-activation by 7-CN would have an impact. We also included a control cell line with a regular Actin 3'UTR (Figure 59A). First of all, we could confirm that purine response is taking place in BSF as well, but it was not altered in the PKAR knockout. However, if the cells were treated with 7-CN during the purine-depletion, the changes in luminescence were almost twice as high compared to the untreated cells and this effect was dependent on PKAR (Figure 59B). In Summary, we could show that PKA is not essential in purine response signaling, but it can enhance expression of the luciferase reporter upon purine depletion.

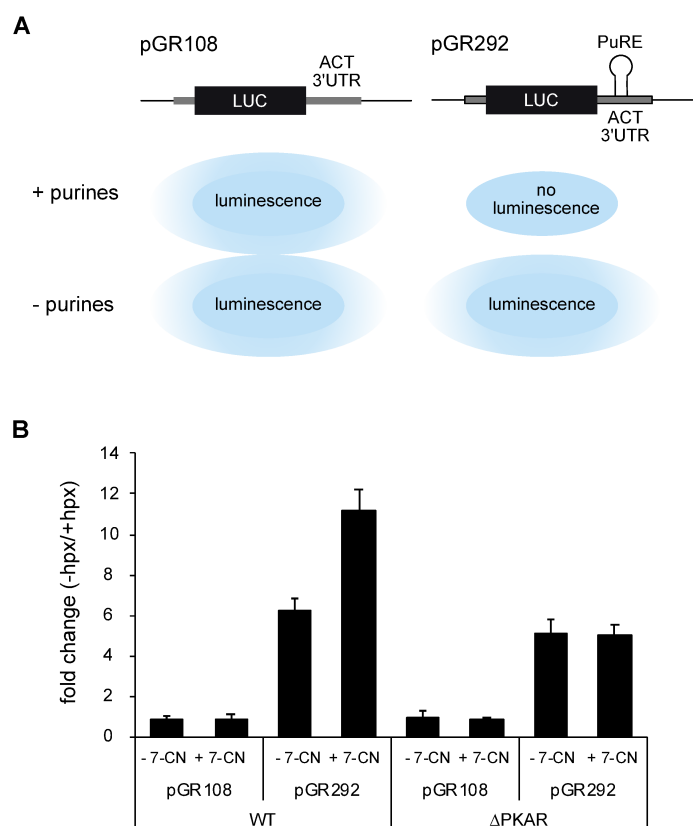


Figure 59: Purine response in pleomorphic BSF. **A:** Schematic representation of luciferase constructs and consequences of purine availability on luminescence readout. **B:** Cells were harvested and resuspended in purine-free medium containing 2% FCS. Depending on the sample, cultures were supplemented with 100 μ M hypoxanthine (hpx) as purine source and 5 μ M 7-CN as PKA activator. Bar chart represents the fold-change of luminescence between -/+ hypoxanthine after 8h incubation. Plotted is the average \pm stdev of n=3.

4 DISCUSSION

4.1 Functions of PKA in PCF

The main scope of this work was to unravel potential functions of TbPKA in the procyclic life cycle stage with a special focus on metabolism. Additionally, we wanted to investigate the requirement of PKA catalytic activity for basic cellular viability.

4.1.1 Role of PKA in metabolism

4.1.1.1 Effects of PKAC2 on central carbon metabolism

Based on the suspected glycosomal localization by (Guther *et al.*, 2014) and the imaging data provided by the tryptag database (Dean *et al.*, 2017), we hypothesized that PKAC2 might play a role in carbon metabolism. After confirmation of the glycosomal localization by glycosome enrichment and purification (chapter 3.4.1.2), we tested this hypothesis by examination of the RXXS*/T* phosphorylation pattern upon switch from a glycolytic carbon source to amino acid metabolism. Indeed, we found phosphorylation of one prominent band under glycerol depletion. Phosphorylation of this band was lost in the PKAC2 knockout, but not in the PKAR knockout. Analysis of the subcellular localization of this band, paired with a phosphoproteomic approach (chapters 3.4.2.2.2, 3.4.2.2.3) led to the preliminary assignment of this protein as PEX14, a member of the glycosomal import machinery. We could confirm PEX14 by GFP- *in situ* tagging in wild type and PKAC2 knockout cells. After GFP-pulldown, we confirmed RXXS*/T* phosphorylation of the fusion protein in the absence of glycerol in the wild-type, but not the PKAC2 knockout (Figure 51). To examine the physiological relevance, we generated homozygous phosphoablative and phosphomimetic mutants of both PEX14 phosphosites. First, we analyzed growth in medium with or without glycerol and did not observe any major phenotypes. Next, we hypothesized that the phosphorylation could have an impact on glycosomal import of a subset of enzymes. While we did not observe differences in steady-state glycosomal protein composition between wild type and the PEX14 phosphomutants, we did observe a loss of regulation of glycosomal protein abundance between cells grown in presence or absence of glycerol. This discrepancy could be explained by the low fold-changes of import differences in combination with potential adaptation mechanisms of the mutants. We thus considered the loss of glycosomal protein regulation by glycerol as the most interesting feature. Furthermore, the proteome comparison of wild type and Δ PKAC2 showed an enrichment for metabolic enzymes amongst the differentially expressed proteins which strengthened the hypothesis of a potential role of PKAC2 in carbohydrate metabolism (chapter 3.3.1).

From the pattern of up- and downregulation of enzymes, we hypothesized that PKAC2 is involved in the regulation of glycolysis and gluconeogenesis (Figure 26). Regulation of these metabolic pathways by PKA is not a new concept. In yeast, PKA is involved in glucose metabolism. In hepatocytes, PKA regulates both these pathways by phosphorylation of transcription factors and the involved enzymes in glycolysis/gluconeogenesis (introduced in 1.2). For *T. brucei*, we identify regulation of metabolic enzymes on proteome level (chapter 3.3.1), but very few regulated phosphorylation sites on metabolic enzymes (chapter 3.3.2). This would indicate that the primary targets involved in this regulation are proteins that regulate gene expression rather than the metabolic enzymes themselves. Based on the BioID interactome and Δ PKAC2 phosphoproteome, it does not seem like there are a lot of glycosomal phosphorylation targets. The most prominent metabolic target of PKAC2 which we could verify is PEX14. Open questions in this pathway, will be discussed in the following paragraphs.

Glycosomal import of PKAC2

First, how is PKAC2 imported into glycosomes? Usually, glycosomal matrix proteins are marked for import via a PTS1 or PTS2 signal. Neither of these are present on PKAC2. Initially, we hypothesized that PKAC2 might be glycosome associated rather than imported. This hypothesis was rejected when we observed that PKAC2 is protected from protease digestion (Figure 39). Alternatively, proteins without PTS signals can be imported by piggybacking. Here the interaction with a PTS-containing protein causes import of the whole complex, as was shown for PEPCK and UGP (Villafranz et al., 2021). After the discovery of PEX14 as a substrate, we propose that PKAC2 import is the result of this kinase-substrate interaction and therefore does not need a PTS signal. The fact that we cannot detect PKAR in glycosomal fractions indicates that PKAC2 is imported either before complex assembly or after dissociation. Whether glycosomal PKAC2 fulfills a function besides the phosphorylation of PEX14 is not clear yet. Based on the phosphoproteomic comparison of wild type and PKAC2 knockout cells (chapter 3.3.2), there is no indication for glycosomal phosphorylation targets with a PKA substrate motif (Supplementary Table 2). However, this phosphoproteomic comparison was done in steady-state culture conditions on a whole cell lysate. It is possible that a glycosomal phosphoproteome might reveal some targets that were missed before due to low abundance. To our knowledge PKAC2 is the only protein kinase localized to this subcellular compartment and could potentially be the antagonist of glycosomal protein phosphatases. Given that PEX14 phosphorylation occurs during glycerol depletion, we would expect elevated PKAC2 import under these conditions, if the piggybacking model applies. Interestingly, we do observe PKAC2 import irrespective of glycerol availability (Figure 39). Yet, it is possible that import is upregulated in

response to glycerol depletion, as the PKAC2 abundance could not be compared quantitatively between both conditions. In the glycosomal proteome, we observed a tendency of higher PKAC2 levels in cells grown in absence of glycerol. Unfortunately, this effect was not statistically significant, which could be due to the dual localization of PKAC2 in the glycosome and flagellum and a minor contamination of the glycosomal fraction with flagella. Both of these cellular structures are enriched with the differential centrifugation method used prior to proteome analysis. Assuming that the predominant flagellar localization is not affected by glycerol, it would most likely quench potential differences in glycosomal import. Whether the import of PKAC2 is regulated quantitatively by changes in glycerol availability still needs to be addressed.

PKAR-independent activation of PAKC2

The second question is how PKAC2 is activated by glycerol depletion, especially considering that PEX14 phosphorylation is a PKAR-independent event. It is possible that PKAC2 needs additional phosphorylations to gain full activity. In the mammalian orthologue, PKAC activity is mediated by two crucial phosphorylation sites. First, S338 in the kinase C-terminal tail is phosphorylated. This phosphorylation allows interaction with PDK1, which then phosphorylates T197 in the activation loop. Both of these phosphorylations are placed before PKAR-PKAC holoenzyme assembly, rendering an activation mechanism that exclusively depends on PKA dissociation by ligands (Romano *et al.*, 2009; Taylor *et al.*, 2012b). In *T. brucei*, phosphoproteomic analyses have reported plenty of phosphosites for PKAC1/2 (Nett *et al.*, 2009; Urbaniak *et al.*, 2013; Zhang *et al.*, 2020), including the equivalents of the S338 and T197 known from mammalian PKA. Due to the extremely high sequence similarity, tryptic digest of PKAC1 and PKAC2 leads to only very few subunit-specific peptides that can be analyzed by mass spectrometry. Therefore, only very few sites can actually be attributed to one subunit specifically. So far, we are only aware of two phosphoproteomic datasets available in the PCF stage, one of which is described here (chapter 3.3.2). In our dataset, we only identified the activation loop phosphorylation (T179 in PKAC1/T181 in PKAC2) and one more phosphorylation on the C-terminal tail (S315 in PKAC1/S317 in PKAC2). The latter could correspond to S338 in the mammalian orthologue and phosphorylation of both these sites should be sufficient to render an active kinase (Romano *et al.*, 2009; Taylor *et al.*, 2012b). Yet, we do not observe any downstream RXXS*/T* substrate phosphorylation increase by nucleoside analogs, even though PKAR-PKAC dissociation is possible (Bachmaier, 2015; Wu, 2021). So far, the only prominent PKA-dependent phosphorylation event we could observe is PEX14 phosphorylation in response to glycerol-depletion. It is possible that some additional post translational modifications are needed to obtain full activity or mediate PEX14 substrate-specificity. The most

prominent phosphorylation target by glycerol-depletion was AMPK α 1 (Table 2). We could confirm changes in AMPK α 1 and AMPK α 2 activity pattern upon this metabolic trigger (Figure 47). This kinase is a known regulator of metabolism and could potentially act upstream of PKAC2 in this pathway. AMPK α is activated by an increase in AMP/ATP ratio (Garcia and Shaw, 2017). A switch from glucose/glycerol to proline metabolism induces a shift from glycolytic to gluconeogenic flux (Wagnies *et al.*, 2018). The cytoplasmic reaction of phosphoglycerate kinase (PGK, step 10 in Figure 3) now consumes ATP instead of generating it. This could contribute to an increase in AMP/ATP ratio activating AMPK α . In addition to that, mitochondrial flux is elevated leading to higher oxidative phosphorylation and production of reactive oxygen species (ROS) (Tirichen *et al.*, 2021), which have also been reported to activate AMPK α in BSF trypanosomes (Saldivia *et al.*, 2016). Activated AMPK α could place some phosphorylation on PKAC2 (directly or via a kinase cascade) in addition to the already established T181 and S317 phosphorylations to increase PKAC2 activity or substrate specificity towards PEX14 (Figure 60A). The fact that we did not observe any additional phosphosites on PKAC2 argues against this hypothesis. However, the cytoplasmic fraction of PKAC2 which we investigate here is minor. Therefore, changes in phosphorylation pattern of this protein fraction could be below detection limit of the mass spectrometry. Alternatively, AMPK α could place the C-terminal phosphorylation on S317, which would facilitate PDK1-mediated phosphorylation of T181 in the activation loop (Figure 60B) giving rise to an active PKAC2 requiring only the two phosphorylation sites we were able to detect by mass spectrometry. Another possibility is that phosphorylation of PEX14 is not induced by enhanced activity of PKAC2, but rather by the inactivation of phosphatases that work antagonistically to PKAC2. In HeLa cells, treatment with diamide, an agent that oxidizes sulfhydryl (-SH) side chains, caused a biphasic effect on PKA activity measured in cell lysates (Humphries *et al.*, 2007). At low concentrations of diamide (up to 100 μ M), PKA activity was increased and inhibited at higher concentrations. Using a variety of phosphatase inhibitors, they confirmed that the increase in PKA activity at low concentrations was the result of phosphatase inhibition by the oxidizing agent. Alternatively, protein oxidation can also be triggered by ROS as oxidizing agents. The PKAC inactivation at high concentrations of diamide is the result of oxidation of the cysteine residue (C199 in mammalian, C183 in PKAC2) in the activation loop (Humphries *et al.*, 2005; Humphries *et al.*, 2002). This mechanism is

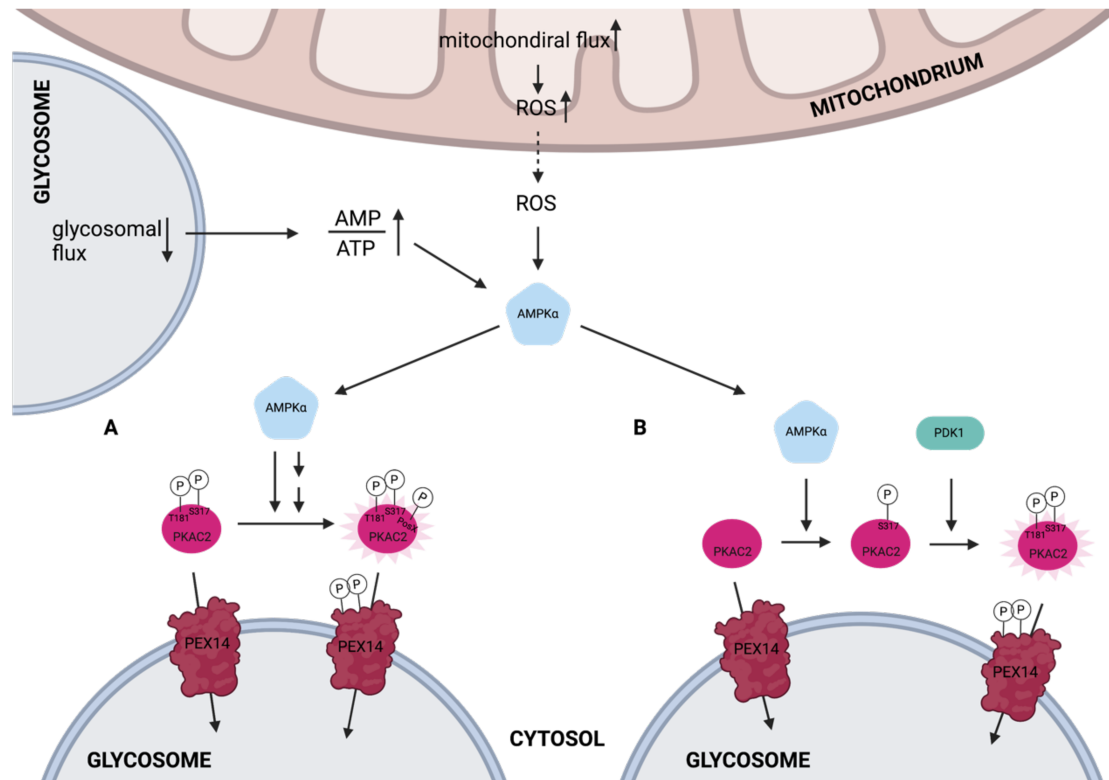


Figure 60: Potential models for PKAC2 activation by glycerol depletion. Glycerol depletion leads to a simultaneous decrease in glycolytic flux and increase in mitochondrial flux. Decrease of glycolytic flux leads to an increased AMP/ATP ratio in the cytosol and elevated ROS production in the mitochondrion. Both of these triggers can activate AMPK α . Activities of both AMPK α subunits are affected by glycerol-depletion. In model **A**, PKAC2 is phosphorylated on S317 and T181 (activation loop). AMPK α mediated phosphorylation of additional residues is needed for full activity. In model **B**, cytoplasmic PKAC2 is unphosphorylated and AMPK α activation leads to phosphorylation of S317 which is necessary for PDK1 recruitment and phosphorylation of the activation loop. Figure was generated using BioRender.com.

independent of the PKAR subunit and we could show that treatment of PCF cells with 1 mM H₂O₂ results in a reduction of RXXS*/T* phosphorylation (Supplementary Figure 9). During the switch from glycerol to proline metabolism, mitochondrial flux is increased and mitochondrial ROS production most likely elevated. A mild increase in ROS levels could lead to phosphatase deactivation without affecting PKAC2 activity. In this model (Figure 61), PKAC2 and phosphatase activity are balanced in the presence of glycerol resulting in unphosphorylated PEX14. A mild increase in ROS levels due to higher mitochondrial flux upon glycerol depletion would result in phosphatase deactivation and shift the balance of PEX14 towards the phosphorylated state. Reversible oxidation of cysteine residues of redox-sensitive signaling molecules was described before, e.g., for the regulation of PKA activity in the cardiovascular system (Cuello et al., 2021). Furthermore, it was recently demonstrated that ROS levels are elevated upon RBP6 overexpression and necessary for progression through the life cycle *in vitro* (Dolezelova et al., 2020). In line with that, overexpression of cytosolic catalase, an H₂O₂ detoxifying enzyme, decreased the efficiency of the tsetse midgut infection rate, indicating that a certain amount of ROS is needed to successfully

progress through the life cycle *in vivo* (Horakova et al., 2020). This necessity of ROS could be explained by oxidative modifications of cysteine residues in signaling molecules that are necessary for initiation or suppression of differentiation events.

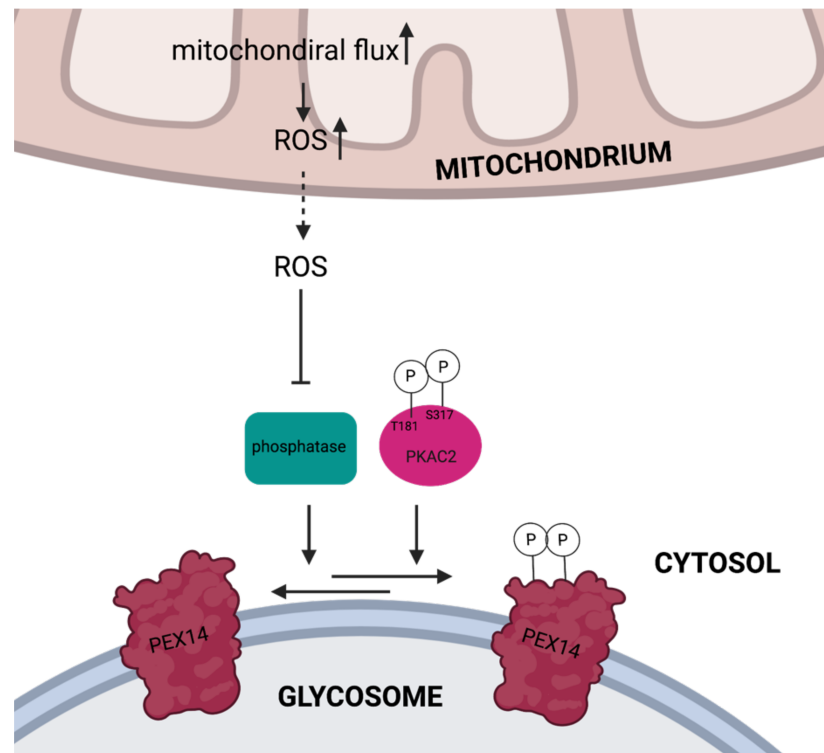


Figure 61: Potential model for increase in PEX14 phosphorylation upon glycerol depletion. In this model, glycerol depletion leads to an increase in mitochondrial flux and ROS generation, mainly due to oxidative phosphorylation. The increase in ROS levels is sufficient to inhibit cytoplasmic protein phosphatases, but not PKAC2. The result is an accumulation of PEX14 in the phosphorylated state. Figure was generated using BioRender.com.

Physiological relevance of PKAC2-dependent PEX14 phosphorylation

At this point we cannot with certainty claim a physiological relevance of the PKAC2-dependent PEX14 phosphorylation event triggered by glycerol depletion. On one hand, we do not observe any severe phenotypes with the PKAC2 knockout or any of the PEX14 phosphomutants. Of course, the experiments here were performed *in vitro* in an extremely rich culture medium, we cannot exclude potential phenotypes under physiological conditions. Since PEX14 is an essential part of the glycosomal import machinery, we focused on a potential role in regulation of glycosomal import. We hypothesized that the phosphorylation could potentially change the interaction with a specific subset of cargo proteins leading to more or less import upon phosphorylation. We expected to see changes in import of some metabolic enzymes which might be necessary to adapt metabolic flux to the current nutrient availability. Surprisingly, this was not the case. While most glycosomal proteins regulated in abundance by glycerol are involved in early steps of glycolysis, gluconeogenesis or nucleotide metabolism, their import was not affected by the mutants. Instead, we observed a moderate (1.5x) up-regulation of PIP39 glycosomal protein levels in the absence of glycerol, which was lost in both PEX14 phosphomutants. PIP39 is a Dx/Dx (T/V) Ser/Thr phosphatase with a predicted citrate binding pocket (Szoor et al., 2010) and plays an important role in

stumpy to procyclic differentiation. In stumpy BSF PIP39 is dephosphorylated and thereby inactivated by the tyrosine phosphatase PTP1. Upon initiation of PCF differentiation by citrate/cis-aconitate, PTP1 is deactivated leading to PIP39 phosphorylation on Y278 and recruitment to the glycosome (Szoor *et al.*, 2010). This glycosomal sequestration is crucial for successful differentiation into procyclic cells. The glycosomal localization is maintained in PCF, but the biological function in this stage is not yet fully investigated. Western blot analysis of PIP39 in BSF and PCF lysates showed a shift in SDS-PAGE migration, indicating that the phosphatase is phosphorylated and therefore most likely active (Szoor *et al.*, 2010). Overexpression or RNAi mediated depletion of PIP39 had no severe growth phenotypes in standard culture conditions (Szöör *et al.*, 2019; Tripathi *et al.*, 2019). Recently, (Tripathi *et al.*, 2019) proposed that PIP39 is involved in maintenance of cellular homeostasis together with Tim50, a mitochondrial DxDx(T/V) phosphatase and part of the mitochondrial translocation machinery. The cross-talk between these two phosphatases is supposed to be mediated via AMPK α . They could observe a 1.5x increase in PIP39 levels upon 8-pCPT-2Me-cAMP treatment (AMPK α -activator) and a decrease in PIP39 levels upon treatment with compound C (AMPK α inhibitor). Furthermore, PIP39 depletion by RNAi resulted in elevated intracellular ROS levels, indicating that PIP39 might be involved in ROS detoxification (Tripathi *et al.*, 2019). Since AMPK α activation by ROS was demonstrated in the BSF stage, it would not be surprising if this feature was conserved in PCF (Saldivia *et al.*, 2016).

In summary, glycerol depletion leads to an increase in PKAC2-dependent PEX14 phosphorylation. This phosphorylation event is independent of the regulatory subunit and hence must involve an alternative activation mechanism of PKA. We propose two models for PKAR-independent increase in PKAC2 activity. The first model involves an upstream acting kinase that is activated by glycerol-depletion and phosphorylates PKAC2 on the C-terminus to render it fully active or confer substrate specificity towards PEX14. We propose AMPK α as a potential upstream acting kinase based on the changes in activity upon glycerol-depletion (Figure 61). In the other model, PKAC2 activity is not altered, but the mild increase in ROS levels causes inhibition of protein phosphatases. These phosphatases would otherwise remove the phosphorylations on PEX14, thereby leading to an accumulation of phosphorylated PEX14. Phosphorylation of PEX14 seems to lead to increase in glycosomal PIP39 protein levels. Based on the finding of (Tripathi *et al.*, 2019), we could image that PIP39 is upregulated to participate in oxidative stress defense by a yet unknown mechanism. Mitochondria are the main source of ROS and glycerol removal will cause an increase in mitochondrial metabolic flux, leading to a higher ROS production. In glycosomes, the only glycolytic

enzyme that are upregulated in response to depletion are hexokinase and glucose-6-phosphate isomerase. Both of these enzymes can produce glucose-6-phosphate which is necessary to feed the pentose phosphate pathway (PPP). This pathway is important for the generation of nucleoside precursors, but also for the supply of reducing agents, such as NADPH. In *T. brucei*, the enzymes which produce NADPH are located predominantly in the cytoplasm, but also in the glycosomes (Duffieux *et al.*, 2000; Heise and Oppendoes, 1999). Assuming that glucose-6-phosphate can cross the glycosomal membrane, it should be able to feed the glycosomal and cytoplasmic branches of the PPP. The reducing agents generated by the PPP are critical for ROS detoxification by the trypanothione pathway (Kovarova and Barrett, 2016). The NADPH consuming step of ROS detoxification by trypanothione reductase is mainly localized in the cytoplasm, but the enzyme was also detected in the glycosomal proteome (Guther *et al.*, 2014). Glycosomal isocitrate dehydrogenase (IDHg) was the most prominently upregulated enzyme upon glycerol depletion and also produces NADH and NADPH during the catalysis of isocitrate to alpha-ketoglutarate (α -KG). There is no evidence of NAD(P)H transport through membranes in *T. brucei*, thus IDHg only contributes to the glycosomal pool. Interestingly, we found two isoforms of thymine-7-hydroxylase, an α -KG consuming enzyme, upregulated along with IDHg. This enzyme catalyzes the modification of thymine to hydroxymethyluracil to formyluracil and finally uracil-carboxylic acid (Simmons *et al.*, 2008). It is possible that IDHg is upregulated to supply these enzymes with the cofactor α -KG to produce modified nucleobases needed for epigenetic remodeling or RNA modification. Modification of RNA could have an effect on the transcript stability or translation initiation and thereby lead to further adaptations. Taken together, it appears as if the function of glycosomes shifts from energy generation to ROS detoxification and potentially further adaptation in the absence of glycolytic carbon sources (Figure 62).

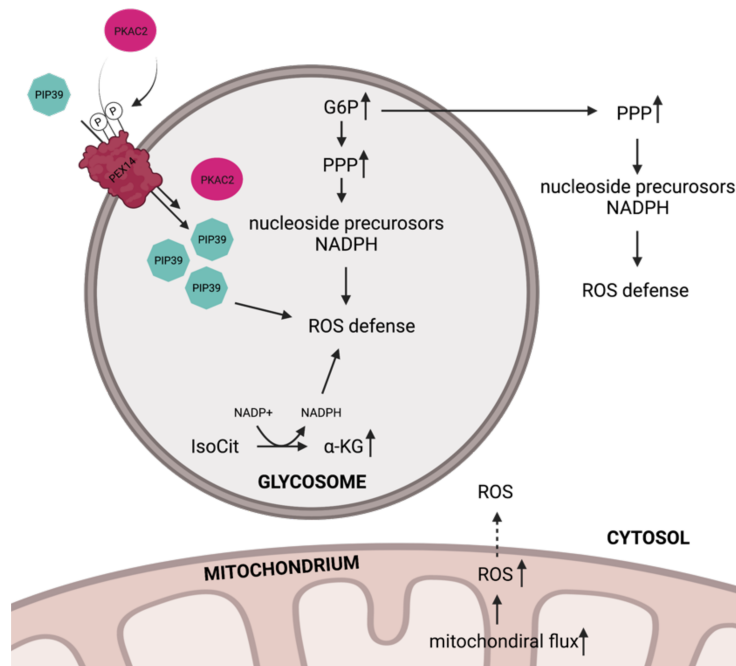


Figure 62: Summary of consequences of glycerol depletion. Glycerol depletion causes PKAC2-dependent PEX14 phosphorylation on two adjacent sites. This phosphorylation appears to promote PIP39 import. Energy production is shifted to the mitochondrion leading to increases in flux and ROS production. Upregulated glycolytic enzymes mainly produce glucose-6-phosphate, which feeds the glycosomal and cytosolic pentose phosphate pathway (PPP) and generates NADPH. Additionally, IDH_g produces NADH and NADPH during catalysis of isocitrate to α -ketoglutarate in the glycosome. NADPH is important for ROS defense in the trypanothione pathway. PIP39 might be involved in ROS detoxification based on (Tripathi et al., 2019). Figure was generated using BioRender.com.

Outlook

It would be extremely interesting to further investigate this proposed model that connects carbon source availability with signaling and organelle remodeling. This can be divided into a PKA upstream and downstream section.

The PKA upstream section concerns the activation mechanism by which PEX14 phosphorylation is mediated, focusing on the proposed post-translational modifications. For that purpose, PKAC2 from cells grown in presence or absence of glycerol could be precipitated and analyzed for differences in phosphorylation pattern by mass spectrometry. If differences in phosphorylation pattern are observed, we could proceed to answer whether AMPK α is involved by RNAi targeting. Using protein phosphatase inhibitors with different specificities towards different types of phosphatases and reducing agents, such as DTT or β -mercaptoethanol, could provide some indication whether phosphatases are involved in PEX14 dephosphorylation in a redox-sensitive manner. It is also possible that both of these mechanisms play a role in PKA activation in PCF. The PKA downstream section concerns the physiological relevance of PEX14 phosphorylation. The first step would be to confirm that PIP39 import is indeed upregulated in absence of glycerol and that the PEX14 phosphorylation is responsible for that upregulation. This can be done by glycosome enrichment and subsequent analysis of PIP39 protein levels. After successful confirmation, we would compare ROS levels from cells grown in presence or absence of glycerol and investigate whether they are affected in the PEX14 phosphomutants. Alternatively, PIP39 could also play a role in further differentiation steps to epimastigotes and metacyclics. These differentiation

steps were shown to be influenced by ROS levels (Dolezelova *et al.*, 2020; Horakova *et al.*, 2020) and PIP39 appears to influence them (Tripathi *et al.*, 2019). So far, functional analysis of PIP39 in the PCF stage is limited. This phosphatase might be important for efficient migration through the tsetse fly. This hypothesis could be tested by infection of tsetse flies with the PEX14 phosphomutants, Δ PKAC2 and a PIP39 depleted line. Progression through the tsetse fly *in vivo* is accompanied by migration through various tissues and morphological changes. It is possible that the necessary adaptations for successful completion of the life cycle are triggered by metabolic signals which are conveyed to signaling proteins or complexes, such as PKA or PIP39.

4.1.1.2 Environmental sensing through glycolytic metabolites

In the previous paragraph, we hypothesized that the physiological relevance of PEX14 phosphorylation could be an increase in glycosomal recruitment of PIP39, a key element of the stumpy to PCF differentiation signaling pathway. In this scenario, the glycolytic metabolites glucose and glycerol would not only act as metabolites for energy generation, but also as environmental signals. In Figure 42 we observed that cultivation of freshly differentiated procyclics (*early* procyclics) in medium containing glucose, but not glycerol, led to growth arrest and eventual cell death. In addition to that, these cells became elongated and showed a decrease in motility. Initially, we hypothesized that early procyclics might not be able to metabolize glucose, but this hypothesis was rejected after the NMR analysis (chapter 2.2.7.5). Trypanosome differentiation is often accompanied by changes in morphology, motility and protein surface coat. During the differentiation from stumpy to procyclics, the cells change their protein surface coat from the variant surface glycoproteins (VSG) in BSF to procyclins in PCF. Composition of this PCF surface coat is affected by availability of glycolytic carbon sources and disturbance of mitochondrial enzyme activity *in vitro* (Morris *et al.*, 2002; Vassella *et al.*, 2000; Vassella *et al.*, 2004). The main procyclin expressed in PCF is EP, a protein of up to 30 tandem repeats of Glu-Pro (Mowatt and Clayton, 1987; Roditi *et al.*, 1987). In addition to that early PCF express the procyclin GPEET, a protein composed of 6 pentapeptide (Gly-Pro-Glu-Glu-Thr) repeats (Mowatt *et al.*, 1989). The latter is down-regulated *in vivo* after 7 days post infection of tsetse flies. *In vitro*, GPEET expression is dependent on glycerol availability during stumpy to PCF differentiation and can be maintained as long as glycerol is present in the culture medium (Vassella *et al.*, 2000). As soon as cells are cultured under glucose only, they undergo morphological changes and a transient growth arrest, which was proposed to mark a further differentiation step to *late* procyclics (Vassella *et al.*, 2000). Alternatively, GPEET re-expression can be triggered by glucose-depletion (Morris *et al.*, 2002) or by downregulation of ASCT-

cycle enzymes (Vassella *et al.*, 2004). Later during the differentiation to epimastigotes, the parasites express BARP (*brucei alanine-rich proteins*) on their surface (Urwyler *et al.*, 2007). Finally, when they reach the salivary glands, metacyclic cells express metacyclic VSGs (mVSGs). *In vitro* differentiation to metacyclics by RBP6 overexpression was demonstrated to be more efficient in glucose and glycerol-free medium (Ziebart, 2016). In summary, many differentiation steps are accompanied by changes in surface coat proteins, which might be important for progression to the next host or tissue. Of these surface coats, GPEET is known to be regulated by metabolic state. It would not be surprising, if small metabolites such as glucose or glycerol would act as metabolic signals or an energy gauge to initiate the next step in this complex life cycle. This could be perceived by interconnection of metabolic pathways with signaling proteins or complexes, such as PKA or PIP39. These signaling complexes could transduce these metabolic signals into a downstream response and initiate adaptation processes such as changes in morphology and surface protein coat, cell cycle arrest or remodeling of metabolic pathways.

4.1.1.3 PKA and nucleoside metabolism

Kinetoplastids cannot synthesize the purine ring *de novo* and rely on purine nucleoside import from their extracellular surroundings (Landfear *et al.*, 2004). The *T. brucei* genome encodes for a variety of nucleoside and nucleobase transporters with different affinities and uptake rates (summary available in (Ortiz *et al.*, 2009)). Inside the cell, the different purines can be interconverted (Arco and Fernandez-Lucas, 2017). One of these conversion enzymes, AMP-deaminase was identified as a potential interaction partner of all three catalytic subunits in both life cycle stages (chapter 3.3.3). Furthermore, glycerol depletion in PCF leads to PKAC2-dependent phosphorylation events and to a downregulation of AMP-deaminase and an upregulation of GMP reductase, two proteins that produce inosine-monophosphate (IMP). IMP can be further broken down to inosine, the most potent physiological PKA activator in BSF (Githure, 2014; Wu, 2021). We tested whether PKA is necessary for the purine response pathway in BSF (chapter 3.4.3) and observed that PKA is not essential but simultaneous activation can enhance the upregulation of the luciferase reporter fused to the purine-dependent regulatory element. In a physiological context this would suggest that PKA activation leads to enhanced expression of the nucleobase transporter NT8. Expression of NT8 is dependent on the RNA binding proteins PuREBP1 and PuREBP2 (Rico-Jimenez *et al.*, 2021). PuREBP1 was identified as a PKA substrate in the BSF phosphoproteome after induction with 7-CN, a potent PKA activator (Bachmaier *et al.*, 2019) and contains one PKA phosphorylation site on S589 (Urbaniak *et al.*, 2013). It is possible that PKA

phosphorylation on this site modifies the RNA binding properties and leads to a higher de-repression of NT8. This effect should be tested in the procyclic stage using the series of PKAC knockouts generated here (chapter 3.2). The purine response pathway was initially described in procyclic cells, which we could reproduce in our lab. We also observed purine response in the procyclic PKAR knockout (T. Thanner, unpublished). We cannot test whether PKA activators would enhance the de-repression in the PCF stage based on the absence of ligand inducibility of PKA in PCF. However, it is still possible that catalytic activity is needed for modification of the PuREBP RNA binding properties, but regulation may not be mediated via PKAR.

Nucleoside transporters are extremely important for trypanosome drug targeting since numerous trypanocidal compounds are taken up by nucleoside transporters (Berg *et al.*, 2010). In this context, simultaneous PKA activation could potentially increase uptake efficiency of these compounds and lead to a lower effective concentration.

4.1.2 PKA is not essential for basic cellular viability in PCF

In addition to the potential metabolic phenotypes, we investigated PKA essentiality in procyclic cells by a series of single, double and triple knockouts. Removal of all PKAC subunits was well tolerated by the cells and showed no major phenotypes in cell viability. Only the PKAC2 and PKAC1/2 knockouts initially displayed a mild increase in PDT which was lost after prolonged culture time. This was not observed for the triple knockout which was a long term procyclic culture. It might indicate that PKA is more crucial in the early procyclic stage shortly after differentiation. We could observe a decrease in substrate phosphorylation pattern (RXXS*/T*), which was mainly due to deletion of PKAC2. From this we concluded that PKA is not essential for basic cellular functions in the procyclic stage, but might be activated under specific circumstances, like changes in nutrient levels. Furthermore, PCFs are only one of several fly stages and differentiate further during progression through the different tissues. It is possible that PKA is needed in a later stage *in vivo*. A complete summary of PKA reverse genetic phenotypes in PCF can be found in Table 4. In contrast to procyclics, BSF cells display an obvious motility and cytokinesis phenotype that corresponds with the flagellar localization. Even though, PKA predominantly localizes to flagella in PCF as well, we do not observe any striking motility phenotypes here. The main reason for this is that motility and cytokinesis are decoupled in the procyclic stage (Broadhead *et al.*, 2006; Ralston *et al.*, 2006). Impaired motility in PCF does not lead to cytokinesis issues and has no effect on cell proliferation. This would explain why we do not observe a cytokinesis phenotype in the PCF stage. We do not observe a striking motility phenotype in the PKAR and PKAC knockouts in culture, but this has not been investigated

in a quantitative manner and is thus not excluded yet. There is still a possibility of a mild motility phenotype which could potentially influence trypanosome migration through the tsetse fly.

Table 4: Summary of PKA phenotypes in PCF *T. brucei* after genetic perturbations.

Sub-unit	Reference	<i>T. brucei</i> strain	Gene manipulation	Phenotype
PKAR	(Bachmaier, 2015)	AnTat 1.1	$\Delta pkar/\Delta pkar$	No obvious phenotypes No co-regulation of other PKA subunits
PKAC2	This work	AnTat 1.1 90-13	$\Delta pkac2/\Delta pkac2$	Growth: mild increase in PDT, lost over prolonged time in culture Loss of PEX14 phosphorylation upon glycerol/glucose-depletion No co-regulation of other PKA subunits
PKAC1/2	This work	AnTat 1.1 90-13	$\Delta pkac1/\Delta pkac1$, $\Delta pkac2/\Delta pkac2$	Growth: mild increase in PDT, lost over prolonged time in culture No co-regulation of other PKA subunits
PKAC3	(Schultze zu Sodingen, 2000)	AnTat 1.1	$\Delta pkac3/\Delta pkac3$	Growth: mild growth phenotype, lost after prolonged time in culture Cytokinesis: no phenotypes No co-regulation of other PKA subunits
PKAC1/2/3	This work	AnTat 1.1	$\Delta pkac1/\Delta pkac1$, $\Delta pkac2/\Delta pkac2$ $\Delta pkac3/\Delta pkac3$	Growth: no effect

4.2 Redundancy of PKAC1 and PKAC2

One of the questions we collectively tried to answer over the past years was whether PKAC1 and PKAC2 are redundant. These two genes share over 90% sequence identity and have most likely emerged from a gene duplication event (Kramer et al., 2007). The life-cycle dependent expression profiles led to the hypothesis that they might have specialized functions. However, the BioID interactome showed more common than specific interaction partners for these two subunits (chapter 3.3.3.3, supplementary tables 3, 5) and the GO analysis of the specific hits showed very similar functional annotations. Reverse genetic analysis in monomorphic BSF, showed quite similar cytokinesis phenotypes for PKAC2 knockout and PKAC1/2 RNAi (Kramer, 2004). PKAC1 in BSF appeared to be essential in the monomorphic strain MITat 1.2, since

heterozygous gene deletion caused a severe growth and cytokinesis phenotype and a homozygous deletion was not possible to obtain (Kramer, 2004). In the pleomorphic AnTat 1.1 strain, RNAi has less severe growth effects and deletion of PKAC1 was possible when PKAC2 was inducibly overexpressed during the course of transfection (Wu, 2021) indicating that PKAC2 might compensate for PKAC1 deletion. However, these cell lines showed no growth phenotype when the PKAC2 overexpression was terminated. Alternatively, this could indicate that these lines have gone through some adaptation mechanism during genetic manipulation and do not require PKAC1 anymore.

The few differences we observe in the protein sequence are located on the extreme N- and C-termini. In mammalian PKA, these regions are important for kinase activity and substrate specificity (Kannan *et al.*, 2007; Tholey *et al.*, 2001). Structural modeling showed that the differences of PKAC1 and PKAC2 lead to slightly different C-terminal surfaces (chapter 3.3.4). Further, these regions are full of phosphorylation sites, which appear to be either life cycle or subunit specific. BSF phosphoproteomes identify higher numbers of phosphosites on PKAC1/2 compared to PCFs. The phosphosites in BSF could also be PKAC1-specific and absent in PCF because this subunit is simply not expressed. Knockout of PKAR is accompanied by a downregulation of PKAC1/2 expression in BSF, but not in PCF. Similarly, this could be a subunit or life cycle specific observation, possibly as a result of the differential phosphorylation patterns. One potential explanation might be that PKAC1 is less stable compared to PKAC2 when not bound in a holoenzyme conformation. Alternatively, some of the phosphorylations in BSF could destabilize the unbound catalytic subunit in BSF. The second seems more likely considering PKAC1 and PKAC2 overexpression experiments (Supplementary Figure 8). When generating TY-PKAC1 and TY-PKAC2 rescue lines in BSF Δ PKAC2, induction of the TY-tagged proteins leads to increase in their expression, while the endogenous PKAC1 is downregulated. This was observed for both, PKAC1 and PKAC2 overexpression, indicating that only a certain amount of catalytic subunit can be stably expressed at a time, possibly limited by the quantity of PKAR. Furthermore, we investigated whether glycosomal localization in PCF was a subunit-specific feature (chapter 3.4.1). Overexpression of a TY-tagged version in the wild type background did show glycosomal import for both PKAC1 and PKAC2. It is not excluded that the efficiency might be different, but in principle both are capable of import. In the context of metabolism, we found that glycerol-depletion causes PKAC2-dependent phosphorylation of PEX14. Attempts to rescue the lack of phosphorylation in the Δ PKAC2 cell line with PKAC1 add-back were inconclusive due to high variability of protein expression levels and differences in sensitivity of different lots of the anti-RXXS*/T* antibody.

In summary (Table 5), in the cases where we were able to differentiate between PKAC1 and PKAC2 they appear redundant. For the rest, it was technically not possible to differentiate between PKAC1 and PKAC2 yet. Even though there appears to be no difference in terms of holoenzyme dissociation and subcellular localization, there might be some important residues which could contribute to differences in kinase activity or substrate specificity. The main remaining unknowns are whether PKAC2 can be responsive to cold shock in BSF and whether PKAC1 can cause PEX14 phosphorylation upon glycerol-depletion. These questions can only be answered in a genetic background that is only expressing the subunit of interest at a high enough concentration. Furthermore, the activation mechanism induced by cold shock remains unknown. In theory, this could still be a PKAC1 specific mechanism that is mediated by sequence differences in N- and C-terminus. In the mammalian system, solving of the PKA holoenzyme structures has unraveled distinct quaternary structures formed by different isoforms, which could form different signaling hubs (Cao et al., 2019). Given that approx. half of the interactors identified by BioID were subunit specific, this might be a possibility. Solving the holoenzyme structures of PKAR-PKAC1/PKAC2 by cryo-EM is a project currently in progress to investigate this hypothesis.

Table 5: Summary of differences between PKAC1 and PKAC2.

Subunit	PKAC1	PKAC2
Co-regulation with PKAR in BSF	Yes ¹	Unknown
Co-regulation with PKAR in PCF	Not expressed	No ²
Essential in BSF culture	dependent on strain and culture method ^{3, 4}	No ³
Subunit specific hits in BioID	47% ⁵	48% ⁵
Isoform specific phosphosites on N-terminus (specific/identified)	4/4 ⁶	0/0 ⁶
Isoform specific Phosphosites on C-terminus (specific/identified)	0/0 ⁶	0/5 ⁶
Flagellar localization in BSF and PCF	Yes ^{7, 8}	Yes ^{7, 8}
Glycosomal localization in PCF	Yes ⁵	Yes ⁵
Dissociation by nucleosides and analogs	Yes ^{1, 4}	Yes ⁴
Activation by cold chock	Yes ¹	Unknown
PEX14 phosphorylation upon glycerol-depletion	Unknown	Yes ⁵
¹ (Bachmaier, 2015); ² (Schulte zu Sodingen, 2000); ³ (Kramer, 2004); ⁴ (Wu, 2021); ⁵ This work; ⁶ (Nett <i>et al.</i> , 2009; Urbaniak <i>et al.</i> , 2012; Zhang <i>et al.</i> , 2020); ⁷ (Krumbholz, 2006); ⁸ tryptag.org		

5 REFERENCES

- Abel, E.S., Davids, B.J., Robles, L.D., Loflin, C.E., Gillin, F.D., and Chakrabarti, R. (2001). Possible roles of protein kinase A in cell motility and excystation of the early diverging eukaryote *Giardia lamblia*. *J Biol Chem* 276, 10320-10329. 10.1074/jbc.M006589200.
- Aleshin, A.E., Zeng, C., Bourenkov, G.P., Bartunik, H.D., Fromm, H.J., and Honzatko, R.B. (1998). The mechanism of regulation of hexokinase: new insights from the crystal structure of recombinant human brain hexokinase complexed with glucose and glucose-6-phosphate. *Structure* 6, 39-50. 10.1016/s0969-2126(98)00006-9.
- Allmann, S. (2014). Developmental adaptations of energy and lipid metabolism in *Trypanosoma brucei* insect forms. Doktor Dissertation (Ludwig-Maximilians-Universität).
- Allmann, S., Mazet, M., Ziebart, N., Bouyssou, G., Fouillen, L., Dupuy, J.W., Bonneau, M., Moreau, P., Bringaud, F., and Boshart, M. (2014). Triacylglycerol Storage in Lipid Droplets in Procyclic *Trypanosoma brucei*. *PLoS One* 9, e114628. 10.1371/journal.pone.0114628.
- Allmann, S., Wargnies, M., Plazolles, N., Cahoreau, E., Biran, M., Morand, P., Pineda, E., Kulyk, H., Asencio, C., Villafraz, O., et al. (2021). Glycerol suppresses glucose consumption in trypanosomes through metabolic contest. *PLoS Biol* 19, e3001359. 10.1371/journal.pbio.3001359.
- Alsford, S., Turner, D.J., Obado, S.O., Sanchez-Flores, A., Glover, L., Berriman, M., Hertz-Fowler, C., and Horn, D. (2011). High-throughput phenotyping using parallel sequencing of RNA interference targets in the African trypanosome. *Genome Res* 21, 915-924. 10.1101/gr.115089.110.
- Arco, J.D., and Fernandez-Lucas, J. (2017). Purine and Pyrimidine Phosphoribosyltransferases: A versatile tool for enzymatic synthesis of nucleoside-5'-monophosphates. *Curr Pharm Des.* 10.2174/1381612823666171017165707.
- Bachmaier, S. (2008). Charakterisierung einer PKA-ähnlichen Kinase in *Trypanosoma brucei*. Diplomarbeit (Ludwig-Maximilians-Universität München).
- Bachmaier, S. (2015). Evolutionary Repurposing of cAMP and PKA Signaling Pathways in Kinetoplastids. Doktor Dissertation (Ludwig-Maximilians-Universität München).
- Bachmaier, S., and Boshart, M. (2013). Kinetoplastid AGC kinases. In *Protein Phosphorylation in Parasites*, C. Doerig, G. Späth, and M. Wiese, eds. (Wiley-VHC Verlag GmbH & Co. KGaA), pp. 99–122. 10.1002/9783527675401.
- Bachmaier, S., Thanner, T., and Boshart, M. (2020). Culturing and Transfection of Pleomorphic *Trypanosoma brucei*. *Methods Mol Biol* 2116, 23-38. 10.1007/978-1-0716-0294-2_2.
- Bachmaier, S., Volpato Santos, Y., Kramer, S., Githure, G.B., Klockner, T., Pepperl, J., Baums, C., Schenk, R., Schwede, F., Genieser, H.G., et al. (2019). Nucleoside analogue activators of cyclic AMP-independent protein kinase A of *Trypanosoma*. *Nat Commun* 10, 1421. 10.1038/s41467-019-09338-z.
- Bachmaier, S., Witztum, R., Tsigankov, P., Koren, R., Boshart, M., and Zilberstein, D. (2016). Protein kinase A signaling during bidirectional axenic differentiation in *Leishmania*. *Int J Parasitol* 46, 75-82. 10.1016/j.ijpara.2015.09.003.
- Baker, N., Catta-Preta, C.M.C., Neish, R., Sadlova, J., Powell, B., Alves-Ferreira, E.V.C., Geoghegan, V., Carnielli, J.B.T., Newling, K., Hughes, C., et al. (2021). Systematic functional analysis of *Leishmania* protein kinases identifies regulators of differentiation or survival. *Nat Commun* 12, 1244. 10.1038/s41467-021-21360-8.
- Balogun, R.A. (1974). Studies on the amino acids of the tsetse fly, *Glossina morsitans*, maintained on in vitro and in vivo feeding systems. *Comp Biochem Physiol A Comp Physiol* 49, 215-222. 10.1016/0300-9629(74)90110-8.
- Bandje, K., Naissant, B., Bigey, P., Lohezic, M., Vayssieres, M., Blaud, M., Kermasson, L., Lopez-Rubio, J.J., Langsley, G., Lavazec, C., et al. (2016). Characterization of an A-kinase anchoring protein-like suggests an alternative way of PKA anchoring in *Plasmodium falciparum*. *Malar J* 15, 248. 10.1186/s12936-016-1275-9.
- Bangs, J.D., Uyetake, L., Brickman, M.J., Balber, A.E., and Boothroyd, J.C. (1993). Molecular cloning and cellular localization of a BiP homologue in *Trypanosoma brucei*. Divergent ER retention signals in a lower eukaryote. *Journal of cell science* 105 (Pt 4), 1101-1113.
- Bao, Y., Weiss, L.M., Ma, Y.F., Kahn, S., and Huang, H. (2010). Protein kinase A catalytic subunit interacts and phosphorylates members of trans-sialidase super-family in *Trypanosoma cruzi*. *Microbes Infect* 12, 716-726. 10.1016/j.micinf.2010.04.014.
- Barraza, C.E., Solari, C.A., Marcovich, I., Kershaw, C., Galello, F., Rossi, S., Ashe, M.P., and Portela, P. (2017). The role of PKA in the translational response to heat stress in *Saccharomyces cerevisiae*. *PLoS One* 12, e0185416. 10.1371/journal.pone.0185416.
- Barraza, C.E., Solari, C.A., Rinaldi, J., Ojeda, L., Rossi, S., Ashe, M.P., and Portela, P. (2021). A prion-like domain of Tpk2 catalytic subunit of protein kinase A modulates P-body formation in response

- to stress in budding yeast. *Biochim Biophys Acta Mol Cell Res* 1868, 118884. 10.1016/j.bbamcr.2020.118884.
- Bastin, P. (2019). The trypanosome journey in the tsetse fly. *Comptes Rendus Biologies* 342, 273-275. 10.1016/j.crv.2019.09.026.
- Bastin, P., Bagherzadeh, Z., Matthews, K.R., and Gull, K. (1996). A novel epitope tag system to study protein targeting and organelle biogenesis in *Trypanosoma brucei*. *Mol Biochem Parasitol* 77, 235-239. 10.1016/0166-6851(96)02598-4.
- Bastin, P., Sherwin, T., and Gull, K. (1998). Paraflagellar rod is vital for trypanosome motility. *Nature* 391, 548. 10.1038/35300.
- Ben-Sahra, I., Howell, J.J., Asara, J.M., and Manning, B.D. (2013). Stimulation of de novo pyrimidine synthesis by growth signaling through mTOR and S6K1. *Science* 339, 1323-1328. 10.1126/science.1228792.
- Berg, M., Van der Veken, P., Goeminne, A., Haemers, A., and Augustyns, K. (2010). Inhibitors of the Purine Salvage Pathway: A Valuable Approach for Antiprotozoal Chemotherapy? *Curr Med Chem* 17, 2456-2481. 10.2174/092986710791556023.
- Bhattacharya, A., Biswas, A., and Das, P.K. (2012). Identification of a protein kinase A regulatory subunit from *Leishmania* having importance in metacyclogenesis through induction of autophagy. *Molecular microbiology* 83, 548-564. 10.1111/j.1365-2958.2011.07950.x.
- Bradley, D., and Beltrao, P. (2019). Evolution of protein kinase substrate recognition at the active site. *PLoS Biol* 17, e3000341. 10.1371/journal.pbio.3000341.
- Breitenlechner, C., Engh, R.A., Huber, R., Kinzel, V., Bossemeyer, D., and Gassel, M. (2004). The typically disordered N-terminus of PKA can fold as a helix and project the myristoylation site into solution. *Biochemistry* 43, 7743-7749. 10.1021/bi0362525.
- Bringaud, F., Baltz, D., and Baltz, T. (1998). Functional and molecular characterization of a glycosomal PPI-dependent enzyme in trypanosomatids: pyruvate, phosphate dikinase. *Proc Natl Acad Sci U S A* 95, 7963-7968. 10.1073/pnas.95.14.7963.
- Bringaud, F., Peyruchaud, S., Baltz, D., Giroud, C., Simpson, L., and Baltz, T. (1995). Molecular characterization of the mitochondrial heat shock protein 60 gene from *Trypanosoma brucei*. *Mol Biochem Parasitol* 74, 119-123. 10.1016/0166-6851(95)02486-7.
- Bringaud, F., Robinson, D.R., Barradeau, S., Biteau, N., Baltz, D., and Baltz, T. (2000). Characterization and disruption of a new *Trypanosoma brucei* repetitive flagellum protein, using double-stranded RNA inhibition. *Mol Biochem Parasitol* 111, 283-297. 10.1016/s0166-6851(00)00319-4.
- Broadhead, R., Dawe, H.R., Farr, H., Griffiths, S., Hart, S.R., Portman, N., Shaw, M.K., Ginger, M.L., Gaskell, S.J., McKean, P.G., and Gull, K. (2006). Flagellar motility is required for the viability of the bloodstream trypanosome. *Nature* 440, 224-227. 10.1038/nature04541.
- Brun, R., and Schönenberger (1979). Cultivation and in vitro cloning or procyclic culture forms of *Trypanosoma brucei* in a semi-defined medium. Short communication. *Acta tropica* 36, 289-292.
- Bubis, J., Martinez, J.C., Calabokis, M., Ferreira, J., Sanz-Rodriguez, C.E., Navas, V., Escalona, J.L., Guo, Y., and Taylor, S.S. (2018). The gene product of a *Trypanosoma equiperdum* ortholog of the cAMP-dependent protein kinase regulatory subunit is a monomeric protein that is not capable of binding cyclic nucleotides. *Biochimie* 146, 166-180. 10.1016/j.biochi.2017.12.010.
- Burkard, G., Fragoso, C.M., and Roditi, I. (2007). Highly efficient stable transformation of bloodstream forms of *Trypanosoma brucei*. *Mol Biochem Parasitol* 153, 220-223. 10.1016/j.molbiopara.2007.02.008.
- Bursell, E. (1963). Tsetse-fly physiology. A review of recent advances and current aims. *Bull World Health Organ* 28, 703-709.
- Calejo, A.I., and Tasken, K. (2015). Targeting protein-protein interactions in complexes organized by A kinase anchoring proteins. *Front Pharmacol* 6, 192. 10.3389/fphar.2015.00192.
- Cao, B., Lu, T.W., Martinez Fiesco, J.A., Tomasini, M., Fan, L., Simon, S.M., Taylor, S.S., and Zhang, P. (2019). Structures of the PKA R1alpha Holoenzyme with the FLHCC Driver J-PKAc1alpha or Wild-Type PKAc1alpha. *Structure* 27, 816-828 e814. 10.1016/j.str.2019.03.001.
- Carling, D., Zammit, V.A., and Hardie, D.G. (1987). A common bicyclic protein kinase cascade inactivates the regulatory enzymes of fatty acid and cholesterol biosynthesis. *FEBS Lett* 223, 217-222. 10.1016/0014-5793(87)80292-2.
- Cembran, A., Masterson, L.R., McClendon, C.L., Taylor, S.S., Gao, J., and Veglia, G. (2012). Conformational equilibrium of N-myristoylated cAMP-dependent protein kinase A by molecular dynamics simulations. *Biochemistry* 51, 10186-10196. 10.1021/bi301279f.
- Cheng, H.C., Kemp, B.E., Pearson, R.B., Smith, A.J., Misconi, L., Van Patten, S.M., and Walsh, D.A. (1986). A potent synthetic peptide inhibitor of the cAMP-dependent protein kinase. *J Biol Chem* 261, 989-992.
- Clayton, C., Adams, M., Almeida, R., Baltz, T., Barrett, M., Bastien, P., Belli, S., Beverley, S., Biteau, N., Blackwell, J., et al. (1998). Genetic nomenclature for *Trypanosoma* and *Leishmania*. *Mol Biochem Parasitol* 97, 221-224. 10.1016/s0166-6851(98)00115-7.
- Corton, J.M., Gillespie, J.G., and Hardie, D.G. (1994). Role of the AMP-activated protein kinase in the cellular stress response. *Curr Biol* 4, 315-324. 10.1016/s0960-9822(00)00070-1.
- Crabbe, A., Jensen, P.O., Bjarnsholt, T., and Coenye, T. (2019). Antimicrobial Tolerance and Metabolic Adaptations in Microbial Biofilms. *Trends Microbiol* 27, 850-863. 10.1016/j.tim.2019.05.003.

- Cuello, F., Herberg, F.W., Stathopoulou, K., Henning, P., and Diering, S. (2021). Regulation of Cardiac PKA Signaling by cAMP and Oxidants. *Antioxidants (Basel)* 10, 10.3390/antiox10050663.
- Darlyuk, I., Goldman, A., Roberts, S.C., Ullman, B., Rentsch, D., and Zilberstein, D. (2009). Arginine homeostasis and transport in the human pathogen *Leishmania donovani*. *J Biol Chem* 284, 19800-19807. 10.1074/jbc.M901066200.
- Davies, S.P., Hawley, S.A., Woods, A., Carling, D., Haystead, T.A., and Hardie, D.G. (1994). Purification of the AMP-activated protein kinase on ATP-gamma-sepharose and analysis of its subunit structure. *Eur J Biochem* 223, 351-357. 10.1111/j.1432-1033.1994.tb19001.x.
- Dawidowski, M., Emmanouilidis, L., Kaleb, V.C., Tripsianes, K., Schorpp, K., Hadian, K., Kaiser, M., Maser, P., Kolonko, M., Tanghe, S., et al. (2017). Inhibitors of PEX14 disrupt protein import into glycosomes and kill *Trypanosoma* parasites. *Science* 355, 1416-1420. 10.1126/science.aal1807.
- De Vit, M.J., Waddle, J.A., and Johnston, M. (1997). Regulated nuclear translocation of the Mig1 glucose repressor. *Mol Biol Cell* 8, 1603-1618. 10.1091/mbc.8.8.1603.
- Dean, S., Sunter, J., Wheeler, R.J., Hodgkinson, I., Gluenz, E., and Gull, K. (2015). A toolkit enabling efficient, scalable and reproducible gene tagging in trypanosomatids. *Open Biol* 5, 140197. 10.1098/rsob.140197.
- Dean, S., Sunter, J.D., and Wheeler, R.J. (2017). TrypTag.org: A Trypanosome Genome-wide Protein Localisation Resource. *Trends Parasitol* 33, 80-82. 10.1016/j.pt.2016.10.009.
- Dejung, M., Subota, I., Bucarius, F., Dindar, G., Freiwald, A., Engstler, M., Boshart, M., Butter, F., and Janzen, C.J. (2016). Quantitative Proteomics Uncovers Novel Factors Involved in Developmental Differentiation of *Trypanosoma brucei*. *PLoS pathogens* 12, e1005439. 10.1371/journal.ppat.1005439.
- Delauw, M.F., Pays, E., Steinert, M., Aerts, D., Van Meirvenne, N., and Le Ray, D. (1985). Inactivation and reactivation of a variant-specific antigen gene in cyclically transmitted *Trypanosoma brucei*. *The EMBO journal* 4, 989-993.
- DeVit, M.J., and Johnston, M. (1999). The nuclear exportin Msn5 is required for nuclear export of the Mig1 glucose repressor of *Saccharomyces cerevisiae*. *Curr Biol* 9, 1231-1241. 10.1016/s0960-9822(99)80503-x.
- Dolezelova, E., Kunzova, M., Dejung, M., Levin, M., Panicucci, B., Regnault, C., Janzen, C.J., Barrett, M.P., Butter, F., and Zikova, A. (2020). Cell-based and multi-omics profiling reveals dynamic metabolic repurposing of mitochondria to drive developmental progression of *Trypanosoma brucei*. *PLoS Biol* 18, e3000741. 10.1371/journal.pbio.3000741.
- Duffieux, F., Van Roy, J., Michels, P.A., and Opperdoes, F.R. (2000). Molecular characterization of the first two enzymes of the pentose-phosphate pathway of *Trypanosoma brucei*. Glucose-6-phosphate dehydrogenase and 6-phosphogluconolactonase. *J Biol Chem* 275, 27559-27565. 10.1074/jbc.M004266200.
- Duvel, K., Yecies, J.L., Menon, S., Raman, P., Lipovsky, A.I., Souza, A.L., Triantafellow, E., Ma, Q., Gorski, R., Cleaver, S., et al. (2010). Activation of a metabolic gene regulatory network downstream of mTOR complex 1. *Mol Cell* 39, 171-183. 10.1016/j.molcel.2010.06.022.
- Dwinger, R.H., Rudin, W., Moloo, S.K., and Murray, M. (1988). Development of *Trypanosoma congolense*, *T vivax* and *T brucei* in the skin reaction induced in goats by infected *Glossina morsitans centralis*: a light and electron microscopical study. *Research in Veterinary Science* 44, 154-163. 10.1016/s0034-5288(18)30831-2.
- Ebikeme, C.E., Peacock, L., Coustou, V., Riviere, L., Bringaud, F., Gibson, W.C., and Barrett, M.P. (2008). N-acetyl D-glucosamine stimulates growth in procyclic forms of *Trypanosoma brucei* by inducing a metabolic shift. *Parasitology* 135, 585-594. 10.1017/S0031182008004241.
- el Kouni, M.H. (2003). Potential chemotherapeutic targets in the purine metabolism of parasites. *Pharmacology & Therapeutics* 99, 283-309. 10.1016/s0163-7258(03)00071-8.
- Engstler, M., and Boshart, M. (2004). Cold shock and regulation of surface protein trafficking convey sensitization to inducers of stage differentiation in *Trypanosoma brucei*. *Genes Dev* 18, 2798-2811. 10.1101/gad.323404.
- Fernandez-Moya, S.M., Carrington, M., and Estevez, A.M. (2014). A short RNA stem-loop is necessary and sufficient for repression of gene expression during early logarithmic phase in trypanosomes. *Nucleic Acids Res* 42, 7201-7209. 10.1093/nar/gku358.
- Fischer Weinberger, R., Bachmaier, S., Dandugudumula, R., Phan, I.Q., Almozino, M., Githure, G.B., Polatoglou, E., Tsiganov, P., Nitzan Koren, R., Myler, P.J., et al. (2021). A divergent protein kinase A in the human pathogen *Leishmania* is associated with developmental morphogenesis. *bioRxiv*. 10.1101/2021.04.24.440790.
- Fort, C., Bonnefoy, S., Kohl, L., and Bastin, P. (2016). Intraflagellar transport is required for the maintenance of the trypanosome flagellum composition but not its length. *Journal of cell science* 129, 3026-3041. 10.1242/jcs.188227.
- Francisco, T., Dias, A.F., Pedrosa, A.G., Grou, C.P., Rodrigues, T.A., and Azevedo, J.E. (2017). Determining the Topology of Peroxisomal Proteins Using Protease Protection Assays. *Methods Mol Biol* 1595, 27-35. 10.1007/978-1-4939-6937-1_3.

- Furuya, T., Kessler, P., Jardim, A., Schnauffer, A., Crudder, C., and Parsons, M. (2002). Glucose is toxic to glycosome-deficient trypanosomes. *Proc Natl Acad Sci U S A* 99, 14177-14182. 10.1073/pnas.222454899.
- Galello, F., Moreno, S., and Rossi, S. (2014). Interacting proteins of protein kinase A regulatory subunit in *Saccharomyces cerevisiae*. *J Proteomics* 109, 261-275. 10.1016/j.jprot.2014.07.008.
- Garcia, D., and Shaw, R.J. (2017). AMPK: Mechanisms of Cellular Energy Sensing and Restoration of Metabolic Balance. *Mol Cell* 66, 789-800. 10.1016/j.molcel.2017.05.032.
- Githure, G.B. (2014). Evolutionary Divergent Ligand Activation of PKA-like Kinase from *Trypanosoma brucei*. PhD Dissertations (Ludwig-Maximilians Universität München).
- Goldman-Pinkovich, A., Kannan, S., Nitzan-Koren, R., Puri, M., Pawar, H., Bar-Avraham, Y., McDonald, J., Sur, A., Zhang, W.W., Matlashewski, G., et al. (2020). Sensing Host Arginine Is Essential for Leishmania Parasites' Intracellular Development. *mBio* 11. 10.1128/mBio.02023-20.
- Goos, C., Dejung, M., Janzen, C.J., Butter, F., and Kramer, S. (2017). The nuclear proteome of *Trypanosoma brucei*. *PLoS One* 12, e0181884. 10.1371/journal.pone.0181884.
- Green, M.R., and Sambrook, J. (2016). Preparation of Plasmid DNA by Alkaline Lysis with Sodium Dodecyl Sulfate: Minipreps. *Cold Spring Harb Protoc* 2016. 10.1101/pdb.prot093344.
- Griffioen, G., Anghileri, P., Imre, E., Baroni, M.D., and Ruis, H. (2000). Nutritional control of nucleocytoplasmic localization of cAMP-dependent protein kinase catalytic and regulatory subunits in *Saccharomyces cerevisiae*. *J Biol Chem* 275, 1449-1456. 10.1074/jbc.275.2.1449.
- Griffioen, G., Branduardi, P., Ballarini, A., Anghileri, P., Norbeck, J., Baroni, M.D., and Ruis, H. (2001). Nucleocytoplasmic distribution of budding yeast protein kinase A regulatory subunit Bcy1 requires Zds1 and is regulated by Yak1-dependent phosphorylation of its targeting domain. *Mol Cell Biol* 21, 511-523. 10.1128/MCB.21.2.511-523.2001.
- Griffith, B.C., Weiss, B.L., Aksoy, E., Mireji, P.O., Auma, J.E., Wamwiri, F.N., Echodu, R., Murilla, G., and Aksoy, S. (2018). Analysis of the gut-specific microbiome from field-captured tsetse flies, and its potential relevance to host trypanosome vector competence. *BMC Microbiol* 18, 146. 10.1186/s12866-018-1284-7.
- Gualdrón-López, M., Brennard, A., Avilan, L., and Michels, P.A. (2013a). Translocation of solutes and proteins across the glycosomal membrane of trypanosomes; possibilities and limitations for targeting with trypanocidal drugs. *Parasitology* 140, 1-20. 10.1017/S0031182012001278.
- Gualdrón-López, M., Chevalier, N., Van Der Smissen, P., Courtoy, P.J., Rigden, D.J., and Michels, P.A.M. (2013b). Ubiquitination of the glycosomal matrix protein receptor PEX5 in *Trypanosoma brucei* by PEX4 displays novel features. *Biochim Biophys Acta* 1833, 3076-3092. 10.1016/j.bbamcr.2013.08.008.
- Guevara, A., Lugo, C., Montilla, A.J., Araujo, N.A., Calabokis, M., and Bubis, J. (2019). Glucose deprivation activates a cAMP-independent protein kinase from *Trypanosoma equiperdum*. *Parasitology* 146, 643-652. 10.1017/S0031182018001920.
- Gunasekera, K., Wüthrich, D., Braga-Lagache, S., Heller, M., and Ochsenreiter, T. (2012). Proteome remodelling during development from blood to insect-form *Trypanosoma brucei* quantified by SILAC and mass spectrometry. *BMC Genomics* 13, 556. 10.1186/1471-2164-13-556.
- Guther, M.L., Urbaniak, M.D., Tavendale, A., Prescott, A., and Ferguson, M.A. (2014). High-confidence glycosome proteome for procyclic form *Trypanosoma brucei* by epitope-tag organelle enrichment and SILAC proteomics. *J Proteome Res* 13, 2796-2806. 10.1021/pr401209w.
- Gwinn, D.M., Shackelford, D.B., Egan, D.F., Mihaylova, M.M., Mery, A., Vasquez, D.S., Turk, B.E., and Shaw, R.J. (2008). AMPK phosphorylation of raptor mediates a metabolic checkpoint. *Mol Cell* 30, 214-226. 10.1016/j.molcel.2008.03.003.
- Haanstra, J.R., van Tuijl, A., Kessler, P., Reijnders, W., Michels, P.A., Westerhoff, H.V., Parsons, M., and Bakker, B.M. (2008). Compartmentation prevents a lethal turbo-explosion of glycolysis in trypanosomes. *Proc Natl Acad Sci U S A* 105, 17718-17723. 10.1073/pnas.0806664105.
- Haesendonckx, S., Tudisca, V., Voordeckers, K., Moreno, S., Thevelein, J.M., and Portela, P. (2012). The activation loop of PKA catalytic isoforms is differentially phosphorylated by Pkh protein kinases in *Saccharomyces cerevisiae*. *Biochem J* 448, 307-320. 10.1042/bj20121061.
- Han, H.S., Kang, G., Kim, J.S., Choi, B.H., and Koo, S.H. (2016). Regulation of glucose metabolism from a liver-centric perspective. *Exp Mol Med* 48, e218. 10.1038/emm.2015.122.
- Hanahan, D., Jessee, J., and Bloom, F.R. (1991). Plasmid transformation of *Escherichia coli* and other bacteria. *Methods in enzymology* 204, 63-113. 10.1016/0076-6879(91)04006-a.
- Hannaert, V., Albert, M.A., Rigden, D.J., da Silva Giotto, M.T., Thiemann, O., Garratt, R.C., Van Roy, J., Opperdoes, F.R., and Michels, P.A. (2003). Kinetic characterization, structure modelling studies and crystallization of *Trypanosoma brucei* enolase. *Eur J Biochem* 270, 3205-3213. 10.1046/j.1432-1033.2003.03692.x.
- Hart, D.T., Misset, O., Edwards, S.W., and Opperdoes, F.R. (1984). A comparison of the glycosomes (microbodies) isolated from *Trypanosoma brucei* bloodstream form and cultured procyclic trypomastigotes. *Mol Biochem Parasitol* 12, 25-35. 10.1016/0166-6851(84)90041-0.
- Haste, N.M., Talabani, H., Doo, A., Merckx, A., Langsley, G., and Taylor, S.S. (2012). Exploring the *Plasmodium falciparum* cyclic-adenosine monophosphate (cAMP)-dependent protein kinase (PfPKA) as a therapeutic target. *Microbes Infect* 14, 838-850. 10.1016/j.micinf.2012.05.004.

- Hawley, S.A., Davison, M., Woods, A., Davies, S.P., Beri, R.K., Carling, D., and Hardie, D.G. (1996). Characterization of the AMP-activated protein kinase kinase from rat liver and identification of threonine 172 as the major site at which it phosphorylates AMP-activated protein kinase. *J Biol Chem* 271, 27879-27887. 10.1074/jbc.271.44.27879.
- Hawley, S.A., Pan, D.A., Mustard, K.J., Ross, L., Bain, J., Edelman, A.M., Frenguelli, B.G., and Hardie, D.G. (2005). Calmodulin-dependent protein kinase kinase-beta is an alternative upstream kinase for AMP-activated protein kinase. *Cell Metab* 2, 9-19. 10.1016/j.cmet.2005.05.009.
- Heathcote, H.R., Mancini, S.J., Strembitska, A., Jamal, K., Reihill, J.A., Palmer, T.M., Gould, G.W., and Salt, I.P. (2016). Protein kinase C phosphorylates AMP-activated protein kinase alpha1 Ser487. *Biochem J* 473, 4681-4697. 10.1042/BCJ20160211.
- Heise, N., and Opperdoes, F.R. (1999). Purification, localisation and characterisation of glucose-6-phosphate dehydrogenase of *Trypanosoma brucei*. *Mol Biochem Parasitol* 99, 21-32. 10.1016/s0166-6851(98)00176-5.
- Herberg, F.W., and Taylor, S.S. (1993). Physiological inhibitors of the catalytic subunit of cAMP-dependent protein kinase: effect of MgATP on protein-protein interactions. *Biochemistry* 32, 14015-14022. 10.1021/bi00213a035.
- Herman, M., Perez-Morga, D., Shtickzelle, N., and Michels, P.A. (2008). Turnover of glycosomes during life-cycle differentiation of *Trypanosoma brucei*. *Autophagy* 4, 294-308. 10.4161/auto.5443.
- Holz, M.K., Ballif, B.A., Gygi, S.P., and Blenis, J. (2005). mTOR and S6K1 mediate assembly of the translation preinitiation complex through dynamic protein interchange and ordered phosphorylation events. *Cell* 123, 569-580. 10.1016/j.cell.2005.10.024.
- Horakova, E., Faktorova, D., Kraeva, N., Kaur, B., Van Den Abbeele, J., Yurchenko, V., and Lukes, J. (2020). Catalase compromises the development of the insect and mammalian stages of *Trypanosoma brucei*. *FEBS J* 287, 964-977. 10.1111/febs.15083.
- Horman, S., Vertommen, D., Heath, R., Neumann, D., Mouton, V., Woods, A., Schlattner, U., Wallimann, T., Carling, D., Hue, L., and Rider, M.H. (2006). Insulin antagonizes ischemia-induced Thr172 phosphorylation of AMP-activated protein kinase alpha-subunits in heart via hierarchical phosphorylation of Ser485/491. *J Biol Chem* 281, 5335-5340. 10.1074/jbc.M506850200.
- Humphrey, S.J., Karayel, O., James, D.E., and Mann, M. (2018). High-throughput and high-sensitivity phosphoproteomics with the EasyPhos platform. *Nat Protoc* 13, 1897-1916. 10.1038/s41596-018-0014-9.
- Humphries, K.M., Deal, M.S., and Taylor, S.S. (2005). Enhanced dephosphorylation of cAMP-dependent protein kinase by oxidation and thiol modification. *J Biol Chem* 280, 2750-2758. 10.1074/jbc.M410242200.
- Humphries, K.M., Juliano, C., and Taylor, S.S. (2002). Regulation of cAMP-dependent protein kinase activity by glutathionylation. *J Biol Chem* 277, 43505-43511. 10.1074/jbc.M207088200.
- Humphries, K.M., Pennypacker, J.K., and Taylor, S.S. (2007). Redox regulation of cAMP-dependent protein kinase signaling: kinase versus phosphatase inactivation. *J Biol Chem* 282, 22072-22079. 10.1074/jbc.M702582200.
- Hurley, R.L., Anderson, K.A., Franzoni, J.M., Kemp, B.E., Means, A.R., and Witters, L.A. (2005). The Ca²⁺/calmodulin-dependent protein kinase kinases are AMP-activated protein kinase kinases. *J Biol Chem* 280, 29060-29066. 10.1074/jbc.M503824200.
- Hurley, R.L., Barre, L.K., Wood, S.D., Anderson, K.A., Kemp, B.E., Means, A.R., and Witters, L.A. (2006). Regulation of AMP-activated protein kinase by multisite phosphorylation in response to agents that elevate cellular cAMP. *J Biol Chem* 281, 36662-36672. 10.1074/jbc.M606676200.
- Inoki, K., Li, Y., Xu, T., and Guan, K.L. (2003). Rheb GTPase is a direct target of TSC2 GAP activity and regulates mTOR signaling. *Genes Dev* 17, 1829-1834. 10.1101/gad.1110003.
- Jia, Y., Marq, J.B., Bisio, H., Jacot, D., Mueller, C., Yu, L., Choudhary, J., Brochet, M., and Soldati-Favre, D. (2017). Crosstalk between PKA and PKG controls pH-dependent host cell egress of *Toxoplasma gondii*. *The EMBO journal* 36, 3250-3267. 10.15252/embj.201796794.
- Johnson, M.A., Snyder, W.B., Cereghino, J.L., Veenhuis, M., Subramani, S., and Cregg, J.M. (2001). *Pichia pastoris* Pex14p, a phosphorylated peroxisomal membrane protein, is part of a PTS-receptor docking complex and interacts with many peroxins. *Yeast* 18, 621-641. 10.1002/yea.711.
- Jones, N.G., Thomas, E.B., Brown, E., Dickens, N.J., Hammarton, T.C., and Mottram, J.C. (2014). Regulators of *Trypanosoma brucei* cell cycle progression and differentiation identified using a kinome-wide RNAi screen. *PLoS pathogens* 10, e1003886. 10.1371/journal.ppat.1003886.
- Jung, J. (2015). Precise timing of the trypanosome cell division cycle
Dissertation (Julius-Maximilians-Universität Würzburg).
- Kabani, S., Fenn, K., Ross, A., Ivens, A., Smith, T.K., Ghazal, P., and Matthews, K. (2009). Genome-wide expression profiling of in vivo-derived bloodstream parasite stages and dynamic analysis of mRNA alterations during synchronous differentiation in *Trypanosoma brucei*. *BMC Genomics* 10, 427. 10.1186/1471-2164-10-427.
- Kannan, N., Haste, N., Taylor, S.S., and Neuwald, A.F. (2007). The hallmark of AGC kinase functional divergence is its C-terminal tail, a cis-acting regulatory module. *Proc Natl Acad Sci U S A* 104, 1272-1277. 10.1073/pnas.0610251104.

- Kelley, L.A., Mezulis, S., Yates, C.M., Wass, M.N., and Sternberg, M.J. (2015). The Phyre2 web portal for protein modeling, prediction and analysis. *Nat Protoc* 10, 845-858. 10.1038/nprot.2015.053.
- Kelly, S., Reed, J., Kramer, S., Ellis, L., Webb, H., Sunter, J., Salje, J., Marinsek, N., Gull, K., Wickstead, B., and Carrington, M. (2007). Functional genomics in *Trypanosoma brucei*: a collection of vectors for the expression of tagged proteins from endogenous and ectopic gene loci. *Mol Biochem Parasitol* 154, 103-109. 10.1016/j.molbiopara.2007.03.012.
- Kessler, P.S., and Parsons, M. (2005). Probing the role of compartmentation of glycolysis in procyclic form *Trypanosoma brucei*: RNA interference studies of PEX14, hexokinase, and phosphofructokinase. *J Biol Chem* 280, 9030-9036. 10.1074/jbc.M412033200.
- Kim, D.I., and Roux, K.J. (2016). Filling the Void: Proximity-Based Labeling of Proteins in Living Cells. *Trends Cell Biol* 26, 804-817. 10.1016/j.tcb.2016.09.004.
- Kim, S.G., Buel, G.R., and Blenis, J. (2013). Nutrient regulation of the mTOR complex 1 signaling pathway. *Mol Cells* 35, 463-473. 10.1007/s10059-013-0138-2.
- Klößner, T. (1996). cAMP-Signaltransduktion in *Trypanosoma brucei*: Klonierung und Charakterisierung von Proteinkinase A- und Phosphodiesterase-Homologen. Doktorarbeit (Ludwig-Maximilians-Universität München).
- Kohl, L., Sherwin, T., and Gull, K. (1999). Assembly of the paraflagellar rod and the flagellum attachment zone complex during the *Trypanosoma brucei* cell cycle. *J Eukaryot Microbiol* 46, 105-109. 10.1111/j.1550-7408.1999.tb04592.x.
- Kolev, N.G., Ramey-Butler, K., Cross, G.A., Ullu, E., and Tschudi, C. (2012). Developmental progression to infectivity in *Trypanosoma brucei* triggered by an RNA-binding protein. *Science* 338, 1352-1353. 10.1126/science.1229641.
- Komori, M., Kiel, J.A., and Veenhuis, M. (1999). The peroxisomal membrane protein Pex14p of *Hansenula polymorpha* is phosphorylated in vivo. *FEBS Lett* 457, 397-399. 10.1016/s0014-5793(99)01087-x.
- Kovarova, J., and Barrett, M.P. (2016). The Pentose Phosphate Pathway in Parasitic Trypanosomatids. *Trends Parasitol* 32, 622-634. 10.1016/j.pt.2016.04.010.
- Kraakman, L., Lemaire, K., Ma, P., Teunissen, A.W., Donaton, M.C., Van Dijck, P., Winderickx, J., de Winde, J.H., and Thevelein, J.M. (1999). A *Saccharomyces cerevisiae* G-protein coupled receptor, Gpr1, is specifically required for glucose activation of the cAMP pathway during the transition to growth on glucose. *Molecular microbiology* 32, 1002-1012. 10.1046/j.1365-2958.1999.01413.x.
- Kramer, S. (2004). Characterization of a PKA-like kinase from *Trypanosoma brucei*. Doktorarbeit (Ludwig-Maximilians-Universität München).
- Kramer, S., Klockner, T., Selmayr, M., and Boshart, M. (2007). Interstrain sequence comparison, transcript map and clonal genomic rearrangement of a 28 kb locus on chromosome 9 of *Trypanosoma brucei*. *Mol Biochem Parasitol* 151, 129-132. 10.1016/j.molbiopara.2006.10.004.
- Krumbholz, C. (2006). A PKA-like kinase important for coordination of flagellar motility in *Trypanosoma brucei*. Doktorarbeit (Ludwig-Maximilians-Universität München).
- Kunkel, J., Luo, X., and Capaldi, A.P. (2019). Integrated TORC1 and PKA signaling control the temporal activation of glucose-induced gene expression in yeast. *Nat Commun* 10, 3558. 10.1038/s41467-019-11540-y.
- Lamour, N., Riviere, L., Coustou, V., Coombs, G.H., Barrett, M.P., and Bringaud, F. (2005). Proline metabolism in procyclic *Trypanosoma brucei* is down-regulated in the presence of glucose. *J Biol Chem* 280, 11902-11910. 10.1074/jbc.M414274200.
- Landfear, S.M., Ullman, B., Carter, N.S., and Sanchez, M.A. (2004). Nucleoside and nucleobase transporters in parasitic protozoa. *Eukaryot Cell* 3, 245-254. 10.1128/EC.3.2.245-254.2004.
- Leighfield, T.A., Barbier, M., and Van Dolah, F.M. (2002). Evidence for cAMP-dependent protein kinase in the dinoflagellate, *Amphidinium operculatum*. *Comp Biochem Physiol B Biochem Mol Biol* 133, 317-324. 10.1016/s1096-4959(02)00148-3.
- Leykauf, K., Treack, M., Gilson, P.R., Nebl, T., Bräulke, T., Cowman, A.F., Gilberger, T.W., and Crabb, B.S. (2010). Protein kinase A dependent phosphorylation of apical membrane antigen 1 plays an important role in erythrocyte invasion by the malaria parasite. *PLoS pathogens* 6, e1000941. 10.1371/journal.ppat.1000941.
- Lippman, S.I., and Broach, J.R. (2009). Protein kinase A and TORC1 activate genes for ribosomal biogenesis by inactivating repressors encoded by Dot6 and its homolog Tod6. *Proc Natl Acad Sci U S A* 106, 19928-19933. 10.1073/pnas.0907027106.
- Locasale, J.W. (2018). New concepts in feedback regulation of glucose metabolism. *Curr Opin Syst Biol* 8, 32-38. 10.1016/j.coisb.2017.11.005.
- London, E., Bloyd, M., and Stratakis, C.A. (2020). PKA functions in metabolism and resistance to obesity: lessons from mouse and human studies. *J Endocrinol* 246, R51-R64. 10.1530/JOE-20-0035.
- Ma, X.M., and Blenis, J. (2009). Molecular mechanisms of mTOR-mediated translational control. *Nat Rev Mol Cell Biol* 10, 307-318. 10.1038/nrm2672.
- MacGregor, P., Szoor, B., Savill, N.J., and Matthews, K.R. (2012). Trypanosomal immune evasion, chronicity and transmission: an elegant balancing act. *Nat Rev Microbiol* 10, 431-438. 10.1038/nrmicro2779.

- Madan, E., Puri, M., Muthuswami, R., Zilberstein, D., and Madhubala, R. (2021). Leishmania parasite arginine deprivation response pathway influences the host macrophage lysosomal arginine sensing machinery. *bioRxiv*. 10.1101/2021.09.01.458453.
- Malenica, K. (2016). Investigation of the Mechanism Underlying PKA activation upon mild acidic stress in *Trypanosoma brucei*. Master Thesis (Ludwig-Maximilians-Universität München).
- Malki-Feldman, L., and Jaffe, C.L. (2009). Leishmania major: effect of protein kinase A and phosphodiesterase activity on infectivity and proliferation of promastigotes. *Exp Parasitol* 123, 39-44. 10.1016/j.exppara.2009.05.010.
- Mantilla, B.S., Marchese, L., Casas-Sanchez, A., Dyer, N.A., Ejeh, N., Biran, M., Bringaud, F., Lehane, M.J., Acosta-Serrano, A., and Silber, A.M. (2017). Proline Metabolism is Essential for *Trypanosoma brucei brucei* Survival in the Tsetse Vector. *PLoS pathogens* 13, e1006158. 10.1371/journal.ppat.1006158.
- Mascher, T., Helmann, J.D., and Unden, G. (2006). Stimulus perception in bacterial signal-transducing histidine kinases. *Microbiol Mol Biol Rev* 70, 910-938. 10.1128/MMBR.00020-06.
- McCartney, R.R., and Schmidt, M.C. (2001). Regulation of Snf1 kinase. Activation requires phosphorylation of threonine 210 by an upstream kinase as well as a distinct step mediated by the Snf4 subunit. *J Biol Chem* 276, 36460-36466. 10.1074/jbc.M104418200.
- Melo-Braga, M.N., Schulz, M., Liu, Q., Swistowski, A., Palmisano, G., Engholm-Keller, K., Jakobsen, L., Zeng, X., and Larsen, M.R. (2014). Comprehensive quantitative comparison of the membrane proteome, phosphoproteome, and sialome of human embryonic and neural stem cells. *Mol Cell Proteomics* 13, 311-328. 10.1074/mcp.M112.026898.
- Merritt, C., and Stuart, K. (2013). Identification of essential and non-essential protein kinases by a fusion PCR method for efficient production of transgenic *Trypanosoma brucei*. *Mol Biochem Parasitol* 190, 44-49. 10.1016/j.molbiopara.2013.05.002.
- Michels, P.A.M., Villafraz, O., Pineda, E., Alencar, M.B., Caceres, A.J., Silber, A.M., and Bringaud, F. (2021). Carbohydrate metabolism in trypanosomatids: New insights revealing novel complexity, diversity and species-unique features. *Exp Parasitol* 224, 108102. 10.1016/j.exppara.2021.108102.
- Milo, R. (2013). What is the total number of protein molecules per cell volume? A call to rethink some published values. *BioEssays* 35, 1050-1055. 10.1002/bies.201300066.
- Misset, O., Bos, O.J., and Opperdoes, F.R. (1986). Glycolytic enzymes of *Trypanosoma brucei*. Simultaneous purification, intraglycosomal concentrations and physical properties. *Eur J Biochem* 157, 441-453. 10.1111/j.1432-1033.1986.tb09687.x.
- Moody, T.W. (2019). Peptide receptors as cancer drug targets. *Ann N Y Acad Sci* 1455, 141-148. 10.1111/nyas.14100.
- Morris, J.C., Wang, Z., Drew, M.E., and Englund, P.T. (2002). Glycolysis modulates trypanosome glycoprotein expression as revealed by an RNAi library. *The EMBO journal* 21, 4429-4438. 10.1093/emboj/cdf474.
- Mowatt, M.R., and Clayton, C.E. (1987). Developmental regulation of a novel repetitive protein of *Trypanosoma brucei*. *Mol Cell Biol* 7, 2838-2844. 10.1128/mcb.7.8.2838-2844.1987.
- Mowatt, M.R., Wisdom, G.S., and Clayton, C.E. (1989). Variation of tandem repeats in the developmentally regulated procyclic acidic repetitive proteins of *Trypanosoma brucei*. *Mol Cell Biol* 9, 1332-1335. 10.1128/mcb.9.3.1332-1335.1989.
- Moyersoen, J., Choe, J., Kumar, A., Voncken, F.G., Hol, W.G., and Michels, P.A. (2003). Characterization of *Trypanosoma brucei* PEX14 and its role in the import of glycosomal matrix proteins. *Eur J Biochem* 270, 2059-2067. 10.1046/j.1432-1033.2003.03582.x.
- Müller, S., Liebau, E., Walter, R.D., and Krauth-Siegel, R.L. (2003). Thiol-based redox metabolism of protozoan parasites. *Trends Parasitol* 19, 320-328. 10.1016/s1471-4922(03)00141-7.
- Mutzel, R., Lacombe, M.L., Simon, M.N., de Gunzburg, J., and Veron, M. (1987). Cloning and cDNA sequence of the regulatory subunit of cAMP-dependent protein kinase from *Dictyostelium discoideum*. *Proc Natl Acad Sci U S A* 84, 6-10. 10.1073/pnas.84.1.6.
- Nett, I.R., Martin, D.M., Miranda-Saavedra, D., Lamont, D., Barber, J.D., Mehler, A., and Ferguson, M.A. (2009). The phosphoproteome of bloodstream form *Trypanosoma brucei*, causative agent of African sleeping sickness. *Mol Cell Proteomics* 8, 1527-1538. 10.1074/mcp.M800556-MCP200.
- Ober, V. (2021). Evolution of ligand specificity of protein kinase A isoforms in the phylum Euglenozoa. Doktorarbeit (Ludwig-Maximilians-Universität).
- Oberholzer, M., Langousis, G., Nguyen, H.T., Saada, E.A., Shimogawa, M.M., Jonsson, Z.O., Nguyen, S.M., Wohlschlegel, J.A., and Hill, K.L. (2011). Independent analysis of the flagellum surface and matrix proteomes provides insight into flagellum signaling in mammalian-infectious *Trypanosoma brucei*. *Mol Cell Proteomics* 10, M111 010538. 10.1074/mcp.M111.010538.
- Okumoto, K., El Shermely, M., Natsui, M., Kosako, H., Natsuyama, R., Marutani, T., and Fujiki, Y. (2020). The peroxisome counteracts oxidative stresses by suppressing catalase import via Pex14 phosphorylation. *Elife* 9. 10.7554/eLife.55896.
- Olmsted, J.B. (1981). Affinity purification of antibodies from diazotized paper blots of heterogeneous protein samples. *J Biol Chem* 256, 11955-11957.
- Opperdoes, F.R. (1984). Localization of the initial steps in alkoxyphospholipid biosynthesis in glycosomes (microbodies) of *Trypanosoma brucei*. *FEBS Lett* 169, 35-39. 10.1016/0014-5793(84)80284-7.

- Opperdoes, F.R., and Szikora, J.P. (2006). In silico prediction of the glycosomal enzymes of *Leishmania major* and trypanosomes. *Mol Biochem Parasitol* 147, 193-206. 10.1016/j.molbiopara.2006.02.010.
- Ortega-Prieto, P., and Postic, C. (2019). Carbohydrate Sensing Through the Transcription Factor ChREBP. *Front Genet* 10, 472. 10.3389/fgene.2019.00472.
- Ortiz, D., Sanchez, M.A., Quecke, P., and Landfear, S.M. (2009). Two novel nucleobase/pentamidine transporters from *Trypanosoma brucei*. *Mol Biochem Parasitol* 163, 67-76. 10.1016/j.molbiopara.2008.09.011.
- Ostling, J., and Ronne, H. (1998). Negative control of the Mig1p repressor by Snf1p-dependent phosphorylation in the absence of glucose. *Eur J Biochem* 252, 162-168. 10.1046/j.1432-1327.1998.2520162.x.
- Parsons, M., Worthey, E.A., Ward, P.N., and Mottram, J.C. (2005). Comparative analysis of the kinomes of three pathogenic trypanosomatids: *Leishmania major*, *Trypanosoma brucei* and *Trypanosoma cruzi*. *BMC Genomics* 6, 127. 10.1186/1471-2164-6-127.
- Pearson, R.B., and Kemp, B.E. (1991). Protein kinase phosphorylation site sequences and consensus specificity motifs: tabulations. *Methods in enzymology* 200, 62-81. 10.1016/0076-6879(91)00127-i.
- Peikert, C.D., Mani, J., Morgenstern, M., Kaser, S., Knapp, B., Wenger, C., Harsman, A., Oeljeklaus, S., Schneider, A., and Warscheid, B. (2017). Charting organellar importomes by quantitative mass spectrometry. *Nat Commun* 8, 15272. 10.1038/ncomms15272.
- Peng, M., Aye, T.T., Snel, B., van Breukelen, B., Scholten, A., and Heck, A.J. (2015). Spatial Organization in Protein Kinase A Signaling Emerged at the Base of Animal Evolution. *J Proteome Res* 14, 2976-2987. 10.1021/acs.jproteome.5b00370.
- Pepperl, J. (2007). Regulation von in vivo-Aktivität der PKA-like kinase in *Trypanosoma brucei*. Diplomarbeit (Ludwig-Maximilians-Universität München).
- Peroutka Iii, R.J., Orcutt, S.J., Strickler, J.E., and Butt, T.R. (2011). SUMO fusion technology for enhanced protein expression and purification in prokaryotes and eukaryotes. *Methods Mol Biol* 705, 15-30. 10.1007/978-1-61737-967-3_2.
- Pilkis, S.J., el-Maghrabi, M.R., and Claus, T.H. (1988). Hormonal regulation of hepatic gluconeogenesis and glycolysis. *Annu Rev Biochem* 57, 755-783. 10.1146/annurev.bi.57.070188.003543.
- Pinna, L.A., and Ruzzene, M. (1996). How do protein kinases recognize their substrates? *Biochim Biophys Acta* 1314, 191-225. 10.1016/s0167-4889(96)00083-3.
- Porstmann, T., Santos, C.R., Griffiths, B., Cully, M., Wu, M., Leever, S., Griffiths, J.R., Chung, Y.L., and Schulze, A. (2008). SREBP activity is regulated by mTORC1 and contributes to Akt-dependent cell growth. *Cell Metab* 8, 224-236. 10.1016/j.cmet.2008.07.007.
- Prinz, B., Harvey, K.L., Wilcke, L., Ruch, U., Engelberg, K., Biller, L., Lucet, I., Erkelenz, S., Heincke, D., Spielmann, T., et al. (2016). Hierarchical phosphorylation of apical membrane antigen 1 is required for efficient red blood cell invasion by malaria parasites. *Sci Rep* 6, 34479. 10.1038/srep34479.
- Ralston, K.S., Lerner, A.G., Diener, D.R., and Hill, K.L. (2006). Flagellar motility contributes to cytokinesis in *Trypanosoma brucei* and is modulated by an evolutionarily conserved dynein regulatory system. *Eukaryot Cell* 5, 696-711. 10.1128/EC.5.4.696-711.2006.
- Reith, P. (2016). Proximity Dependent Biotinylation Reveals Potential Interaction Partners of *Trypanosoma brucei* Protein Kinase A Regulatory Subunit. Masterarbeit (Ludwig-Maximilians-Universität München).
- Rico-Jimenez, M., Ceballos-Perez, G., Gomez-Linan, C., and Estevez, A.M. (2021). An RNA-binding protein complex regulates the purine-dependent expression of a nucleobase transporter in trypanosomes. *Nucleic Acids Res* 49, 3814-3825. 10.1093/nar/gkab181.
- Rico, E., Rojas, F., Mony, B.M., Szoor, B., Macgregor, P., and Matthews, K.R. (2013). Bloodstream form pre-adaptation to the tsetse fly in *Trypanosoma brucei*. *Front Cell Infect Microbiol* 3, 78. 10.3389/fcimb.2013.00078.
- Rieck, T. (2001). Funktionelle Genanalyse durch RNA-Interferenz vermittelte Repression in *Trypanosoma brucei*. Diplomarbeit (Freie Universität Berlin).
- Robitaille, A.M., Christen, S., Shimobayashi, M., Cornu, M., Fava, L.L., Moes, S., Prescianotto-Baschong, C., Sauer, U., Jenoe, P., and Hall, M.N. (2013). Quantitative phosphoproteomics reveal mTORC1 activates de novo pyrimidine synthesis. *Science* 339, 1320-1323. 10.1126/science.1228771.
- Roditi, I., Carrington, M., and Turner, M. (1987). Expression of a polypeptide containing a dipeptide repeat is confined to the insect stage of *Trypanosoma brucei*. *Nature* 325, 272-274. 10.1038/325272a0.
- Rojas, F., and Matthews, K.R. (2019). Quorum sensing in African trypanosomes. *Curr Opin Microbiol* 52, 124-129. 10.1016/j.mib.2019.07.001.
- Rojas, F., Silvester, E., Young, J., Milne, R., Tettey, M., Houston, D.R., Walkinshaw, M.D., Perez-Pi, I., Auer, M., Denton, H., et al. (2019). Oligopeptide Signaling through TbGPR89 Drives Trypanosome Quorum Sensing. *Cell* 176, 306-317 e316. 10.1016/j.cell.2018.10.041.
- Romano, R.A., Kannan, N., Kornev, A.P., Allison, C.J., and Taylor, S.S. (2009). A chimeric mechanism for polyvalent trans-phosphorylation of PKA by PDK1. *Protein Sci* 18, 1486-1497. 10.1002/pro.146.

- Rose, C., Casas-Sánchez, A., Dyer, N.A., Solórzano, C., Beckett, A.J., Middlehurst, B., Marcello, M., Haines, L.R., Lisack, J., Engstler, M., et al. (2020). *Trypanosoma brucei* colonizes the tsetse gut via an immature peritrophic matrix in the proventriculus. *Nat Microbiol* 5, 909-916. 10.1038/s41564-020-0707-z.
- Ross, F.A., MacKintosh, C., and Hardie, D.G. (2016). AMP-activated protein kinase: a cellular energy sensor that comes in 12 flavours. *FEBS J* 283, 2987-3001. 10.1111/febs.13698.
- Rotureau, B., Subota, I., Buisson, J., and Bastin, P. (2012). A new asymmetric division contributes to the continuous production of infective trypanosomes in the tsetse fly. *Development* 139, 1842-1850. 10.1242/dev.072611.
- Rotureau, B., and Van Den Abbeele, J. (2013). Through the dark continent: African trypanosome development in the tsetse fly. *Front Cell Infect Microbiol* 3, 53. 10.3389/fcimb.2013.00053.
- Roux, K.J., Kim, D.I., Raida, M., and Burke, B. (2012). A promiscuous biotin ligase fusion protein identifies proximal and interacting proteins in mammalian cells. *J Cell Biol* 196, 801-810. 10.1083/jcb.201112098.
- Saldivia, M., Ceballos-Perez, G., Bart, J.M., and Navarro, M. (2016). The AMPKalpha1 Pathway Positively Regulates the Developmental Transition from Proliferation to Quiescence in *Trypanosoma brucei*. *Cell Rep* 17, 660-670. 10.1016/j.celrep.2016.09.041.
- Salmon, D. (2018). Adenylate Cyclases of *Trypanosoma brucei*, Environmental Sensors and Controllers of Host Innate Immune Response. *Pathogens* 7. 10.3390/pathogens7020048.
- Salt, I.P., Johnson, G., Ashcroft, S.J., and Hardie, D.G. (1998). AMP-activated protein kinase is activated by low glucose in cell lines derived from pancreatic beta cells, and may regulate insulin release. *Biochem J* 335 (Pt 3), 533-539. 10.1042/bj3350533.
- Sanz, P., Alms, G.R., Haystead, T.A., and Carlson, M. (2000). Regulatory interactions between the Reg1-Glc7 protein phosphatase and the Snf1 protein kinase. *Mol Cell Biol* 20, 1321-1328. 10.1128/mcb.20.4.1321-1328.2000.
- Sastri, M., Barraclough, D.M., Carmichael, P.T., and Taylor, S.S. (2005). A-kinase-interacting protein localizes protein kinase A in the nucleus. *Proc Natl Acad Sci U S A* 102, 349-354. 10.1073/pnas.0408608102.
- Saxton, R.A., and Sabatini, D.M. (2017). mTOR Signaling in Growth, Metabolism, and Disease. *Cell* 168, 960-976. 10.1016/j.cell.2017.02.004.
- Schenk, R., Bachmaier, S., Bringaud, F., and Boshart, M. (2021). Efficient flavinylation of glycosomal fumarate reductase by its own ApbE domain in *Trypanosoma brucei*. *FEBS J* 288, 5430-5445. 10.1111/febs.15812.
- Schulte zu Sodingen, C. (2000). Molekulargenetische Untersuchungen zur Differenzierung von *Trypanosoma brucei*. Doktorarbeit (Universität Konstanz).
- Schummer, A., Maier, R., Gabay-Maskit, S., Hansen, T., Muhlhauser, W.W.D., Suppanz, I., Fadel, A., Schuldiner, M., Girzalsky, W., Oeljeklaus, S., et al. (2020). Pex14p Phosphorylation Modulates Import of Citrate Synthase 2 Into Peroxisomes in *Saccharomyces cerevisiae*. *Front Cell Dev Biol* 8, 549451. 10.3389/fcell.2020.549451.
- Scott, J.D., Glaccum, M.B., Fischer, E.H., and Krebs, E.G. (1986). Primary-structure requirements for inhibition by the heat-stable inhibitor of the cAMP-dependent protein kinase. *Proc Natl Acad Sci U S A* 83, 1613-1616. 10.1073/pnas.83.6.1613.
- Shabb, J.B. (2001). Physiological substrates of cAMP-dependent protein kinase. *Chem Rev* 101, 2381-2411. 10.1021/cr000236l.
- Shalaby, T., Liniger, M., and Seebeck, T. (2001). The regulatory subunit of a cGMP-regulated protein kinase A of *Trypanosoma brucei*. *Eur J Biochem* 268, 6197-6206. 10.1046/j.0014-2956.2001.02564.x.
- Shaw, R.J., Bardeesy, N., Manning, B.D., Lopez, L., Kosmatka, M., DePinho, R.A., and Cantley, L.C. (2004). The LKB1 tumor suppressor negatively regulates mTOR signaling. *Cancer Cell* 6, 91-99. 10.1016/j.ccr.2004.06.007.
- Shoji, S., Titani, K., Demaille, J.G., and Fischer, E.H. (1979). Sequence of two phosphorylated sites in the catalytic subunit of bovine cardiac muscle adenosine 3':5'-monophosphate-dependent protein kinase. *Journal of Biological Chemistry* 254, 6211-6214. 10.1016/s0021-9258(18)50345-8.
- Simmons, J.M., Muller, T.A., and Hausinger, R.P. (2008). Fe(II)/alpha-ketoglutarate hydroxylases involved in nucleobase, nucleoside, nucleotide, and chromatin metabolism. *Dalton Trans*, 5132-5142. 10.1039/b803512a.
- Slice, L.W., and Taylor, S.S. (1989). Expression of the catalytic subunit of cAMP-dependent protein kinase in *Escherichia coli*. *J Biol Chem* 264, 20940-20946.
- Smith, J.J., and Aitchison, J.D. (2009). Regulation of peroxisome dynamics. *Curr Opin Cell Biol* 21, 119-126. 10.1016/j.ceb.2009.01.009.
- Smith, T.K., Bringaud, F., Nolan, D.P., and Figueiredo, L.M. (2017). Metabolic reprogramming during the *Trypanosoma brucei* life cycle. *F1000Res* 6. 10.12688/f1000research.10342.2.
- Soberg, K., and Skalhegg, B.S. (2018). The Molecular Basis for Specificity at the Level of the Protein Kinase a Catalytic Subunit. *Front Endocrinol (Lausanne)* 9, 538. 10.3389/fendo.2018.00538.

- Solari, C.A., Tudisca, V., Pugliesi, M., Nadra, A.D., Moreno, S., and Portela, P. (2014). Regulation of PKA activity by an autophosphorylation mechanism in *Saccharomyces cerevisiae*. *Biochem J* 462, 567-579. 10.1042/BJ20140577.
- Steichen, J.M., Kuchinskas, M., Keshwani, M.M., Yang, J., Adams, J.A., and Taylor, S.S. (2012). Structural basis for the regulation of protein kinase A by activation loop phosphorylation. *J Biol Chem* 287, 14672-14680. 10.1074/jbc.M111.335091.
- Stein, S.C., Woods, A., Jones, N.A., Davison, M.D., and Carling, D. (2000). The regulation of AMP-activated protein kinase by phosphorylation. *Biochem J* 345 Pt 3, 437-443.
- Steinberg, R.A., Cauthron, R.D., Symcox, M.M., and Shuntoh, H. (1993). Autoactivation of catalytic (C alpha) subunit of cyclic AMP-dependent protein kinase by phosphorylation of threonine 197. *Mol Cell Biol* 13, 2332-2341. 10.1128/mcb.13.4.2332-2341.1993.
- Sternlieb, T., Schoijet, A.C., Genta, P.D., Vilchez Larrea, S.C., and Alonso, G.D. (2021). An AMP-activated protein kinase complex with two distinctive alpha subunits is involved in nutritional stress responses in *Trypanosoma cruzi*. *PLoS Negl Trop Dis* 15, e0009435. 10.1371/journal.pntd.0009435.
- Stewart, G.C. (2015). The Exosporium Layer of Bacterial Spores: a Connection to the Environment and the Infected Host. *Microbiol Mol Biol Rev* 79, 437-457. 10.1128/MMBR.00050-15.
- Subota, I., Julkowska, D., Vincensini, L., Reeg, N., Buisson, J., Blisnick, T., Huet, D., Perrot, S., Santi-Rocca, J., Duchateau, M., et al. (2014). Proteomic analysis of intact flagella of procyclic *Trypanosoma brucei* cells identifies novel flagellar proteins with unique sub-localization and dynamics. *Mol Cell Proteomics* 13, 1769-1786. 10.1074/mcp.M113.033357.
- Sugi, T., Ma, Y.F., Tomita, T., Murakoshi, F., Eaton, M.S., Yakubu, R., Han, B., Tu, V., Kato, K., Kawazu, S., et al. (2016). *Toxoplasma gondii* Cyclic AMP-Dependent Protein Kinase Subunit 3 Is Involved in the Switch from Tachyzoite to Bradyzoite Development. *mBio* 7. 10.1128/mBio.00755-16.
- Supek, F., Bosnjak, M., Skunca, N., and Smuc, T. (2011). REVIGO summarizes and visualizes long lists of gene ontology terms. *PLoS One* 6, e21800. 10.1371/journal.pone.0021800.
- Szoor, B., Ruberto, I., Burchmore, R., and Matthews, K.R. (2010). A novel phosphatase cascade regulates differentiation in *Trypanosoma brucei* via a glycosomal signaling pathway. *Genes Dev* 24, 1306-1316. 10.1101/gad.570310.
- Szőör, B., Simon, D.V., Rojas, F., Young, J., Robinson, D.R., Krüger, T., Engstler, M., and Matthews, K.R. (2019). Positional Dynamics and Glycosomal Recruitment of Developmental Regulators during *Trypanosome* Differentiation. *mBio* 10. 10.1128/mBio.00875-19.
- Taylor, S.S., Ilouz, R., Zhang, P., and Kornev, A.P. (2012a). Assembly of allosteric macromolecular switches: lessons from PKA. *Nat Rev Mol Cell Biol* 13, 646-658. 10.1038/nrm3432.
- Taylor, S.S., Keshwani, M.M., Steichen, J.M., and Kornev, A.P. (2012b). Evolution of the eukaryotic protein kinases as dynamic molecular switches. *Philos Trans R Soc Lond B Biol Sci* 367, 2517-2528. 10.1098/rstb.2012.0054.
- Taylor, S.S., Kim, C., Cheng, C.Y., Brown, S.H., Wu, J., and Kannan, N. (2008). Signaling through cAMP and cAMP-dependent protein kinase: diverse strategies for drug design. *Biochim Biophys Acta* 1784, 16-26. 10.1016/j.bbapap.2007.10.002.
- Taylor, S.S., Wu, J., Bruystens, J.G.H., Del Rio, J.C., Lu, T.W., Kornev, A.P., and Ten Eyck, L.F. (2021). From structure to the dynamic regulation of a molecular switch: A journey over 3 decades. *J Biol Chem* 296, 100746. 10.1016/j.jbc.2021.100746.
- Tetley, L., and Vickerman, K. (1985). Differentiation in *Trypanosoma brucei*: host-parasite cell junctions and their persistence during acquisition of the variable antigen coat. *Journal of cell science* 74, 1-19.
- Tholey, A., Pipkorn, R., Bossemeyer, D., Kinzel, V., and Reed, J. (2001). Influence of myristoylation, phosphorylation, and deamidation on the structural behavior of the N-terminus of the catalytic subunit of cAMP-dependent protein kinase. *Biochemistry* 40, 225-231. 10.1021/bi0021277.
- Tirichen, H., Yaigoub, H., Xu, W., Wu, C., Li, R., and Li, Y. (2021). Mitochondrial Reactive Oxygen Species and Their Contribution in Chronic Kidney Disease Progression Through Oxidative Stress. *Frontiers in Physiology* 12. 10.3389/fphys.2021.627837.
- Toda, T., Cameron, S., Sass, P., Zoller, M., and Wigler, M. (1987). Three different genes in *S. cerevisiae* encode the catalytic subunits of the cAMP-dependent protein kinase. *Cell* 50, 277-287. 10.1016/0092-8674(87)90223-6.
- Trefts, E., and Shaw, R.J. (2021). AMPK: restoring metabolic homeostasis over space and time. *Mol Cell* 81, 3677-3690. 10.1016/j.molcel.2021.08.015.
- Treitl, M.A., and Carlson, M. (1995). Repression by Ssn6-Tup1 is directed by Mig1, a repressor/activator protein. *Proc Natl Acad Sci U S A* 92, 3132-3136. 10.1073/pnas.92.8.3132.
- Treitl, M.A., Kuchin, S., and Carlson, M. (1998). Sfn1 protein kinase regulates phosphorylation of the Mig1 repressor in *Saccharomyces cerevisiae*. *Mol Cell Biol* 18, 6273-6280. 10.1128/mcb.18.11.6273.
- Trindade, S., Rijo-Ferreira, F., Carvalho, T., Pinto-Neves, D., Guegan, F., Aresta-Branco, F., Bento, F., Young, S.A., Pinto, A., Van Den Abbeele, J., et al. (2016). *Trypanosoma brucei* Parasites Occupy and Functionally Adapt to the Adipose Tissue in Mice. *Cell Host Microbe* 19, 837-848. 10.1016/j.chom.2016.05.002.

- Tripathi, A., Singha, U.K., Paromov, V., Hill, S., Pratap, S., Rose, K., and Chaudhuri, M. (2019). The Cross Talk between TbTim50 and PIP39, Two Aspartate-Based Protein Phosphatases, Maintains Cellular Homeostasis in *Trypanosoma brucei*. *mSphere* 4. 10.1128/mSphere.00353-19.
- Tsigankov, P., Gherardini, P.F., Helmer-Citterich, M., Spath, G.F., Myler, P.J., and Zilberstein, D. (2014). Regulation dynamics of *Leishmania* differentiation: deconvoluting signals and identifying phosphorylation trends. *Mol Cell Proteomics* 13, 1787-1799. 10.1074/mcp.M114.037705.
- Tsigankov, P., Gherardini, P.F., Helmer-Citterich, M., Spath, G.F., and Zilberstein, D. (2013). Phosphoproteomic analysis of differentiating *Leishmania* parasites reveals a unique stage-specific phosphorylation motif. *J Proteome Res* 12, 3405-3412. 10.1021/pr4002492.
- Tudisca, V., Recouvreux, V., Moreno, S., Boy-Marcotte, E., Jacquet, M., and Portela, P. (2010). Differential localization to cytoplasm, nucleus or P-bodies of yeast PKA subunits under different growth conditions. *Eur J Cell Biol* 89, 339-348. 10.1016/j.ejcb.2009.08.005.
- Tudisca, V., Simpson, C., Castelli, L., Lui, J., Hoyle, N., Moreno, S., Ashe, M., and Portela, P. (2012). PKA isoforms coordinate mRNA fate during nutrient starvation. *Journal of cell science* 125, 5221-5232. 10.1242/jcs.111534.
- Tyanova, S., and Cox, J. (2018). Perseus: A Bioinformatics Platform for Integrative Analysis of Proteomics Data in Cancer Research. *Methods Mol Biol* 1711, 133-148. 10.1007/978-1-4939-7493-1_7.
- Tyanova, S., Temu, T., and Cox, J. (2016a). The MaxQuant computational platform for mass spectrometry-based shotgun proteomics. *Nat Protoc* 11, 2301-2319. 10.1038/nprot.2016.136.
- Tyanova, S., Temu, T., Sinitcyn, P., Carlson, A., Hein, M.Y., Geiger, T., Mann, M., and Cox, J. (2016b). The Perseus computational platform for comprehensive analysis of (prote)omics data. *Nat Methods* 13, 731-740. 10.1038/nmeth.3901.
- Tyler, K.M., Matthews, K.R., and Gull, K. (1997). The bloodstream differentiation-division of *Trypanosoma brucei* studied using mitochondrial markers. *Proc Biol Sci* 264, 1481-1490. 10.1098/rspb.1997.0205.
- Uboldi, A.D., Wilde, M.L., McRae, E.A., Stewart, R.J., Dagley, L.F., Yang, L., Katris, N.J., Hapuarachchi, S.V., Coffey, M.J., Lehane, A.M., et al. (2018). Protein kinase A negatively regulates Ca²⁺ signalling in *Toxoplasma gondii*. *PLoS Biol* 16, e2005642. 10.1371/journal.pbio.2005642.
- Urbaniak, M.D., Guther, M.L., and Ferguson, M.A. (2012). Comparative SILAC proteomic analysis of *Trypanosoma brucei* bloodstream and procyclic lifecycle stages. *PLoS One* 7, e36619. 10.1371/journal.pone.0036619.
- Urbaniak, M.D., Martin, D.M., and Ferguson, M.A. (2013). Global quantitative SILAC phosphoproteomics reveals differential phosphorylation is widespread between the procyclic and bloodstream form lifecycle stages of *Trypanosoma brucei*. *J Proteome Res* 12, 2233-2244. 10.1021/pr400086y.
- Urwiler, S., Studer, E., Renggli, C.K., and Roditi, I. (2007). A family of stage-specific alanine-rich proteins on the surface of epimastigote forms of *Trypanosoma brucei*. *Molecular microbiology* 63, 218-228. 10.1111/j.1365-2958.2006.05492.x.
- van der Plaats, J.B. (1974). Cyclic 3',5'-adenosine monophosphate stimulates trehalose degradation in baker's yeast. *Biochem Biophys Res Commun* 56, 580-587. 10.1016/0006-291x(74)90643-3.
- Vassella, E., and Boshart, M. (1996). High molecular mass agarose matrix supports growth of bloodstream forms of pleomorphic *Trypanosoma brucei* strains in axenic culture. *Mol Biochem Parasitol* 82, 91-105. 10.1016/0166-6851(96)02727-2.
- Vassella, E., Den Abbeele, J.V., Bütikofer, P., Renggli, C.K., Furger, A., Brun, R., and Roditi, I. (2000). A major surface glycoprotein of *trypanosoma brucei* is expressed transiently during development and can be regulated post-transcriptionally by glycerol or hypoxia. *Genes Dev* 14, 615-626.
- Vassella, E., Probst, M., Schneider, A., Studer, E., Renggli, C.K., and Roditi, I. (2004). Expression of a major surface protein of *Trypanosoma brucei* insect forms is controlled by the activity of mitochondrial enzymes. *Mol Biol Cell* 15, 3986-3993. 10.1091/mbc.e04-04-0341.
- Vertommen, D., Van Roy, J., Szikora, J.P., Rider, M.H., Michels, P.A., and Opperdoes, F.R. (2008). Differential expression of glycosomal and mitochondrial proteins in the two major life-cycle stages of *Trypanosoma brucei*. *Mol Biochem Parasitol* 158, 189-201. 10.1016/j.molbiopara.2007.12.008.
- Villafranz, O., Baudouin, H., Mazet, M., Kulyk, H., Dupuy, J.W., Pineda, E., Botte, C., Inaoka, D.K., Portais, J.C., and Bringaud, F. (2021). The *Trypanosoma* UDP-Glucose Pyrophosphorylase Is Imported by Piggybacking into Glycosomes, Where Unconventional Sugar Nucleotide Synthesis Takes Place. *mBio* 12, e0037521. 10.1128/mBio.00375-21.
- Walsh, B., and Hill, K.L. (2021). Right place, right time: Environmental sensing and signal transduction directs cellular differentiation and motility in *Trypanosoma brucei*. *Molecular microbiology* 115, 930-941. 10.1111/mmi.14682.
- Walsh, D.A., Perkins, J.P., and Krebs, E.G. (1968). An Adenosine 3',5'-Monophosphate-dependant Protein Kinase from Rabbit Skeletal Muscle. *Journal of Biological Chemistry* 243, 3763-3765. 10.1016/s0021-9258(19)34204-8.
- Wargnies, M., Bertiaux, E., Cahoreau, E., Ziebart, N., Cruzols, A., Morand, P., Biran, M., Allmann, S., Hubert, J., Villafranz, O., et al. (2018). Gluconeogenesis is essential for trypanosome

- development in the tsetse fly vector. *PLoS pathogens* 14, e1007502. 10.1371/journal.ppat.1007502.
- Wargnies, M., Plazolles, N., Schenk, R., Villafranz, O., Dupuy, J.W., Biran, M., Bachmaier, S., Baudouin, H., Clayton, C., Boshart, M., and Bringaud, F. (2021). Metabolic selection of a homologous recombination-mediated gene loss protects *Trypanosoma brucei* from ROS production by glycosomal fumarate reductase. *J Biol Chem* 296, 100548. 10.1016/j.jbc.2021.100548.
- Weiss, B.L., Maltz, M.A., Vigneron, A., Wu, Y., Walter, K.S., O'Neill, M.B., Wang, J., and Aksoy, S. (2019). Colonization of the tsetse fly midgut with commensal *Kosakonia cowanii* *Zambiae* inhibits trypanosome infection establishment. *PLoS pathogens* 15. 10.1371/journal.ppat.1007470.
- Welch, E.J., Jones, B.W., and Scott, J.D. (2010). Networking with AKAPs: context-dependent regulation of anchored enzymes. *Mol Interv* 10, 86-97. 10.1124/mi.10.2.6.
- Wheeler, R.J. (2021). A resource for improved predictions of *Trypanosoma* and *Leishmania* protein three-dimensional structure. *PLoS One* 16, e0259871. 10.1371/journal.pone.0259871.
- Wiemer, E.A., L, I.J., van Roy, J., Wanders, R.J., and Opperdoes, F.R. (1996). Identification of 2-enoyl coenzyme A hydratase and NADP(+)-dependent 3-hydroxyacyl-CoA dehydrogenase activity in glycosomes of procyclic *Trypanosoma brucei*. *Mol Biochem Parasitol* 82, 107-111. 10.1016/0166-6851(96)02710-7.
- Wilde, M.L., Triglia, T., Marapana, D., Thompson, J.K., Kouzmitchev, A.A., Bullen, H.E., Gilson, P.R., Cowman, A.F., and Tonkin, C.J. (2019). Protein Kinase A Is Essential for Invasion of *Plasmodium falciparum* into Human Erythrocytes. *mBio* 10. 10.1128/mBio.01972-19.
- Wirtz, E., Leal, S., Ochatt, C., and Cross, G.A. (1999). A tightly regulated inducible expression system for conditional gene knock-outs and dominant-negative genetics in *Trypanosoma brucei*. *Mol Biochem Parasitol* 99, 89-101. 10.1016/s0166-6851(99)00002-x.
- Wishart, D.S., Feunang, Y.D., Marcu, A., Guo, A.C., Liang, K., Vazquez-Fresno, R., Sajed, T., Johnson, D., Li, C., Karu, N., et al. (2018). HMDB 4.0: the human metabolome database for 2018. *Nucleic Acids Res* 46, D608-D617. 10.1093/nar/gkx1089.
- Woods, A., Dickerson, K., Heath, R., Hong, S.P., Momcilovic, M., Johnstone, S.R., Carlson, M., and Carling, D. (2005). Ca²⁺/calmodulin-dependent protein kinase kinase-beta acts upstream of AMP-activated protein kinase in mammalian cells. *Cell Metab* 2, 21-33. 10.1016/j.cmet.2005.06.005.
- Wu, Q. (2021). The trypanosomatid protein kinase A activation mechanism - a target for structure-based inhibitor development. Doktor Dissertation (Ludwig-Maximilians-Universität).
- Yamashita, K., Tamura, S., Honsho, M., Yada, H., Yagita, Y., Kosako, H., and Fujiki, Y. (2020). Mitotic phosphorylation of Pex14p regulates peroxisomal import machinery. *J Cell Biol* 219. 10.1083/jcb.202001003.
- Yonemoto, W., Garrod, S.M., Bell, S.M., and Taylor, S.S. (1993). Identification of phosphorylation sites in the recombinant catalytic subunit of cAMP-dependent protein kinase. *Journal of Biological Chemistry* 268, 18626-18632. 10.1016/s0021-9258(17)46675-0.
- Zhang, N., Jiang, N., Zhang, K., Zheng, L., Zhang, D., Sang, X., Feng, Y., Chen, R., Yang, N., Wang, X., et al. (2020). Landscapes of Protein Posttranslational Modifications of African *Trypanosoma Parasites*. *iScience* 23, 101074. 10.1016/j.isci.2020.101074.
- Zheng, J., Knighton, D.R., Xuong, N.H., Taylor, S.S., Sowadski, J.M., and Ten Eyck, L.F. (1993). Crystal structures of the myristylated catalytic subunit of cAMP-dependent protein kinase reveal open and closed conformations. *Protein Sci* 2, 1559-1573. 10.1002/pro.5560021003.
- Ziebart, N., Emmy (2016). Metabolic Signals and Pathways in Development of *Trypanosoma brucei*. PhD Thesis (Ludwig-Maximilians-Universität München).
- Ziegelbauer, K., Quinten, M., Schwarz, H., Pearson, T.W., and Overath, P. (1990). Synchronous differentiation of *Trypanosoma brucei* from bloodstream to procyclic forms in vitro. *Eur J Biochem* 192, 373-378. 10.1111/j.1432-1033.1990.tb19237.x.
- Zikova, A., Verner, Z., Nenarokova, A., Michels, P.A.M., and Lukes, J. (2017). A paradigm shift: The mitoproteomes of procyclic and bloodstream *Trypanosoma brucei* are comparably complex. *PLoS pathogens* 13, e1006679. 10.1371/journal.ppat.1006679.
- Zilberstein, D., and Myler, P.J. (2021). Arginine sensing in intracellular parasitism of *Leishmania*. *Curr Opin Microbiol* 64, 41-46. 10.1016/j.mib.2021.09.003.
- Zomer, A.W., Michels, P.A., and Opperdoes, F.R. (1999). Molecular characterisation of *Trypanosoma brucei* alkyl dihydroxyacetone-phosphate synthase. *Mol Biochem Parasitol* 104, 55-66. 10.1016/s0166-6851(99)00141-3.
- Zomer, A.W., Opperdoes, F.R., and van den Bosch, H. (1995). Alkyl dihydroxyacetone phosphate synthase in glycosomes of *Trypanosoma brucei*. *Biochim Biophys Acta* 1257, 167-173. 10.1016/0005-2760(95)00066-l.
- Zurita-Martinez, S.A., and Cardenas, M.E. (2005). Tor and cyclic AMP-protein kinase A: two parallel pathways regulating expression of genes required for cell growth. *Eukaryot Cell* 4, 63-71. 10.1128/EC.4.1.63-71.2005.

6 CURRICULUM VITAE

Kristina Malenica

Personal Details

E-Mail	Kristina.Malenica@lmu.de
Date of birth	September 18, 1992
Place of birth	Munich, Germany

Education

01/2017 – 05/2022	<p>phD thesis in the lab of Prof. Michael Boshart, LMU, Munich</p> <p>“Protein kinase A mediated adaptation of trypanosomes to the insect host environment”</p>
10/2014 – 12/2016	<p>Master of science at LMU, Munich</p> <p>focus on molecular and cell biology</p> <p>Master's thesis: “<i>Investigation of the mechanism underlying PKA activation by mild acidic stress in Trypanosoma brucei</i>” in the lab of Prof. Michael Bosart</p>
10/2011 – 10/2014	<p>Bachelor of Science at LMU, Munich</p> <p>focus on molecular biology</p> <p>Bachelor's thesis: “<i>Identification and characterization of TRPM channel genetic interactors</i>” in the lab of Prof. Barbara Conradt, LMU Munich</p>
09/2003 – 07/2011	<p>University entrance diploma at Asam-Gymnasium, Munich</p>

Scholarships, work experience and volunteer engagement

Since 09/2017	Membership at the LSM graduate school student council
10/2013 – 11/2016	Membership at the LMU student council
11/2014 – 12/2016	Student jobs as a course helper at LMU Munich faculty of biology and medicine
01/2016 – 04/2016	Lehre@LMU Förderpreis for the project: „ <i>Expression & purification of Trypanosoma brucei protein kinase A using cell-free expression systems</i> “
04/2015 – 01/2016	Student job at the medical diagnosis lab <i>Labor Becker, Olgemöller and Kollegen</i> , S2 security level
04/2015 – 10/2015	Deutschlandstipendium provided by Roche Diagnostics GmbH
10/2014 – 10/2015	Participation at the LMU P2P mentoring program as a mentor for freshmen students

Meetings and conferences

04/2016	6 th meeting ACETOTRYP/GLYCONOV (Frauenchiemsee, Germany)
04/2018	28 th annual meeting of the german society for parasitology (Berlin, Germany, poster presentation)
05/2019	9 th meeting GLYCONOV (Bombannes, France, talk)
07/2019	Today-LMU meeting on trypanosome metabolism (Tokyo, Japan, talk)

Teaching experience

2017 - 2020	Yearly organization of practical course Genetik 2 for bachelor students, preparation and presentation of lectures for the practical course
2017 – 2021	Supervision of bachelor and master student project
2018 - 2020	Supervision of bachelor theses

Skills and training

Trainings

02/2020	Good Clinical Practice (GCP) basic course for Scientists (GMP Academy)
09/2019	Good Manufacturing Practice (GMP) course (GMP Academy)
06/2019	Self and time management for natural sciences (Sabine Lerch)
02/2019	Scientific Writing (Science craft)
09/2017	Statistical literacy (Science craft)
06/2017	9 th MaxQuant Summer School (Berlin, Germany)
05/2017	Adobe Illustrator Course (LMU Munich)
03/2017	Getting Published and Understanding Peer Review (Science craft)

Languages

German	native
English	9 years in school and one seminar <i>“English for Biology”</i> (focus on communication)
French	5 years in school and DELF certificate level B1
Croatian	native

Computer

familiar with Microsoft Office, Adobe Illustrator and Photoshop, CLC Main workbench, ImageJ, GraphPad Prism, MaxQuant, Perseus

7 ACKNOWLEDGEMENTS

First of all, I would like to express my gratitude to Prof. Michael Boshart for his supervision on this continuously developing project. I am very grateful for all the discussions we had and the great support he offered. I really appreciate that there was always time to discuss science.

Many thanks to all the thesis committee members for their time and interest, especially PD Dr. Bettina Bölter, who agreed to being the second reviewer.

Moreover, I would also like to thank the members of my thesis advisory committee, Prof. Thorben Cordes and Prof. Nicolai Siegel for their support and feedback along the way.

I am very grateful for all the collaboration partners, especially Frederic Bringaud and his lab, who provided us with his expert knowledge on metabolism along with numerous antibodies and protocols. I would also like to thank Emanuel Tetaud, without his CRISPR protocol, the generation of some cell lines would not have been possible or very tedious.

Many thanks to the LSM coordinators Francisca Rosa Mende and Nadine Hamze for their support and the organization of all these great method and soft skill courses. A great thanks goes to the LSM student council, I really enjoyed being a part of it.

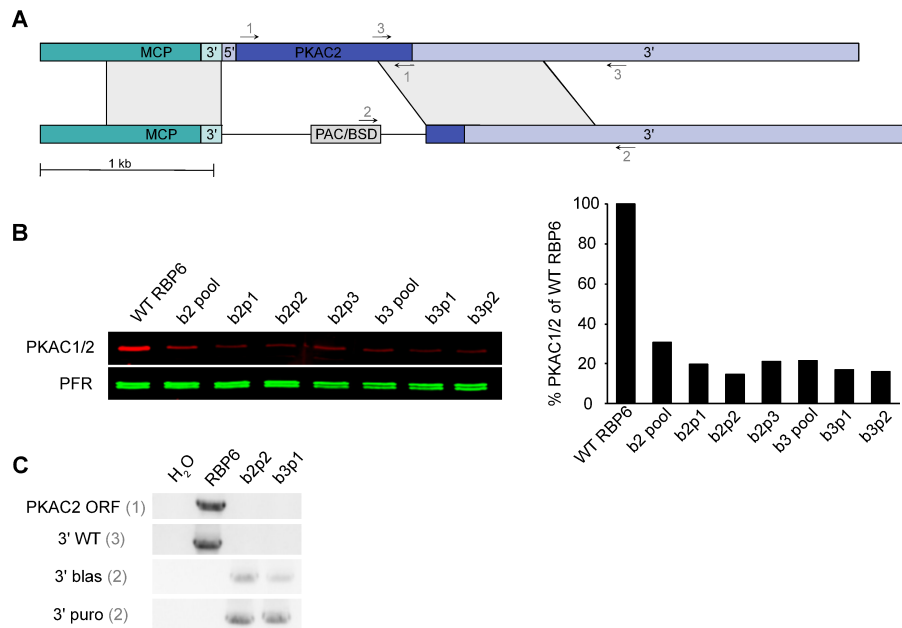
Thank you to all the former and present lab members of the AG Boshart for providing such a great work atmosphere and support. Especially to Sabine for sharing her expertise on everything and Qingping for being a great office and labmate and for introducing me to hotpot.

A big thanks also goes to all the members of the Broscamps & Cordes group, especially Theresa, Astrid, Vroni, Gustavo, Giacomo and Helge, who increased the fun level of phd in and outside the institute with beer fridays, Dnd mondays, party saturdays and lake sundays. It was an amazing time!

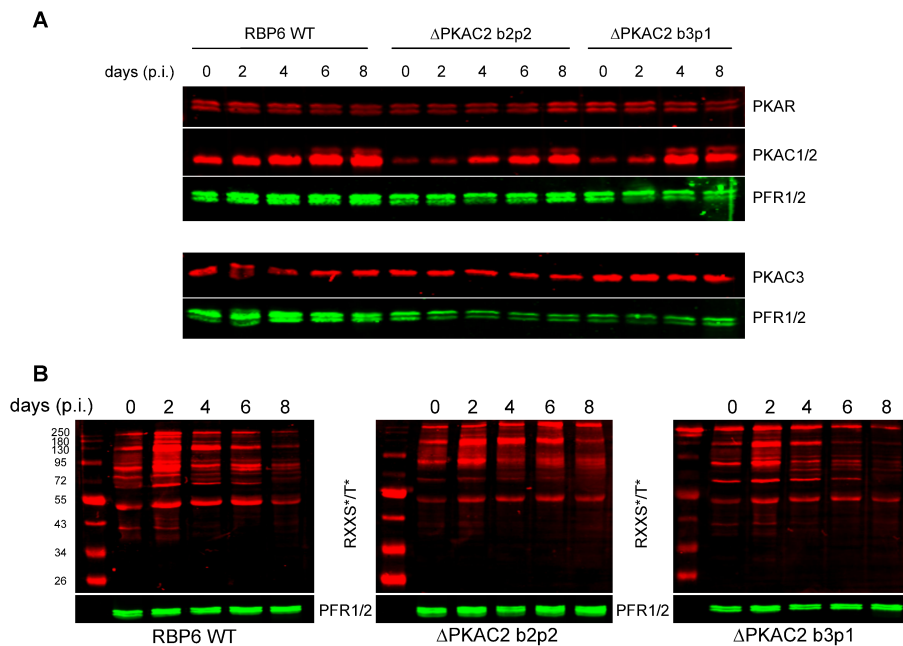
I would also like to thank Lisa and Lari for all the nice coffee breaks we had, they are really missed.

Finally, I would like to thank my family and friends for all their support throughout all these years of "school". I want to especially thank Roman for the constant love, support and encouragement.

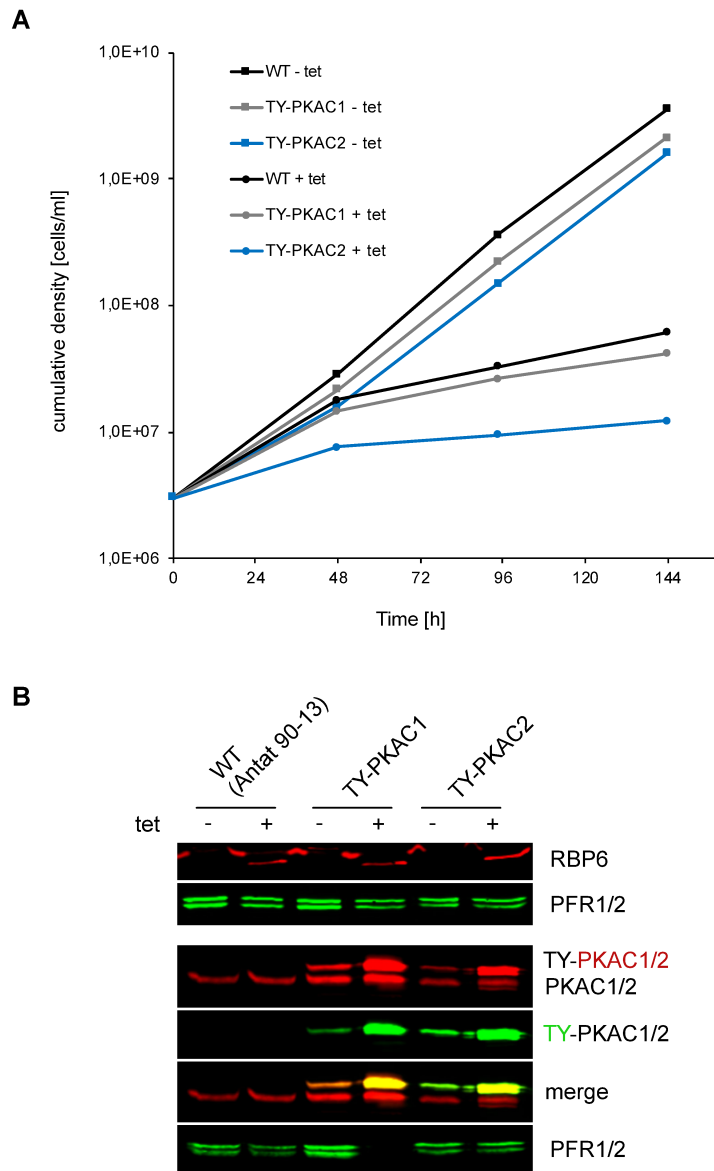
8 SUPPLEMENTARY DATA



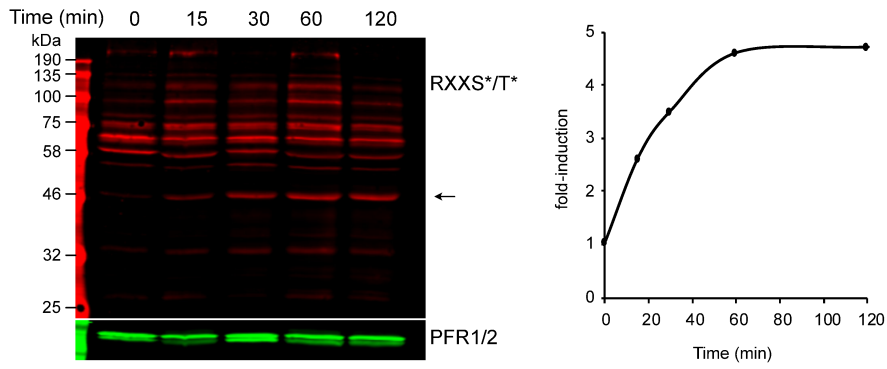
Supplementary Figure 1: Generation and validation of EATRO 1125 T7T RBP6^{Ti} Δ PKAC2. **A:** Schematic representation of knockout strategy. **B:** Western blot analysis of remaining PKAC1 expression after PKAC2 knockout. Plot on the right shows quantification of signal intensity normalized to the PFR loading control. **C:** PKAC2 knockout of the two clones with the lowest expression levels of PKAC1 was verified by integration PCR using the primers indicated in **A**.



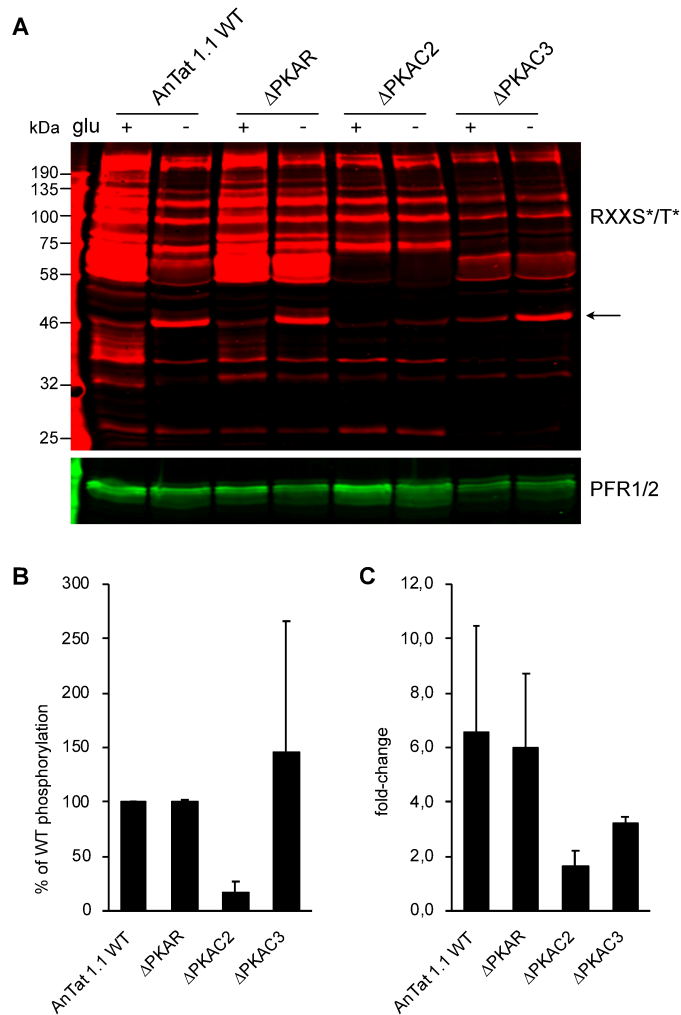
Supplementary Figure 2: Western blot analysis of *in vitro* differentiation by RBP6 overexpression of wild type and two independent PKAC2 knockout clones. **A:** Expression levels of PKA subunits. PFR was used as a loading control. **B:** RXXS^T substrate phosphorylation throughout differentiation. PFR was used as a loading control.



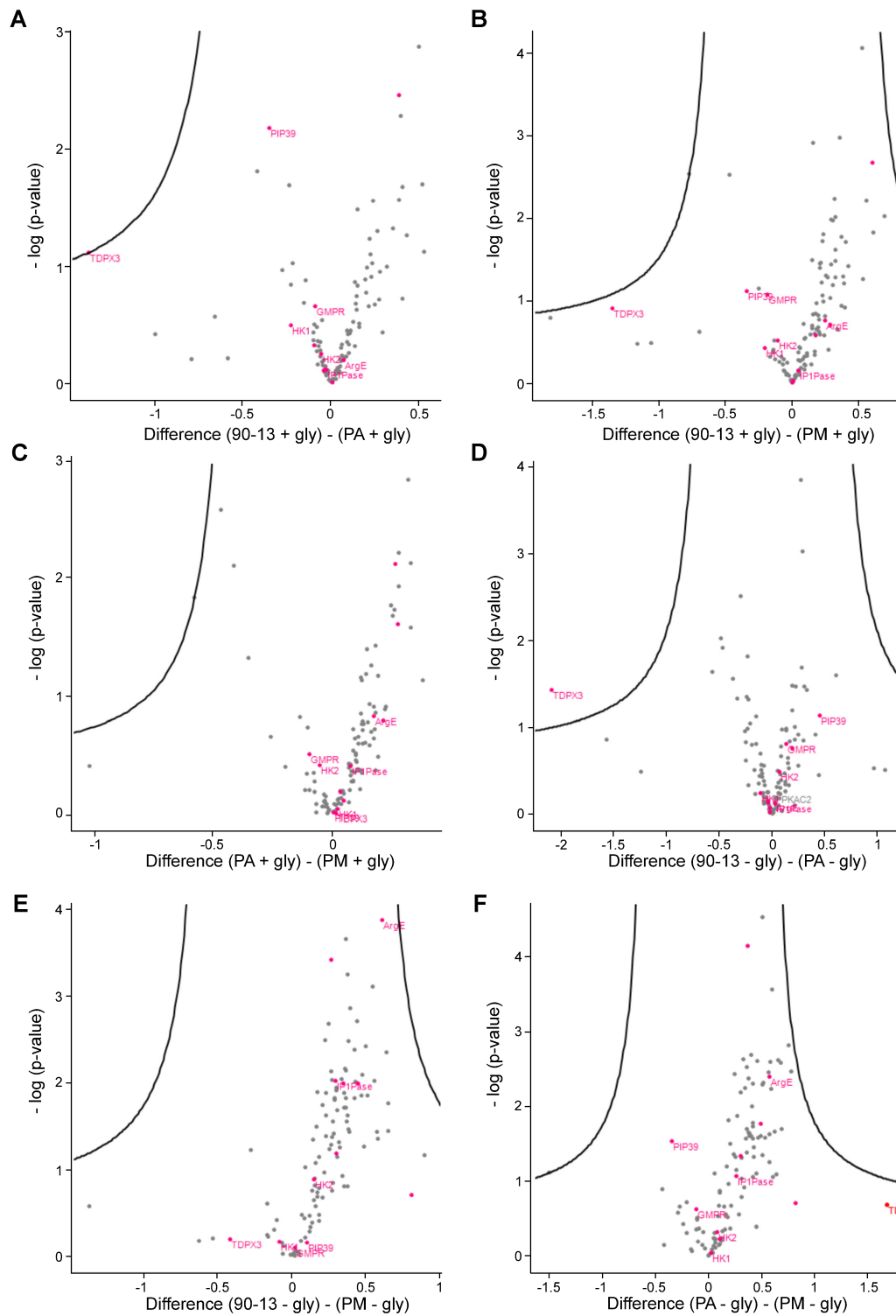
Supplementary Figure 3: RBP6 *in vitro* differentiation experiment of TY-PKAC1 and TY-PKAC2 overexpression (OE). **A:** Growth arrest upon RBP6 OE. **B:** Expression levels of RBP6 and PKAC1/2 throughout the course of differentiation. PKAC1/2 is expressed from a leaky tetracycline (tet) inducible promoter leading to constitutive overexpression and upregulation upon tet-induction. RBP6 is inducible overexpressed upon tetracycline addition. PFR was used as a loading control.



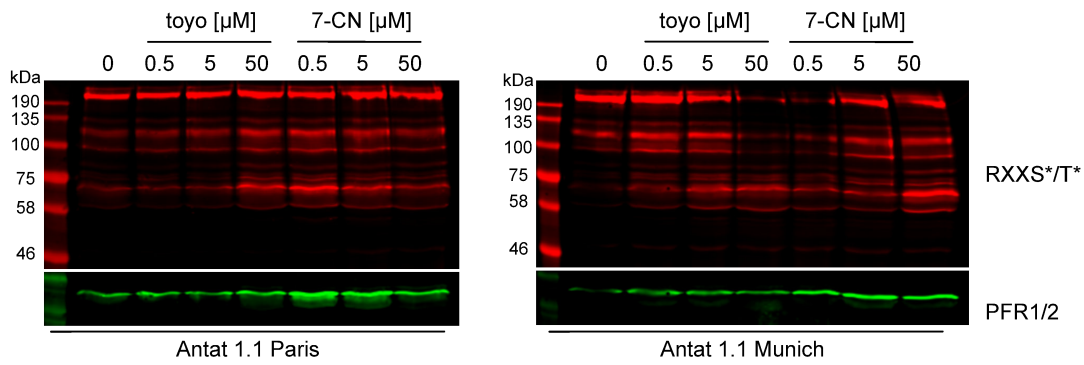
Supplementary Figure 4: Time course of glycerol-depletion in AnTat 1.1 Paris strain.



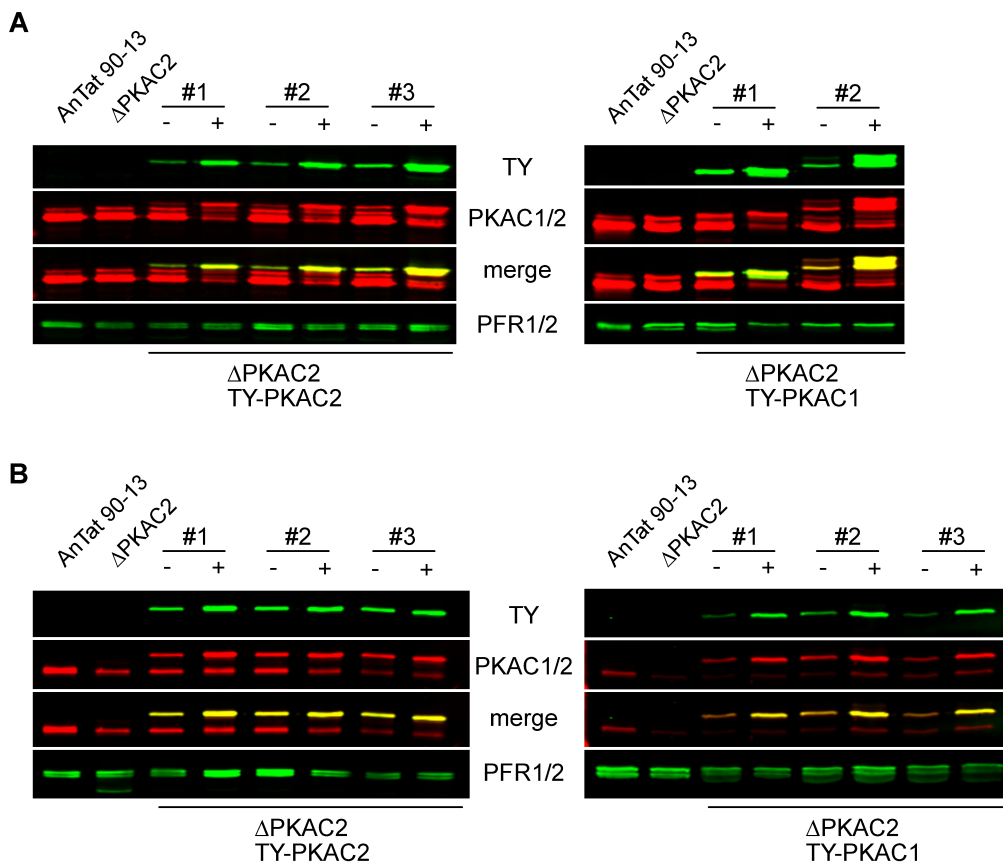
Supplementary Figure 5: Glucose-depletion in AnTat 1.1 wild-type and PKA null mutant cell lines. **A:** representative western blot of 3 independent experiments. Arrow indicates regulated phosphoband. **B:** Intensity of the phosphoband after 60 min glucose-depletion compared to wild type. PFR was used as a loading control. **C:** Fold-change of the phosphoband between +/- glucose.



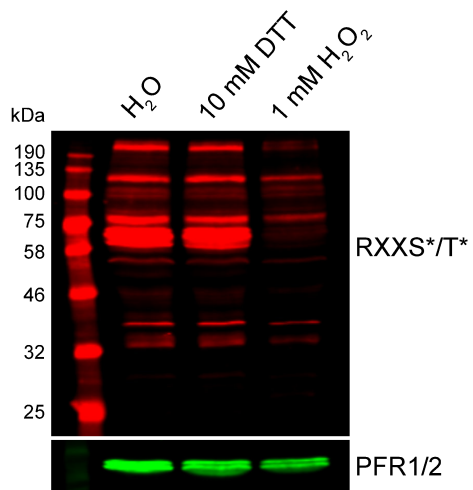
Supplementary Figure 6: Comparison of glycosomal protein abundance in 90-13 wild type and PEX14 phosphomutant cell lines. Volcano plots were generated using a Student's t-test with the significance cut-offs of FDR = 0.05 and S0 = 0.5 in Perseus. Proteins marked in pink were identified as glycerol-regulated in the wild type, but not the PEX14 phosphomutants.



Supplementary Figure 7: PKA activation by nucleoside analogs in PCF cells. Cells were resuspended at a concentration of 10^8 /ml in SDM79 and recovered from centrifugation for 10 min at 27°C. Toyocamycin (toyo) and 7-cyano-7-deazainosine (7-CN) were added at the indicated concentrations for 15 min. Cells were harvested by centrifugation and resuspended in SDS loading buffer. Phosphorylation of PKA substrates was analyzed by anti-RXXS*/T* PKA substrate antibody on western blot. PFR was used as a loading control. Even though there are some blotting irregularities, there appears to be no major effect of the compounds on RXXS*/T* phosphorylation.



Supplementary Figure 8: Regulation of PKAC1/2 expression levels in Δ PKAC2 background. **A:** Inducible overexpression of TY-PKAC1 or TY-PKAC2 in BSF leads to downregulation of endogenous PKAC1. **B:** Tet-inducible overexpression of TY-PKAC1 or TY-PKAC2 in PCF does not affect endogenous PKAC1 level. PFR was used as a loading control.



Supplementary Figure 9: Effect of hydrogen peroxide on RXXS*/T* phosphorylation. AnTat 90-13 procyclic cells were harvested and resuspended in fresh SDM79. After 10 min recovery at 27°C, cells were treated with 1 mM H₂O₂ or 10 mM DTT for 30 min. Samples were taken and analyzed by western blot using anti-RXXS*/T* antibody. PFR was used as a loading control.